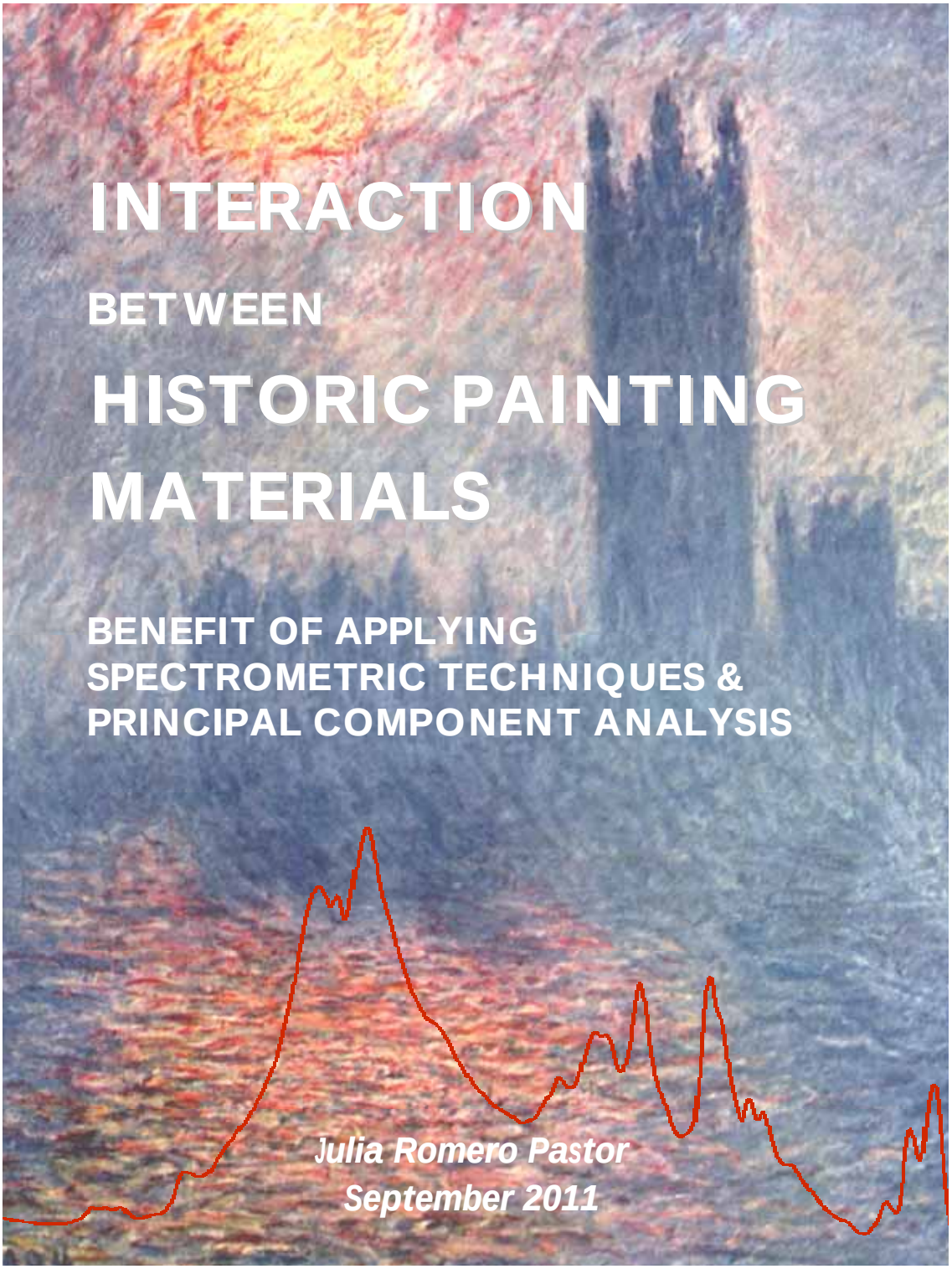
INTERACTION
BETWEEN
HISTORIC PAINTING
MATERIALS
BENEFIT OF APPLYING
SPECTROMETRIC TECHNIQUES &
PRINCIPAL COMPONENT ANALYSIS
Julia Romero Pastor
September 2011

UNIVERSIDAD DE GRANADA

FACULTAD DE CIENCIAS

Departamento de Mineralogía y Petrología

Grupo de Investigación RMN-179: "Mineralogía y Geoquímica de los ambientes Sedimentario y Metamórfico"

TESIS DOCTORAL

"INTERACTION BETWEEN HISTORIC PAINTING MATERIALS. BENEFIT OF APPLYING SPECTROMETRIC TECHNIQUES AND PRINCIPAL COMPONENT ANALYSIS"

presentada por

Julia Romero Pastor

para optar al grado de

Doctorado Europeo

Granada, Septiembre de 2011

Editor: Editorial de la Universidad de Granada
Autor: Julia Romero Pastor
D.L.: GR 956-2012
ISBN: 978-84-694-9404-2

UNIVERSIDAD DE GRANADA

FACULTAD DE CIENCIAS

Departamento de Mineralogía y Petrología

"INTERACTION BETWEEN HISTORIC PAINTING MATERIALS. BENEFIT OF APPLYING SPECTROMETRIC TECHNIQUES AND PRINCIPAL COMPONENT ANALYSIS"

Tesis Doctoral presentada por Julia Romero Pastor para optar al Grado de Doctor por la Universidad de Granada

Granada, Septiembre de 2011

Fdo. Julia Romero Pastor

VºBº DE LOS DIRECTORES:

Fdo. Dra. Carolina Cardell Fernández
Profesora Titular.
Dpto. Mineralogía y Petrología.
Universidad de Granada

Fdo. Dra. Natalia Navas Iglesias
Profesora Titular.
Dpto. Química Analítica.
Universidad de Granada

Fdo. Dr. Alejandro Rodríguez-Navarro
Profesor Titular.
Dpto. Mineralogía y Petrología.
Universidad de Granada

"Woman Reading a Setter"

Johannes Vermeer

(1632-1675)

A mis padres

Tesis evaluada por:

Dr. David Hradil
Institute of Inorganic Chemistry, Academy of Science of CR
Prague, Czech Republic

Dr. Roberto Todeschini
Department of Environmental Sciences. University of Milano-Bicocca
Milano, Italy

INDICE

Abstract

This PhD Thesis study historical painting materials, the interaction among their chemical constituents and the deterioration caused by accelerated ageing processes by their exposure under diverse environmental conditions. The use of routine and advanced analytical techniques applied to the study of painting materials was evaluated by multivariate analysis method (Principal Component Analysis; PCA). The aim of this work was to demonstrate the ability of these analytical techniques and PCA to discriminate painting model samples according to their differing composition, states of ageing or the interactions among the different components of the painting materials. To this end, different inorganic pigments and proteinaceous binders were used to reproduce similar historical tempera paintings, used historically in the decoration of wall paintings in historical buildings. The final goal of this investigation was to study the behavior of the pigments and binders when they are mixed, and their mineralogical and chemical stability, to examine their compatibility in real painting samples. In this regard, a novel approach was applied to identify inorganic and organic components from polychromes from the 14th century Islamic University –*Madrasah Yusufiyya*– in Granada (Spain).

Firstly, in the first three studies of this PhD Thesis the work was focused on the study of fresh historical tempera model samples according to historical recipes. In this regard, the PCA demonstrated the potential benefits of the use of Diffuse Reflectance Infrared Fourier transform spectroscopy (DRIFTS) versus transmittance-Fourier transform infrared spectroscopy (T-FTIR) to evaluate the capability of the multivariate analysis method to discriminate samples according to their composition. To the second and third work, tempera model samples were prepared with historical pigments (azurite, lapis lazuli, smalt, cinnabar, minium, raw Sienna, lead white, chalk, gypsum) and proteinaceous binder (i.e. egg yolk). In the second paper, the chemometric analysis of Raman spectra by PCA allowed the identification of historical pigments and binders as well as degradation processes. From the

other point of view, the third work focused on the effectiveness of applying PCA to Raman Microscopy data to identify the interaction processes between the pigments and the binders.

In a following stage, the research was focused on the accelerated ageing processes of the tempera model samples by alteration agents (i.e. UV radiation and low temperature) and the use of PCA to discriminate their effect on the painting materials. Three studies based on PCA are presented to achieve these goals. The PCA were performed on analytical data of T-FTIR, RM, Attenuated Total Reflectance-Fourier Transform Infrared (ATR-FTIR) Spectroscopy and Matrix-Assisted Laser Desorption/Ionization-Time of Flight Mass Spectroscopy (MALDI-TOF MS). Firstly, the analysis of FTIR data by PCA allowed the detection of physico-chemical changes occurring in painting model samples due to the exposure to UV radiation, providing insights into age-induced alterations of animal based glue and the protective effect of azurite. For the second study of this section, the molecular and mineralogical changes of organic binders (i.e. animal based glue and albumin) during an accelerated thermal aging test were detected while the mineral (i.e. hydroxyapatite or quartz) used as an internal standard remained stable. This methodology based on the use of internal standards was also proposed to check the quality of spectrometric analysis and validate the results of PCA. Finally, the effect of UV radiation on tempera paintings was also evaluated by direct analysis of IR data and the use of PCA to analyse mass data of MALDI-TOF MS for the third study. The main goal was the identification of the role of historical pigments such as cinnabar and azurite on the chemical stability of the animal glue during the UV irradiation.

Regarding the real painting samples, the seventh study shows the benefits of characterizing historic paintings via compositional and microtextural data from Micro-X-Ray Diffraction (μ-XRD) combined with molecular information acquired with RM along depth profiles in paint stratigraphies. Also, information obtained give in sights regarding the manufacture of pigments,

decay processes and the painting technique which was used to discriminate between the original Nasrid paintings and Christian historical interventions

This PhD Thesis represents an advance in the field of Cultural Heritage Science and particularly in studying historical tempera paintings. It shows for the first time the potential benefits of the application of PCA to identify historical pigments and proteinaceous binders on tempera model samples and to study their interactions physico-chemical. Finally, general conclusions and future work perspectives are presented.

Acronyms and Abbreviations

ATR-FTIR	Attenuated Total Reflectance Infrared Fourier Transform
A/P	Ratios of azelaic and palmitic acids
API	Average Intensity of peaks
AL	All layers
Anh	Anhydrite
Az	Azurite
B	Barite
BSE	Backscattered Electron Mode
BC	Black carbon
BG	Brunswick green
C	Calcite
Cer	Cerussite
ΔC*	Chroma
DRIFTS	Diffuse Reflectance Infrared Fourier Transform Spectroscopy
Dol	Dolomite
EDS or EDX	X-Ray Energy Dispersive Spectrometer
GC-MS	Gas Chromatography-Mass Spectroscopy
G	Gold
Gy	Gypsum
GL	Ground layer
H	Hematite
HRTEM	High Resolution Transmission Electron Microscopy
Hy	Hydrocerussite
ΔH*	Hue
IR	Infrared
ΔL*	Brightness
MALDI TOF	Matrix Assisted Laser Desorption Ionisation Time of Flight
MS	Mass Spectrometry
Mi	Minium
μ-XRD	Micro-X-Ray Diffraction
OM	Optical Microscopy
PCA	Principal Component Analysis
PC(s)	Principal Component(s)
P/S	Ratios of palmitic and stearic acids
Q	Quartz
RM	Raman Microscopy
SEM	Scanning Electron Microscopy
SE	Secondary Electron Mode
Sm	Smalt
2D	Two dimensional
ΔE_{cmc}	Total color
TNP	Total number of peaks
T-FTIR	Transmittance-Fourier Transforms Infrared Spectroscopy

UV	Ultraviolet radiation
Ult	Ultramarine
V	Vermilion
XRD	X-Ray Diffraction
ZW	Zinc white

1. Introducción

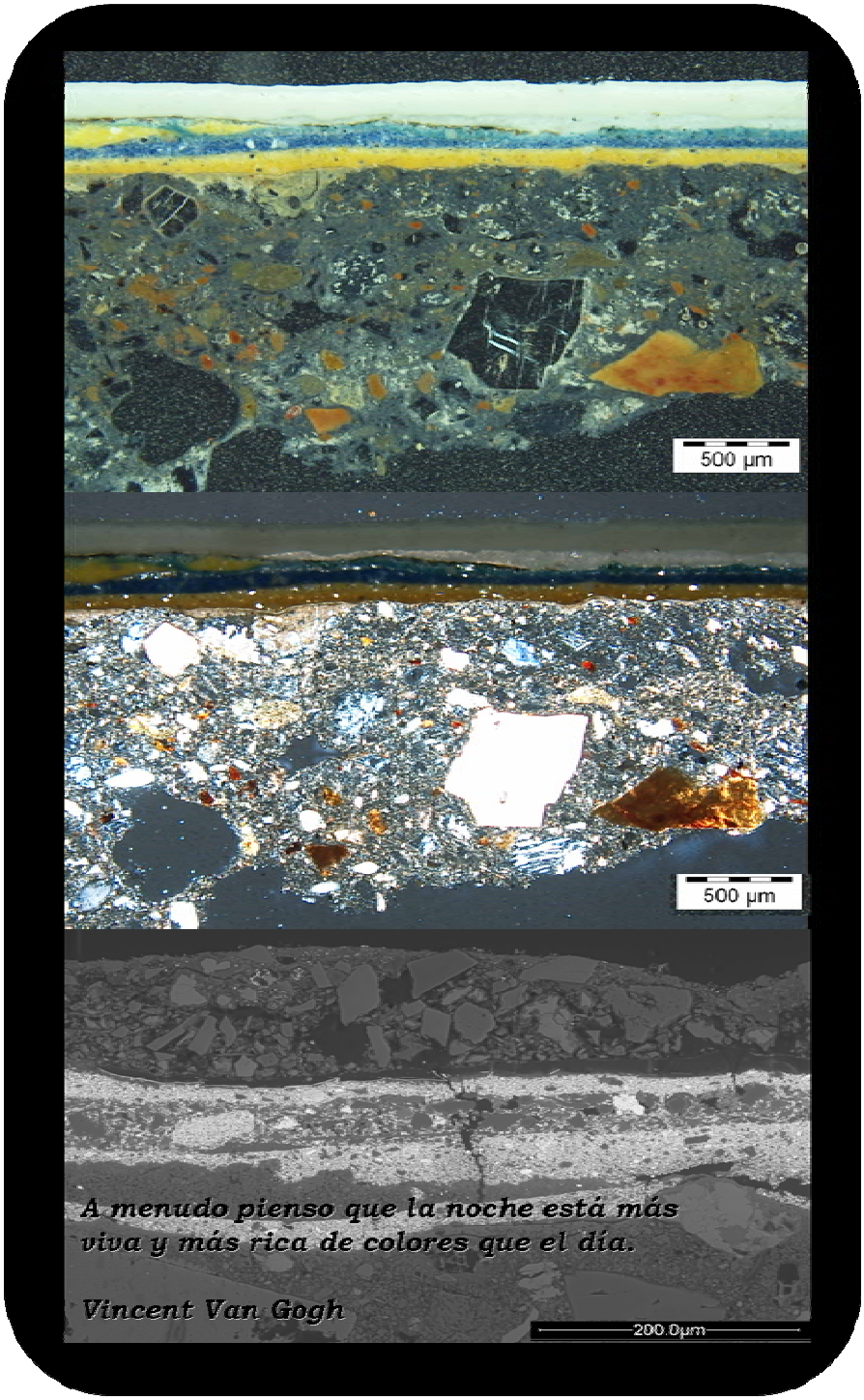

En esta Tesis Doctoral se estudian materiales pictóricos y sus interacciones, en particular, en temples proteicos de pigmentos tradicionales. En este Capítulo introductorio se hace una revisión del estado actual de este campo de investigación desde el punto de vista histórico y científico.

This Doctoral Thesis is based on the study of painting materials and the physico-chemical interactions, in particular, on historical tempera paintings. In the first Chapter, a review was carried out about the state of the art in this field research from a historical and scientific perspective.

1. Introducción

1.1. Análisis científico del Patrimonio Pictórico

El análisis científico de las obras pictóricas ha contribuido en las últimas décadas a un profundo conocimiento de las paletas artísticas, así como de las técnicas y materiales pictóricos utilizados en cada época histórica (Prieto et al., 2005; Cardell-Fernández y Navarrete-Aguilera, 2006). Este avance ha sido posible gracias al desarrollo y el uso de técnicas y metodologías científicas de análisis (Ferreti, 1993). En particular, el estudio científico del Patrimonio Pictórico ha permitido la caracterización tanto de pinturas rupestres, realizadas con técnicas sencillas y materiales naturales (i.e. tierras ocres, negro de carbón, etc.), como la caracterización completa de obras pictóricas mucho más complejas tales como pinturas al óleo o al fresco (Fig.1.1) (Hall et al., 2007; Cardell et al., 2009; Monico et al., 2011).

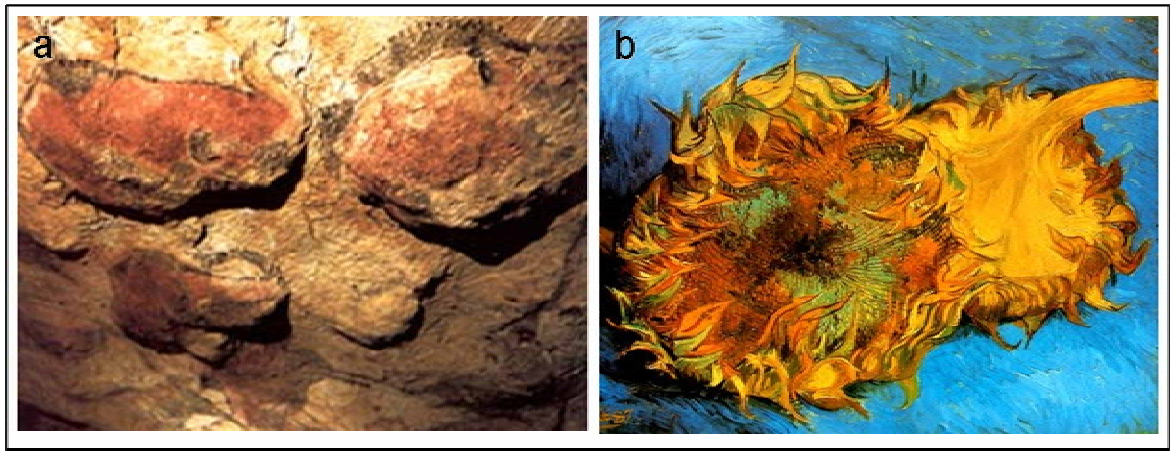

Figura 1.1. Ejemplos de obras de arte pictóricas a lo largo de la Historia: a) Pinturas rupestres de Altamira (Paleolítico Superior, 15.000–12.000 a.C) realizadas con pigmentos tierra y carbón vegetal; b) Pintura al óleo de V. Van Gogh (1853-1890) ejecutada con amarillo de cromo sobre fondo azul de Prusia (Monico et al., 2011).

Por otra parte, en los últimos años, una línea de investigación en auge es aquella dedicada al estudio del deterioro de materiales pictóricos históricos

expuestos a diferentes agentes de alteración (Tabla 1.1). La respuesta de una obra pictórica a tales agentes de deterioro debe ser estudiada en detalle, ya que provocan alteraciones físicas, químicas y/o mineralógicas, que repercuten profundamente en el estado de conservación de la obra (Maravelaki-Kalaitzaki, 2005; Cotte et al., 2006; Kotulanová et al, 2009; Moussa et al., 2009). De igual manera, se necesita conocer la repercusión de los diferentes tratamientos y metodologías de intervención (e.g. limpieza) en obras pictóricas, para evaluar su efecto a largo plazo (Gaetani y Santamaria, 2000). A este respecto, los principios de la *Conservación Preventiva* están orientados a propiciar unas condiciones ambientales favorables de almacenaje, transporte y exposición de las obras pictóricas, que reduzcan al máximo su degradación, y eviten tratamientos curativos innecesarios (Art. 4 de ICOMOS-UNESCO, 2003).

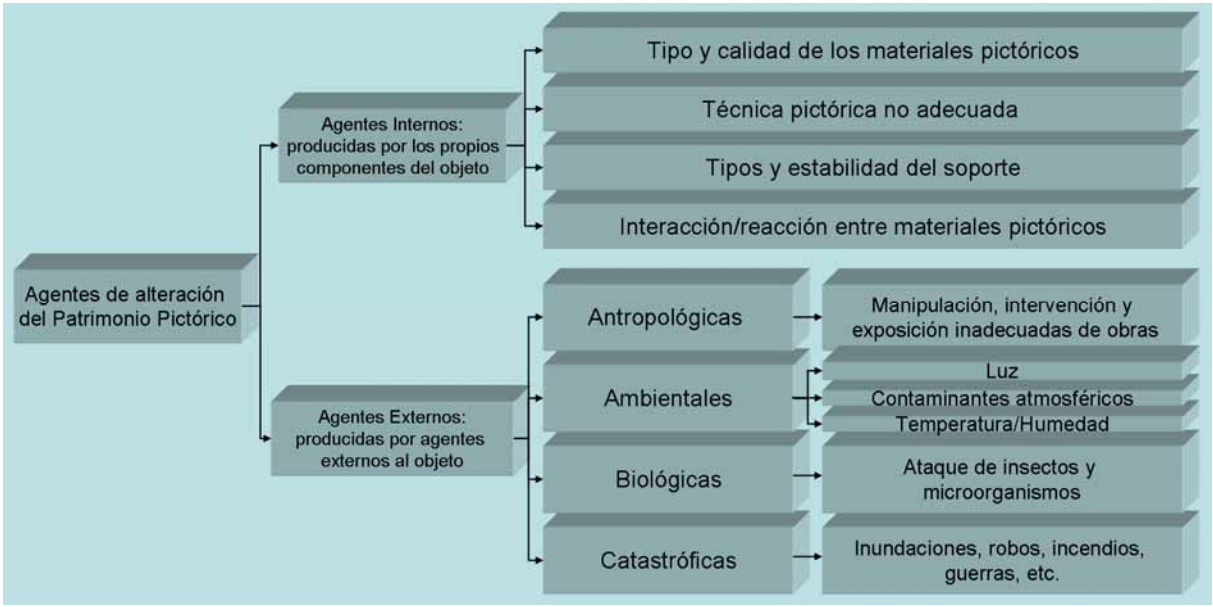

Tabla 1.1. Resumen de agentes de alteración del Patrimonio Pictórico.

Por otra parte, las técnicas de análisis contribuyen a la autentificación de obras pictóricas de dudoso origen, así como la detección de intervenciones históricas, que permiten poner en valor la obra pictórica (Ionescu et al., 2004). Todo ello, facilita la labor del restaurador y/o del historiador-

conservador durante los procesos de intervención o catalogación (Bianchin et al., 2007).

En este contexto científico surge en el año 2006 en Reino Unido el concepto de *Heritage Science*, anglicismo que engloba la investigación, la conservación, la interpretación y la gestión de las obras del Patrimonio Cultural e Histórico (House of Lords, 2006). Las tres estrategias básicas de *Heritage Science* son: (1) profundizar en el estudio del deterioro de los materiales histórico-artísticos; (2) mejorar su gestión para un correcto almacenaje-exposición, incluyendo estudios científicos sobre los efectos perjudiciales del cambio climático, y; (3) desarrollar tecnologías de análisis portátiles, no destructivas y económicamente accesibles (Williams, 2009). Estas tres estrategias básicas lógicamente se extrapolan al Patrimonio Pictórico, fomentándose la investigación, gestión y conservación de toda obra pictórica con valor histórico y/o artístico.

A pesar de las nuevas técnicas analíticas desarrolladas actualmente, el carácter único e histórico de las obras pictóricas hace que su caracterización no sea sencilla. Ello se debe, por una parte, a la complejidad de los materiales pictóricos a estudiar, ya sea por su naturaleza como por los procesos de envejecimiento/alteración que han sufrido. En la figura 1.2 se ejemplifican algunos efectos negativos que puede sufrir una obra pictórica, p.ej. cambios cromáticos por envejecimiento del barniz, pérdida de material pictórico por la cristalización de sales en superficie, hendidura por acto de vandalismo, o daños físicos y químicos debido al microbiodeterioro de soportes textiles. Por otro lado, hay que considerar la pequeña cantidad de muestra normalmente accesible, que hace aún más compleja y limitada su representatividad frente al conjunto de la obra pictórica. Ante estas limitaciones es recomendable el uso de técnicas de análisis no destructivas o microdestructivas, así como la combinación de técnicas tradicionales y/o avanzadas que permitan la caracterización completa de la muestra pictórica.

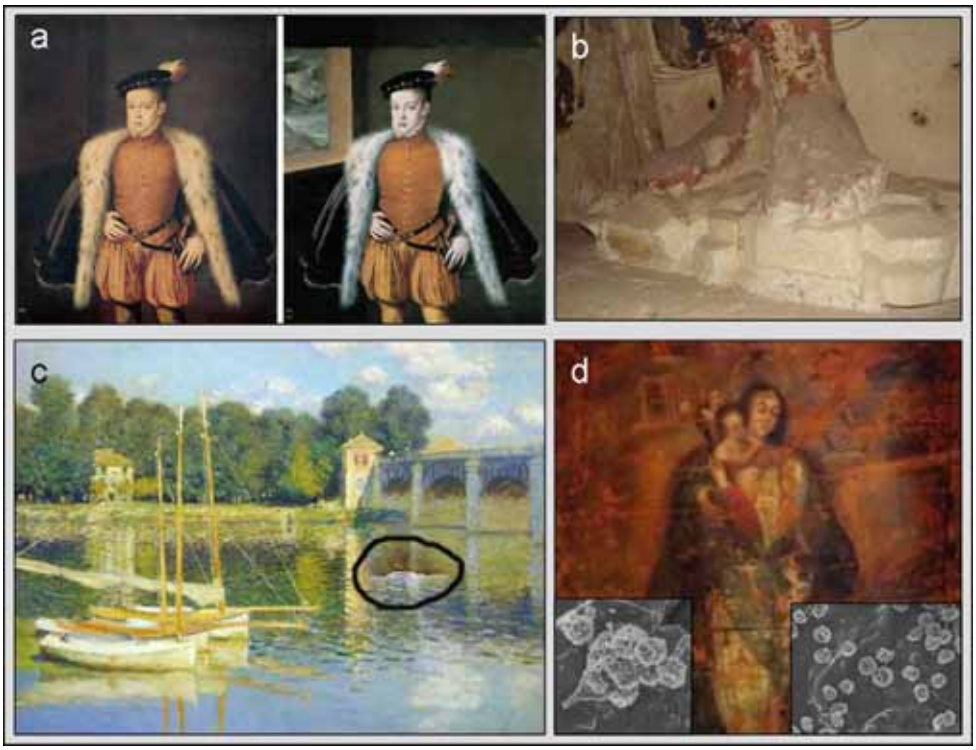

Figura 1.2. Ejemplos de alteraciones en el Patrimonio Pictórico: a) cambios cromáticos provocados por envejecimiento del barniz; lienzo al óleo de A. Sánchez Coello, "*El príncipe Don Carlos*" (1557) (www.museodelprado.es); b) pérdida de policromía por formación de sales, Iglesia de S. Jerónimo, Granada (siglo XVIII) (Tesis Doctoral Cardell, 1998); c) caso de vandalismo sobre un lienzo al óleo de C. Monet, "*Puente de Argenteuil*" (1874), (www.artespain.com); d) contaminación microbiológica por *Alternaria* (hongo) y *Bacillus Micrococcus* (bacteria) en "*Inmaculada con niño*" (Anónimo, siglo XVI-XVII) (Tesis Doctoral Poyatos, 2007).

Las llamadas técnicas de análisis tradicionales se usan de forma rutinaria en la caracterización de materiales pictóricos, aportando información imprescindible para alcanzar resultados satisfactorios en procesos de restauración e interpretación histórico-artísticos de la obra pictórica. Entre estas técnicas de análisis cabe destacar: i) las técnicas de microanálisis y microtexturales como Microscopía Electrónica de Barrido (SEM-EDS – Scanning Electrón Microscopy-Energy Dispersive X-Ray Spectroscopy) que proporciona información sobre la composición elemental e imágenes topográficas del material inorgánico (Cardell et al., 2009; Weber et al., 2009); ii) la Difracción de Rayos X (XRD – X-Ray Diffraction) que proporciona datos

de la composición mineralógica (Duran et al., 2009, 2010); iii) técnicas espectrométricas y cromatográficas que posibilitan el análisis molecular de materiales, tales como la Espectrometría Infrarroja con Transformada de Fourier (FTIR – Fourier Transform Infrared Spectroscopy) y la Cromatografía de Gases (GC-Gas Chromatography), y líquida (HPLC-High Performance Liquid Chromatography) (Gautier et al., 2007; Checa-Moreno et al., 2008; Marras et al., 2010).

En los últimos años, el uso de técnicas no destructivas y micro-destructivas en el estudio del Patrimonio Pictórico ha supuesto un avance en el estudio científico de las obras pictóricas. Estas técnicas se caracterizan por necesitar una cantidad de muestra mucho menor que otras técnicas tradicionales, debido a su alta sensibilidad analítica. Entre dichas técnicas cabe destacar la Espectrometría Infrarroja por Transformada de Fourier en modo reflectancia (DRIFTS y ATR-FTIR – Diffuse Reflectance Infrared Fourier Transform y Attenuated Total Reflectance, respectivamente) (Silva et al., 2006); la Espectroscopía Raman y su modificación técnica por acoplamiento a un microscopio óptico, i.e. la Microscopía Raman (RM – Raman Microscopy) (Burgio et al., 2001; Vandenabeele et al., 2000, 2007; Castro et al, 2008; Appolonia et al., 2009); la Espectrometría de Masas de Desorción/Ionización Láser Asistida por Matriz con Detector de Tiempo de Vuelo (MALDI-TOF MS – Matrix Assisted Laser Desorption Ionisation Time of Flight Mass Spectrometry) (Hynek et al., 2004; Kuckova et al., 2005, 2007) y la Micro-difracción de Rayos X (μ-XRD – Micro X-Ray Diffraction) (Herrera y Videla, 2009; Kotulanová et al., 2009; Schmidt et al, 2009). Todas estas técnicas analíticas se han empleado en esta Tesis Doctoral para caracterizar muestras pictóricas tanto réplicas (elaboradas en laboratorio) así como muestras reales.

Otras técnicas analíticas de interés son la Microscopía Electrónica de Transmisión (TEM – High Resolution Transmission Electron Microscopy) (Fig. 1.3) (Polette-Niewold et al., 2007), la Difracción de Rayos X con

incidencia rasante (GIXRD – Grazing Incidente X-Ray Diffraction) (Bueno et al., 2006; Duran et al., 2008) y otras técnicas de análisis basadas en el uso de radiación Sincrotrón (Van der Snickt et al., 2009; Duran et al., 2010; Monico et al., 2011), las cuales se tiene previsto utilizar en un futuro dentro de esta línea de investigación (Capítulo 12).

Por otra parte, una tendencia en los últimos años en este campo de investigación es la caracterización de obras pictóricas mediante metodologías basadas en el uso conjunto de varias técnicas de análisis (Correia et al., 2008; Appolonia et al., 2009; Osticioli et al., 2009). Además, en los últimos años está en auge el uso de técnicas de análisis multivariantes de datos para la extracción de información relevante en el estudio de obras pictóricas (Trafela et al., 2007; Rosi et al., 2009).

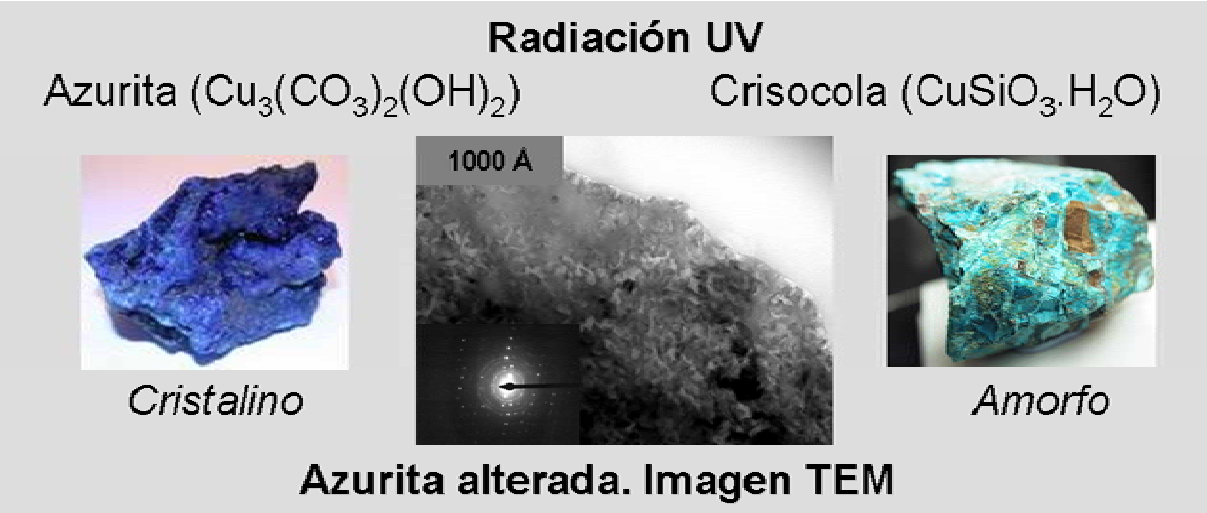

Figura 1.3. Ejemplo de alteración mineralógica detectada por TEM. Se observa la transformación de la azurita (material cristalino) a crisocola (material amorfo) en los borde del grano mineral debido al impacto de la radiación UV. (Investigación en desarrollo de la autora).

A este respecto, las técnicas de análisis multivariantes son una herramienta extremadamente útil que permite sintetizar la información obtenida a partir de técnicas de análisis. Este campo de investigación surge de la necesidad de extraer la máxima y más correcta información posible de un gran volumen

de datos analíticos obtenidos de las obras pictóricas. En los últimos años, el número de referencias sobre metodologías de estudio de materiales pictóricos que han aplicado técnicas de análisis multivariante ha aumentado considerablemente. En particular, aquellas relacionadas con el Análisis de las Componentes Principales (PCA – Principal Component Analysis; Musumarra y Fichera, 1998).

1.2. Quimiometría. Aplicación al Patrimonio Cultural y Pictórico

La Quimiometría es una disciplina química que hace uso de diferentes herramientas matemáticas y estadísticas para el análisis e interpretación de datos analíticos. Aunque inicialmente surgió como una ciencia al servicio de la Química Analítica, en los últimos años su aplicación se ha extendido a muchas otras disciplinas (Einax, 2008). Su ventaja reside en la capacidad para, por ejemplo, diseñar procesos óptimos de medida en experimentos complejos, aplicar técnicas de agrupamiento o *clustering*, seguimiento de parámetros ambientales, etc., y para extraer la máxima información analítica posible a partir de un gran número de datos experimentales.

Entre las técnicas quimiométricas más usadas se encuentran las técnicas multivariantes, las cuales permiten analizar simultáneamente un gran número de variables como por ejemplo, los datos espectrales obtenidos a partir de técnicas espectrométricas. Un ejemplo de variables multivariantes es un espectro de infrarrojos (IR), donde se representa datos para un intervalo de longitudes de onda de la región del infrarrojo.

Una de las técnicas multivariantes más ampliamente usada en el Patrimonio Cultural es el Análisis de las Componentes Principales (PCA). Esta técnica permite sintetizar un gran conjunto de datos, crear estructuras de interdependencia entre variables cuantitativas y crear unas nuevas variables

que son función lineal de las originales y que pueden representarse gráficamente (Métodos de Proyección) (Wold et al., 1987; Ericsson et al., 2006). Utilizando como ejemplo los espectros FTIR, el PCA permite analizar una matriz de datos con tantas columnas como espectros de muestras analizadas (K muestras), y tantas filas como amplio sea el intervalo de longitudes de onda del espectro de IR y su precisión espectral (N observaciones) (Fig. 1.4). El PCA genera nuevas variables, llamadas Componentes Principales (*Principal Components*, PCs) que son más fácilmente interpretables y que contienen la información espectral más relevante del sistema estudiado.

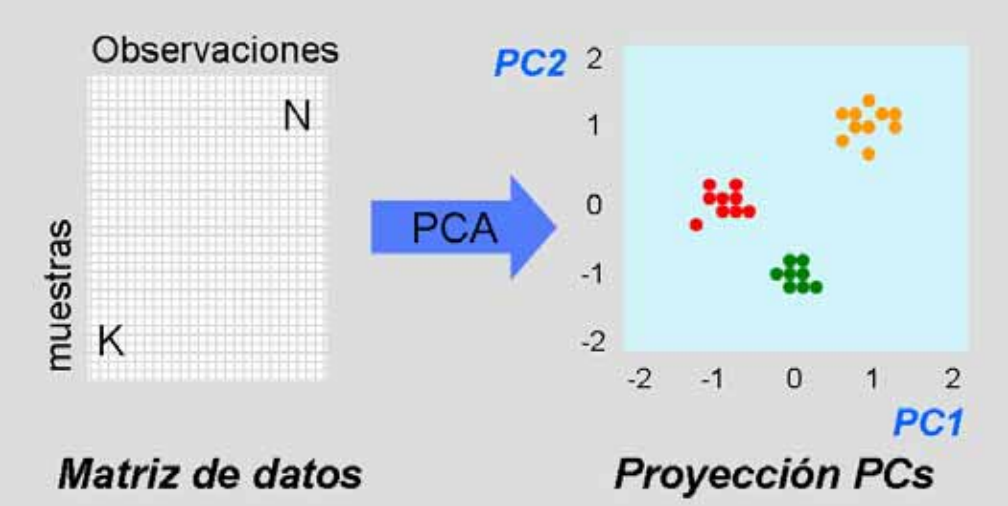

Figura 1.4. Esquema simplificado del Análisis en Componentes Principales (PCA). La matriz de datos formada por K muestras y N observaciones da lugar a nuevas variables (Componentes Principales, PCs) que pueden representarse gráficamente (ver capítulo 3).

En general, la aplicación de la Quimiometría al campo del Patrimonio Cultural se ha extendido ampliamente en las dos últimas décadas. De hecho, son numerosas las referencias a metodologías analíticas que hacen uso de técnicas multivariantes en el estudio de materiales característicos del Patrimonio Cultural e Histórico. Según la revisión bibliográfica de Musumarra y Fichera (1998), el uso de la Quimiometría en el campo del Patrimonio Cultural a finales de la década de los noventa se centraban en la clasificación y estudios de procedencia de materiales arqueológicos, tales

como cerámicas, metales, vidrios, porcelanas y textiles (Mirti, 1990; Glinsman y Hayek, 1993; Mirti et al., 1993; Rutledge et al., 1993; Pollard y Hatcher, 1994; Yap y Hua, 1994; Swerts et al., 1994; Neff, 1994; Brodie y Steel, 1996; Castellano et al., 1996; Cork et al., 1996; Troia et al., 1996).

Por ejemplo, en estos últimos años, con el empleo de este tipo de metodologías al estudio de morteros ha permitido, correlacionar el cociente aglutinante/agregado de muestras artificiales para predecir el comportamiento de morteros reales (Rampazzi et al., 2006), o caracterizar los daños provocados por la presencia de sales de nitratos en morteros y ladrillos (Maguregui et al., 2008). En el campo de la Arqueología, las técnicas quimiométricas han permitido establecer el origen de esculturas de alabastro con canteras concretas (Castro et al., 2008). Por otro lado, el diseño de "modelos predictivos de comportamiento" ha hecho posible comparar los resultados en muestras modelo con muestras reales (Trafela et al., 2007). Desde el punto de vista de la conservación, los estudios quimiométricos de vidriados de Sainte-Chapelle de Paris han permitido la datación y distinción entre vidriados originales y modernos (Colomban et al., 2007). Por lo que respecta al uso de PCA a obras pictóricas, éste ha permitido, por ejemplo, la asignación de frescos a diferentes autores en función de la composición de sus morteros (Giuffrida et al., 1993).

Asimismo, en el estudio de materiales pictóricos, el análisis de datos mediante PCA ha permitido identificar pigmentos artificiales muy complejos en obras pictóricas contemporáneas (Rosi et al., 2010), y distinguir entre pigmentos artificiales y naturales, como el llamado ultramar (aluminosilicato sintético) y lapislázuli (pigmento mineral constituido principalmente por lazurita), respectivamente (Osticiolli et al, 2009). Además, la aplicación del PCA ha permitido identificar aglutinantes proteicos de diferente naturaleza a partir de espectros Raman (Nevin et al., 2007). Otra ventaja sustancial del uso del PCA es que facilita la interpretación de una gran cantidad de datos espectroscópicos procedentes de materiales sometidos a procesos de

envejecimiento acelerado (Bacci et al., 2001; Marengo et al., 2004, 2006; Lau et al., 2008; Manzano et al., 2009). Concretamente, este tipo de estudio es el abordado en esta Tesis Doctoral. En particular, en los capítulos 4 al 10 se presentan trabajos de investigación sobre análisis espectrométricos de muestras pictóricas de laboratorio llamadas, de aquí y en adelante, réplicas pictóricas. La aplicación de PCA a los datos espectrales ha permitido discriminar las muestras en función de su composición y reconocer procesos de alteración química o modificaciones mineralógicas de los materiales pictóricos involucrados. Más aún, el PCA ha revelado las ventajas al aplicar determinadas técnicas analíticas, y sus condiciones de trabajo más adecuadas para el estudio de los materiales pictóricos.

1.3. Materiales y técnicas pictóricas. Paletas históricas

La elección de materiales pictóricos utilizados a lo largo de la Historia para la realización de las pinturas artísticas viene determinada por las necesidades expresivas de cada cultura, el tipo de civilización y por las materias primas disponibles. Además, todo ello está condicionado por los factores climáticos y los fines a lo que se destina la obra pictórica. La elaboración tradicional de los materiales artísticos empleados en las obras pictóricas está basada en la mezcla de pigmentos con aglutinantes para la decoración de un soporte. En algunos casos, este soporte tiene un valor añadido, por ejemplo, decoración de labrados, esculturas o relieves de madera, escayola, piedra, etc., tomando el nombre de policromía.

Según la definición del diccionario de la Real Academia Española (RAE, 2001), pigmento se define como "*materia colorante que se usa en la pintura*". En sentido estricto, un pigmento artístico es una sustancia que confiere su color a otro material, ya sea por su mezcla con él o por aplicación a su superficie (Mayer, 1988). Los pigmentos se pueden dividir en inorgánicos, i.e. minerales (e.g. lapislázuli), tierras naturales (e.g. tierras verdes), tierras

tostadas (e.g. *Sienna* tostada) y artificial (e.g. azul esmalte u óxido de zinc); y orgánicos, los cuales pueden ser naturales – de origen animal (e.g. cochinilla) y vegetal (e.g. índigo) – y artificiales (e.g. rojo de alizarina) (Mayer, 1988; Calvo, 1997). Por otro lado, un aglutinante se define como "*sustancia en la que se diluyen los pigmentos para preparar barnices o pinturas*". En este sentido, los aglutinantes pueden ser inorgánicos, e.g. carbonato cálcico, y orgánicos, e.g. gomas, colas, aceites, etc. (Calvo, 1997).

La elaboración tradicional de las obras pictóricas se basa en la superposición de capas pictóricas sobre una o varias capas de preparación, normalmente de color blanco, bol rojo en caso de dorado bruñido, o verdacho (preparación verde) muy utilizada como capa de preparación de carnaciones verdosas (Matteni y Moles, 2001). En el caso de pinturas al temple y al óleo, el soporte debe tener una superficie sólida e impermeable (Mayer, 1989). En ocasiones, ésto se consigue mediante la aplicación de una capa de imprimación que produce una superficie rugosa, adecuada para la aplicación de las capas pictóricas propiamente dichas (Fig.1.5a). Además, en la pintura al óleo se aplica una capa superficial protectora de barniz (Fig.1.5b). A esta ordenación sucesiva de capas pictóricas y preparatorias se denomina estratigrafía pictórica. Una estratigrafía pictórica consta de en una superposición de capas cuyo tamaño de partícula a menudo decrece hacia la superficie.

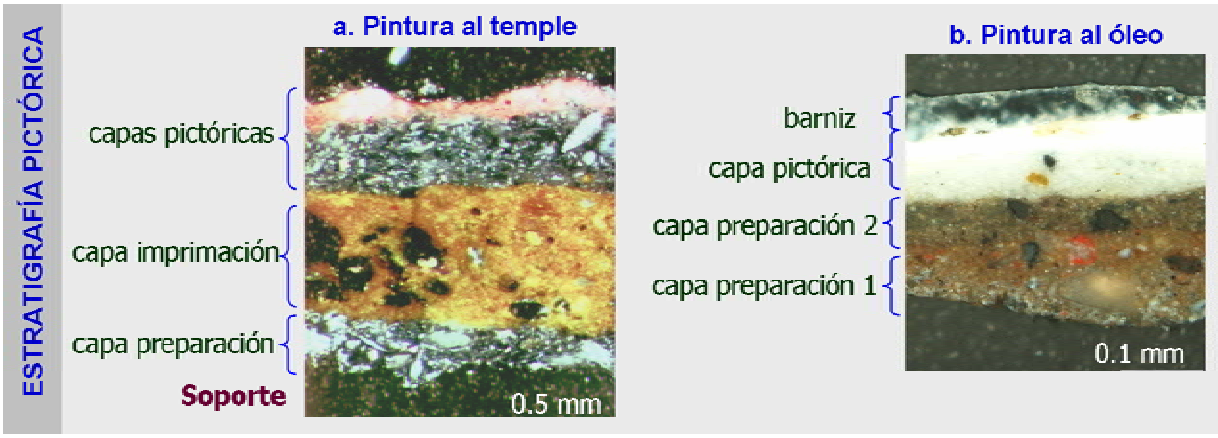

Figura 1.5. Imagen de estratigrafías pictóricas al microscopio óptico-petrográfico: a) Imagen de policromía procedente de Iglesia del Monasterio de San Jerónimo (Cardell, 1998); b) pintura al óleo sobre lienzo (Anónimo, S. XIX) (informe interno de la autora).

El uso de determinados pigmentos viene determinado por la naturaleza del aglutinante con que son mezclados y el soporte sobre el que la pintura se aplica. Así, la técnica pictórica se establece en base al aglutinante utilizado (Tabla 1.2). Entre las técnicas pictóricas más utilizadas a lo largo de la Historia destacan aquellas empleadas en la decoración pictórica integrada en una construcción, i.e. pintura mural (Calvo, 1997). Una técnica pictórica empleada en la pintura mural es la pintura al fresco (e.g. *buon fresco*). La pintura al fresco se basa en la aplicación de pigmentos disueltos en agua sobre un revoco húmedo de cal. Cuando la cal se transforma en carbonato cálcico por contacto con el CO_2 atmosférico, el pigmento queda englobado en su seno. Una variante del *buon fresco* es la técnica pictórica al *fresco secco*, que consiste en decorar con pintura al temple la argamasa de cal seca (Fig. 1.6a) (Mayer, 1988).

La pintura al temple es una técnica pictórica en la que se emplean aglutinantes proteicos de diferente naturaleza, tales como colas animales, huevo, leche o sangre, para la aplicación del pigmento (Kuckova et al., 2007). Existen otras técnicas pictóricas utilizadas principalmente en la llamada pintura de caballete; es decir, aquella pintura transportable cuyo soporte puede ser madera, lienzo o metal (Fig. 1.6 b, c) (Calvo, 1997). Entre estas

técnicas pictóricas se encuentran la técnica al óleo, la encáustica y la técnica acrílica (ésta última más extendida desde el siglo XIX), cuyos aglutinantes son respectivamente aceites secantes, ceras de abeja y polímeros sintéticos (Tabla 1.2).

TÉCNICA PICTÓRICA	AGLUTINANTE
Fresco	carbonato cálcico
Fresco seco	pintura sobre pared de cal seca
Encáustica	cera
Temple	aglutinante proteico
Óleo	aceites
Acrílica	polímeros sintéticos

Tabla 1.2. Descripción de las técnicas pictóricas en función del aglutinante usado.

Si realizamos una breve revisión del Patrimonio Pictórico a lo largo del tiempo, en la Prehistoria el hombre usó materiales pictóricos de gran sencillez en su composición, siendo habitual encontrar pigmentos naturales obtenidos de zonas geográficamente adyacentes a la obra pictórica (Fig. 1a). Éste es el caso de las pinturas de Grottes de la Garenne (Saint-Marcel, Francia) o Benquerencia de la Serena (Badajoz, España) donde los pigmentos utilizados fueron hematites (Fe_2O_3), hidróxidos de hierro, carbón vegetal y negro de manganeso mezclados con silicatos como cuarzo (SiO_2), caolinita ($Al_2(OH)_4[Si_2O_5]$), feldespatos ($KAlSi_3O_8$) y/o gehlenita ($Ca_2Al(AlSi)O_7$) (Prieto et al., 2000; Jezequel et al., 2011). Los aglutinantes orgánicos identificados eran también materiales que tenían al alcance, tales como sangre, orina o leche (Calvo, 1997).

En el Antiguo Egipto (3150 – 31 a. C.) predominan las pinturas murales realizadas al temple. Los pigmentos inorgánicos eran disueltos en agua y aglutinados con cola, goma y huevo, aplicándose en zonas concretas y sin mezclar colores (Mayer, 1988). Además, los egipcios emplearon pigmentos naturales y sintéticos, cuya naturaleza y manufactura ha permitido construir un esquema cronológico preciso, distinguiendo, por otra parte, su origen local o importado (El Goresy, 2000, Cardell, 2008). Entre los pigmentos blancos más utilizados en este periodo se encuentran el yeso ($CaSO_4.2H_2O$) o la anhidrita ($CaSO_4$), la calcita ($CaCO_3$) y la huntita ($Mg_3Ca(CO_3)_4$) (Tabla 1.3). Los pigmentos amarillos más utilizados fueron variantes de óxidos y oxi-hidróxidos de hierro como la goetita (FeO(OH)) y la lepidocrocita (γ-FeOOH), así como el oropimente (As_2S_3) (Uda et al., 2000). Como pigmento naranja utilizaron el rejalgar (As_4S_4) y como pigmento rojo hematites. Entre los pigmentos negros se han identificado negro carbón, procedente de la calcinación de madera o huesos de animal, y negro humo (El Goresy, 2000; Eastaugh et al., 2004; Cardell, 2008). Los pigmentos azules y verdes fueron mayoritariamente pigmentos sintéticos elaborados a partir de la Dinastía IV (2630 a.C. – 2500 a.C.). Existe un conocimiento profundo de su fabricación y aplicación, el cual puede usarse como patrón cronológico de la ejecución de las pinturas murales (Uda et al., 2000). En primer lugar se elaboró y utilizó como pigmento azul un vidrio rico en cobre y posteriormente un vidrio verde con hierro y potasio. Seguidamente, se empleó el azul egipcio y más tarde una variedad verdosa de la wollastonita. Por último, se hizo uso del pigmento azul amarna que corresponde a una espinela rica en cobre (El Goresy, 2000). Por otra parte, las investigaciones sobre el contenido orgánico de las pinturas egipcias han revelado la presencia de aglutinantes orgánicos, tales como colas animales y ceras de abeja, además de materiales resinosos usados como barniz (Chiviari et al., 1995).

La cultura griega (1100 –146 a.C.) contribuyó con nuevos pigmentos como el blanco de plomo artificial (cerusita, $PbCO_3$), ya comentado por Vitruvio

(arquitecto, escritor e ingeniero romano) en el siglo I a.C., el minio (Pb_3O_4) y el litargirio (γ-PbO), además de usar algunos de los pigmentos de épocas históricas anteriores (Perrault, 1761; Eastaugh et al., 2004) (Tabla 1.3). Por otra parte, introdujeron nuevas técnicas pictóricas como la pintura al fresco (prácticamente idéntico al *buon fresco* italiano del Renacimiento), y la pintura encáustica (Miliani et al., 2010). Los mejores ejemplos de pinturas murales al fresco de este periodo son los del Palacio de Cnossos (1600 a.C) pintados con tierras naturales como ocre amarillo (óxidos e hidróxidos de hierro), hematites y negro mineral (grafito), entre otros (Tabla 1.3), encontrándose junto a estas pinturas otras al fresco *secco* (Fig. 1.6a) (Mayer, 1988). Ya Vitruvio recomendaba la preparación de la pintura mural con siete capas de mortero: la primera (*trusilación*) para enrasar las paredes; a continuación tres capas de cal y arena, y tres de estuco (*intocado*) para la decoración romana (Perrault, 1761; Rallo, 2003). Los romanos usaron los pigmentos egipcios y griegos pero aportaron otros como el púrpura Murex (también llamado púrpura Tyrian), que se obtenía a partir de las glándulas del molusco del género del mismo nombre (Mazzocchin et al., 2004; Barnett et al., 2006). Además, los romanos explotaron las minas de Almadén (Ciudad Real, España) para la extracción de cinabrio (HgS) (siglo IV a.C.) (Mactaggard, 1990; Easteaugh, 2004).

En la Edad Media Cristiana (siglos V al XV d.C) surgieron una gran cantidad de estilos artísticos (prerrománicos, románicos y góticos) influenciados por la situación religiosa y económica pero también por la situación política y cultural. En particular, en la Península Ibérica surgieron diferentes estilos islámicos (siglos del VIII al XV) derivados de la ocupación musulmana. Los estilos cristianos se basaron principalmente de la técnica al fresco *secco* empleando temples de vivos colores y gran expresividad mediante el uso de algunos pigmentos como bermellón, tierras de diferentes tonos de rojos y ocres (Rallo, 2003) (Tabla 1.3). Por lo que respecta al estilo islámico, en concreto, el arte pictórico Nazarí (1238–1492) alcanzó su punto culminante con las policromías de la Alhambra de Granada, España (Cardell-Fernández

y Navarrete-Aguilera, 2006; Cardell et al., 2009). En los Palacios Nazaríes de la Alhambra se han identificado como pigmento naranja, el minio; pigmentos rojos como el bermellón, minio y hematites; pigmentos azules como el lapislázuli y la azurita; verdes de malaquita; oro y estaño como colores metálicos; así como negros de carbón, negro de hueso y negro vegetal (Cardell et al., 2004) (Tabla 1.3).

El Renacimiento (siglos XV y XVI) se caracterizó por la aplicación de pinturas murales al fresco *secco* decoradas con temples al huevo, y la introducción de las primeras pinturas al óleo aglutinadas con aceites de linaza y nuez principalmente (Fig. 1.6b) (Mayer, 1988). A partir de 1400 se intensifican los intercambios comerciales con Oriente, con el consiguiente aumento de materiales pictóricos disponibles (Tabla 1.3). A partir del siglo XVII, comenzó a decaer el uso de la técnica al temple, siendo sustituida por la pintura al óleo. Este hecho se debió al profundo conocimiento tecnológico de los aceites y su mayor estabilidad a ciertos ambientes, lo que favoreció su aplicación tanto en imprimaciones, como en capas pictóricas en pintura de caballete (Mayer, 1988). En el Renacimiento aparecen pigmentos como el esmalte, que es un vidrio de cobalto. Este pigmento azul artificial sustituyó a la azurita y el lapislázuli por su menor valor económico y mayor estabilidad química (Eastaugh et al., 2004).

El siglo XVIII en Europa, se caracterizó por la aparición de pigmentos artificiales a base de cianuros como el azul de Prusia ($Fe_4[Fe(CN)_6]_3$) o cromatos como el verde Brunswick, elaborado con la mezcla de azul de Prusia, amarillo de cromo ($PbCrO_3$) y barita ($BaSO_4$) (Eastaugh et al., 2004). Además, destacan los colores Marte, cuya composición la forman óxidos de hierro de tonalidades variables entre rojo y negro, en función del ambiente de oxidación y la temperatura de síntesis (Eastaugh et al., 2004; Barnett et al., 2006). En los siglos XIX y XX predominó la elaboración de pigmentos sintéticos de origen orgánico, como los derivados naftalenos (añil tioíndigo o el rojo de naftol, Pedrola, 1998). También en este momento se elaboraron

pigmentos de cromo (verdes de hidróxidos y óxidos de cromo) y blancos como el Litopón (mezcla de ZnS y $BaSO_4$) o blanco de zinc (ZnO), los cuales reemplazaron al blanco de plomo (Eastaugh et al., 2004). La sustitución de los pigmentos tradicionales por otros más modernos ha sido una práctica muy habitual durante toda la Historia. Este hecho se ha visto impulsado por la necesidad de emplear pigmentos más baratos, más estables a las técnicas pictóricas de moda, y de menor riesgo para la salud del artista. Entre los pigmentos tradicionales sustituidos por su toxicidad pueden mencionarse el cinabrio, el blanco de plomo o el verde Veronés ($Cu(C_2H_3O_2)_2.3Cu(AsO_2)_2$, entre otros (Mayer, 1988; Pedrola, 1998; Barnett et al., 2006) (Tabla 1.3).

Esta Tesis Doctoral se ha centrado en el estudio de temples proteicos de pigmentos tradicionales. La escasez de información biográfica existente sobre la caracterización de temples proteicos, sus procesos de alteración debido al medio ambiente al que están expuestos, los productos de degradación resultantes y las reacciones de interacción entre los pigmentos inorgánicos y el aglutinante han motivado que sea esta técnica pictórica la investigada en esta Tesis Doctoral (Odlyha et al., 2000).

Tradicionalmente, los temples proteicos se han clasificado como magros (aquellos realizados a partir de material proteico como colas animales) y grasos (aquellos materiales naturales que contienen tanto proteínas como aceites en su composición, i.e. yema de huevo) (Mayer, 1988). Para el desarrollo de esta Tesis Doctoral se han elaborado réplicas pictóricas de laboratorio a partir de materiales pictóricos tradicionales. En particular, los aglutinantes proteicos seleccionados han sido: cola animal, albúmina y yema de huevo, a los que se han añadido pigmentos y cargas históricos como son la azurita, lapislázuli, azul esmalte, cinabrio, minio, Sienna natural, blanco de plomo, yeso, calcita y cuarzo. La descripción completa acerca de la elaboración de las réplicas pictóricas se detalla en el capítulo 3 “Materiales y Métodos” de esta Tesis Doctoral.

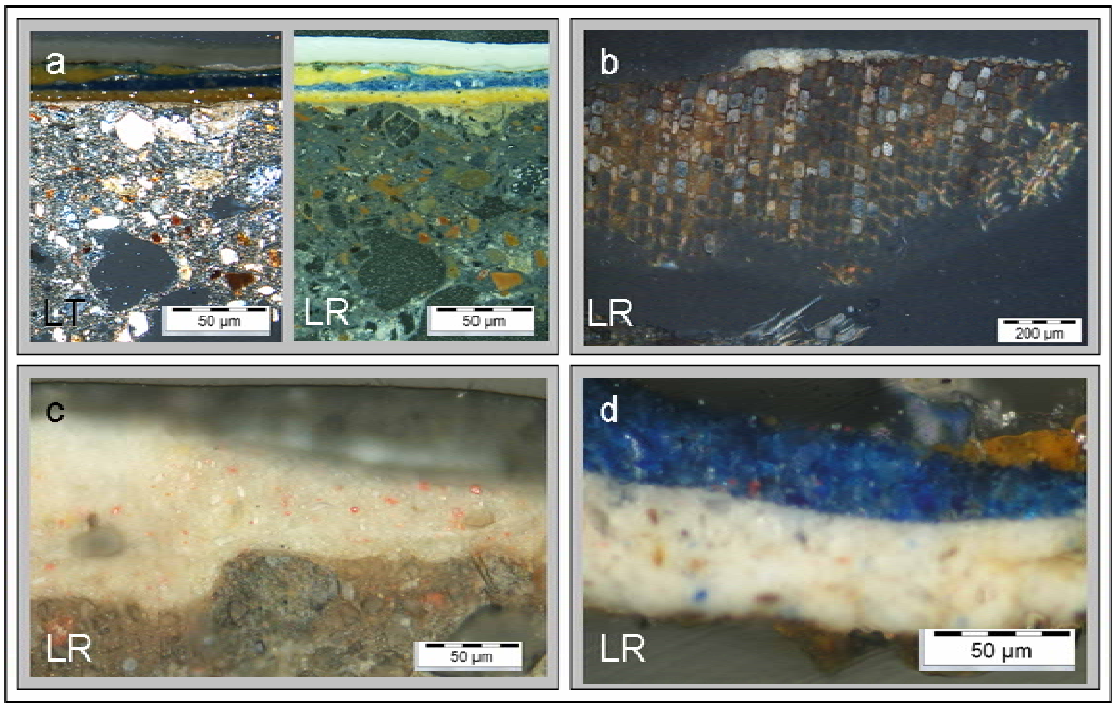

Figura 1.6. Imágenes de microscopía óptica-petrográfica de estratigrafías pictóricas: a) pintura mural al *fresco secco*, Villacarrillo, Jaén (siglo XVII); b) pintura al óleo sobre artesonado de madera, Palacio de la Madraza (Granada) (siglo XVIII); c) pintura al óleo sobre lienzo (Anónimo, siglo XIX) (Imágenes a,b,c de informes internos de la autora); y d) policromía de lapislázuli al temple sobre yesería Nazarí, Alhambra (siglo XIV) (informe interno de Dra. Cardell). Imágenes con luz transmitida (LT) y luz reflejada (LR).

Pigmentos	Blancos	Negros	Pardos	Amarillos	Rojos	Violetas	Azules	Verdes	Aglutinantes
PREHISTORIA	Cuarzo[11]	Negro de Vid[7,11] Carbón vegetal[10,11] Tierra Negra[6,10,11] Óxido de Manganeso[6,10,11] Negro de Hueso[1] Pirolusita[4,5,11]	Tierras de Sombra [6,7,10]	Limonita[7] Goetita[5,10,11] Jarosita[10]	Hematites[6,10] Ocres rojos [6,10,11] Goetita [6,10]			Tierra Verde[7] (glaucomita y celadonita)	Sangre[1] Savia[1] Óleo de plantas[1]
EGIPTO, GRECIA Y ROMA	*[5] Calcita[5,6] Anhidrita[4] Huntita[4,5] Yeso[4,5,6] Blanco de Plomo[7] Arcillas[6]	* Grafito mineral[10] Carbón orgánico[10] carbón amorfo[10] Magnetita[4] Negro de marfil[7]	* Betún de Judea[7]	* Oropimente[4,5,6] Litargio[7]	*[4,5] Realgar[7] Cinabrio[7] Bermellón[7] Minio[7] Kermes[7] Rubia[7]	Murex[3,7,11]	Azul Egipcio[4,6]	Tierra Verde[7] Verde Egipcio[4,6] Malaquita[7,8] Verdigris[9]	Colas animales[1,2,5] Gomas[2] Clara de huevo[2] Cera de abeja[1,2,5]
EDAD MEDIA (Siglo V al XV) **Pintura Cristiana y pintura Nazarí (1238-1492 d.C.)**	*[8] Blanco de hueso[8] Blanco de cáscara de huevo[1] Concha calcinada[1,7]	*	*	* Goma Gutta[7]	*		Lapislázuli[7,8] Azurita[8]	*	Colas animales[1,10] Gomas[2] Huevo (clara y yema)[2,8] Caseína[1]
RENACIMIENTO (Siglo XV al XVI)	*	*	*	* Amarillo de Nápoles[3]	*		Lapislázuli[10] Esmalte[7] Azurita[1,3,7]	*	Colas animales[2,5] Huevo[2] Aceites[1,6]
Siglo XVII	*	*	* Pardo de Van Dick[3]	*	*		Esmalte[7,6] Azurita[4,5,6]	Tierra Verde[7] Malaquita[7,8] Verdigris[9]	Colas animales[2,5] Clara de Huevo[2]
Siglo XVIII	Blanco de Zinc[3] Barita[7]	* Negro de Marte[7]	* Sepia[7] Bistre[3,7] Pardo de Marte[3,7]	* Amarillo de Marte[7,11] Amarillo de Cromo[7]	* Rojo de Marte[7]	Violeta de Marte[7]	Esmalte[7] Azul de Prusia[3,7]	Verde de Cobalto[7] Verde Veronés[7] Verdigris[7,9] Verde Brunswick[7]	Cera[2] Aceites[1,6]
Siglo XIX	Blanco de Zinc[3]		*	* Cadmio metálico[7,11] Amarillo de Zinc[7] Amarillo de Cadmio[7] Amarillo de Barita[7] Amarillo Indio[6]	* Alizarina[7]	Violeta de Cobalto[7]	Azul Ultramar[6] Azul de Prusia[7,3] Azul Cobalto[7] Azul Cerúleo[7]	Verde de Cobalto[7] Verde de Cromo (viridian)[7]	Acrílicos[1]
Siglo XX	Blanco de Titanio[7,6]	*		* Amarillo de Cromo[7] Amarillo de Barita[7]	Alizarina[7] Kermes[7]	Violeta de Cobalto[7]	Azul Cerúleo[7] Azul de Prusia[3,7]	Verde de Cobalto[7] Verde de Cromo (viridian)[7]	Acrílicos[1]

Tabla 1.3: Clasificación histórica de la aparición de pigmentos y aglutinantes en el antiguo Egipto y Europa. (1) Mayer, 1988; (2) Chiviari et al., 1995; (3) Pedrola, 1998; (4) El Goresy (2000); (5) Uda et al., 2000; (6) Hradil et al, 2003; (7) Eastaugh et al., 2004; (8a-b) Cardell et al, 2006, 2009; (9) De la Roja et al., 2007; (10) Menu, 2009; (11) Jezequel et al., 2011. (*)Se continuó usando pigmentos de etapas históricos anteriores.

1.4. Análisis de la interacción pigmento-aglutinante

Una cuestión clave en el estudio de materiales pictóricos, además de su caracterización completa de sus componentes, es el estudio de las posibles interacciones que se producen entre ellos. En particular, la interacción entre materiales pictóricos tiene un papel muy importante en el estado de conservación de la obra pictórica, en la que influye el ambiente al que está expuesta. Por ejemplo, en el caso de interacciones entre aglutinantes oleosos con pigmentos que contienen elementos metálicos, se ha constatado que algunos de estos pigmentos actúan como catalizadores de los procesos de oxidación del aceite, dando lugar a su envejecimiento prematuro o a cambios cromáticos (Colombini et al., 1999; Gimeno-Adelantado et al., 2001; Colombini et al., 2002; Plater et al., 2003; Cotte et al., 2007). Por otra parte, la interacción de algunos pigmentos, en cuya composición se encuentra el plomo, hierro, cadmio, manganeso y cobre, con los ésteres de los ácidos grasos de aceites secantes, o aquellos contenidos en la yema de huevo, produce la formación de carboxilatos metálicos, mediante procesos de saponificación. Esta interacción química provoca alteración en el poder cubriente del pigmento (Plater et al., 2003). En particular, es bien conocido como un ambiente húmedo favorece la formación de jabones de plomo por degradación de pigmentos con plomo (e.g. minio o blanco de plomo) en pinturas al óleo (Cotte et al., 2007). Por otra parte, la formación de carboxilatos de cobre juega un papel muy relevante en los reemplazamientos pseudomórficos de la azurita ($2CuCO_3.Cu(OH)_2$) por malaquita ($Cu_3(CO_3)_2(OH)_2$) en presencia de aceites secantes que conlleva un viraje de color (Mazzeo et al., 2008).

Otros estudios, en cambio, muestran los efectos positivos de la interacción pigmento-aglutinante en la estabilidad de la obra pictórica. En estos estudios se discute el papel protector del material proteico que “envuelve” al pigmento mineral y evita su fotoenvejecimiento (Price, 2000) (Fig. 1.7). Otros trabajos muestran el efecto positivo de los complejos proteicos (e.g. yema de

huevo) con pigmentos que contienen elementos metálicos. En este caso, la formación de un complejo metal-proteína retiene al ión metálico y le impide actuar como catalizador de la reacción de oxidación de material orgánico (Price, 2000; Ropret et al., 2007). También se ha demostrado que ciertos pigmentos pueden estabilizar las resinas terpénicas contenidas en barnices y aglutinantes orgánicos durante la exposición a la radiación ultravioleta (Doménech-Carbó et al., 2006). En este caso concreto, el blanco de plomo y el ocre amarillo se comportan como eficaces agentes absorbentes de la radiación UV protegiendo la resina. Sin embargo, la formación de complejos metálicos en temples proteicos o el papel de las proteínas en los mecanismos de alteración química y/o transformación mineralógica de pigmentos inorgánicos han sido menos investigados, constituyendo ambos objetivos de esta Tesis Doctoral (Vallance, 1997; Colombini et al., 1999).

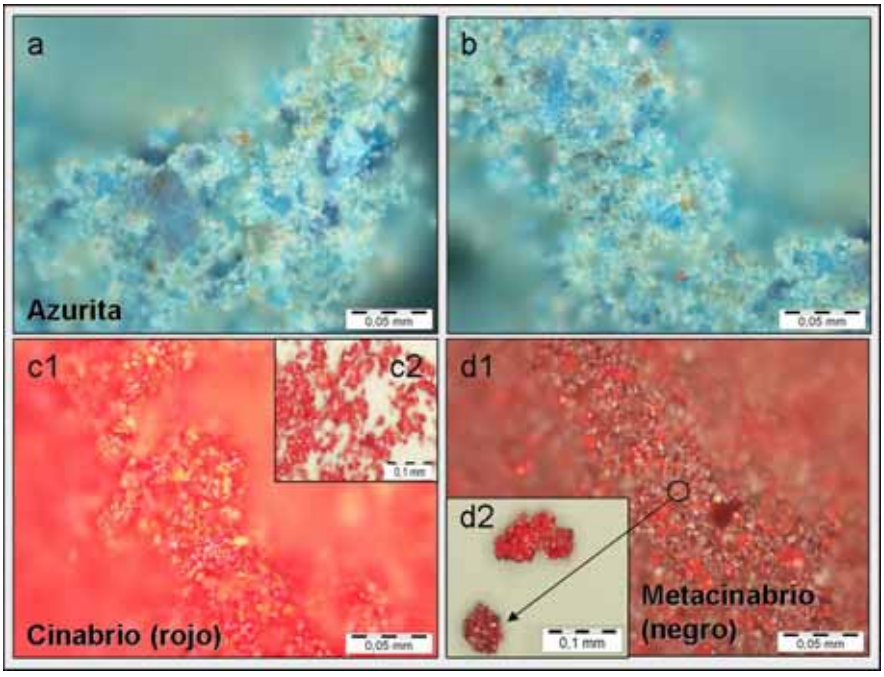

Figura 1.7. Imágenes de microscopía óptica-petrográfica con luz reflejada de temples de cola de conejo (colágeno) envejecidos con radiación UV: a) con azurita, previa exposición; b) azurita tras 2500 h de exposición. Nótese la estabilidad mineralógica del pigmento; c1) cinabrio (trigonal), previo a la exposición; c2) Imagen de detalle de cristales de cinabrio, d1) cinabrio alterado tras la exposición a 3000 h; d2) Nótese el oscurecimiento propio del metacinabrio negro (cúbico). (Informe interno de la autora).

1.5. Referencias

Appolonia L., Vaudan D., Chatel V., Aceto M., Mirti P. (2009). Combined use of FORS, XRF and Raman spectroscopy in the study of mural paintings in the Aosta Valley (Italy). Anal. Bioanal. Chem. 395, 2005–2013.

Bacci M., Fabbri M., Piccolo M., Porcinai S. (2001). Non-invasive fibre optic FTIR reflectance spectroscopy on painted layers. Identification of materials by means of PCA and Mahalanobis distance. Anal. Chim. Acta 446, 15–21.

Barnett J.R., Miller S., Pearce E. (2006). Colour and art: A brief history of pigments. Opt. Laser Technol 38, 445–453.

Bianchin S., Casellato U., Favaro M., P.A. Vigato. (2007). Painting technique and state of conservation of wall paintings at Qusayr Amra, Amman e Jordan. J. Cult. Herit. 8, 289–293.

Brodie N.J., Steel L. (1996). Cypriot black-on-red ware: towards a characterization. Archaeom. 38, 263–278.

Bueno J., Espejo T., Pérez J.L., Justo Á. (2006). Colour in the Seventeenth-Century Miniaturas of Spanish Choir Books. Restaurator, 143–161.

Burgio L., Clark R.J.H. (2001). Library of FT-Raman spectra of pigments, minerals, pigment media and varnishes, and supplement to existing library of Raman spectra of pigments with visible excitation. Spectrochim. Acta A. 57, 1491–1521.

Calvo A. (1997). Conservación y Restauración. Materiales, técnicas y procedimientos de la “A” a la “Z”. Serbal. Barcelona.

Castellano A., D’Innocenzo A., Pagliara C., Raho F. (1996). Composition and origin of Iapygian pottery from Roca Vecchia, Italy. Archaeom. 38, 59–65.

Cardell C. (1998). Tesis Doctoral: "Cristalización de sales en calcarenitas: aplicación al Monasterio De San Jerónimo, Granada". Departamento de Mineralogía y Petrología, Universidad de Granada. Granada.

Cardell-Fernández C., Navarrete-Aguilera C, y Rodríguez-Gordillo, J. (2004). Pigments in polychrome architectural and ornamental elements in The Alhambra (Granada, Spain): archaeological considerations. 34th International Symposium on Archaeometry, 176–177, Zaragoza.

Cardell-Fernández C., Navarrete-Aguilera C. (2006). Pigment and plasterwork analyses of *Nasrid* polychromed lacework stucco in the Alhambra (Granada, Spain). Stud. Conserv. 51, 161–176.

Cardell C. (2008). Examen visual y estado de conservación de la decoracion arquitectónica interna de la tumba QH33 de Qubbet El-Hawa Asuán. BAEDE, 18, 7–19.

Cardell C., Rodríguez-Simón L., Guerra I., Sánchez-Navas A. (2009). Analysis of Nasrid polychrome carpentry at the hall of the Mexuar palace, Alhambra complex (Granada, Spain) combining microscopic, chromatographic and spectroscopic methods. Archaeom. 51, 637–657.

Castro K., Sarmiento A., Maguregui M., Martínez-Arkarazo I., Etxebarria N., Angulo M., Barrutia M.U., Gonzalez-Cembellín J.M., Madariaga J.M. (2008). Multianalytical approach to the analysis of English polychromed alabaster sculptures: μ-Raman, μ-EDXRF, and FTIR spectroscopies. Anal. Bioanal. Chem. 392, 755–763.

Checa-Moreno R., Manzano E., Mirón G., Capitan-Vallvey L.F. (2008). Comparison between traditional strategies and classification technique (SIMCA) in the identification of old proteinaceous binders. Talanta, 75, 697–704

Chiavari G., Fabbri D., Galletti G. C., Mazzeo R. (1995). Use of analytical pyrolysis to characterize Egyptian painting layers. Chromatographia 40, 594–600.

Colomban P., Tournie A. (2007). On-site Raman identification and dating of ancient/modern stained glasses at the Sainte-Chapelle, Paris. J. Cult. Herit. 8, 242–256.

Colombini M.P., Modugno F., Giacomelli, A. (1999). Two procedures for suppressing interference from inorganic pigments in the analysis by gas chromatography-mass spectrometry of proteinaceous binders in paintings. J. Chromatogr. A. 846, 101–111.

Colombini M. P., Modugno F., Fuoco R., Tognazzi A. (2002). A GC-MS study on the deterioration of lipidic paint binders. Microchem. J. 73, 175–185.

Cotte M., Susini J., Metrich N., Moscato A., Gratziu C., Bertagnini A., Pagano M. (2006). Blackening of Pompeian cinnabar paintings: X-ray microspectroscopy analysis. Anal. Chem. 78, 7484–7492.

Cotte M., Checroun E., Susini J., Walter P. (2007). Micro-analytical study of interactions between oil and lead compounds in paintings. Appl. Phys. A 89, 841–848.

Correia A. M., Oliveira M. J. V., Clark R. J. H., Ribeiro M. I., Duarte M. L. (2008). Characterization of Pousa o Pigments and Extenders by Micro-X-ray Diffractometry and Infrared and Raman Microspectroscopy. Anal. Chem. 80, 1482-1492.

Cork C.R., Cooke W.D., Wild J.P. (1996). The use of image analysis to determine yarn twist level in archaeological textiles. Archaeom. 38, 337–345.

De la Roja J. M., San Andrés M., Sancho N., Santos-Gómez S. (2007). Variations in the Colorimetric Characteristics of Verdigris Pictorial Films

Depending on the Process Used to Produce the Pigment and the Type of Binding Agent Used in Applying It. Color Res. Appl. 32, 414–424.

Doménech-Carbó M.T., Kuckova S., de la Cruz-Cañizares J., Osete-Cortina L. (2006). Study of the influencing effect of pigments on the photoageing of terpenoid resins used as pictorial media. J. Chromatogr. A 1121, 248–258.

Duran A., Herrera L.K., Jiménez de Haro M.C., Justo A., Pérez-Rodríguez J.L. (2008). Non-destructive analysis of cultural heritage artefacts from Andalucía, Spain, by X-ray difraction with Gobel mirrors. Talanta 76, 183–188.

Duran A., Perez-Rodriguez J. L., Espejo T., Franquelo M. L., Castaing J, Walter P. (2009). Characterization of illuminated manuscripts by laboratory-made portable XRD and micro-XRD systems, Anal. Bioanal. Chem. 395, 1997–2004.

Duran A., Castaing J., Walter P. (2010). X-ray diffraction studies of Pompeian wall paintings using synchrotron radiation and dedicated laboratory made systems. Appl. Phys. A 99, 333–340.

Eastaugh N., Walsh V., Chaplin T., Siddall R. (2004). Pigment Compendium: A Dictionary of Historical Pigments. Butterworth-Heinemann, Oxford.

Einax J.W. (2008). Chemometrics in analytical chemistry. Anal. Bioanal. Chem. 390, 1225–1226.

El Goresy, A. (2000). Polychromatic Wall Painting Decorations in Monuments of Pharaonic Egypt: Compositions, Chronology and Painting Technique. Ed. S. Sherratt, Petros M. Nomikos and The Thera Foundation, Athens, Greece. Proceedings of the First International Symposium: The wall paintings of Thera, vol. I, 49–70.

Ericsson L., Johansson E., Kettaneh-Wold N., Trygg J., Wikström C., Wold S. (2006). Multi- and Megavariate Data Analysis. Part I. Basic Principles and Applicacions. Umetrics. Umea.

Ferreti M. (1993). Scientific Investigation of Works of Art. ICCROM. International Centre for the Study of the Preservation and the Restoration of Cultural Property. Rome.

Gaetani M.C. y Santamaria U. (2000). The laser cleaning of wall paintings. J. Cult Herit. 1, 199–207.

Gautier G., Colombini M.P. (2007). GC-MS identification of proteins in wall painting samples: A fast clean-up procedure to remove copper-based pigment interferences. Talanta 73, 95–102.

Gimeno-Adelantado J.V., Mateo-Castro R., Doménech-Carbo M.T., Bosch-Reig F., Doménech-Carbó A., Casas-Catalán M.J., Osete-Cortina L. (2001). Identification of lipid binders in paintings by gas chromatography. Influence of the pigments. J. Chromatogr. A 922, 385–390.

Giuffrida R., Matteini M., Musumarra G., Rizzi M. (1993). Multivariate characterization of mortars in wall paintings by physicochemical analysis. J. Cult Herit. 2, 99–114.

Glinsman L.A., Hayek L.C. (1993). A multivariate analysis of Renaissance portrait medals: an expanded nomenclature for defining alloy composition. Archaeom. 35, 49–67.

Hall K., Meiklejohn I., Arocena J. (2007). The thermal responses of rock art pigments: Implications for rock art weathering in southern Africa. Geomorph. 91, 132–145.

Herrera L.K., Videla H.A. (2009). Surface analysis and materials characterization for the study of biodeterioration and weathering effects on cultural property. Int. Biodeter. Biodegr. 63, 813–822.

House of Lords (2006). Science and Technology Comité. Science and Heritage. 9th Report of Session 2005/06. London.

Hynek R., Kuckova S., Hradilova J. (2004). Matrix-assisted laser desorption/ionization time-of-flight mass spectrometry as a tool for fast identification of protein binders in color layers of paintings. Rapid Commun., Mass Spectrom. 18, 189–190.

Hradil D., Grygara T., Hradilova J., Bezdicka P. (2003). Clay and iron oxide pigments in the history of painting. Appl. Clay Sci. 22, 223– 236**.**

ICOMOS-UNESCO (2003). Principios para la Preservación, Conservación y Restauración de Pinturas Murales. Ratificados por la 14ª Asamblea General del ICOMOS-UNESCO. Zimbabwe.

Ionescu O. H., Mohanua D., Stoica A. I., Baiulescu G. E. (2004). Analytical contributions to the evaluation of painting authenticity from Princely church of Curtea de Arges. Talanta 63, 815–823.

Jezequel P., Wille G., Beny C., Delorme F., Jean-Prost V., Cottier R., Breton J., Dure F., Despriee J. (2011). Characterization and origin of black and red Magdalenian pigments from Grottes de la Garenne (Vallée moyenne de la Creuse-France): a mineralogical and geochemical approach of the study of prehistorical paintings. J. Archaeol. Sci., 38, 1165–1172.

Kotulanová E., Bezdicka P., Hradil D., Hradilová J., Svarcová S., Grygar T. (2009). Degradation of lead-based pigments by salt solutions. J. Cult Herit. 10, 367–378.

Kuckova S., Nemec I., Hynek R., Hradilova J., Grygar T. (2005). Analysis of organic colouring and binding components in colour layer of art works. Anal. Bioanal. Chem. 382, 275–282.

Kuckova S., Hynek R., Kodicek M. (2007). Identification of proteinaceous binders used in artworks by MALDI-TOF mass spectrometry. Anal Bioanal. Chem. 388, 201–206.

Lau D., Kappen P., Strohschnieder M., Brack N., Pigram P. J. (2008). Characterization of green copper phase pigments in Egyptian artifacts with X-ray absorption spectroscopy and principal components analysis. Spectrochim. Acta B 63, 1283–1289.

Mactaggard P., Mactaggard A. (1990). A Pigment Microscopist's Notebook. 5th Revision. Mac & Me Ltd., Welwyn, Herts.

Maguregui M., Sarmiento A., Martínez-Arkarazo I., Angulo M., Castro K., Arana G., Etxebarria N., Madariaga J.M. (2008). Analytical diagnosis methodology to evaluate nitrate impact on historical building materials. Anal. Bioanal. Chem. 391, 1361–1370.

Manzano E., Navas N., Checa-Moreno R., Rodriguez-Simón L., Capitán-Vallvey L.F. (2009). Preliminary study of UV ageing process of proteinaceous paint binder by FT-IR and principal component analysis. Talanta, 77, 1724–1731.

Manzano E., Romero-Pastor J., Navas N., Rodríguez-Simon L., Cardell C. (2010). A study of the interaction between rabbit glue binder and blue copper pigment under UV radiation: a spectroscopic and PCA approach. Vibrat. Spectrosc. 53, 260–268.

Matteni M., Moles A. (2001). La química en la restauración. Ed. Nerea. Sevilla.

Maravelaki-Kalaitzaki P. (2005). Black crusts and patinas on Pentelic marble from the Parthenon and Erechtheum (Acropolis, Athens): Characterization and origin. Anal. Chim. Acta 532, 187–198.

Mayer R. (1988). Materiales y Técnicas del Arte. Hermann Blume. Madrid.

Marengo E., Robotti E., Liparota M.C., Gennaro M.C. (2004). Monitoring of pigmented and wooden surfaces in accelerated ageing processes by FT-Raman spectroscopy and multivariate control charts. Talanta 63, 987–1002.

Marengo E., Liparota M. C., Robotti E., Bobba M. (2006). Monitoring of paintings under exposure to UV light by ATR-FT-IR. Spectroscopy and multivariate control charts. Vibrat. Spectrosc. 40, 225–234.

Marras S., Pojana, G. Ganzerla R., Marcomini A. (2010). Study and characterization of mural paintings from XIX Century in a noble Venetian (Italy) Palace. Microchem. J., 96, 397–405.

Mazzeo R., Prati S., Quaranta M., Joseph E., Kendix E., Galeotti M. (2008). Attenuated total reflection micro FTIR characterisation of pigment-binder interaction in reconstructed paint films. Anal. Bioanal. Chem. 392, 1–12.

Mazzocchin G.A., Agnoli F., Salvadori M. (2004). Analysis of Roman age wall paintings found in Pordenone, Trieste and Montegrotto. Talanta 64, 732–741.

Menu M. (2009). L'analyse de l'art préhistorique. The analysis of prehistoric art. L'anthropologie 113, 547–558.

Mirti P. (1990). Roman pottery from Augusta Praetoria Aosta, Italy.: a provenance study. Archaeom. 32, 163–175.

Mirti P., Casoli A., Appolonia L. (1993). Scientific analysis of roman glass from Augusta Praetoria. Archaeom. 35, 225–240.

Miliani C., Daveri A., Spaabaek L., Romani A., Manuali V., Sgamellotti A., B. Giovanni Brunetti. (2010). Bleaching of red lake paints in encaustic mummy portraits. Appl. Phys. A 100, 703–711.

Monico L., Van der Snickt G., Janssens K., de Nolf W., Miliani C., Dik J., Radepont M., Hendriks E., Geldof M., Cotte M. (2011). Degradation Process of Lead Chromate in Paintings by Vincent van Gogh Studied by Means of Synchrotron X-ray Spectromicroscopy and Related Methods. 2. Original Paint Layer Samples. Anal. Chem., 83, 1224–1231.

Moussa A.M.A., Kantiranis N., Voudouris K. S., Stratis J.A., Ali M.F., Christaras V. (2009). The Impact of Soluble Salts on the Deterioration of haraonic and Coptic Wall Paintings at Al Qurna, Egypt: Mineralogy and Chemistry. Archaeom. 51, 292–308.

Musumarra G., Fichera M. (1998). Chemometric and Cultural Heritage. Chemom. Intell. Lab. Syst. 44, 363–372.

Neff H. (1994). RQ-mode principal component analysis of ceramic compositional data. Archaeom. 36, 115–130.

Nevin A., Osticioli I., Anglos D., Burnstock A., Cather S., Castellucci E., (2007). Raman Spectra of Proteinaceous Materials Used in Paintings: A Multivariate Analytical Approach for Classification and Identification. Anal. Chem. 79, 6143–6151.

Odlyha M., Cohen N.S., Foster G.M., West R. (2000). Dosimetry of paintings: determination of the degree of chemical change in museum exposed test paintings (azurite tempera) by thermal and spectroscopic analysis Thermochim. Acta 365, 53–63.

Osticioli I., Mendes N. F. C., Porcinai S., Cagnini A., Castellucci E. (2009). Spectroscopic analysis of works of art using a single LIBS and pulsed Raman setup. Anal. Bioanal. Chem. 394, 1033–1041.

Pedrola A. (1998). Materiales, procedimientos y técnicas pictóricas. Ariel. Madrid.

Perrault C. (1761). Compendio de los diez libros de arquitectura de Vitruvio. Real Academia de las Ciencias de Paris. Paris.

Plater M. J., De Silva B., Gelbrich T., Hursthouse M. B., Higgitt C. L., Saunders D. R. (2003). The characterisation of lead fatty acid soaps in "protrusions" in aged traditional oil paint. Polyhedron. 22, 3171–3179.

Prieto A.C., Jiménez J., Pérez B., Leal L. (2000). Analytical techniques for characterizing polychromated coatings on quartzite samples from a prehistorical cave. Proceedings of the 9th International Congress on Deterioration and Conservation of Stone, 619–628.

Prieto A.C., Guedes A., Dória A., Noronha F. (2005). Characterization of pigments in a limestone sculpture "las tres generaciones" (Cathedral's museum of Santiago de Compostela, Spain) by optical microscopy and Micro-Raman Spectroscopy. Can. J. Anal. Sci. Spectrosc. 50, 88–96.

Price M. (2000). A Renaissance of Colour: particle separation and preparation of azurite for use in oil painting. Leonardo 33, 281–288.

Pollard A.M., Hatcher H. (1994). The chemical analysis of oriental ceramic body compositions: Part I. Wares from North China. Archaeom. 36, 41–62.

Polette-Niewold L.A., Manciu F.S., Torres B., Alvarado M., Chianelli R.R. (2007). Organic/inorganic complex pigments: Ancient colors Maya Blue. J. Inorg. Biochem. 101, 1958–1973.

Poyatos F. (2007). Tesis Doctoral: "Procesos de Microbiodeterioro en pinturas sobre lienzo del Museo de Bellas Artes de Granada: Examen visual y Gráfico". Departamento de Pintura. Universidad de Granada. Granada.

Rallo Gruss C. (2003). La pintura mural hispano-musulmana. ¿Tradición o innovación?. Al-Qantara XXIV 1, 109–137.

Rampazzi L., Pozzi A., Sansonetti A., Toniolo L., Giussani B. (2006). A chemometric approach to the characterisation of historical mortars. Cement Concrete Res. 36, 1108–1114.

Real Academia Española (RAE) (2001). Diccionario de la Lengua Española, vigésima segunda edición. Madrid.

Ropret P., Zoubek R., Sever Škapin A., Bukovec P. (2007). Effects of ageing on different binders for retouching and on some binder–pigment combinations used for restoration of wall paintings. Mater. Charact. 58, 1148–1159.

Rosi F., Burnstock A., Jan Van den Berg K., Miliani C., Giovanni B. Brunetti, Sgamellotti A. (2009). A non-invasive XRF study supported by multivariate statistical analysis and reflectance FTIR to assess the composition of modern painting materials. Spectrochim. Acta A: Mol. Biomol. Spectros., 71, 1655–1662.

Rosi F., Miliani C., Clementi C., Kahrim K., Presciutti F., Vagnini M., Manuali V., Daveri A., Cartechini L., Brunetti B.G., Sgamellotti A. (2010). An integrated spectroscopic approach for the non-invasive study of modern art materials and techniques. Appl. Phys. A 100, 613–624.

Rutledge D.N., Guesnier S., Lahanier C., Ducauze C.J. (1993). Classification of gallo–roman ceramics from the Bordeaux region by multidimensional statistical analysis of their chemical composition. Chemometr. Intell. Lab. Syst. 19, 111– 117.

Schmidt C. M., Walton M. S., Trentelman K. (2009). Characterization of Lapis Lazuli Pigments Using a Multitechnique Analytical Approach:

Implications for Identification and Geological Provenancing. Anal. Chem. 81, 8513–8518.

Silva C.E., Silva L.P., Edwards H.G.M., De Oliveira L.F.C. (2006). Diffuse reflection FTIR spectral database of dyes and pigments. Anal. Bioanal. Chem., 386, 2183– 2191.

Swerts J., Aerts A., De Biscop N., Adams F., Van Espen P. (1994). Age determination of Chinese porcelain by X-ray fluorescence and multivariate analysis. Chemometr. Intell. Lab. Syst. 22, 97–105.

Trafela T., Strlič M., Kolar J., Lichtblau D.A., Anders M., Mencigar P.D., Pihlar B. (2007). Nondestructive analysis and dating of historical paper based on IR spectroscopy and chemometric data evaluation. Anal. Chem. 79, 6319–6323.

Troia S.O., Cro A., Gueli A.M., La Rosa V., Mazzoleni P., Pezzino A., Romeo M. (1996). Characterization and thermoluminescence dating of prehistoric pottery sherds from Milena. Archaeom. 38, 113–128.

Uda M., Sassa S., Taniguchi K., Nomura S., Yoshimura S., Kondo J., Iskander N., Zaghloul B. (2000). Touch-free in situ investigation of ancient Egyptian pigments. Naturwissenschaften 87, 260–263.

Vallance S. L. (1997). Applications of Chromatography in Art Conservation: Techniques Used for the Analysis and Identification of Proteinaceous and Gum Binding Media. Analyst 122, 75–81.

Vandenabeele P., Wehling B., Moens L., Edwards H., De Reu M., Van Hooydonk G. (2000). Analysis with micro-Raman spectroscopy of natural organic binding media and varnishes used in art. Anal. Chim. Acta. 407, 261–274.

Vandenabeele P., Castro K., Hargreaves M., Moens L., Madariaga J.M., (2007). Comparative study of mobile Raman instrumentation for art analysis. Anal. Chim. Acta. 588, 108–116.

Van Der Snickt G., Dik J., Cotte M., Janssens K., Jaroszewicz, J., De Nolf W., Groenewegen J., Van Der Loeff L. (2009). Characterization of a degraded cadmium yellow (CdS) pigment in an oil painting by means of synchrotron radiation based X-ray techniques. Anal. Chem. 81, 2600–2610.

Williams J. (2009). The role of science in the management of the UK's heritage. National Heritage Science Strategy. London.

Weber J., Prochaska W., Zimmermann N. (2009). Microscopic techniques to study Roman renders and mural paintings from various sites. Mater. Charact. 60, 586–593.

Wold S., Esbensen K., Geladi P. (1987). Principal Component Analysis. Chemom. Intell. Lab. Syst. 2, 37–52.

Yap C.T., Hua Y. (1994). A study of Chinese porcelain raw materials for Ding Xing, Gongxian and Dehua wares. Archaeom. 36, 63–76.

2. Objetivos y Estructura

Este Capítulo 2 expone los objetivos planteados en esta Tesis Doctoral y la secuencia de la investigación seguida para cada trabajo.

The second Chapter "Objectives and Structure" shows the main goals of this Doctoral Thesis and the sequence of the research followed.

2. Objetivos y Estructura

2.1. Objetivos

Con el fin de profundizar en la caracterización de materiales pictóricos y sus interacciones, incluidas aquellas establecidas bajo determinadas condiciones ambientales, se han planteado los siguientes objetivos en esta Tesis Doctoral:

1) Puesta a punto de metodologías de análisis innovadoras que hagan uso de herramientas multivariantes de análisis para caracterizar los materiales pictóricos.

2) Puesta a punto de metodologías de análisis innovadoras que hagan uso de herramientas multivariantes de análisis para estudiar posibles interacciones entre componentes pictóricos de diferente naturaleza, concretamente entre componentes inorgánicos (pigmentos azules, rojos, blancos y cargas) y componentes orgánicos (e.g. aglutinantes proteicos tales como cola animal, yema de huevo y albúmina).

3) Desarrollo de metodologías analíticas que puedan ser aplicables en el estudio del proceso de envejecimiento de materiales pictóricos sometidos a diferentes condiciones ambientales mediante el empleo de muestras pictóricas de laboratorio.

4) Establecimiento de metodologías de análisis *ad hoc* de muestras pictóricas reales a partir de diversas técnicas analíticas y/o estadísticas, que maximicen la información analítica y minimicen la cantidad de muestra a estudiar y el impacto sobre la obra pictórica.

2.2. Estructura

La consecución de estos objetivos ha dado lugar a los capítulos 4 a 10 de la presente Memoria de Tesis Doctoral, que corresponden a siete trabajos de investigación ya publicados (Capítulos 4, 5, 6 y 7), aceptados y en proceso de publicación (Capítulo 10), enviados y en proceso de revisión (Capítulo 8), o enviados (Capítulo 9). Previamente en el capítulo 3 se presentan los Materiales y Métodos empleados a lo largo de todos los trabajos. Finalmente en el capítulo 11 se exponen las conclusiones generales, y en el capítulo 12, se exponen las perspectivas de trabajo futuras iniciadas con esta Tesis Doctoral. A continuación se detallan brevemente el contenido de los capítulos 4 al 12 y sus objetivos.

Capítulo 4: El objetivo concreto de este capítulo es evaluar mediante PCA la Espectrometría Infrarroja en dos modos de trabajo, i.e. transmisión (T-FTIR) y reflexión (DRIFTS), en el estudio de réplicas pictóricas. Tradicionalmente, T-FTIR ha sido el modo de empleo más extendido de la Espectroscopía de Infrarrojos. En este trabajo se pone de manifiesto una mayor idoneidad del modo T-FTIR en el estudio del material proteico presente en una muestra pictórica. Sin embargo, el empleo de DRIFTS, una novedosa técnica en el campo de del Patrimonio Pictórico, proporciona bandas de absorción mejor definidas que permiten mejorar el estudio del pigmento inorgánico.

- *Benefits of applying combined diffuse reflectance FTIR spectroscopy and principal component analysis for the study of blue tempera historical painting.* (2008). N. Navas, **J. Romero-Pastor**, E. Manzano, C. Cardell. Analytica Chimica Acta 630, 141–149.

Capítulo 5: En este capítulo el objetivo es estudiar la capacidad de la aplicación combinada de la Microscopía Raman (RM) y PCA para discriminar pigmentos históricos y sus temples de huevo. Se demuestra que la aplicación de diferentes tratamientos matemáticos a los espectros Raman, y en concreto, de la primera derivada del espectro permite discriminar réplicas

pictóricas en función de su composición específica. Asimismo, estos análisis permiten detectar procesos de alteración de ciertos pigmentos producidos durante el proceso de medida. En este trabajo se propone por primera vez el empleo de la primera derivada del espectro Raman para poder abordar a continuación el análisis multivariante de los datos espectrales en muestras pictóricas.

- *Raman spectroscopic discrimination of pigments and tempera paint model samples by principal component analysis on first-derivative spectra.* (2010). N. Navas, **J. Romero-Pastor**, E. Manzano, C. Cardell. J. Raman Spectroscopy 41, 1486–1493.

Capítulo 6: Una vez se han caracterizado los materiales pictóricos de temples de huevo en el capítulo anterior, en el capítulo 6 se estudia la interacción de dichos pigmentos inorgánicos con la estructura proteica. Mediante RM y PCA se demuestra la interacción con los componentes proteicos de pigmentos como azurita, yeso, calcita, esmalte y lapislázuli al estudiar la banda espectral de C-H de la proteína (3100-2800 cm^{-1}), región en la cual no aparece ninguna banda Raman característica de estos pigmentos. En este trabajo se propone, por tanto, una estrategia novedosa y original para el estudio y la detección de la interacción pigmento-aglutinante proteico.

- *Assessment of Raman Microscopy coupled with Principal Component Analysis to examine egg yolk-pigment interaction based on the protein C-H stretching region (3100 - 2800 cm^{-1}).* (2011). **J. Romero-Pastor**, C. Cardell, E. Manzano, Á. Yebra-Rodríguez, N. Navas. J. Raman Spectroscopy, (doi: 10.1002/jrs.2977).

Una vez realizados estos estudios sobre réplicas pictóricas sin envejecimiento previo, en los siguientes capítulos 7, 8 y 9, se recogen los trabajos de investigación basados en el proceso de alteración acelerada de

réplicas pictóricas, tanto por tratamientos térmicos como por exposición a radiación ultravioleta.

Capítulo 7: En este capítulo se aborda el estudio de réplicas pictóricas envejecidas por radiación UV, en particular, de temples proteicos de azurita. Como ya ha quedado demostrado en el capítulo 3, el uso de T-FTIR es adecuado para la caracterización de réplicas pictóricas elaboradas con pigmento inorgánico y proteína. Por ello, esta técnica espectroscópica se ha usado, junto con otras técnicas complementarias, para identificar el efecto de la radiación UV sobre los materiales pictóricos. Este trabajo pone de manifiesto la estabilidad de la azurita frente a la radiación UV, y la capacidad estabilizadora de dicho pigmento sobre el envejecimiento del material proteico.

- *A study of the interaction between rabbit glue binder and blue copper pigment under UV radiation: A spectroscopic and PCA approach*. (2010). E. Manzano, **J. Romero-Pastor**, N. Navas, L.R. Rodríguez-Simón, C. Cardell. Vibrational Spectroscopy 53, 260–268.

Capítulo 8: Este capítulo recoge el estudio del envejecimiento acelerado a baja temperatura (< 250ºC) de réplicas pictóricas. El objetivo es evaluar mediante PCA la calidad de los datos espectroscópicos obtenidos por RM y ATR-FTIR y para discriminar alteraciones químicas o modificaciones mineralógicas en los materiales pictóricos. Para ello se ha incorporado un patrón interno de naturaleza mineral a diversos medios proteicos de uso tradicional en la elaboración de temples. Este trabajo demuestra la capacidad de dichas técnicas para este propósito e identifica procesos de alteración producidos sobre el material orgánico presente en las réplicas pictóricas.

- *Internal mineral standard and PCA as tools to validate the quality of spectroscopy data of thermally aged composite materials* (2011). **J. Romero-**

Pastor, C. Cardell, A. Yebra-Rodríguez, A. B. Rodríguez- Navarro. J. European Mineralogy. (*Submitted paper, acepted for revison April 2011*).

Capítulo 9: En este trabajo se estudia el fotoenvejecimiento de la cola de conejo y sus temples (azurita y cinabrio) por radiación UV proponiéndose a su vez una metodología novedosa que combina el análisis multivariante (i.e. PCA) de los espectros de masas (mapas peptídicos resultado de la digestión con tripsina) registrados por MALDI-TOF MS y el estudio de la estructura secundaria del colágeno de la cola mediante T-FTIR. Se estudia así la interacción de dos pigmentos inorgánicos (azurita y cinabrio) con el material proteico y su efecto sobre el envejecimiento. La metodología utilizada facilita la interpretación del proceso de envejecimiento de las réplicas pictóricas de cola de conejo, tanto pura como en presencia de pigmento. Los resultados obtenidos sugieren diferentes formas de interacción pigmento-aglutinante y de fotoenvejecimiento de la cola de conejo para cada réplica pictórica estudiada.

- *Pigment-proteinaceous binder interaction study under UV ageing conditions by MALDI-TOF-MS and Principal Component Analysis* (2011). **J. Romero-Pastor**, N. Navas, S. Kuckova, A. Rodríguez-Navarro, E. Manzano, C. Cardell. Journal of Mass Spectrometry. (*Submitted paper*, July 2011).

Capítulo 10: En este capítulo se estudian los materiales pictóricos en muestras reales procedentes del Palacio de la Madraza, Granada (Siglo XIV) mediante una metodología novedosa basada en el uso combinado de µ-XRD, RM, SEM-EDX y CG-MS. Una de las novedades del trabajo es la aplicación de la µ-XRD para el estudio textural de los pigmentos minerales encontrados en las estratigrafías pictóricas. Gracias a ello, este estudio ha permitido la identificación de procesos de manufactura, naturaleza y alteración de los pigmentos minerales presentes, así como la datación de pinturas

procedentes de intervenciones históricas en función de la técnica pictórica utilizada.

- *Compositional and quantitative microtextural characterization of Historic Paintings by means of Micro-X-Ray Diffraction and Raman Microscope* (2011). **J. Romero-Pastor**, A. Duran, A. B. Rodríguez- Navarro, R. Van Grieken, C. Cardell. Analytical Chemistry. (*Paper in press*, June 2011).

Capítulo 11: En este capítulo se exponen las conclusiones globales derivadas de la investigación realizada en esta Tesis Doctoral.

Capítulo 12: El desarrollo de parte de los capítulos anteriores ha supuesto profundizar en una línea previamente iniciada y dirigida al estudio y caracterización mediante técnicas quimiométricas de materiales pictóricos, especialmente centrada en aquellos materiales en los que el aglutinante es de naturaleza proteica. El estudio de muestras pictóricas reales procedentes de La Alhambra y del Monasterio de San Jerónimo (ambos monumentos en la ciudad de Granada) es uno de los objetivos futuros para la aplicación de algunas de las metodologías propuestas. Además, se trabaja con otros materiales pictóricos a nivel de laboratorio para su completa caracterización, evaluación y el estudio de los procesos de alteración e interacción entre ellos.

3. Materiales y Métodos

En este capítulo 3 de Materiales y Métodos se incluye una descripción y justificación detallada de los materiales pictóricos utilizados para la elaboración de las réplicas pictóricas, las muestras reales procedentes del edificio histórico estudiado (Palacio de la Madraza, Granada), así como las técnicas analíticas y quimiométricas utilizadas en el desarrollo de esta Tesis Doctoral.

In third Chapter 3 of "Materials and Methods" includes a brief detailed history of painting materials use to elaborate pictorial replicas, real painting samples from monuments (Madrasah Palace, Granada, Spain) and the analytical and chemometric techniques used in the development of this Doctoral Thesis.

3. Materiales y Métodos

En esta Tesis Doctoral se han seleccionado para su estudio materiales pictóricos utilizados tradicionalmente en la elaboración de temples proteicos según se describe en recetas de la Edad Media y Renacimiento (Pacheco, 1990). Para el estudio de dichos materiales y de posibles interacciones físicas, químicas y/o mineralógicas se han preparado réplicas pictóricas monocomponentes, elaboradas con un pigmento o con un aglutinante, y réplicas pictóricas binarias de pigmento-aglutinante proteico. Además, en este Capítulo se detallan las muestras pictóricas reales tomadas del edificio histórico y su localización.

Finalmente, se expondrán las técnicas de análisis utilizadas en los siguientes capítulos de esta Tesis Doctoral. Entre estas técnicas incluimos tanto las analíticas como quimiométricas, de las cuales se ha evaluado su capacidad analítica y se ha determinado las condiciones idóneas de utilización para el estudio de los materiales pictóricos seleccionados. También se ha evaluado el beneficio que suponen en el estudio de muestras pictóricas reales.

3.1. Materiales pictóricos

3.1.1. Reseña histórica de materiales pictóricos

Los **pigmentos históricos** inorgánicos seleccionados para su estudio en esta Tesis Doctoral se detallan en la tabla 3.1. En concreto, se seleccionaron tres grupos de pigmentos en función de sus características cromáticas: pigmentos azules, rojos y blancos.

Entre los pigmentos azules adquiridos a *Kremer Pigments GmbH & Co* (Madrid), encontramos la **azurita** ($Cu_3(CO_3)_2(OH)_2$. Este pigmento ha sido el más importante en la pintura europea hasta finales del siglo XVII. Este pigmento mineral tiene un color azul brillante que a menudo era confundido

con el lapislázuli (Ballirano et al., 2006). El **lapislázuli** se obtiene de la roca semipreciosa del mismo nombre que está constituida principalmente por lazurita ($Na_{8-10}Al_6Si_6O_{24}S_{2-4}$), mineral de lustre vítreo-deslucido a graso. La primera vez que hay constancia del uso del lapislázuli como pigmento fue en el siglo VI y VII d.C. en temples afganos (Eastaugh et al., 2004; Barnett et al., 2006). El lapislázuli tuvo un uso extensivo durante los siglos XIV y XV, en manuscritos y pinturas italianas, para decorar sólo las túnicas de Cristo y la Virgen, debido a su alto valor económico (Eastaugh et al., 2004; Marano et al., 2006). También se ha estudiado el **azul esmalte**, que a diferencia de los anteriores, es un pigmento artificial constituido por un vidrio de potasio y cobalto. Este pigmento azul, más económico, se empezó a usar en Italia durante los siglos XIV y XV, sustituyendo a la azurita y el lapislázuli durante el siglo XVII (Borgia et al., 2002).

Entre los pigmentos rojos, adquiridos en *Caremi Pigmentos* (Sevilla), se seleccionaron varios pigmentos históricos como son el cinabrio, el minio y la *Sienna* natural. La composición del **cinabrio** y bermellón es sulfuro de mercurio (HgS) y sólo difieren en su origen natural o sintético, respectivamente. Este pigmento rojo intenso ya se explotaba de forma extensiva por los romanos en las Minas de Almadén (Ciudad Real) (Eastaugh et al., 2004). Otro de los pigmentos rojos utilizados en esta Tesis Doctoral ha sido el **minio**, óxido de plomo (Pb_3O_4). Este pigmento rojo es uno de los más antiguos y comúnmente utilizados a lo largo de la historia, especialmente, en la decoración de manuscritos (Mayer, 1988; Eastaugh et al., 2004; Barnett et al., 2006). Por último, la ***Sienna* natural**, originaria de la región italiana que le aporta el nombre, corresponde a una arcilla de composición variable rica en óxidos de hierro y otros elementos (e.g. hematites, goetita, magnetita, óxido de manganeso, etc.) (Hradil et al., 2003). Por tanto, este pigmento presenta una amplia gama de tonos cromáticos desde amarillos hasta rojos (Froment et al., 2008). Este pigmento mineral ha sido muy utilizado desde la Prehistoria hasta nuestros días, debido a su estabilidad cromática y su abundancia (Mayer, 1988; Hradil et al., 2003).

Los pigmentos blancos se han seleccionado en función de su uso como pigmentos y/o como cargas históricas. Todos ellos se adquirieron en *Caremi Pigmentos* (Sevilla). El **blanco de plomo** o cerusita, ($PbCO_3$), es el pigmento blanco más utilizado desde la época Greco-Romana hasta la actualidad (Scott et al., 2009), aunque ha sido sustituido progresivamente por otros pigmentos menos tóxicos como el Blanco de Titanio (TiO_2) o el Blanco de Zinc (ZnO) (Mayer, 1988; Doerner, 2005; Pedrola, 1998). La **calcita** ($CaCO_3$) es un pigmento mineral natural usado desde época romana (Eastaugh et al., 2004). El uso de la calcita en las capas pictóricas es muy común como pigmento y carga. Además, cabe destacar su importante función aglutinante en pinturas al fresco (Eastaugh et al., 2004). También el **yeso** ($CaSO_4 \cdot 2H_2O$), pigmento mineral natural, ha sido utilizado para los ensayos de esta Tesis Doctoral por su extensa aplicación en pintura a lo largo de la Historia (Heywood, 2001). El yeso se ha utilizado tradicionalmente en capas preparatorias y/o en capas pictóricas, como pigmento y/o carga (tabla 3.1). Por otra parte, el yeso constituye una de las materias primas más importantes en el arte Nazarí (época islámica en España, siglos XIII al XV) al emplearse para la elaboración de las llamadas yeserías (Cardell-Fernández y Navarrete-Aguilera, 2006). Por último, el **cuarzo** (SiO_2) es uno de los minerales más utilizados como carga pictórica en la elaboración de capas pictóricas, ya que proporciona volumen sin modificar el color de las capas, y es mineralógicamente muy estable. Por ejemplo, el cuarzo se ha encontrado como carga capas azules elaboradas con azurita (Price 2000; Hradil et al., 2003). Además, se han utilizando muestras de hueso natural, cuya composición mayoritaria se basa en hidroxiapatito ($Ca_{10}[PO_4]_6[OH]_2$) y colágeno. Los pigmentos de "hueso" se han utilizado como pigmento blanco y negro desde la época griega hasta la Edad Media (Cardell et al., 2009b).

Por lo que respecta a los **aglutinantes orgánicos** usados en esta Tesis Doctoral, se han seleccionado dos materiales proteicos para la elaboración de réplicas pictóricas: a) **cola de conejo (colágeno)** de dos marcas comerciales (*Sigma-Aldrich*, Barcelona; *Productos de Conservación*, Madrid) y

b) albúmina; ésta última de dos fuentes proteicas diferentes: **yema de huevo natural** compuesta principalmente de albúmina, ovoalbúmina y ácidos grasos (Mayer, 1988), y **albúmina liofilizada** de la marca comercial *Kremer Pigments GmbH & Co.* (Madrid).

Nombre del pigmento (español e inglés)	Composición química	Origen	Uso histórico	Imagen*
Azurita (Azurite)	$Cu_3(CO_3)_2(OH)_2$	Natural	Egipto → S. XVII	
Lapislázuli (Lapis lazuli)	Principal fase mineral: lazurita ($Na_{8-10}Al_6Si_6O_{24}S_{2-4}$)	Natural	S. VI → Renacimiento	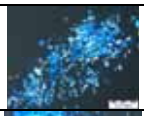
Esmalte (Smalt)	Vidrio de cobalto y potasio	Artificial	S. XIV→XVIII	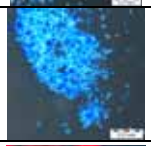
Cinabrio (Cinnabar)	HgS	Natural	Roma → S. XVIII	
Minio (Minium)	Pb_3O_4	Artificial	Roma → Actualidad	
Sienna natural (Raw Sienna)	Arcillas ricas en Fe_2O_3	Natural	Prehistoria → Actualidad	
Blanco de Plomo (Lead White)	$(PbCO_3)_2$	Artificial	Grecia-Roma → S. XVII	
Calcita (Chalk)	$CaCO_3$	Natural	Prehistoria → S. XVII	
Yeso (Natural Gypsum)	$CaSO_4 \cdot 2H_2O$	Natural	Egipto-Grecia-Roma → S. XVII	
Cuarzo (Quartz)	SiO_2	Natural	Prehistoria → S. XVII	
Hueso Natural	Mayoritariamente Hidroxiapatito $Ca_{10}[PO_4]_6[OH]_2$	Natural	Grecia-Roma→ Edad Media	

Tabla 3.1. Composición y características de los pigmentos tradicionales utilizados en esta Tesis Doctoral. *Imágenes a microscopio óptico-petrográfico con luz reflejada, nícoles cruzados y a 4X.

Estos compuestos se han utilizado para elaborar temples magros (cola de conejo) y grasos (yema de huevo). Ambos tipos de aglutinantes tienen propiedades de viscosidad, elasticidad y flexibilidad similares, lo que los convierten en materiales muy adecuados para la elaboración de pintura mural (Sangrando et al., 2010). Una diferencia sustancial entre ambos medios proteicos es la presencia de ácidos grasos en la yema de huevo, que proporcionan mayor brillo y flexibilidad a la pintura que aquellas elaboradas mediante temples de cola (Mayer, 1988).

3.1.2. Preparación de réplicas pictóricas

Para la elaboración de las réplicas pictóricas a partir de los materiales pictóricos anteriormente detallados se han aplicado recetas tradicionales del Renacimiento y Edad Media (Pacheco, 1990). De esta manera se han simulado estratigrafías pictóricas que contienen pigmento y/o aglutinante proteico. En particular, en los Capítulos 4, 7 y 9 de esta Tesis Doctoral se han preparado réplicas pictóricas de cola de conejo y sus temples correspondientes. Para los capítulos 5 y 6, las réplicas pictóricas se prepararon a base de yema de huevo y sus temples; y en el Capítulo 8 se elaboraron réplicas pictóricas de albúmina liofilizada con cuarzo y otras a base de hueso natural (Tabla 3.2).

Preparación de las réplicas pictóricas de pigmento puro

Para preparar las colecciones de réplicas pictóricas de pigmento puro, se ha tomado una cantidad conocida de cada pigmento y depositado en forma de cráter (vidrio de reloj) en cuyo interior se añade un volumen conocido de agua (ultra-pura Milli-Q) y se agita hasta que la mezcla no gotee. A continuación, se aplica sobre un soporte de vidrio en capas sucesivas. Antes de la aplicación de la capa siguiente se debe comprobar que la capa anterior se ha secado. Tras la aplicación de la última capa se realiza el control del secado hasta pesada constante (Fig.3.1).

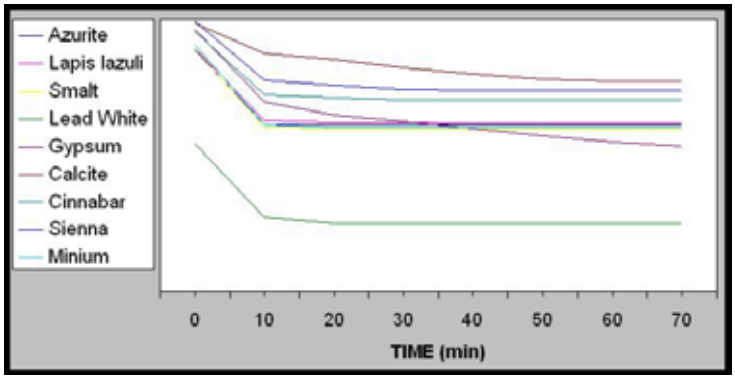

Fig. 3.1. Control de secado de las réplicas pictóricas de pigmento puro.

Preparación de las réplicas pictóricas de aglutinante puro

a) Réplicas de cola de conejo (colágeno)

Para la preparación de réplicas pictóricas con cola de conejo se han tomado 10g de cola de conejo comercial *Sigma-Aldrich* (Barcelona) o *Productos de Conservación* (Madrid) y se han diluido al 10% en agua (ultra-pura MILLIQ). La cola debe hidratarse durante 24 horas, agitando el sólido regularmente durante este tiempo. Una vez hidratado se calienta la mezcla al "baño María", siempre a una temperatura inferior a 50°C, hasta obtener una solución homogénea (Pacheco, 1990). Se deja enfriar y se conserva en un recipiente cerrado a una temperatura inferior a 10°C, hasta el momento de su uso. La preparación de las réplicas pictóricas basadas en cola de conejo pura se realizó sobre un porta de vidrio (76x26x1mm), aplicándose capas sucesivas de cola mediante pincel, previo secado de la anterior y hasta pesada constante (Fig.3.2).

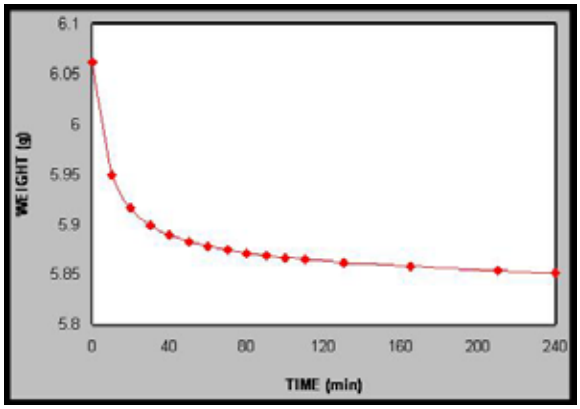

Fig. 3.2. Control de secado de la muestra de cola de conejo

b) Réplicas de yema de huevo natural

Para la preparación de las réplicas con yema de huevo natural, se pincha la yema con una aguja y se vierte el contenido en un recipiente adecuado para su posterior aplicación, tanto para la preparación de réplicas pictóricas puras (material de referencia), como para la preparación de réplicas pictóricas con los pigmentos antes citados. Este proceso incluye el secado a peso constante, como muestra la Figura 3.3. (Mayer, 1988; Pacheco, 1990).

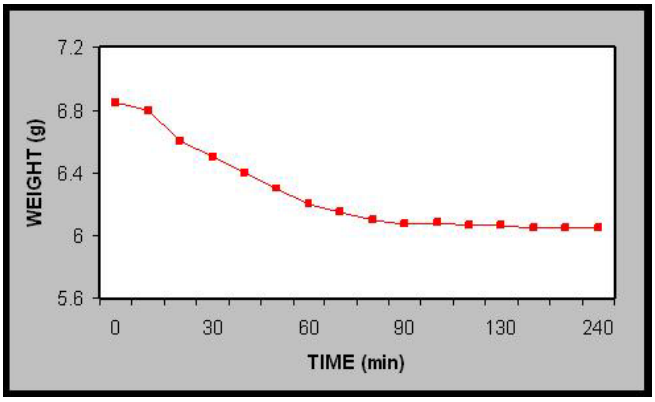

Fig. 3.3. Control de secado de la muestra de yema de huevo natural puro.

Preparación de las réplicas pictóricas de pigmento – aglutinante

a) "Mezcla Ideal" Pigmento – Aglutinante (I-Mixt)

Se han elaborado réplicas pictóricas de pigmento-aglutinante "ideales" según recetas tradicionales (Pacheco, 1990). Para ello, a los pigmentos anteriormente citados se les añaden sucesivamente volúmenes conocidos de cola de conejo en caliente (T<50 °C) o yema de huevo. La réplica pictórica pigmento-aglutinante ideal (I-Mixt) es adecuada si tras realizar pinceladas finas sobre un soporte de vidrio, la pasta pictórica seca se retira limpiamente con una punta de madera fina (Mayer, 1988; Pacheco, 1990). Dicha mezcla ideal se ha aplicado en capas sucesivas sobre el soporte de vidrio, tras el secado de la capa anterior. Tras la aplicación de la última capa se realiza el control periódico del secado hasta pesada constante (Fig.3.4).

b) "Mezclas no Ideales" pigmento – aglutinante

Con el objetivo de estudiar la influencia que ejerce la proporción pigmento-aglutinante (CVCP, Concentración Volumétrica Crítica de Pigmento) sobre los procesos de alteración en una película pictórica se han preparado mezclas no ideales de pigmento-aglutinante (Capítulo 7). Estas mezclas no ideales se han elaborado a base de azurita y cola de conejo. En particular, se han preparado réplicas pictóricas con una proporción diluida *(Mixt-g)* y concentrada en cola de conejo *(Mixt-G)*, como se describe a continuación:

b.1) Réplicas pictóricas con una proporción diluida en cola de conejo *(Mixt-g)*

Una vez conocido el volumen de aglutinante necesario para preparar la mezcla ideal azurita-cola de conejo (5.2/1, p/v), se toma aproximadamente un tercio de dicho volumen para preparar la colección llamada mezcla diluida y la misma cantidad de azurita, es decir, 5.2/0.4 (p/v). Posteriormente, se aplica sobre el soporte de vidrio y se realiza el control periódico del secado hasta pesada constante (Fig.2.4.).

b.2) Réplicas pictóricas con una proporción concentrada en cola de conejo *(Mixt-G)*

De igual manera, se han preparado las réplicas pictóricas con una proporción concentrada de cola de conejo, en concreto, con el triple del volumen que en la mezcla ideal y la misma cantidad de azurita, es decir, en una proporción 5.2/3 (p/v). A continuación, se extiende sobre el porta de vidrio y se realiza el control del proceso de secado (Fig.3.4.).

Para el secado de las réplicas pictóricas de laboratorio se ha usado el *Sistema Gel Air Dryer, BIO-RAD Laboratorios S.A.* (Madrid), y para el control de peso durante el secado se usó una balanza analítica *METTLER-TOLEDO modelo AE163*, con un rango entre 0-30 y 0-160 g y con una precisión de 0.1 y 0.1 mg, respectivamente.

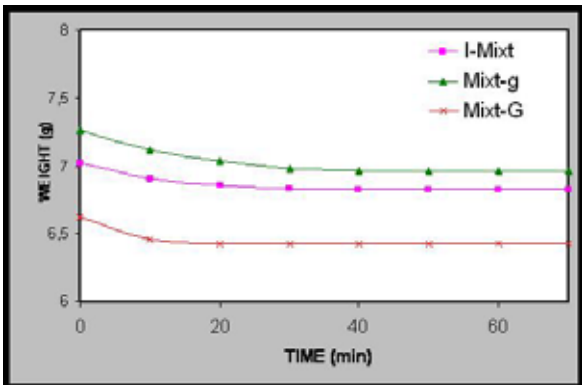

Fig. 3.4. Control del secado de réplicas pictóricas azurita-colágeno con una proporción ideal (IMixt), diluida (Mixt-g) y concentrada (Mixt-G) en cola de conejo (Mixt-g).

Preparación de las réplicas pictóricas cuarzo/albúmina

Las réplicas pictóricas que contienen cuarzo y albúmina se han elaborado a partir de cuarzo (SiO_2) en polvo mezclado con albúmina liofilizada (Kremer Pigmentos GmbH & Co.KG, CI: PB 63.250; Madrid). Se han preparado cuatro mezclas con diferente contenido de cuarzo [30%, 50%, 70% y 90% (p/p)].

Preparación de las réplicas pictóricas hidroxiapatito/colágeno

Estas réplicas pictóricas se prepararon a partir de hueso de gallina (fémur) para el trabajo de investigación que constituye el Capítulo 8. Este biomaterial contiene hidroxiapatito (70%) y un 30% de materia orgánica (fundamentalmente colágeno) (Cardell et al., 2009b; Le Blond et al., 2009). Las muestras de hueso fresco han sido molidas en un mortero de ágata y se ha pulverizado en un equipo de criomolienda (*modelo CertiPrep 6750, Freezer/Mill, SPEX*), para su posterior tratamiento y análisis directamente sobre la muestra pulverizada.

Nº Capítulo Tesis Doctoral	Pigmento	Aglutinante	Proporción
4	azurita	Colágeno (cola de conejo)	Mezcla Ideal*
	lapislázuli		
	esmalte		
5 y 6	Blanco de Plomo	Yema de huevo (natural de gallina)	Mezcla Ideal*
	calcita		
	yeso		
	azurita		
	lapislázuli		
	esmalte		
	cinabrio		
	minio		
	Sienna natural		
7	azurita	Colágeno (cola de conejo)	Mezcla Ideal** (5.2/1 p/v)**
			Mezcla diluida (5.2/0.4 p/v)**
			Mezcla concentrada (5.2/3 p/v)**
8	Cuarzo	Albúmina (liofilizada)	30%, 50%, 70%, 90% (p/p)***
	Hueso natural (hidroxiapatito y colágeno)		70% hidroxiapatito y 30% colágeno
9	azurita	Colágeno (cola de conejo)	Mezcla Ideal** (5.2/1 p/v)*
	cinabrio		

*(recetas tradicionales Medievales; Pacheco, 1990);
** (p/v): peso de pigmento (g)/ volumen de aglutinante (ml);
***(p/p): % en peso de pigmento/aglutinante (g/g).

Tabla 3.2. Composición de las réplicas pictóricas elaboradas y estudiadas según la aparición en Tesis Doctoral.

3.1.3. Muestras pictóricas reales

Para el estudio de materiales pictóricos reales, se han tomado muestras del Palacio de la Madraza de Granada (antigua Universidad *Madrasha Yusufiyya*) que fue construido por Yusuf I (dinastía nazarí, 1238-1492) en 1349. Fue el centro religioso y comercial de la antigua *Madinat Garnata* (en la actualidad centro de la ciudad de Granada). La *Madrasha Yusufiyya* fue la primera Universidad Islámica del reino Nazarí. Poco después de la conquista Cristiana en 1492, la Madraza se convirtió en Casa del Cabildo, sufriendo desde entonces numerosas reformas para adaptarse a sus nuevas funciones. Entre ellas, la más importante fue la realizada en el siglo XVI. Dos estancias nuevas tienen su origen en esta reforma, la Sala de la Entrada y la Sala de Caballeros XXIV (Fig. 3.5) (Gómez Moreno, 1982; Cruz Cabrera y Gómez-Moreno Calera, 2007).

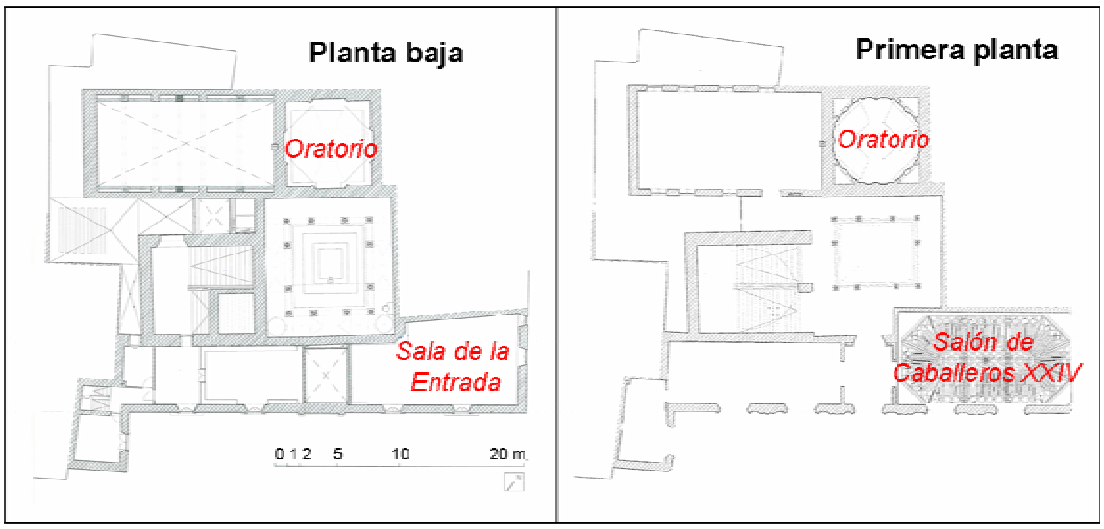

Fig.3.5. Plano del Palacio de la Madraza (Granada).

En la actualidad, la única sala Nazarí que se conserva de la Madraza original es el *Oratorio*, decorado con yeserías policromadas en rojo, azul, verde y dorado (Fig.3.6.). Sin embargo, esta sala también ha sido objeto de varias intervenciones a partir del siglo XIX, sufriendo la más importante

restauración en 1893 (Gómez Moreno, 1982; Cruz Cabrera y Gómez-Moreno Calera, 2007).

Fig.3.6. Imágenes del Palacio de la Madraza (Granada): a) Decoración del Oratorio basada en yeserías policromadas y artesonado policromado (S. XIV); b) detalle de yesería policromada. Nótese la pérdida de material pictórico por la alteración de la policromía original.

La *sala de la Entrada y El Salón de Caballeros XXIV* se construyeron durante la misma reforma del edificio del siglo XVI, sin embargo, sólo el *Salón de Caballeros XXIV* se decoró en el momento de su construcción con artesonado de madera policromada en colores rojos, negros, blancos y azules (Fig.3.7a). En cambio, la *sala de la Entrada* se decoró con pinturas murales y sobre policromía sobre madera (alfarje) entre los siglos XVIII y XIX, según referencias biográficas (Gómez-Moreno, 1982; Cruz Cabrera y Gómez-Moreno Calera, 2007). Las decoraciones en este caso consisten en motivos geométricos de tonos rojos y ocres (Fig.3.7.b).

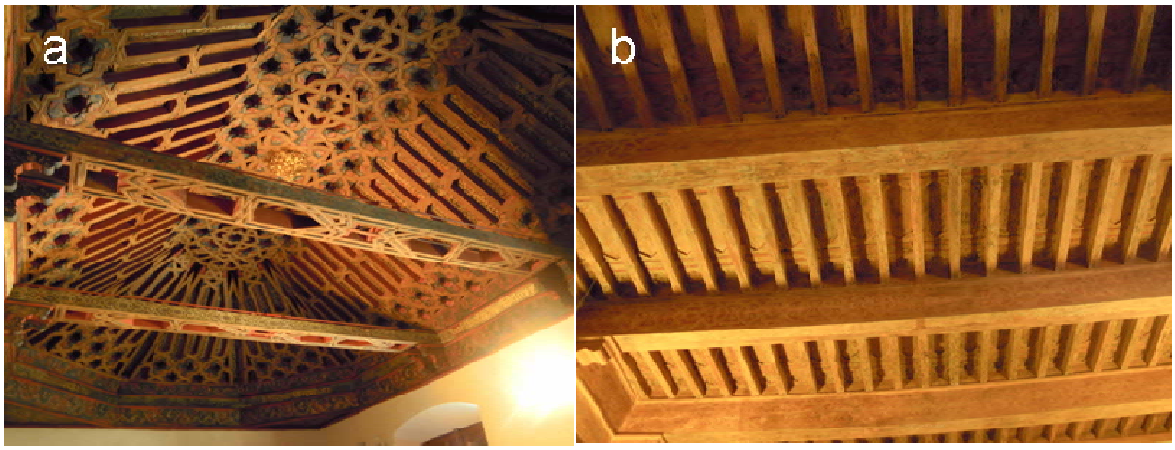

Fig. 3.7. Salas añadidas al Palacio de la Madraza (S. XVI): Sala de Caballeros XXIV decorada con artesonado policromado (a) y Sala de la Entrada decorado con alfarje (b) y pintura mural.

Durante el muestreo realizado para esta Tesis Doctoral, se han tomado diecinueve muestras pictóricas de diferentes zonas: siete muestras del *Oratorio,* seis de pintura sobre yesería policromada y una muestra de policromía sobre madera del artesonado que cubre la estancia. Por otra parte, del *Salón de Caballeros XXIV* se han tomado seis muestras de los colores representativos de la decoración del artesonado. Asimismo, de *sala de la Entrada* se han tomado seis muestras, tanto de la pintura mural como de la policromía sobre madera del alfarje. El muestreo se ha basado en i) la ubicación de las pinturas dentro del edificio, ii) el color en superficie observado en diferentes sustratos (yesería, madera, pintura mural) y iii) posibles intervenciones históricas. El método para el muestreo se ha basado en la extracción de la muestra de la policromía o pintura mural mediante bisturí, y su conservación en un vial *Eppendorf* etiquetado.

3.2. Técnicas Analíticas

Con objeto de cumplir los objetivos marcados en este Tesis Doctoral (Capítulo 2), se han evaluado técnicas analíticas tradicionales como por ejemplo, la Espectrometría de Infrarrojos en modo transmisión (modo Transmitancia), así como otras más novedosas en el campo del Patrimonio

Pictórico, como son: la Espectrometría de Infrarrojos en modo reflexión (en modo Reflectancia Difusa y en modo Reflectancia Total Atenuada), la Microscopía Raman, la Microdifracción de Rayos X, y la Espectrómetría de Masas de Desorción/Ionización asistida por Láser con Detector de Tiempo de Vuelo.

3.2.1. Técnicas Espectroscópicos

a) Espectrometría de Infrarrojos con transformada de Fourier en modo Transmitancia (Transmittance- Fourier Transform Infrared Spectroscopy, T-FTIR)

El mecanismo de interacción entre las moléculas y la radiación infrarroja induce oscilaciones y vibraciones en las moléculas que hace que los enlaces que los unen se estiren o flexionen. Todos los movimientos combinados dan como resultado varios tipos de movimientos relativos o modos de vibración, como los que se muestran en la Fig. 3.8.

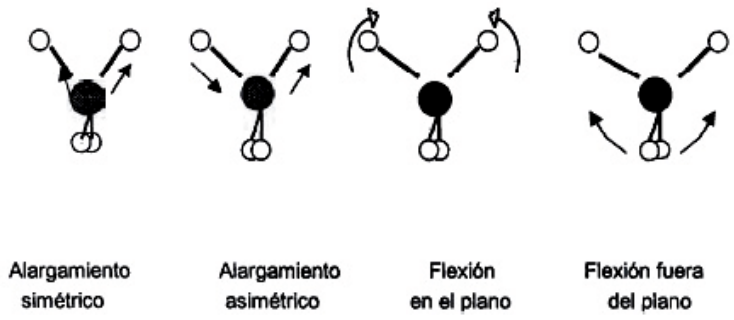

Fig. 3.8. Tipos de vibración molecular, alargamiento (stretching) y flexión (flexion). Imagen tomada de García Sánchez (1990)

La radiación IR al interaccionar con las moléculas del compuesto analizado hace que los fotones con unas energías características sean absorbidos, y el espectro de la radiación transmitida presenta unas bandas características

de absorción. Cada frecuencia de luz absorbida por una molécula corresponde a la vibración de un enlace específico y, por tanto, proporciona información de los tipos de enlace que presenta una muestra. Así cada molécula efectúa este tipo de movimiento a frecuencias específicas y bien conocidas. Además, la señal obtenida proporciona información cuantitativa del contenido de una molécula en función de su intensidad.

La espectrometría IR trabaja típicamente en el intervalo del infrarrojo, que va de 4000 a 400 cm^{-1} de longitud de onda. Por esta razón, la espectrometría de IR es sensible a la presencia de determinados grupos funcionales, tales como C=O, CH_2, OH, entre otros, ya que estos grupos poseen bandas de absorción características del infrarrojo (Álvarez-Lloret, 2008).

En el campo del arte, el uso de la espectrometría de IR está muy extendido desde hace años y se ha establecido como una técnica de rutina para el análisis e identificación de muestras pictóricas (Daniilia et al., 2000; Edreira et al., 2001). Su ventaja fundamental, para el análisis de materiales pictóricos es que permite estudiar tanto los componentes inorgánicos (pigmentos y cargas) como los componentes orgánicos (ceras, aceites secantes y proteínas que componen barnices y aglutinantes). Por tanto, esta técnica combinada con otras, e.g. SEM-EDX, XRD y GC-MS, permite una caracterización muy completa de obras pictóricas (Manzano et al., 2000).

En nuestro caso, para el análisis de réplicas pictóricas mediante T-FTIR se ha utilizado un espectrómetro de IR por Transformada de Fourier (FTIR) modelo *Nicolet 20SXB* disponible en Centro de Instrumentación Científica de la Universidad de Granada (CIC). Los espectros se registraron de 4000 a 400 cm^{-1}, con una resolución de 2 cm^{-1} y 200 barridos. La técnica por Transformada de Fourier permite medir la longitud de onda de forma absoluta sin necesidad de hacer medidas de referencia o calibrados en longitud de onda. En nuestros estudios, para el análisis de muestras en modo Transmitancia, se ha utilizado una cantidad de muestra entre 30-50µg diluida al 1% en una pastilla prensada de KBr.

b) Espectrometría de Infrarrojos con transformada de Fourier en modo Reflectancia Difusa (Diffuse Reflectance Infrared Fourier Transform Spectroscopy, DRIFTS)

Hasta ahora son escasos los trabajos de investigación que hacen uso de esta técnica analítica. Sin embargo, ésta se ha utilizado para la elaboración de una base de datos de pigmentos y colorantes, y para el estudio de restos orgánicos en materiales arqueológicos (Silva et al., 2006; Blee et al., 2010).

La reflexión de la radiación IR puede ser de dos tipos: especular y difusa (Fig. 3.9). La reflectancia difusa tiene lugar en todas las direcciones como consecuencia de un fenómeno de absorción y dispersión. Predomina cuando los materiales de la superficie reflectante son débilmente absorbentes a la radiación de onda incidente, y cuando la penetración de la radiación es grande con respecto a la longitud de onda. Este tipo de reflexión es la que se estudia mediante Espectroscopía por Reflectancia Difusa (DRIFT).

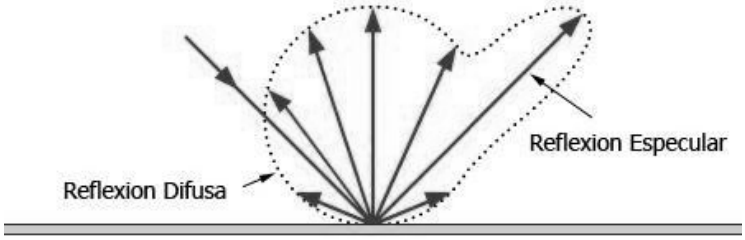

Fig. 3.9. Componentes especular y difusa

Esta técnica requiere de un porta-muestras especial que se integra en el espectrómetro de infrarrojos por Transformada de Fourier. Este accesorio óptico consta de unos espejos que permiten colimar el haz sobre la superficie de la muestra y registrar el espectro de IR por reflexión difusa (Fig.3.10). Este dispositivo permite medir la componente de reflexión difusa

producida por la muestra en el rango IR de 4000 y 400 cm^{-1} con una resolución de hasta 0,5 cm^{-1}. (Escribano, 1989).

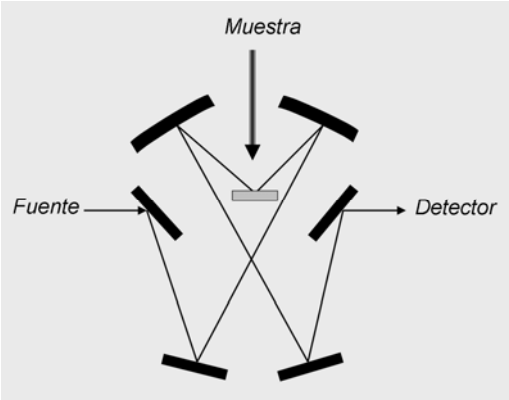

Fig. 3.10. Accesorio óptico para obtener la reflexión difusa en FTIR

La ventaja principal del modo reflectancia difusa, es que el haz de IR incide directamente sobre la muestra en polvo sin necesidad de prepararla en forma de pastilla. Otra ventaja de este modo de trabajo es la pequeña cantidad de muestra que se necesita para el análisis (5-10 μg). Por otra parte, para medir una muestra hay que molerla en un mortero de ágata para reducir el tamaño de grano y añadir KBr hasta diluir la muestra al 5%. La mezcla finamente dividida se coloca sobre el portamuestra circular de 3 mm de diámetro, y mediante una leve presión se busca tener la superficie lo más libre de irregularidades. A continuación, se coloca en el accesorio anterior y se empieza la medida.

En nuestro caso, para el análisis de muestras pictóricas se ha utilizado un espectrómetro de infrarrojos por Transformada de Fourier modelo *Nicolet 20SXB* disponible en el CIC, y un accesorio portamuestras *Spectra-Tech modelo Collector* (Sutton, Surrey, Reino Unido) que permite medir las muestras mediante reflectancia difusa.

c) *Espectrometría de Infrarrojos con transformada de Fourier en modo Reflectancia Total Atenuada (Attenuated Total Reflectance Infrared Fourier Transform ATR-FTIR Spectroscopy)*

El modo ATR de Espectrometría de Infrarrojos se basa en la reflexión total de la radiación en la interfase de dos medios de índice de refracción muy diferente. La radiación penetra unas micras (0.5-5µm) en el material de índice de refracción más bajo, y se genera un espectro de absorción de la muestra. Por ello, es necesario que el cristal sobre el que se coloca la muestra tenga un alto índice de refracción (e.g. diamante). Generalmente, los equipos de ATR-FTIR logran aumentar la sensibilidad mediante reflexiones internas múltiples, es decir, el haz choca repetidamente con la muestra y tras varias reflexiones llega al detector (Fig.3.11).

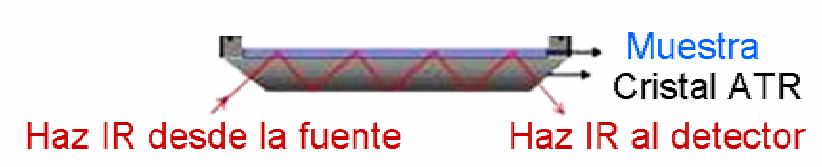

Fig. 3.11. Portamuestra accesorio para ATR-FTIR.

El modo ATR-FTIR requiere una cantidad de muestra muy pequeña para el análisis (3 µg), y no necesita mezclar la muestra con KBr. La muestra pulverizada se coloca sobre un cristal de diamante (3 mm de diámetro) y se presiona para maximizar el área de contacto de la muestra con el cristal. Una limitación de esta técnica es el intervalo espectral, restringido por la ausencia de señal a longitudes de onda inferiores a 650 cm^{-1} debido a la absorción del diamante. Esto impide el estudio de aquellos materiales en los que sus bandas características se encuentran en esta región. Este es el caso de pigmentos rojos como cinabrio o hematites, que tienen sus principales bandas de absorción entre 600 y 200 cm^{-1} (Burgio y Clark, 2001).

En nuestros estudios, se ha hecho uso de un espectrómetro *JascoFTIR6200* (Jasco, Tokio, Japón) equipado con un accesorio ATR de cristal de diamante

(*MIRacleTM accesorio ATR, Pike Tecnología*) disponible en el CIC. Para cada medida se registraron 200 barridos, con una resolución de 2 cm^{-1} en la región de 4000 cm^{-1} a 650 cm^{-1}. El tratamiento de los espectros se realizó con el software Spectra Manager JASCO v.2.

d) Espectroscopía Raman (Raman Spectroscopy)

La Espectroscopía Raman se basa en la dispersión inelástica de la luz al incidir sobre la materia. Cuando un haz de luz monocromática (por ejemplo, un haz de luz láser) incide sobre un material, la mayor parte de dicha luz es dispersada elásticamente con la misma longitud de onda de la luz incidente (dispersión *Rayleigh*). Sin embargo, una pequeña parte de la energía luminosa incidente (alrededor de una millonésima) es dispersada inelásticamente (debido a una pequeña absorción), siendo esta segunda la denominada dispersión Raman, que permite caracterizar el material a estudiar (Bañares y Ximena, 1998; Boanza et al., 2002).

El acoplamiento de un espectrómetro Raman a un microscopio óptico permite hacer análisis puntuales de los componentes de la muestra con una gran resolución espacial. La resolución espacial varía de acuerdo con las características ópticas de dicho microscopio, alcanzándose una resolución de hasta 1 µm. La Microscopía Raman (RM) es una técnica analítica muy fiable, sensible, no destructiva (a priori) y especialmente adecuada para estudiar materiales pictóricos. Además permite trabajar in situ, sin necesidad de tomar muestra de la obra pictórica (Vandenabeele et al., 2000, 2007; Pérez-Alonso et al., 2006). El análisis mediante Microscopía Raman permite además identificar los componentes orgánicos más comúnmente usados en pinturas como son la caseína, la yema de huevo, resinas, etc., así como los pigmentos inorgánicos presentes en la mayoría de las obras de arte pictóricas (Burgio y Clark., 2001).

Durante el desarrollo de esta Tesis Doctoral, para el análisis de muestras se utilizaron dos equipos de Microscopía Raman *(Renishaw Invia Raman microscope system)*: un equipo de los Servicios Técnicos de la Universidad de Jaén y otro del laboratorio *Micro and Trace Analysis Centre (MiTAC)* de la Universidad de Amberes (Bélgica), éste último, durante una estancia predoctoral de la doctoranda. Ambos equipos disponen de dos fuentes de excitación láser: un láser diodo de 785 nm y un láser ión de Ar (modelo Láser-Physics), refrigerado por aire, con una potencia de salida de 300mW y 20mW, respectivamente. Asimismo, los equipos disponen de un detector CCD refrigerado por un sistema Peltier (-70ºC) y un microscopio Leica DMLM. En ambos equipos la resolución espacial fue de 1 μm.

Los espectros se registraron mediante la colocación de las muestras en la platina del microscopio óptico, y se analizaron con un objetivo de 20x ó 50x. La zona a estudiar se enfocó usando la videocámara o los objetivos oculares. Para evitar la degradación de los materiales pictóricos inducida por el láser, se redujo la intensidad de éste y posteriormente se confirmó visualmente la ausencia de daños en la zona estudiada. En todos los casos, la potencia del láser se mantuvo entre 0.2 y 20 mW. Por otra parte, para optimizar las condiciones de medida se ajustó la potencia del láser, el número de espectros acumulados y los tiempos de integración (máximo 20s) para cada muestra. Para el control de las aplicaciones del instrumento y tratamiento de los datos se hizo uso del Software Wire 2.0.

e) Espectrofotometría Visible (Spectrophotometry)

Esta técnica se ha usado para analizar la variación del color en las réplicas pictóricas de azurita y cola de conejo, durante los procesos de envejecimiento con radiación UV. A lo largo del transcurso de los experimentos, las muestras pictóricas frescas y envejecidas se analizaron

periódicamente para valorar los cambios cromáticos sufridos durante el proceso de envejecimiento acelerado.

Para el análisis de las muestras se ha utilizado un equipo *Hunterlab Ultrascan* con el que se ha medido la reflectancia difusa espectral. Los espectros se registraron en el intervalo de longitud de onda del visible de 375 y 750 nm, con una resolución espectral de 5 nm. Las curvas de reflectancia espectral y las coordenadas de cromaticidad CIE-1931 se calcularon con una iluminación D65. Los datos cromáticos se expresaron como coordenadas del espacio colorimétrico CIELAB (luminosidad, saturación, tono y color total) y los parámetros CIE (x, y, z), que definen los colores rojo, verde y azul, respectivamente (Duran-Suárez et al., 1995). La fórmula de diferencia de color CMC (2:1) se usó para comparar espectrofotométricamente las muestras pictóricas envejecidas con respecto a las correspondientes muestras sin envejecer. En general, estas diferencias son visualmente apreciables si el cambio en el valor de diferencia de color total es superior a tres unidades (Duran-Suárez et al., 1995).

3.2.2. Técnicas de Difracción de Rayos-X (X-ray Diffraction, XRD)

a) Difracción de Rayos-X convencional (método de polvo cristalino)

Esta técnica se ha usado para determinar la composición mineral de todos pigmentos. El difractómetro utilizado es el modelo Philips PW-1710 con geometría Bragg-Brentano y rendija automática. Las condiciones de trabajo fueron las siguientes: radiación CuKα (λ = 1.5405Å), 40kV de voltaje y 40 mA de intensidad de corriente. El recorrido de barrido estuvo comprendido entre 3 y 60° en 2θ, siendo la velocidad de barrido del goniómetro de 0.01° 2θ s^{-1}. Previamente, se molieron los pigmentos finamente en un mortero de ágata hasta un tamaño de partícula inferior a 40 μm. La adquisición

automática de los datos y la evaluación e identificación de los minerales se realizó con el programa *Xpowder* (Martín-Ramos, 2004).

b) Microdifracción de Rayos-X (Micro X-Ray Diffraction, μ-XRD)

La Microdifracción de Rayos-X es una técnica no destructiva que permite el análisis directo de la composición mineralógica en un punto concreto de la muestra con alta precisión espacial. Es una técnica complementaria que proporciona información detallada de los minerales presentes en las muestras y permite identificar los pigmentos originales y los productos de alteración (Cardell et al., 2007; Duran et al., 2009; 2010a; 2010b).

En esta Tesis Doctoral, los análisis se han realizado directamente en las secciones delgadas pulidas de las muestras pictóricas tomadas del Palacio de la Madraza (Granada). Para ello se utilizó un difractómetro de Rayos-X diseñado y fabricado en el laboratorio del *Centre de Recherche et de Restauration des Musées de France del Louvre Museum (Paris, Francia)* durante una estancia predoctoral de la doctoranda en dicho Centro. Este μ-XRD está equipado con un tubo de rayos-X (*Rigaku MSC MicroMax micro-foco*) y un ánodo de cobre. El pequeño tamaño del haz de rayos-X (0.5 mm) permite analizar un área muy pequeña de la muestra. Para el registro de los patrones de difracción bidimensionales (2D) se usaron placas fotográficas (*image plate*). Los patrones de difracción 2D contienen información más detallada y completa de la mineralogía y microtextura de la muestra que los diagramas de difracción convencionales (Fig.3.12). Para el análisis mineralógico se convirtieron estos patrones 2D en difractogramas 2θ, análogos a los registrados con un difractómetro de polvo convencional, utilizando el programa informático *XRD2DScan* (Rodríguez-Navarro, 2006a; Rodríguez-Navarro et al., 2006b). Estos diagramas lineales se analizaron con los programas *Eva* y *XPowder* (Martín-Ramos, 2004) con los que se identificaron las fases minerales presentes. Para ello se utilizó la base de datos DPF-2 (ICDD, EE.UU.).

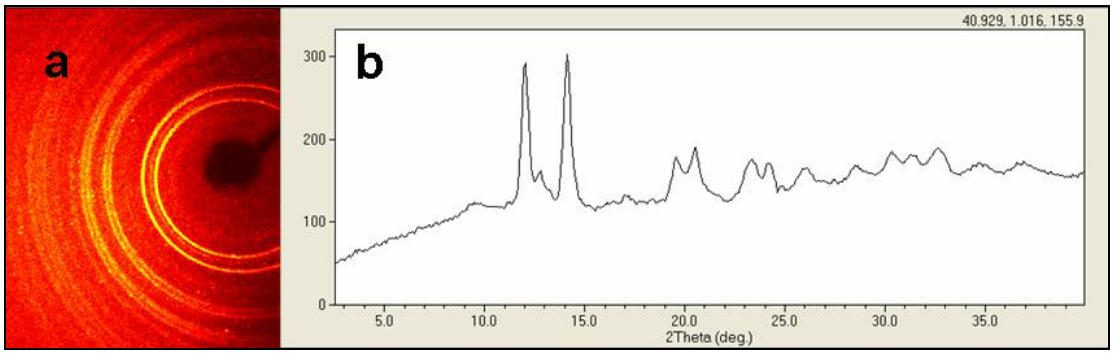

Fig. 3.12. Diagrama 2D y barrido 2θ calculado de un cinabrio.
(Imagen tomada de Cardell et al., 2007)

El uso de placas fotográficas permite la recopilación de datos de forma razonablemente rápida (10 minutos por cada punto de la muestra) con buena resolución angular (Duran et al. 2009; Duran et al., 2010a; 2010b). Los experimentos de μ-XRD se realizaron en el modo de reflexión con un ángulo de incidencia próxima a 10 grados. Se utilizó un colimador de 500 micras para limitar el tamaño del haz para el microanálisis. Para cada muestra, se realizaron análisis a lo largo de una línea de 1 mm y se tomaron las medidas cada 10 ó 50 ó 200 μm, desde la superficie de la estratigrafía hacia las capas inferiores. Sin embargo, debido al pequeño espesor de algunas capas (de c.a. 10 μm), las medidas no corresponden exactamente a capas individuales. No obstante, es posible obtener información muy útil sobre la evolución de la composición en función del espesor de la muestra (Duran et al. 2009; Duran et al., 2010a; 2010b).

Los patrones 2D constan de anillos de Debye-Scherrer y cada anillo corresponde a un conjunto específico de planos cristalográficos {hkl} de una fase mineral en particular (Fig. 3.13), formados por las reflexiones de los granos minerales iluminados por el haz de rayos-X orientados de tal de forma que cumplen la condición de la condición de difracción de la Ley de Bragg. De acuerdo a las características microtexturales de la muestra, los anillos muestran variaciones en la intensidad y continuidad. Así, para un tamaño fijo del haz de rayos-X, dependiendo del tamaño de granos minerales, el número de granos iluminados será más grande para los

materiales nano-o microcristalinos, y menor para granos minerales más gruesos. Por lo tanto, es posible obtener información microtextural de los pigmentos presentes en las muestras.

Específicamente, cuando se observan anillos irregulares constituidos por reflexiones aisladas, se puede deducir que el material mineral es escaso (Rodríguez-Navarro, 2006a, Rodríguez-Navarro et al., 2006b). Por otra parte, el número total de los picos (TNP) de un anillo es un indicador del número de granos que cumplen la condición de difracción, y del tamaño de dichos granos minerales. Otra de las características texturales obtenidas es la intensidad media de los picos (API) a lo largo de un anillo de Debye-Scherrer (Fig.3.13). Este dato se relaciona con el tamaño de los granos minerales. De hecho, la intensidad de estos picos es directamente proporcional al tamaño, lo cual permite cuantificar el tamaño de los granos minerales. Asimismo, esta técnica permite la cuantificación de los tamaños de grano de diferentes fases minerales presentes de manera independiente mediante el análisis de los anillos asociadas a cada mineral (Rodríguez-Navarro, 2006a, Rodríguez-Navarro et al., 2006b).

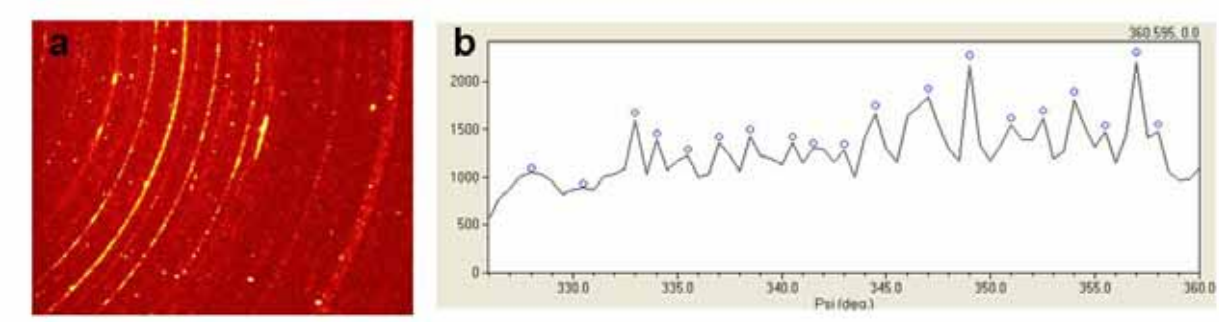

Fig. 3.13. a) Patrón de difracción 2D de una muestra de pintura mural; se observan anillos de Debye-Scherrer continuos y punteados. b) Perfil de intensidades correspondiente a un anillo de Debye-Scherrer.

3.2.3. Técnicas Microscópicas

a) Microscopía Óptica-Petrográfica (Optical Petrographic Microscopy, OM)

Los materiales pictóricos utilizados para la elaboración de réplicas de laboratorio, además de las muestras pictóricas reales se han examinado con un microscopio óptico petrográfico (Olympus BX60) perteneciente al Dpto. de Mineralogía y Petrología de la Universidad de Granada. El sistema está equipado con una cámara digital para el registro de microfotografías (Olympus DP10). El objetivo de usar esta técnica ha sido obtener una visión microscópica en detalle de los materiales pictóricos. Además, en el caso de las estratigrafías pictóricas es posible observar la disposición, morfología y color de las capas pictóricas. Para ello se ha utilizado un microscopio petrográfico de luz polarizada con luz transmitida y luz reflejada.

b) Microscopía Electrónica de Barrido con Microanálisis de Energía Dispersiva de Rayos-X (Scanning Electron Microscope with Energy-Dispersive X-Ray, SEM-EDX)

Esta técnica, disponible en el CIC, se ha aplicado para estudiar la composición química y las características texturales y morfológicas de las muestras pictóricas. Se ha utilizado un equipo *Inca 350 versión 17 Oxford* para análisis de electrones secundarios (SE) y retrodispersados (BSE). Ambos modos de trabajo son complementarios, ya que proporcionan información estructural y topográfica en el modo SE y composición elemental en el modo BSE. Las condiciones de trabajo han sido una corriente de 1.3nA, 20 eV/ch de resolución y un tiempo de adquisición de 50 s. Para este tipo de análisis la muestra no requiere preparación, sólo el montaje sobre un soporte y la metalización con carbono o con oro para fotografías de alta resolución (Manzano et al., 2000).

3.2.4. Técnicas de Espectrometría de Masas

a) Espectrometría de Masas de Desorción/Ionización asistida por Láser con Detector de Tiempo de Vuelo (Matrix-Assisted Laser Desorption/Ionization, Time of Flight Mass Spectrometry, MALDI-TOF MS)

Los análisis realizados mediante MALDI-TOF MS se realizaron en los laboratorios del Departamento de Química de la *Charles University* de Praga, Republica Checa) durante la estancia predoctoral de la doctoranda a dicho Centro. Para ello, se ha utilizado un espectrómetro de masas *(Bruker-Daltonics Biflex IV)* equipado con un láser de nitrógeno estándar (337 nm), en modo de reflexión. Se emitieron 200 pulsos de láser para cada espectro, utilizando el software *Xmass (Bruker)* para el registro de los espectros de masas. Antes de iniciar una sesión, se calibró el equipo con un estándar comercial de mezcla de péptidos *(Pepmix, Bruker)*.

Durante el proceso de medida de masas, los analitos cristalizados en una matriz apropiada se ionizaron mediante la acción de un láser. Esta fuente de ionización suele acoplar a un analizador de Tiempo de Vuelo (TOF, Time-of-Flight) en el que los iones se separan en función de su relación masa-carga. Para ello, a la salida de la fuente de ionización, los iones se aceleran por un campo eléctrico (ca. 30 kV) y llegan a una zona de deriva libre de campos. El voltaje de aceleración proporciona a todos los iones la misma energía cinética y, por lo tanto, distintas velocidades en función de sus relaciones masa-carga. Los iones más ligeros viajan a mayor velocidad a lo largo de la zona de deriva y llegan antes al detector, el cual registra los "tiempos de vuelo" de cada uno de los distintos iones. A partir de los tiempos de vuelo se determinan las relaciones masa-carga de los iones detectados y medidos por el espectrómetro de Masas.

Este tipo de Espectrometría de Masas se usó para el análisis de aglutinantes proteicos. En proteómica, está muy extendido el análisis de los aglutinantes

proteicos de alto peso molecular mediante técnicas tradicionales como HPLC o GC-MS, las cuales requieren una hidrólisis total y la identificación de aminoácidos liberados dada su complejidad (Marinach et al., 2004). En los últimos años, el uso de la espectrometría MALDI-TOF MS para estudiar obras del Patrimonio Pictórico ha supuesto un gran avance, pues permite identificar los diferentes aglutinantes proteicos usados tradicionalmente, así como sus procesos de degradación (Hynek et al., 2004). Estos análisis requieren un tratamiento previo de digestión mediante enzimas para fragmentar la proteína en pépticos conocidos. Las enzimas (normalmente tripsinas) se unen a la proteína sólo entre ciertos aminoácidos, fragmentándola (Ma et al., 2001). Los péptidos resultantes de esta fragmentación son característicos de cada proteína inicial y constituyen "una huella digital de masa" que permite la identificación fiable, mediante la comparación con espectros de masas de referencia (Kuckova et al., 2005, 2007). Hasta el momento, este método se ha utilizado principalmente para la caracterización de muestras pictóricas compuestas de material proteico. Sin embargo, esta técnica es de gran utilidad para estudiar el envejecimiento de materiales pictóricos frente a agentes de alteración (Kuckova et al., 2009).

b) Cromatografía de Gases con Detector de Masas (Gas Chromatography-Mass Spectroscopy, GC-MS).

Los análisis de masas mediante Cromatografía de Gases se han realizado con un espectrómetro de Masas *Plataform II* (*Micromass Instruments, Reino Unido*) acoplado a un cromatógrafo de gases *Carlo Erba 8060 (Thermo Instruments, EE.UU.,* disponible en el CIC. La GC-MS permite la separación de moléculas orgánicas en la columna del cromatógrafo que son analizadas y medidas conforme llegan al espectrómetro de masas. La GC-MS se ha utilizado en nuestro caso para identificar los compuestos orgánicos, en particular, la presencia de aceites secantes, ceras y/o barnices presentes en las muestras pictóricas reales.

La cantidad de muestra necesaria para este análisis es inferior a 5 mg. Cada muestra pictórica se disuelve en 25 ml de benceno, 25 ml de hidróxido de trimetil amonio (*m-trifluorometilfenilamonio) (Meth Prep II, Alltech),* y la mezcla se agita durante unos 40 minutos a temperatura ambiente. Es necesario un microlitro de esta solución para realizar el análisis mediante GC-MS. La columna capilar utilizada fue de sílice fundida (HP-5MS), siendo la fase estacionaria de 5% metilpolisiloxano fenil-95%, con 30 m. de longitud, 0.25 mm de diámetro y una película de 0.25 mm de espesor. El gas transportador fue helio a un caudal de 1.2 ml min^{-1}. Las muestras se inyectaron en el modo *splitless*. Los espectros de masas se registraron en el intervalo de masas desde 50 hasta 550 m/z y la generación de iones fue debida a una fuente de ionización por impacto de electrones a 70 eV, trabajando a una temperatura de la fuente de 210ºC. Por otro lado, la adquisición y procesado de datos se llevó a cabo con un sistema de *MassLynx v.4.0 datos* (Mills, 1966; Romero-Noguera et al., 2008).

3.3. Estudio multivariante de datos espectrales mediante Análisis de Componentes Principales

3.3.1. Pretratamiento matemático de datos espectrales

El Análisis de las Componentes Principales (PCA) requiere la manipulación previa de los datos espectrales para hacer más efectiva la extracción de información del análisis de las Componentes Principales.

En esta memoria de Tesis Doctoral se han realizado diferentes tipos de pretratamientos matemáticos de datos espectrales, e.g. suavizado de espectros, corrección de la línea base, conversión a escala logarítmica y de derivadas. En esta Tesis Doctoral la manipulación de dichos datos se realizó mediante *Excel 2000* (*Microsoft Corporation, EE.UU.*) y el programa de

acceso libre *Spectrum Viewer 2.1b*. Dependiendo de los datos espectrales analizados fue necesario uno o varios de estos tratamientos previos. En particular, el uso de las derivadas es un tratamiento bien conocido que permite eliminar información que no es relevante y que de otra manera dificultaría el análisis de los datos. Por otra parte, también se ha aplicado la operación de la segunda derivada para reducir la fluorescencia en los espectros Raman (O´Grady et al., 2001; Weis et al., 2004). Sin embargo, este último tratamiento tiene el inconveniente de reducir considerablemente la sensibilidad espectral. La primera derivada en algunos casos (espectros Raman) permite obtener datos espectrales de mayor resolución espectral que los originales (Kauffman et al., 2007).

En los diferentes estudios descritos en esta Memoria de Tesis Doctoral, la aplicación de logaritmos y primera derivada ha generado datos espectrales que proporcionaron un mejor reconocimiento y evaluación del análisis estadístico. En particular, los mejores resultados se obtuvieron con la aplicación de la primera derivada, ya que las bandas de vibración con mayor intensidad en los espectros originales fueron puntos singulares (x=0) en los espectros derivados, permitiendo reconocer con mayor facilidad las bandas de absorción más relevantes. Se denominan *puntos singulares ó estacionarios,* a los valores de la variable en los que se anula la derivada f´(x) de una función f(x), es decir, si f´(x)=0. En estos puntos, existen máximos relativos en la función f(x) (Fig.3.14). Esto proporciona una mayor resolución espectral a los datos utilizados en el análisis estadístico y permite discriminar mejor los cambios en la composición química y mineralógica de las muestras.

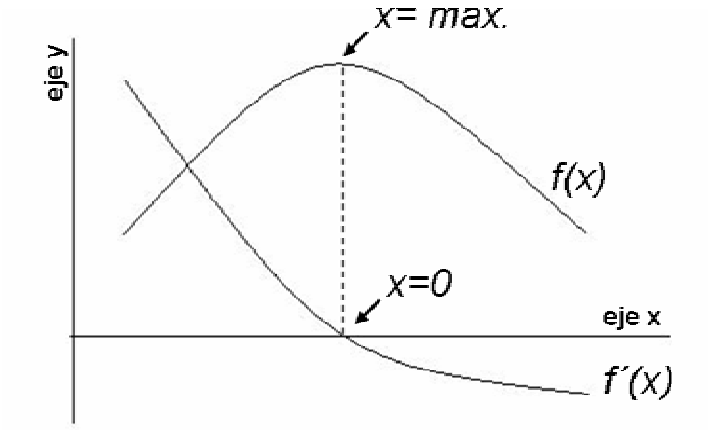

3.14. Representación gráfica para la función f(x) y su derivada f´(x).

3.3.2. Análisis de las Componentes Principales (Principal Component Analysis, PCA)

El PCA es una técnica estadística que permite la síntesis de la información. El método PCA puede encuadrarse dentro del conjunto de técnicas multivariantes. Esta técnica permite sintetizar un gran conjunto de datos y crear estructuras de interdependencia entre variables cuantitativas para crear unas nuevas variables que son función lineal de las originales, y de las que se puede hacer una representación gráfica (Fig.3.15) (Wold et al., 1987).

El objetivo del PCA es reducir la dimensión de un conjunto de p variables a un conjunto m, de menor número de variables, para facilitar la interpretación de los datos (Fig.3.15). Las nuevas variables, las componentes principales (*Principal Components, PC*), contienen lo esencial de las variables originales; ya que son una combinación lineal de ellas. Además tienen las siguientes propiedades: a) son ortogonales (cada componente representa una dirección del espacio de las variables originales); b) no están correlacionadas; c) la primera componente es la que más varianza contiene y la j-ésima tiene más varianza que la j-1 ésima...,d)

las primeras j componentes dan la solución de mínimos cuadrados del modelo:

$$y = ax + b \qquad \text{(Ec. 3.1)}$$

El PCA es una técnica estadística capaz de evaluar las capacidades instrumentales y analíticas de ciertas técnicas. Para datos analíticos se estima que el 95 % de la variabilidad debería ser explicada por dos o tres componentes principales. Si se cumple esto, existe un modelo estadístico que permita la interpretación de las nuevas variables (componentes principales) (Fig.3.15) (Johnson, 2000). El análisis de componentes sólo es apropiado en aquellos casos en que todas las variables son medidas en las mismas unidades y tienen varianzas con tamaño muy semejantes. Si una variable tiene una varianza mayor a las demás, dominará la primera componente principal sin importar la estructura de las covarianzas de las variables; por lo tanto, no se puede realizar el PCA. En este caso, sería más adecuado aplicar la matriz de correlación, para que todas las variables respuesta tengan la misma importancia (Jackson, 1991).

Matemáticamente si se dispone de una tabla de datos X_{np}, con n filas que corresponden al número de muestras y p columnas al número de variables, cada elemento x_{ij} de la matriz X es el valor que corresponde a la muestra i-ésima al medir sobre ella la variable j-ésima, X_j. Para facilitar la descripción formal de las componentes principales se supondrá que los datos de la matriz X están autoescalados. El autoescalado consiste en un centrado seguido de una normalización donde $x'_{i,m}$ es el dato autoescalado, $x_{i,m}$ es el dato antes del autoescalado, x_m la media de la columna m y s_m la desviación estándar de la columna m. De esta forma, la media y la varianza de las nuevas variables autoescaladas es de 0 y 1 respectivamente (Todeschini, 1998).

$$x'_{i,m} = \frac{x_{i,m} - \bar{x}_m}{s_m} \qquad \text{(Ec. 3.2)}$$

La primera componente principal (PC1) es una combinación lineal de las p variables X_j de modo que la proyección de los objetos sobre ella tenga la mayor varianza posible. La varianza es un parámetro adecuado para medir la elongación de la nube de puntos que forma los objetos al representarlos en un espacio de p dimensiones (Real-García, 2010). Formalmente se trata de encontrar los coeficientes a_{1j} j=1,...p tales que se alcance el máx(Var (PC1)) siendo:

$$PC1 = a_{11}X_{11} + a_{12}X_{12} + \ldots + a_{1p}X_p \qquad \text{(Ec. 3.3)}$$

con la restricción:

$$a^2_{11} + a^2_{12} + \ldots + a^2_{1p} = 1 \qquad \text{(Ec. 3.4)}$$

Esta restricción es necesaria para que la ecuación. 3.1 no conduzca a la obtención del máximo haciendo los coeficientes arbitrariamente grandes. Los coeficientes a_{1j} son los "loading" de la primera componente.

El valor de z_{i1}, "score", es el valor que para la muestra i-ésima toma la primera componente al sustituir en (Ec. 3.1) los valores de las p variables (x_{i1}, x_{i2},..., x_{ip}). Geométricamente en la proyección ortogonal sobre el eje determinado por la primera componente principal:

$$z_{i1} = a_{11}X_{11} + a_{12}X_{12} + \ldots + a_{1p}X_p \qquad \text{(Ec. 3.5)}$$

Así cada objeto tiene un valor sobre la primera componente principal; la varianza de las puntuaciones o scores es la varianza de la primera compones que se anota por Var (PC1) = I_1.

La segunda componente principal (PC2) se halla de modo similar, como una nueva combinación lineal de las variables originales (Real-García, 2010),

pero teniendo en cuenta que esta vez la mayor varianza explicada posible será la restante una vez considerada la primera de las componentes, max (Var (CP2)) siendo:

$$PC2= a_{21}X_{21} + a_{22}X_{22} +\ldots+a_{2p}X_p \qquad \text{(Ec. 3.6)}$$

con las restricciones:

$$a^2_{21} + a^2_{22} +\ldots+a^2_{2p}=1 \qquad \text{(Ec. 3.7)}$$

Las restricciones de la ecuación anterior obligan a que el vector formulado por los loadings sea ortonormal al vector del loading PC1 (Fig.3.16). Si el número de objetos n es menor que el de variable sólo se pondrá obtener n componentes ya que los datos están en un espacio de dimensión n. Para no complicar la notación introduciendo un nuevo índice supondremos que se tienen p componentes (Real-García, 2010).

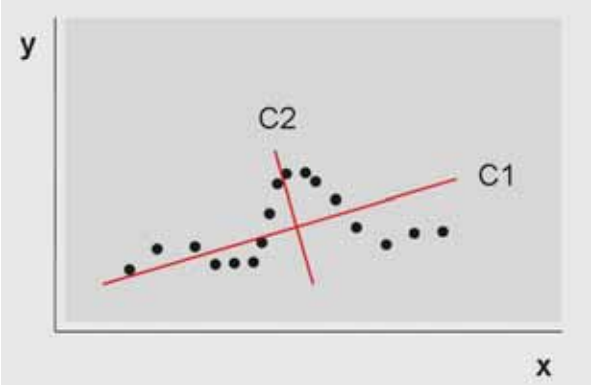

Fig. 3.15. Nuevo sistema de coordenadas ortogonales (C1 y C2).

En conjunto las PCs son unos nuevos ejes cartesiano en el espacio p dimensional en el eje j-ésimo es la componente PCj. Los escores de las muestras, es decir, las coordenadas de las muestras en estos ejes computados como en la ecuación (3.4) se agrupan como columnas de una matriz Z tal que:

$$Z_{np}=X_{np}A^t_{pp} \qquad \text{(Ec. 3.8)}$$

Cada fila de A_{pp} está formada por los loadings de la componente principal j-ésima. Esta matriz es ortogonal por lo que su inversión, (App)-1 coincide con su transpuesta A_{pp} pudiéndose transformar la ecuación 3.8 en:

$$X_{np}=Z_{np}A_{pp} \qquad \text{(Ec. 3.9)}$$

Donde X_{np} en la matriz de datos autoescalados descompuesta en Z_{np} (matriz de scores) y A_{pp} (matriz de loadings). La matriz de loadings da información acerca de la contribución de las variables originales a las componentes principales. Si los datos están autoescalados estos loadings son la correlación entre la variable y la componente (Real-García, 2010).

Si ponemos como ejemplo de técnica analítica la espectrometría de infrarrojos (IR), la señal espectral que se obtiene es el resultado de la interacción de la materia con la radiación IR. Para cada longitud de onda la muestra absorbe de forma diferente. Por tanto, el espectro de IR se puede expresar como (x_i, y_i), longitud de onda (x) y Absorbancia (y), los cuales se pueden representar gráficamente y observar como varía la absorbancia en función de la longitud de onda (Fig.3.16). Asimismo, podemos definir un nuevo sistema de coordenadas con el que representemos toda la información de los datos originales (x_i, y_i) y que, además, estos ejes de coordenadas sean ortogonales, como muestra la Figura 3.15. Los datos (x_i, y_i) puede ser representados de una manera tal que sus proyecciones sobre el nuevo primer eje de coordenadas recojan la mayor cantidad posible de variación (C1), y las proyecciones sobre el segundo eje recoja el resto de variación (C2).

La información de cada espectro que forma la matriz de datos se ve reducida a un punto, que se sitúa según su peso estadístico en una posición concreta en la proyección de las nuevas coordenadas C1 y C2. A estas nuevas coordenadas las llamaremos componentes principales, y a cada punto, *scores (S)*. Estos puntos *S* se obtienen de la representación del peso estadístico o *loading (L)* de cada valor de longitud de onda para cada nueva

componente principal. Por lo tanto, la matriz original de datos X, *siendo* $X = (x_i, y_i)$, es la combinación lineal de las nuevas coordenadas, y por tanto, se cumple: $X = S\ L^T$, donde L^T es la transpuesta de la matriz L.

En esta Tesis Doctoral, el PCA de los datos espectrales se ha realizado mediante el programa *Statistical Product and Service Solutions program* (*SPSS, para Window ver. 15, EE.UU.)*. Sin embargo, la preparación de las matrices de datos necesarias para el PCA se realizó empleando el programa *Excel 2003 (Microsoft Corporation, EE.UU.)*.

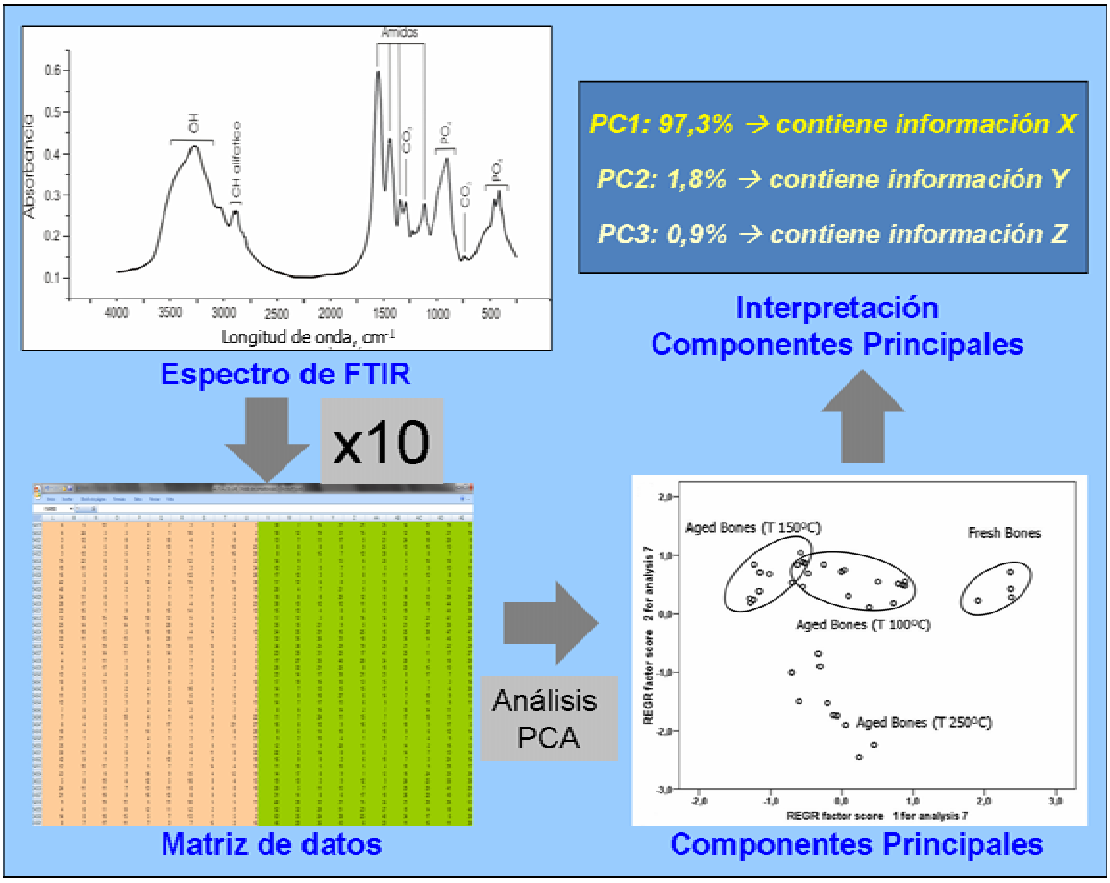

Fig.3.16. Esquema resumen del proceso de análisis de datos espectrales por PCA (Imagen espectro de FTIR tomada de Álvarez-Lloret, 2008).

3.4. Envejecimiento acelerado de réplicas pictóricas

a) Envejecimiento acelerado por radiación UV

Este tipo de ensayo se ha realizado empleando una cámara de envejecimiento acelerado por radiación UV, *Modelo Suntest CPS, Heraeus* (Hanau, Alemania) y equipada con una lámpara de Xenon, disponible en el Dpto. de Química Analítica de la Universidad de Granada. El filtro de UV empleado limita la radiación a 295 nm de longitud de onda. La irradiación se realizó a 765 $W.m^{-2}$ y el rango de temperaturas en las muestras estuvo a 30±5°C y una humedad relativa de 15±5% medido con un termohigrómetro *OREGON*, *modelo EMR812HGN* (Pórtland, Oregon, USA). (ANEXO I y II). Las réplicas pictóricas se expusieron a radiación UV por un máximo de 3000 horas, tiempo durante el cual se realizó un control periódico (ver capítulos 7 y 9).

b) Envejecimiento térmico acelerado.

Este tipo de ensayo se ha realizado sobre muestras de cuarzo/albúmina y de hueso natural pulverizado. Paralelamente, ambos tipos de muestras se dividieron en cuatro fracciones, las cuales sufrieron diferente tratamiento térmico, es decir, una fracción se reservó como muestra de control y no se le aplicó ningún proceso de alteración. Para las tres muestras cuarzo/albúmina restantes se realizó un calentamiento controlado de quince minutos a 150 º C, 200 º C y 250 º C, respectivamente. Para ello se ha hecho uso de una mufla *Termo Thermolyne Científico, mod. F4791026 (USA)* y de unos crisoles de porcelana para contener la muestra durante el proceso de calentamiento. Del mismo modo, el hueso en polvo se dividió en cuatro fracciones y se realizó el mismo proceso de calentamiento para tres de ellas. En este caso, las muestras de hueso pulverizado se calentaron a 100 º C, 150 º C y 250 º C, respectivamente. Una vez realizado el tratamiento térmico, las muestras se conservaron en viales *Eppendorf* etiquetados para su posterior análisis mediante ATR-FTIR (ver capítulo 8).

3.5. Referencias

Álvarez-Lloret P. (2008). Tesis Doctoral: "Alteración de la mineralización del hueso debida a la exposición a contaminantes". Departamento de Mineralogía y Petrología, Universidad de Granada. Granada.

Ballirano P., Maras A. (2006). Mineralogical characterization of the blue pigment of Michelangelo's fresco "The Last Judgment". Am. Mineral 91, 997–1005.

Bañares M. A., Ximena R. (1998). Instituto de Catálisis y Petroleoquímica (CSIC). Espectroscopía Raman. Memoria 1998. Madrid.

Barnett J.R., Miller S., Pearce E. (2006). Colour and art: A brief history of pigments. Opt. Laser Technol. 38, 445–453.

Baonza V.G., San Andrés M., Polo L., de la Rioja J.M., Sanz E. (2002). Análisis de pigmentos por microscopía Raman: Espectros Raman de referencia de algunos pigmentos de interés artístico. PH Boletín 38, 71–78.

Blee A.J., Walshe K., Pring A., Quinton J.S., Lenehan C.E. (2010). Towards the identification of plant and animal binders on Australian stone knives. Talanta 82, 745–750.

Borgia I., Brunettia B., Mariania I., Sgamellottia A., Cariati F., Fermob P., Mellinic M., Vitic C., Padelettid G. (2002). Heterogeneous distribution of metal nanocrystals in glazes of historical pottery. Appl. Surf. Sci. 185, 206–216.

Burgio L., Clark R. J.H. (2001). Library of FT-Raman spectra of pigments, minerals, pigment media and varnishes, and supplement to existing library of Raman spectra of pigments with visible excitation. Spectrochim. Acta A. 57, 1491–1521.

Cardell-Fernández C., Navarrete-Aguilera C. (2006). Pigment and plasterwork analyses of Nasrid polychromed lacework stucco in the Alhambra (Granada, Spain). Stud. Conserv. 51, 161–176.

Cardell C., J. Romero-Pastor, M. Bethencourt, A. Rodríguez-Navarro. (2007) Macla 7, 21–21.

Cardell C., Rodríguez-Simón L., Guerra I., Sánchez-Navas A. (2009a). Analysis of Nasrid polychrome carpentry at the hall of the Mexuar palace, Alhambra complex (Granada, Spain) combining microscopic, chromatographic and spectroscopic methods. Archaeom. 51, 637–657.

Cardell C., Guerra I., Romero-Pastor J., Cultrone G., Rodriguez-Navarro A. (2009b). Innovative Analytical Methodology Combining Micro-X-Ray Diffraction, Scanning Electron Microscopy-Based Mineral Maps, and Diffuse Reflectance Infrared Fourier Transform Spectroscopy to Characterize Archeological Artifacts. Anal. Chem. 81, 604–611.

Cruz-Cabrera J.P., Gómez-Moreno Calera J.M. (2007). Informe interno del Dpto de Historia del Arte. Universidad de Granada. Granada.

Johnson D. E. (2000). Métodos Multivariados Aplicados al Análisis de datos. International Thomson, México.

Daniilia S., Sotiropoulou S., Bikiaris, D. Salpistis C., Karagiannis G., Chryssoulakis Y., Price B. A., Carlson J. H. (2000). Panselinos' Byzantine wall paintings in the Protaton Church, Mount Athos, Greece: a technical examination. J. Cult. Herit. 1, 91–110.

Duran A., Pérez-Rodríguez J.L., Jiménez de Haro M.C. (2009). Study of the gilding technique used in polychromed stones and ceramics by dedicated laboratory-made micro X-ray diffraction and complementary techniques. Anal. Bioanal. Chem. 394, 1671–1677.

Duran A., Siguenza M.B., Franquelo M.L., Jimenez de Haro M.C., Justo A., Perez-Rodriguez J.L. (2010a). Murillo's paintings revealed by spectroscopic techniques and dedicated laboratory-made micro X-ray diffraction. Anal. Chim. Acta. 671, 1–8.

Duran A., Castaing J., Walter P. (2010b). X-ray diffraction studies of Pompeian wall paintings using synchrotron radiation and dedicated laboratory made systems. Appl. Phys. A. 99, 333–340.

Durán-Suárez J., García-Beltrán A., Rodríguez-Gordillo J. (1995). Colorimetric cataloguing of stone materials (biocalcarenite) and evaluation of the chromatic effects of different restoring agents. Sci. Total Environ. 167, 171–180.

Doerner, M. (2005). Los materiales de la pintura y su empleo en el arte. Ed. Reverté 6th edición. Barcelona.

Eastaugh N., Walsh V., Chaplin T., Siddall R. (2004). Pigment Compendium: A Dictionary of Historical Pigments. Butterworth-Heinemann, Oxford.

Edreira M.C., Feliu M.J., Fernández-Lorenzo C., Martín J. (2001). Roman wall paintings characterization from Cripta del Museo and Alcazaba in Mérida (Spain): chromatic, energy dispersive X-ray flurescence spectroscopic, X-ray diffraction and Fourier transform infrared spectroscopic analysis. Anal. Chim. Acta. 434, 331–345.

Escribano R. (1989). Sociedad Española de Óptica. Curso de Espectrometría Infrarroja por Transformada de Fourier. Universidad de Zaragoza. Jaca.

Froment F., Tournie A., Colomban P. (2008). Raman identification of natural red to yellow pigments: ochre and iron-containing ores. J. Raman Spectrosc. 39, 560–568.

García-Bueno A., Medina-Flores V. (2004) The Nasrid plasterwork at "qubba Dar al-Manjara l-kubra" in Granada: Characterisation of materials and techniques. J. Cult. Herit. 5, 75–89.

García Sánchez M.A. (1990). Manual de Espectrometría IR, Universidad Autónoma Metropolitana. Izlapalapa.

Gómez Moreno M. (1982). Guía de Granada, 1892. Ed. Facsímil. Universidad de Granada-Fundación Gómez-Moreno, Granada.

Heywood A. (2001). The use of huntite as a white pigment in Ancient Egypt. Colour and Painting in Ancient Egypt, British Museum Press, London.

Hradil D., Grygara T., Hradilova J., Bezdicka P. (2003). Clay and iron oxide pigments in the history of painting. Appl. Clay Sci. 22, 223–236.

Hynek R., Kuckova S., Hradilova J. (2004). Matrix-assisted laser desorption/ionization time-of-flight mass spectrometry as a tool for fast identification of protein binders in color layers of paintings. Rapid Commun., Mass Spectrom. 18, 1896–1900.

Jackson J. E. (1991). A User's Guide to Principal Components. John Wiley & Sons, Inc., New York.

Kauffman J. F., Dellibovi M., Cunninghamb C. R. (2007). Raman spectroscopy of coated pharmaceutical tablets and physical models for multivariate calibration to tablet coating thickness. J. Pharm. Biomed. Anal. 43, 39–48.

Kuckova S., Nemec I., Hynek R., Hradilova J., Grygar T. (2005), Analysis of organic colouring and binding components in colour layer of art Works. Anal. Bioanal. Chem. 382, 275–282.

Kuckova, R. Hynek, M. Kodicek. (2007). Identification of proteinaceous binders used in artworks by MALDI-TOF mass spectrometry Anal. Bioanal. Chem. 388, 201–206.

Kuckova S., Crhova M., Vankova L.; Hnizda A., Hynek R., Kodicek M. (2009). Towards proteomic analysis of milk proteins in historical building materials. Int. J. Mass Spectrom. 284, 42–46.

Le Blond S., Guilminot E., Lemoine G., Huet N., Mevellec J.Y. (2009). FT-Raman spectroscopy: A positive means of evaluating the impact of whale bone preservation treatment. Vib. Spectrosc. 51, 156–161.

Ma Y., Lu Y., Zeng H., Ron D. Mo W., Neubert T.A. (2001) Characterization of phosphopeptides from protein digests using matrix-assisted laser desorption/ionization time-of-flight mass spectrometry and nanoelectrospray quadrupole time-of-flight mass spectrometry. Rapid Comun. Mass Spectrom. 15, 1693–1700.

Manzano E., García-Bueno A., Gonzalez-Casado A., del Olmo M. (2000). Mortars, pigments and binding media of wall paintings in the 'Carrera del Darro' in Granada, Spain. J. Cult. Herit. 1, 19–28.

Marano D., Catalana I.M., Monno A. (2006). Pigment identification on "Pietà" of Barletta, example of Renaissance Apulian sculpture: A Raman microscopy study. Spectrochim. Acta A. 64, 1147–1150.

Marinach C., Papillon M.C., Pepe C., (2004). Identification of binding media in works of art by gas chromatography–mass spectrometry. J. Cult. Herit. 5, 231–240.

Martín-Ramos J.D. (2004) Using XPowder: A software package for Powder X-Ray diffraction analysis. (GR 1001/04. ISBN 84–609–1497–6).

Mayer R. (1988). Materiales y Técnicas del Arte. Hermann Blume. Madrid.

Mills J.S. (1966). The gas chromatographic examination of paint media. Part I: fatty acid composition and identification of dried oil films. Stud. Conserv. 11, 92–107.

O'Grady A., Dennis A. C., Denvir D., McGarvey J. J., Bell S. E. J. (2001). Quantitative Raman Spectroscopy of Highly Fluorescent Samples Using Pseudosecond Derivatives and Multivariate Analysis. Anal. Chem. 73, 2058–2065.

Pacheco F. (1990). El arte de la pintura. Cátedra, Madrid.

Pedrola A. (1998). Materiales, procedimientos y técnicas pictóricas. Ariel. Madrid.

Pérez-Alonso M., Castro K., Madariaga J.M. (2006). Investigation of degradation mechanisms by portable Raman spectroscopy and thermodynamic speciation: The wall painting of Santa María de Lemoniz (Basque Country, North of Spain). Anal. Chim. Acta. 571, 121–128.

Price M. (2000). A Renaissance of Colour: particle separation and preparation of azurite for use in oil painting. Leonardo. 33, 281–288.

Real-García B.D. (2010). Tesis Doctoral: "Optimización del funcionamiento de Procedimientos Analíticos en Cromatografía y Espectroscopía mediante el uso de Diseños de Experimentos y Quimiométricos". Departamento de Química. Área de Química Analítica. Universidad de Burgos.

Rodríguez-Navarro A.B. (2006a). XRD2DScan: new software for polycrystalline materials characterization using two-dimensional X-ray diffraction. J. Appl. Cryst. 39, 905–909.

Rodríguez-Navarro A.B., Alvarez-Lloret P., Ortega-Huertas M., Rodriguez-Gallego M. (2006b). Automatic Crystal Size Determination in the Micrometer

Range from Spotty X-Ray Diffraction Rings of Powder Sample. J. Am. Ceram. Soc. 89, 2232–2238.

Romero-Noguera, J.; Bolivar-Galiano, F. C.; Ramos-López, J. M.; Fernández-Vivas, M. A.; Martín-Sánchez. (2008). Study of biodeterioration of diterpenic varnishes used in art painting: Colophony and Venetian turpentine. I. Inter. Biodeter. Biodegr. 62, 427–433.

Sangrando R., Piazza R., Cairns W.R.L., Izzo F. C., Vianello A., Zendri E., Gambado A. (2010). Quantitative determination of un-derivatised amino acids in artistic mural paintings using high-performance liquid chromatography/electrospray ionization triple quadrupole mass spectrometry. Anal. Chim. Acta. 675, 1–7.

Scott D.A., Warmlander S., Mazurek J., Quirke S. (2009). Examination of some pigments, grounds and media from Egyptian cartonnage fragments in the Petrie Museum, University College London. J. Archaeol. Sci. 36, 923–932.

Silva C.E., Silva L.P., Edwards H.G.M., L. De Oliveira F.C., (2006). Diffuse reflection FTIR spectral database of dyes and pigments. Anal. Bioanal. Chem. 386, 2183–2191.

Todeschini, R. (1998). Introduzione alla Chimiometria. EdiSES, Napoli.

Vandenabeele P., Wehling B., Moens L., Edwards H., De Reu M., Van Hooydonk G. (2000). Analysis with micro-Raman spectroscopy of natural organic binding media and varnishes used in art. Anal. Chim. Acta. 407, 261–274.

Vandenabeele P., Castro K., Hargreaves M., Moens L., Madariaga J.M. (2007). Comparative study of mobile Raman instrumentation for art analysis. Anal. Chim. Acta. 588, 108–116.

Weis T. L., Jiang Y., Grant E. R. (2004). Toward the comprehensive spectrochemical imaging of painted works of art: a new instrumental approach. J. Raman Spectrosc. 35, 813–818.

Wold S., Esbensen K., Geladi P. (1987). Multi-Way Principal Components-and PLS Analysis. Chemom. Intell. Lab. Syst. 2, 41–56.

4. Beneficio del uso conjunto de DRIFT y PCA para el estudio de temples históricos azules

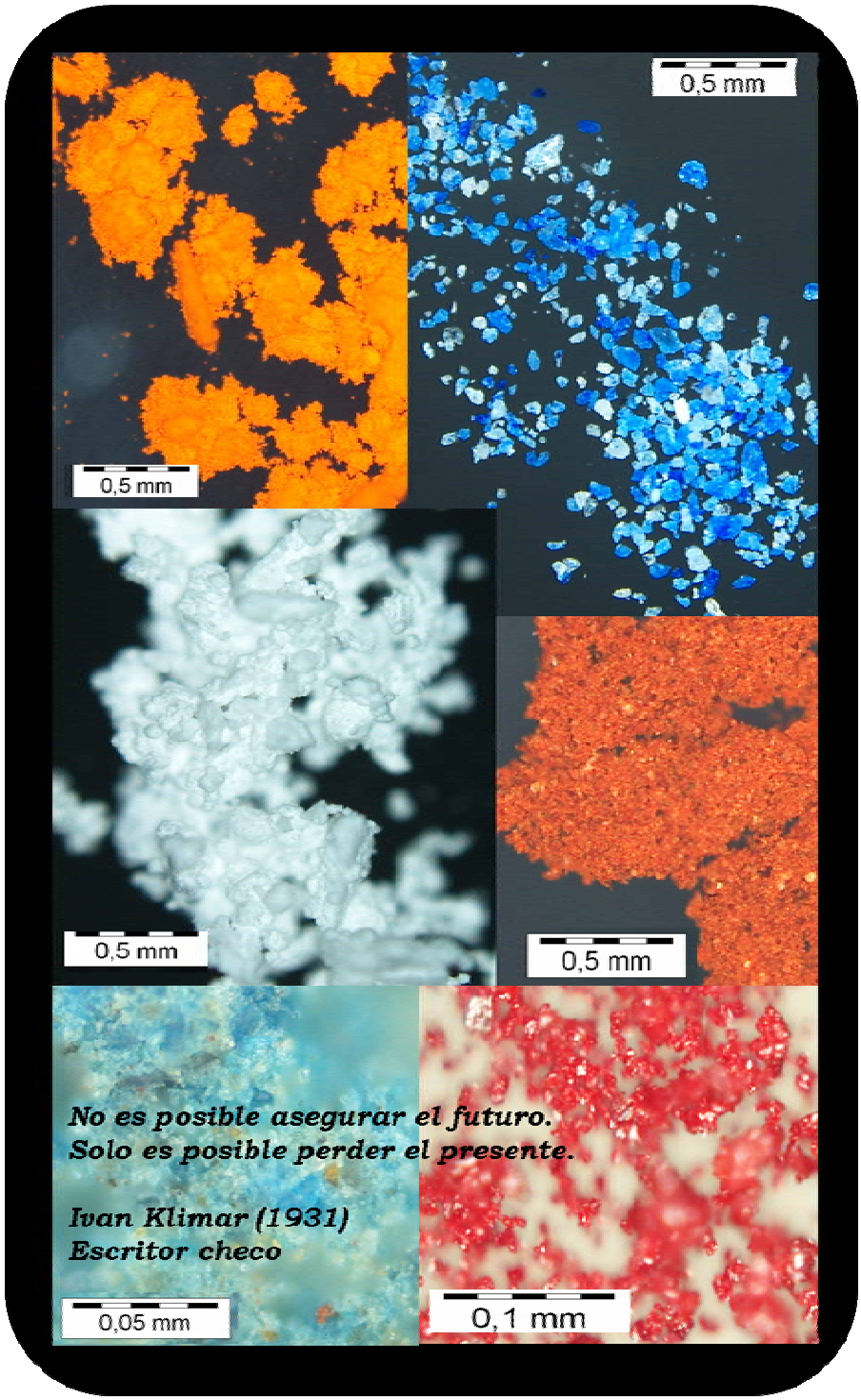

Benefits of applying combined diffuse reflectance FTIR spectroscopy and principal component analysis for the study of blue tempera historical painting. (2008). N. Navas, **J. Romero-Pastor**, E. Manzano, C. Cardell. Analytica Chimica Acta 630, 141–149.

Resumen

Un aspecto de gran interés en la investigación científica del Patrimonio Histórico-Artístico consiste en la puesta a punto de procedimientos y metodologías de análisis para el estudio de materiales pictóricos. Las técnicas analíticas no-destructivas o incluso técnicas que requieran la extracción de unas decenas de µg de muestra presentan importantes ventajas en el análisis de obras pictóricas. La Espectrometría Infrarroja con Transformada de Fourier en su modo Transmitancia (T-FTIR) se ha utilizado con frecuencia para el estudio simultáneo de materiales pictóricos inorgánicos y orgánicos, p. ej. pigmentos y aglutinantes. No obstante, limitaciones relacionadas con la cantidad de muestra necesaria para preparar la pastilla de BrK, el tamaño de partícula y los efectos negativos sobre la línea base del espectro son algunas desventajas de esta técnica cuando se emplea para la caracterización de muestras pictóricas. Una alternativa es la Espectrometría Infrarroja con Transformada de Fourier en modo Reflectancia, en concreto, la medida de la reflectancia difusa, conocida como DRIFT. En el análisis mediante DRIFT se requiere menor cantidad de muestra (~ 5 - 10 µg), y se realiza directamente sobre la muestra en polvo mezclada con BrK, lo que supone una notable ventaja en el análisis de muestras pictóricas. No obstante, ha sido una técnica poco utilizada en el estudio de materiales pictóricos.

Este capítulo evalúa la aplicación de ambas técnicas de FTIR en el análisis de réplicas pictóricas de pigmentos históricos azules, tanto puros como de sus temples azules de cola. Este trabajo se centra principalmente en las ventajas del análisis multivariante mediante PCA de los datos espectrales obtenidos por DRIFT. Se han analizado tanto réplicas pictóricas puras, esto es pigmentos puros (azurita, lapislázuli y esmalte) y aglutinante puro (cola de conejo), como las mezclas pigmento-aglutinante (temples de cola). En este Capítulo 4 se discuten comparativamente los resultados del análisis visual de los espectros así como la ventaja del empleo del análisis multivariante de los datos espectroscópicos obtenidos por T-FTIR y DRIFT. Los resultados muestran la complementariedad de ambas técnicas de FTIR en el estudio y caracterización de materiales pictóricos, y una mejor capacidad del PCA en la discriminación de réplicas pictóricas de acuerdo a su diferente composición. De hecho, se

pudo discriminar entre los pigmentos azurita, lapislázuli y esmalte puros, sus temples de cola y muestras de cola pura.

ANALYTICA CHIMICA ACTA 630 (2008) 141–149

available at www.sciencedirect.com

ScienceDirect

journal homepage: www.elsevier.com/locate/aca

Benefits of applying combined diffuse reflectance FTIR spectroscopy and principal component analysis for the study of blue tempera historical painting

Natalia Navas[a,*], *Julia Romero-Pastor*[b], *Eloisa Manzano*[a], *Carolina Cardell*[b]

[a] *Dept. of Analytical Chemistry, University of Granada, Fuentenueva s/n, 18071 Granada, Spain*
[b] *Dept. of Mineralogy and Petrology, University of Granada, Fuentenueva s/n, 18071 Granada, Spain*

ARTICLE INFO

Article history:
Received 26 June 2008
Received in revised form
29 September 2008
Accepted 2 October 2008
Published on line 14 October 2008

Keywords:
Diffuse reflectance infrared Fourier transform spectroscopy
Transmittance-spectroscopy
Principal component analysis
Blue tempera paintings
Painting heritage conservation

ABSTRACT

This paper explores the application of diffuse reflectance infrared Fourier transform spectroscopy (DRIFTS) to the examination of historic blue pigments and blue tempera paintings commonly found on works of art. The discussion is mainly focused on the practical benefits of using this technique joined to principal component analysis (PCA), a powerful multivariate analysis tool. Thanks to the study of several replica samples that contain either pure blue pigments (azurite, lapis lazuli and smalt), or pure binder (rabbit glue) and mixtures of each of the pigments with the binder (*tempera* samples), different aspects of these benefits are highlighted. Comparative results of direct spectra and multivariate analysis using transmittance-Fourier transform infrared spectroscopy (T-FTIR) are discussed throughout this study. Results showed an excellent ability of PCA on DRIFT spectra for discriminating replica samples according to differing composition. Several IR regions were tested with this aim; the fingerprint IR region exhibited the best ability for successfully clustering the samples. The presence of the binder was also discriminated. Only using this approach it was possible to completely separate all the studied replica samples. This demonstrates the potential benefits of this approach in identifying historical pigments and binders for conservation and restoration purposes in the field of Cultural Heritage.

1. Introduction

Scientific study of artwork is of interest in order to test the suitability of analytical techniques on matrices different from those classically examined. Historical paintings are often heterogeneous microlayered materials made of complex mixtures of inorganic and organic compounds applied on diverse supports, as for instance stone, canvas, wood and paper. Since ancient times, painters have tried out a variety of organic materials to mix with inorganic pigments. These components can be simultaneously present in different layers of paint stratigraphy, making the recognition of paint constituents a difficult challenge for chemists [1–3]. The identification of pigments and binders when mixed is one of the most important tasks in the field of painting heritage, in order to establish suitable actions for both restoration and conservation and allow proper preservation.

Spectroscopic techniques offer great potential to solve many of the problems associated with the characterisation of the materials constituting works of art. Fourier transform infrared spectroscopy in its traditional mode of transmittance (T-FTIR) is particularly important because of the variety

* *Corresponding author*. Tel.: +34 958 243388; fax: +34 958 243328.
E-mail address: natalia@ugr.es (N. Navas).
0003-2670/$ – see front matter © 2008 Elsevier B.V. All rights reserved.
doi:10.1016/j.aca.2008.10.008

of information contained in the spectra – i.e. data of both organic and inorganic compounds – and because of its variety of possibilities for sample measurements. Therefore, T-FTIR spectroscopy has become one of the most important analytical techniques in the field of Cultural Heritage [4,5]. In addition, it is a reasonable low cost technique compared with other analytical methods. However, T-FTIR has limitations related to particle size (when minerals are present) and the negative effect on spectrum baseline. On the other hand, sampling restrictions imposed in artworks limit the amount of sample to work with, which in the particular case of T-FTIR technique makes it difficult to prepare the pellet and to acquire a standard spectrum. In the case of composite materials like ancient paintings, the interpretation of the T-FTIR spectra may be extremely arduous to resolve. By contrast, interesting results could be achieved by analysing the specimen in reflectance mode (diffuse reflectance infrared Fourier transform (DRIFT) spectroscopy) though at present this technique has been scarcely used in Cultural Heritage [6] contrary to other scientific fields [7–9]. Recently, reflectance spectroscopy in the UV–visible region has shown to be useful for environmental monitoring conditions in museums [10,11].

DRIFTS refers to a particular FTIR sampling technique based on reflectance measurements [12]. The increasing application of DRIFTS is related to the development of optical devices using special attachments for standard spectrometers [13]. This technique is particularly useful in the investigations of powdered samples. Moreover, it is accepted to be a very low impact method since only a very small quantity of powdered sample is needed (~5–10 μg) unlike the T-FTIR mode (~30–50 μg) [14]. This makes it very attractive in the field of Painting Cultural Heritage, where non-destructive techniques and/or micro-destructive techniques are preferred. Nevertheless, in the specialised literature only one article has been found regarding the application of DRIFT spectroscopy to characterise paintings components, providing a diffuse reflectance FTIR spectral database of 25 dyes and pigments [6]. Thus, the present work represents an advance in this research field, since for the first time a study of the application of factorial analysis such as principal component analysis (PCA) is used to compare T-FTIR and DRIFTS spectral data obtained from historical pigments and binders. Application of chemometrics tools for the characterisation and conservation of Cultural Heritage is a well-established procedure [15]. Several works have recently demonstrated the usefulness of these approaches for calibrations [16], ageing detection [17–19], classification [20,21], and dating purposes [22].

This paper describes the benefits of using DRIFT spectroscopy versus T-FTIR spectroscopy, each joined with PCA as a tool in Heritage Science. Three blue pigments, i.e. azurite ($Cu_3(CO_3)_2(OH)_2$), lapis lazuli ($Na_6Ca_2(Al_6Si_6O_{24})S_2$) and smalt (Co-K silicate glass), and rabbit glue as binder (proteinaceous medium) were selected to carry out this study since they have been widely used through historical epochs. Seven replicate samples, i.e. pure pigment samples, pure glue sample and pigment/glue mixture samples (*tempera* samples), were prepared and measured with both molecular vibrational techniques, i.e. T-FTIR and DRIFT, which allowed direct evaluation of the obtained spectral data. Comparative discussion of the direct spectra obtained by both spectroscopic modes is discussed throughout this work. PCA was performed separately on the spectral data from both FTIR modes to evaluate the capability of this multivariate tool to discriminate between different sample compositions. Only when the PCA was performed on the spectral data from DRIFT, it was possible to successfully discriminate all replicate samples by their composition.

2. Experimental

2.1. Reagents

Reagents were chosen based on their widespread use through history, in particular during the Middle Ages and Renaissance. Azurite is a non-expensive hydrated copper carbonate mineral of composition $Cu_3(CO_3)_2(OH)_2$. It was the most important pigment in European paintings until near the end of the 17th century. Azurite has a bright blue colour that sometimes resembles lapis lazuli, and the two were often confused [23]. In addition to azurite, by far the most important blue in the Middle Ages was lapis lazuli. This vivid rich blue pigment is made by grinding the semi-precious rock lapis lazuli whose main constituent is the mineral lazurite ($Na_{8-10}Al_6Si_6O_{24}S_{2-4}$). The first noted use of the stone as pigment was in 6th- and 7th-century AD cave paintings in Afghan temples. Lapis lazuli pigment found its most extensive use in 14th and 15th centuries, illuminating manuscripts and Italian panel paintings, often reserved for the cloaks of Christ and the Virgin. It is famous for having been the most expensive pigment [23]. Smalt is an artificial pigment made of fine to coarsely ground potassium cobalt glass. The blue colour is due to small amounts of cobalt added as cobalt oxide during manufacture. Since ancient times, smalt was used to colour and decorate glasses, though powdered cobalt glass was also employed as pigment. Smalt was an important pigment in European oil paintings. In Italy it was little used in the 14th and 15th centuries but became a substitute for azurite and lapis lazuli in the 17th century [24].

The azurite and smalt pigments were purchased from Kremer Pigments GmbH & Co. KG (Madrid, Spain). Pigment references are: 10,200 natural azurite (CI: PB 30.77420) with particle size 0–120 μm, and 10,010 blue smalt (CI: PB 32.77365) with particle size 0–80 μm. The lapis lazuli was supplied by Caremi Pigmentos (Sevilla, Spain). Pigment reference is natural Lapis lazuli Afghanistan, medium blue.

The standard protein binder selected was rabbit skin glue (collagen). This binder has been used since ancient times, mostly in traditional woodworking, gilding and paintings due to its high strength, viscosity and elasticity. It was purchased from Sigma (Barcelona, Spain).

Potassium bromide was used as a non-absorbing reference material for the spectroscopic background measurement. It was purchased from Merck (Damstadt, Germany).

2.2. Replica samples

Seven painting replica samples were prepared to emulate real paint layers according to old master recipes to obtain standards similar to those used by medieval artists [25]. The first, second and third replicas comprise each of the three pure pig-

Table 1 – Replica sample composition.

Replica sample	Binder	Pigment
Pure samples		
1	–	Azurite
2	–	Lapis lazuli
3	–	Smalt
4	Rabbit glue	–
Tempera samples		
5	Rabbit glue	Azurite
6	Rabbit glue	Lapis lazuli
7	Rabbit glue	Smalt

ments (azurite, lapis lazuli and smalt), and the fourth replica the pure rabbit glue binder (Table 1). Preparation of the pure pigment samples was as follows: 5 g of powder pigment was formed as a crater-shaped mass and six drops of pure water (total volume of 30 μL) were added until a dense paste was attained. Then, four layers of the obtained paste were sequentially spread out with a paintbrush in fine coats on a glass slide. Each layer needs to dry thoroughly before applying the next. This is the traditional way to obtain an opaque painted layer and to guarantee full luminosity of the colour, otherwise it immediately appears dead. The pure binder sample (fourth replica) was prepared as follows: 10 g of rabbit glue was diluted 10% in ultra pure water (MILIQ) by gently adding the glue to the water during 24 h, and stirring periodically. Next the obtained blend was gradually heated in a bain-marie below 50 °C to obtain a homogeneous mixture. Then the glue was carefully spread on a glass slide with a paintbrush in six successive fine coats, each applied after the previous layer had dried to a constant weight using a gel air dryer system.

The fifth, sixth and seventh replicas include mixtures between glue and each of the pure pigments, i.e. azurite, lapis lazuli and smalt, thus blue tempera replicate samples were obtained. They were prepared by blending the pigment with the glue – both components elaborated as above – in a ratio 5.2:1 (w/v) (Table 1). Next, mixtures were spread on glass slides in three fine coats. This procedure was adapted to emulate real paint layers as found in ancient paintings. *Tempera* is a painting method in which finely ground pigments are mixed with a solidifying proteinaceous binding agent, such as egg, animal glue and casein [26]. Well known from antiquity, *tempera* was the exclusive panel medium in the Middle Ages and the early Renaissance, and in Italy it was not supplanted by oil until *ca.*1500.

2.3. *Instrument and software*

The FTIR spectra were collected using a NICOLET spectrometer 20SXB, working in transmission mode (T-FTIR) and diffuse reflectance mode (DRIFT). The instrument was connected to a Pentium 200 and the instrument software was OMNIC v 4.1, running under Windows 2000 Professional (Microsoft Corporation, USA).

The T-FTIR spectra were registered from 3999 to 400 cm^{-1} with a resolution of 2 cm^{-1} and 200 scans. Each replica sample was characterised by 10 T-FTIR spectra, except the pure glue replica sample (25 T-FTIR spectra). These spectra were obtained from KBr pellets prepared by homogeneously mixing aliquots removed from seven random locations on the glass slide (KBr in 1%). In this way, T-FTIR spectra were independent from the position where the powder micro-sample was taken from the glass slide. Baseline correction was performed in all T-FTIR spectra.

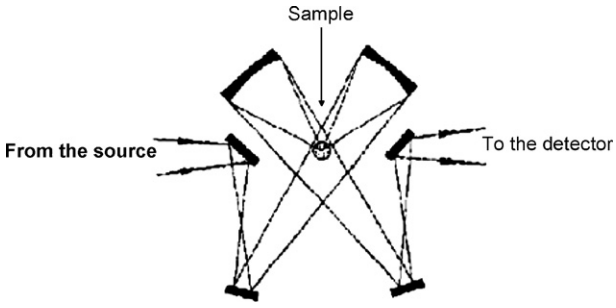

Fig. 1 – Sample compartment and optical accessories for measuring diffuse reflection in the spectroscopic equipment.

In order to better discriminate the Fresnel reflectance, the SPECTRA-TECH attachment Model COLLECTOR (Sutton, Surrey, England, SM1 1TH) was used to measure the diffuse reflectance in the FTIR spectrometer. This optical accessory uses a focusing mirror to collimate the beam on the sample surface and collect the IR energy (Fig. 1). Aliquots were also taken from seven random places from each replica sample and later mixed with the potassium bromide used as diluent and for the background spectra. The mixture (5% in KBr) was placed in a micro-sample cup (3 mm diameter). In this case, the sample consumed in the preparation of the KBr medium is reduced compare to that required for T-FTIR analysis, using only 1–5 μg of powder sample. For comparison purposes, DRIFTS spectra were scanned at the same experimental conditions (resolving power 2 cm^{-1} and 200 scans) as in transmission mode. Likewise each replica sample was characterised by 10 DRIFT spectra, except for pure glue replica sample (25 DRIFT spectra). These spectra were converted to Kubelka–Munk units [12].

Chemometric data analysis was done using Statistical Product and Service Solutions program (SPSS, for Windows Ver. 15, USA) and Excel 2000 (Microsoft Corporation, USA).

3. Results and discussion

3.1. *Direct spectrometric analysis*

Scientific examination and comparative investigation of historical pigments in the laboratory is fundamental to further analyse and understand real painted artworks, in addition to be of particular usefulness for conservators. Furthermore, knowledge of the properties of ancient pigments and their response and sensitivity to specific spectroscopic methods are relevant in Science Heritage. In this context, the three blue pigments, i.e. azurite, lapis lazuli and smalt were investigated by means of diffuse reflectance infrared spectroscopy (DRIFTS) and transmittance Fourier transform infrared spectroscopy for comparison purposes.

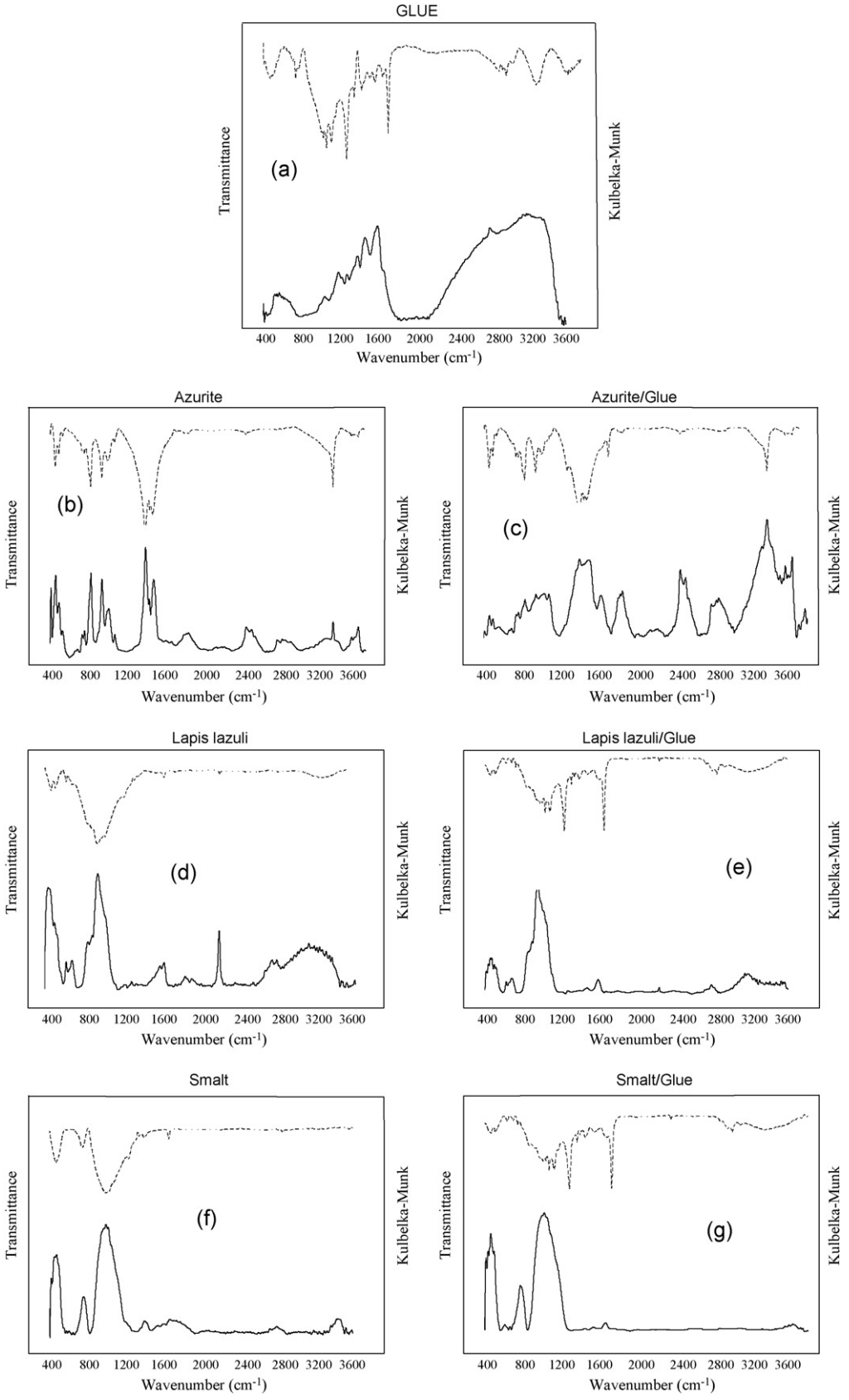

Fig. 2 – DRIFT (*lower*) and T-FTIR (*upper*) spectra of the seven replica samples: (a) pure glue (collagen), (b) pure azurite, (c) azurite/glue, (d) pure lapis lazuli, (e) lapis lazuli/glue, (f) pure smalt, and (g) smalt/glue.

Table 2 – Main IR absorption bands of the blue pigments and their temperas for identifications purposes.

Replica sample	Description	Vibrational wavenumber (cm^{-1})	
		T-FTIR	DRIFT
Pure rabbit glue	Collagen	700 (δ (NH) wagging band) 1290 (amide band II) 1730 (amide band I) 3310 (N–H stretching mode)	680, 3000 [31]
Pure azurite	$Cu_3(CO_3)_2(OH)_2$	840 (carbonate stretching [28]) 1430 (carbonate stretching [28])	840 (as in T-FTIR) 1430 (as in T-FTIR)
Azurite/rabbit glue	$Cu_3(CO_3)_2(OH)_2$/collagen	840 (carbonate stretching [28]) 1430 (carbonate stretching [28])	840 (as in T-FTIR) 1430 (as in T-FTIR) 1890, 2510, 2890
Pure lapis lazuli	$Na_{8-10}Al_6Si_6O_{24}S_{2-4}$	460 (O–Si–O deformation mode [29,30]) 990 (O–Si–O anti-symmetric stretching mode [29,30])	460 (as in T-FTIR) 990 (as in T-FTIR)
Lapis lazuli/rabbit glue	$Na_{8-10}Al_6Si_6O_{24}S_{2-4}$/collagen	460 (O–Si–O deformation mode [29,30]) 990 (O–Si–O anti-symmetric stretching mode [29,30]) 1290 (amide band II) 1730 (amide band I)	460 (as in T-FTIR) 990 (as in T-FTIR)
Pure smalt	Potassium silicate glass with some cobalt oxide	480 (O–Si–O deformation mode [29,30]) 1030 (O–Si–O anti-symmetric stretching mode [29,30])	480 (as in T-FTIR) 1030 (as in T-FTIR)
Smalt/rabbit glue	Potassium silicate glass with some cobalt oxide/collagen	480 (O–Si–O deformation mode [29,30]) 1030 (O–Si–O anti-symmetric stretching mode [29,30]) 1290 (amide band II) 1730 (amide band I)	480 (as in T-FTIR) 1030 (as in T-FTIR)

Fig. 2 shows simultaneously both the DRIFT (lower) and the T-FTIR (upper) spectra of the seven replica samples. The main vibrational wavenumbers observed in all these spectra are recorded in Table 2.

For the replica samples studied in the present work, the comparison of the DRIFT spectra with the T-FTIR in terms of baseline shows no clear advantage of one technique over the other, since the quality of both type of spectra were similar for both pure replica samples and tempera replica samples. The position of the absorption bands was also similar in DRIFT and T-FTIR spectra, except in the case of pure glue replica sample. However, the relative intensity of the bands was clearly different, being more intense in the case of DRIFT spectra, particularly the secondary absorption bands [27]. This characteristic of DRIFT spectra, i.e. the most prominent vibrational bands, reveals this technique more suitable for purposes of identification and characterisation of pigments, both when pure or mixed with binder.

Specifically, pure azurite presents bands at 1430 and 840 cm^{-1} that can be assigned to carbonate stretching [28] and a band at 3430 cm^{-1} related to the O–H stretching mode (Fig. 2b). Pure lapis lazuli and pure smalt present two prominent and specific bands that can be used as markers for the silicate group [29,30]. The observed bands at 460 and 480 cm^{-1} respectively are related to the (O–Si–O) deformation mode, whereas the bands at 990 cm^{-1} (lapis lazuli) and 1030 cm^{-1} (smalt) are assigned to the (Si–O–Si) anti-symmetric stretching mode.

DRIFT and T-FTIR spectra for the pure glue replica samples were not entirely complementary (Fig. 2a). T-FTIR showed a prominent amide band I at 1730 cm^{-1} and the combined N–H deformation and C–N stretching vibration, the amide II of the secondary amides, at 1290 cm^{-1} [31]. The band at 3310 cm^{-1} was assigned to the N–H stretching modes. In addition, there is a very wide δ (NH) wagging band at around 700 cm^{-1}. DRIFT spectra showed two wide bands in accordance with previous work [31] located at around 1680 and 3200 cm^{-1}.

The presence of glue in the replica pigment samples introduced several changes in both types of spectra, DRIFT and T-FTIR. The T-FTIR spectra of azurite when pure or mixed with glue were similar, with only a small band at 1730 cm^{-1} (the amide band I) indicating the presence of the binder. Lapis lazuli and smalt glue tempera samples can be distinguished from their corresponding pure replica samples by the amide bands I and II in the T-FTIR spectra (1730 and 1290 cm^{-1}, respectively) attributed to the presence of glue. These bands were not detected in the corresponding DRIFT spectra. By visual examination of the lapis lazuli and smalt DRIFT spectra – the two silicate-based pigments – it was not possible to distinguish the presence of glue in the replica samples. In the case of azurite, the presence of glue in the replica sample could be detected mainly by means of the DRIFT spectra, since bands at around 1890, 2510, 2890 and 3430 cm^{-1} increased their relative intensity with respect to the corresponding DRIFT spectra of the pure azurite samples.

Consistent with these results, direct analysis of the spectra obtained by the two spectroscopic FTIR modes showed that DRIFT spectra better identify pigments, both when pure or mixed with binder. This ability was also extended to the identification of the glue when mixed with azurite. This information

is relevant since it will permit further investigation of the azurite/glue interaction by DRIFT spectra. Nevertheless in the case of the silicate-based pigments (lapis and smalt), T-FTIR better identified the presence of glue. As is usual in Heritage Science due to the complexity of the samples analysed, a combination of analytical techniques provides better and more complete information [32].

3.2. PCA analysis on DRIFT and T-FTIR spectroscopic data

Chemometric evaluation of spectral data is well accepted as a powerful tool for different purposes, including sample identification and recognition [33]. Among the different chemometric tools, PCA is a powerful data-mining technique that reduces data dimensionality obtaining more interpretable representation of the system under investigation [34,35]. In addition, valuable information about the most important variables involved in the process studied is also obtained.

In this work aimed at evaluating the ability to extract information from DRIFT and T-FTIR spectral data, PCA was performed separately on each. Thus, a matrix was built for each type of spectral data, DRIFT and T-FTIR, which includes the seven replica samples. In this way, for multivariate analysis each matrix was formed by 85 IR spectra, since each sample was characterised by 10 FT-IR and 10 DRIFT spectra (except pure glue replica samples characterised by 25 spectra of each IR mode). The PCs were obtained using both the covariance data matrices (scaling by mean-centered data) and the correlation data matrixes (scaling by unit variance). Similar to previous work [19,36], results were better when PCA was performed on correlation data matrices, so the results shown and discussed here correspond to autoscaled data. A simple centring data procedure is often adopted for spectral data [18,37] because the commonly applied autoscaling procedure assigns the same relevance to each IR spectral region. Thus spectral regions with small variation – no relevant IR bands – can acquire the same importance as large IR bands related to important functional groups. This problem was avoided in this work because only IR regions containing absorption bands were selected to apply PCA (not the whole IR spectrum). The IR regions selected to perform the multivariate analysis are shown in Table 3. PCA was performed independently on these IR regions. The fingerprint IR region was tested due to its unique absorption pattern for every sample. The wavenumber interval 2100–3600 cm^{-1} was chosen according to results from previous work [19,36]. These studies found this IR region quite informative when glue was present in the replica samples, thus it was also tested in the present work. The other IR regions were selected from a visual examination of the IR spectra obtained with both T-FTIR and DRIFT, where an absorption band was observed.

Table 3 – IR regions studied by PCA.

IR intervals (cm^{-1})	
600–1200	Fingerprint
1200–2000	Azurite band
2100–2700	Azurite band, lapis lazuli band
2100–3600	Glue most informative IR region[a]

[a] From previous work [19,36].

The highest quality information for the two FTIR modes was obtained using the IR region in the wavenumber interval 600–1200 cm^{-1}, the fingerprint region. The main absorption bands of the two silicate-based pigments (lapis and smalt) are also found here. PCA on the wavenumber interval 1200–2000 cm^{-1} allowed separation according to chemical class, that is, glue, azurite (pure and mixed with glue) and the silicate-based pigments (pure and mixed with glue). This result is justified since absorption bands of azurite that separate this pigment from the others compounds are found in this IR region. The wavenumber interval 2100–2700 cm^{-1} also separated the replica samples, although less clearly, despite containing information on the absorption bands of azurite and lapis lazuli. The last IR region tested, 2100–3600 cm^{-1}, showed the ability to separate replica samples, but again less clearly than the fingerprint region. The results of the corresponding PCA in terms of explained variance (%) and cumulative explained variance (%) for each FTIR mode, and for the two IR regions with the best ability to discriminate samples are shown in Table 4.

The results obtained by applying PCA separately on the DRIFT and T-FTIR spectral data in the fingerprint region are summarised in Figs. 3 and 4. These figures show the score plot

Table 4 – PCA performed on DRIFT and T-FTIR spectral data.

IR region	PC	DRIFT		T-FTIR	
		Variance account (%)	Variance accumulated (%)	Variance account (%)	Variance accumulated (%)
600–1200 cm^{-1}	PC1	59.3	59.3	58.1	58.1
	PC2	23.0	82.4	34.3	92.4
	PC3	13.0	95.4	4.0	96.4
	PC4	2.4	97.8	2.0	98.4
	PC5	1.1	98.9	0.9	99.3
2900–3600 cm^{-1}	PC1	58.9	58.9	47.4	47.4
	PC2	21.5	80.4	25.2	72.6
	PC3	9.9	90.4	11.1	83.6
	PC4	6.0	96.4	6.6	90.2
	PC5	1.5	97.9	5.2	95.4

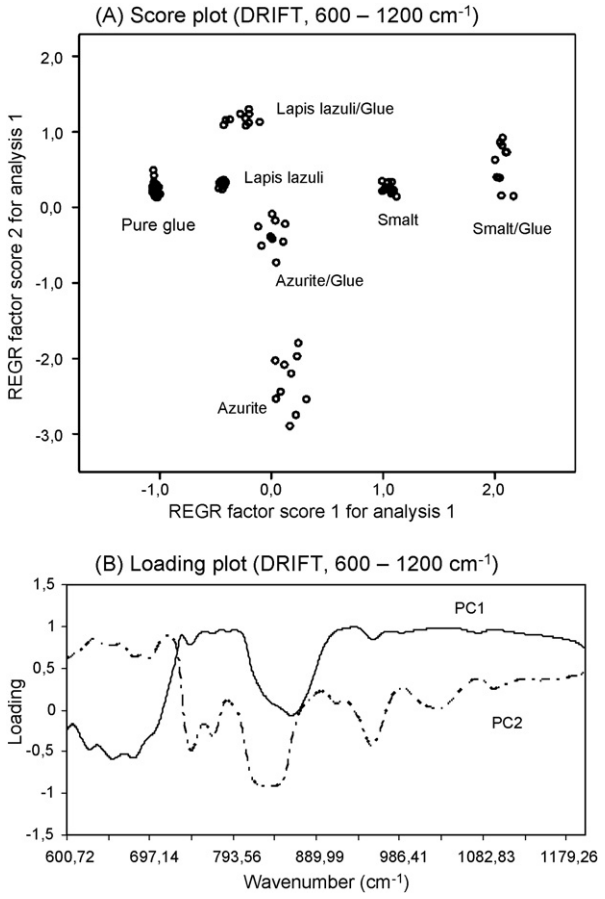

Fig. 3 – Results of the PCA performed on the DRIFT spectral data using the IR wavenumber interval 400–1200 cm^{-1} (fingerprint): (A) score plot (DRIFT, 600–1200 cm^{-1}) of PC1 and PC2; (B) loading plot (DRIFT, 600–1200 cm^{-1}) of PC1 and PC2.

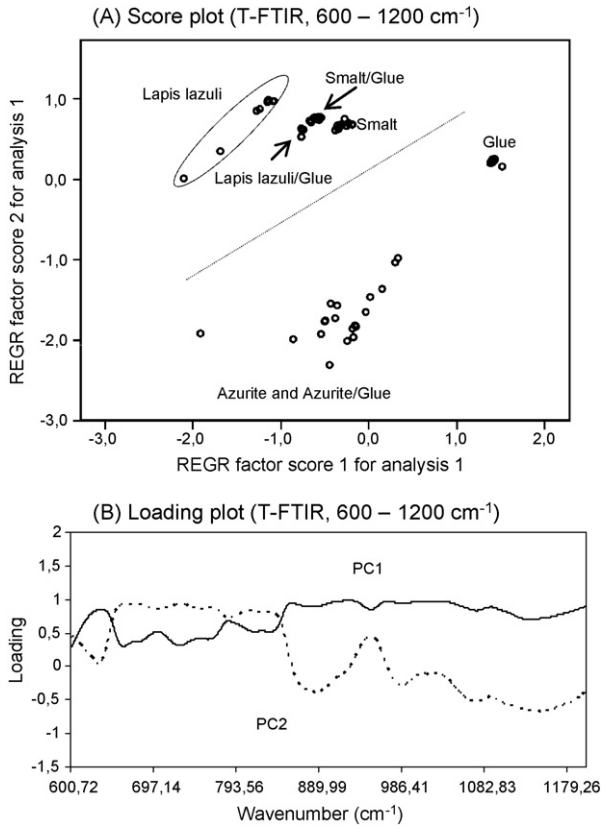

Fig. 4 – Results of the PCA performed on the T-FTIR spectral using the IR wavenumber interval 400–1200 cm^{-1} (fingerprint): (A) score plot (T-FTIR, 600–1200 cm^{-1}) of PC1 and PC2; (B) loading plot (T-FTIR, 600–1200 cm^{-1}) of PC1 and PC2.

of all the replica samples in the plane of the two first principal components, PC1 and PC2. The loading plot of the two first PCs is also included for each spectroscopy mode.

In the case of DRIFT spectral data (Fig. 3), seven clusters were clearly distinguished, according to replica sample composition. The score plot shows the most positive values on PC1 for smalt/glue replica samples, followed by pure smalt, with the most negative values for glue replica samples. The lapis lazuli/glue sample scored highest for PC2, followed by pure lapis lazuli, with the most negative scores for pure azurite. These results, combined with the analysis of the loading plot, suggested that the spectral variability explained by PC1 (59.3% of the total variance) was mainly related to the presence of the pigment smalt in the replica sample. The main absorption band of the smalt pigment was located in the wavenumber interval with the highest loading values for PC1 (900–1200 cm^{-1}), as well as its characteristic absorption band at 780 cm^{-1} (734–806 cm^{-1}). This behaviour of the replica samples allowed separation of the smalt pigment from its mixture with glue, since the presence of glue increased the absorption bands in those regions. In contrast pure glue exhibited the smallest absorption in those IR regions. The loadings for PC2 (23% of the total variance) indicated that a large fraction of spectral variability was due to the spectral region 600–734 cm^{-1}, where an absorption band of lapis lazuli at 660 cm^{-1} was located. Again, the presence of glue in the replica samples produces an increment of the characteristic absorption bands of the silicate-based pigment lapis lazuli, and this fact was correlated with the highest scores for PC2 for this replica sample. Therefore, it was possible to perfectly group replica samples of lapis lazuli with and without glue in two well-separated clusters. The pure azurite replicate samples presented the most negative score for this PC2. The negative loadings for the wavenumber interval 820–852 cm^{-1} suggested that the absorption band of azurite at 840 cm^{-1} determined separation along this PC2. In the case of azurite, the presence of glue in the replica samples decreased the absorption in this IR band, with scores shifted to more positive values.

In a similar way, PCA was performed on the T-FTIR spectral data, to evaluate whether the difference due to the diverse sample composition could be detected as in the case of DRIFT spectral data. Fig. 4 shows clearly a lesser capability of this approach to discriminate sample composition since five clusters instead of seven were distinguished in the score plot in the plane of the two first PCs (92.4% of the total variance). The replicate samples containing azurite (pure or mixed with glue) were separated from glue and from a cluster formed by all replica samples containing silicate-based pigments (pure or

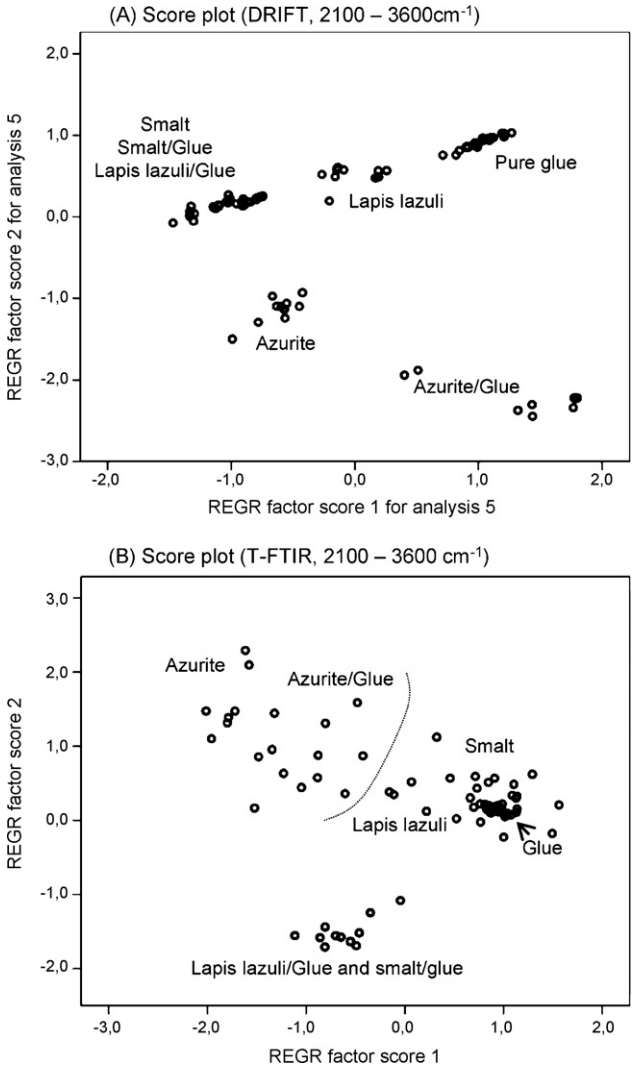

Fig. 5 – Score plot of PC1 and PC2 of the replica samples using the IR region between 2100 and 3600 cm^{-1}: (A) DRIFT spectral data, score plot (DRIFT, 2100–3600 cm^{-1}); (B) T-FTIR spectral data, score plot (T-FTIR, 2100–3600 cm^{-1}).

mixed with glue). An in-depth analysis of this cluster showed the separation of the pure lapis lazuli and pure smalt samples. Nevertheless when glue was present in the sample, the two silicate-based pigments were not distinguished. In addition, the loading values for PC1 were quite similar, making their interpretation difficult.

The results of applying this approach in the other IR region previously cited were less conclusive, particularly when the T-FTIR spectral data were used. As an example, Fig. 5B represents the scores of the first two relevant PCs for both FTIR modes in the wavenumber interval 2100–3600 cm^{-1}. The capability of clustering samples by composition was again clearly better when DRIFT data were used (Fig. 5A). In this case, samples were grouped in five clusters: pure azurite, azurite/glue, pure glue, pure lapis lazuli and a cluster containing pure smalt, smalt/glue and lapis lazuli/glue. In the score plot for the T-FTIR data, only replicate samples containing glue mixed with the silicate-based pigments (lapis lazuli and smalt) were clearly separated from the rest of the samples that grouped in a large cluster. The distribution of the samples in this cluster was as follows: pure azurite with the most negative scores for PC1, azurite/glue samples were shifted to more positive values, and pure smalt, pure lapis lazuli and pure glue had the highest scores. Thus, only PCA performed on DRIFT spectral data in the fingerprint region enabled the discrimination of all replicate samples.

Based on these results, it can be concluded that the application of PCA to DRIFT spectra represents an improvement over the same approach using T-FTIR. The presence of the most prominent vibrational bands in the DRIFT spectra, in addition to permitting direct analysis for identification purpose, also benefits the application of data exploration techniques like PCA.

4. Conclusions

For the conservator concerned with the identification of materials, concretely blue pigments and their corresponding temperas, PCA performed on DRIFT spectral data has marked advantages when compared the results obtained with the same approach but using T-FTIR spectral data. Multivariate analysis of DRIFT data demonstrated better ability to discriminate replica samples according to known composition. Moreover, it was possible to group in different clusters samples that differed only in terms of the presence of glue. This is the first attempt to use this approach in Heritage Science, and the results are very promising to identify pigments and temperas used in historical paintings.

Regarding direct analysis of DRIFT and T-FTIR spectra, the complementary use of both spectroscopic modes are highly recommended. Pigment identification in art paintings will certainly benefit from the use of DRIFT spectra since these are easier to interpret. The presence of glue in tempera can be confirmed by the occurrence of several characteristics absorption bands in the corresponding T-FTIR spectra.

Acknowledgements

Financial support for this work was provided by Spanish Science Ministry Projects BHA2003-08671 and HUM-2006-09262/ARTE, the Andalusian Research Group RNM-179, and a research contract from the Junta de Andalucía awarded to C. Cardell. We wish to thank A. Kowalski for English revision.

REFERENCES

[1] A. Nevin, I. Osticioli, D. Anglos, A. Burnstock, S. Cather, E. Castellucci, Anal. Chem. 79 (2007) 6143.
[2] D. Lau, C. Villis, S. Furman, M. Livett, Anal. Chim. Acta 610 (2008) 15.
[3] C. Cardell, L. Rodríguez-Simón, I. Guerra, A. Sánchez-Navas, Archaeometry, doi:10.1111/j.1475-4754.2008.00438.x, in press.
[4] G. Bitossi, R. Giorgi, M. Mauro, B. Salvadori, L. Dei, Appl. Spectrosc. Rev. 40 (2005) 187.
[5] K. Castro, A. Sarmiento, E. Princi, M. Pérez-Alonso, M.D. Rodríguez-Laso, S. Vicini, J.M. Madariaga, E. Pedemonte, Trends Anal. Chem. 26 (2007) 347.

[6] C.E. Silva, L.P. Siva, H.G.M. Edwards, L.F.C. De Oliveira, Anal. Bioanal. Chem. 386 (2006) 2183.
[7] M. Mecozzi, E. Pietrantonio, Mar. Chem. 101 (2006) 27.
[8] O. Carmody, J. Kristof, R.L. Frost, E. Mako, J.T. Kloprogge, S. Kokot, J. Colloid Interface Sci. 287 (2005) 43.
[9] K. Poellaenen, A. Haekkinen, S. Reinikainen, J. Rantanen, M. Karjalainen, M. Louhi-Kultanen, L. Nystroem, J. Pharmaceut. Biomed. 38 (2005) 275.
[10] M. Bacci, C. Cucci, A.L. Dupont, B. Lavédrine, M. Piccolo, S. Porcinai, Environ. Sci. Technol. 37 (2003) 5687.
[11] M. Bacci, C. Cucci, M. Piccolo, S. Porcinai, B. Radicati, Environ. Sci. Technol. 34 (2000) 2865.
[12] D.E. Leyden, R.S.S. Murthy, Trends Anal. Chem. 7 (1988) 164.
[13] M. Hrebicík, G. Budínová, T. Godarská, D. Vlácil, S.B. Vogenseh, K. Volka, J. Mol. Struct. 410–411 (1997) 527.
[14] H. Gunzler, H. Gremlich, IR Spectroscopy, Wiley, VCH, Germany, 2002.
[15] G. Musumarra, M. Fichera, Chemom. Intell. Lab. Syst. 44 (1998) 363.
[16] E. Marengo, M.C. Liparota, E. Robotti, M. Bobba, Anal. Chim. Acta 553 (2005) 111.
[17] E. Marengo, E. Robotti, M.C. Liparota, M.C. Gennaro, Anal. Chem. 75 (2003) 5567.
[18] E. Robotti, M. Bobba, A. Panepinto, E. Marengo, Anal. Bioanal. Chem. 388 (2007) 1249.
[19] E. Manzano, J. Romero, N. Navas, A. García-Beltrán, L. Rodríguez-Simón, C. Cardell, Anal. Bioanal. Chem., submitted for publication.
[20] A. Jurado-López, M.D. Luque de Castro, Anal. Bioanal. Chem. 380 (2004) 706.
[21] R. Checa-Moreno, E. Manzano, G. Mirón, L.F. Capitán-Vallvey, Talanta 75 (2008) 697.
[22] T. Trafela, M. Strlic, J. Kolar, D.A. Lichtblau, M. Anders, D.P. Mencigar, B. Pihlar, Anal. Chem. 79 (2007) 6319.
[23] N. Eastaugh, V. Walsh, T. Chaplin, R. Siddall, Pigment Compendium. A Dictionary of Historical Pigments, Butterworth-Heineman, Oxford (England), 2004.
[24] J.R. Barnett, S. Miller, E. Pearce, Opt. Laser Technol. 38 (2006) 445.
[25] F. Pacheco in El arte de la pintura, Ed. Cátedra, Madrid, Spain, 1990.
[26] L. Masschelein-Kleiner, Ancient Binding Media, Varnishes and Adhesives, ICCROM, Rome, Italy, 1995.
[27] D.A. Skoog, F.J. Holler, T.A. Nieman, Principles of Instrumental Analysis, 5th ed., McGrawHill, Madrid, Spain, 1992, p. 451.
[28] G.W. Taylor, Stud. Conserv. 28 (1983) 153.
[29] N.B. Colthup, L.H. Daly, S.E. Wiberley, Introduction to Infrared and Raman Spectroscopy, 3rd ed., Academic, San Diego, CA, USA, 1990.
[30] L.J.R. Marshall, J.R. Williams, M.J. Almond, S.D.M. Atkinson, S.R. Cook, W. Matthews, J.L. Mortimore, Spectrochim. Acta A 61 (2005) 233.
[31] W. Kautek, S. Penzien, A. Conradi, D. Leichtfried, L. Puchinger, J. Cult. Heritage 4 (2003) 179s.
[32] V. Desnica, K. Furic, B. Hochleitner, M. Mantler, Spectrochim. Acta B 58 (2003) 681.
[33] P. Geladi, B. Sethson, J. Nystroem, T. Lillhonga, T. Lestander, J. Burger, Spectrochim. Acta B 59 (2004) 1347.
[34] S. Wold, K. Esbensen, P. Geladi, Chemom. Intell. Lab. Syst. 2 (1987) 37.
[35] J.E. Jackson, A User's Guide to Principal Components, John Wiley & Sons Inc., New York, 1991.
[36] E. Manzano, N. Navas, R. Checa-Moreno, L. Rodríguez-Simón, L.F. Capitán Vallvey, Talanta, submitted for publication.
[37] D.L. Massart, B.G.M. Vanderginste, S.N. Deming, Y. Micotte, L. Kaufman, Chemometrics: A Textbook, Elsevier, Amsterdam, Holland, 1988.

Conclusiones

Uno de los resultados a destacar de este trabajo proviene del examen visual de los espectros obtenidos mediante DRIFT y T-FTIR que pone de manifiesto la complementariedad de la información obtenida en las muestras pictóricas por ambas técnicas. Por una parte, la caracterización del pigmento en las réplicas pictóricas se realiza con mayor eficacia mediante el empleo de la técnica DRIFT, ya que proporciona espectros más definidos, con bandas de absorción más intensas que los espectros obtenidos por T-FTIR. En cambio, la presencia de bandas de T-FTIR características y bien definidas debidas al material proteico (cola de conejo) en las réplicas pictóricas, hace que esta otra técnica proporcione mayores ventajas a la hora de la identificación de dicho material en las réplicas de temples azules de cola. En concreto, se observa como las bandas de absorción secundarias en las réplicas de cola pura registradas mediante DRIFT son de menor intensidad que las obtenidas mediante T-FTIR.

En cuanto al análisis multivariante, este ha sido más eficaz en el caso de los espectros DRIFT y especialmente en la región espectral correspondiente a la huella dactilar, i.e. 600 - 1200 cm^{-1}. El PCA de datos DRIFT y T-FTIR se ha realizado por separado y en dos regiones espectrales diferentes, concretamente entre 600 - 1200 cm^{-1} (huella dactilar -*fingerprint*-) y entre 2100 - 3600 cm^{-1}. La primera se eligió por sus características de huella dactilar, y la segunda por proporcionar bandas relacionadas con el material proteico. El PCA realizado con datos espectrales registrados mediante DRIFT ha mostrado ventajas cuando se comparan los resultados obtenidos con el mismo procedimiento pero utilizando datos espectrales de T-FTIR. En particular, los resultados obtenidos mediante el PCA de espectros registrados mediante DRIFT en la región comprendida entre 600-1200 cm^{-1} permite una mejor discriminación de las réplicas pictóricas estudiadas, separándose en grupos diferentes en función de su composición (azurita, lapislázuli y esmalte puros, cola pura y sus correspondientes temples de cola). Esto puede ser atribuido a que en dicha región espectral se localizan las bandas características de los pigmentos estudiados. Sin embargo, el mismo estudio realizado con los datos T-FTIR no separa entre si las réplicas pictóricas de lapislázuli, esmalte y temple de

esmalte, así como las réplicas pictóricas que contiene azurita. No es por tanto capaz de discriminar todas las muestras en función de su composición.

Por otra parte, los resultados obtenidos en la región del espectro entre 2100 y 3600 cm^{-1} para ambos modos de trabajo, DRIFT y T-FTIR, son similares, no consiguiéndose una separación de todas las réplicas pictóricas en función de su composición, aunque los resultados fueron siempre sensiblemente mejores cuando se emplearon espectros registrados mediante DRIFT. Por lo tanto, se puede concluir que la región espectral con mayor capacidad para la discriminación de las réplicas pictóricas azules estudiadas es la comprendida entre 600 - 1200 cm^{-1}.

5. Discriminación de pigmentos y temples mediante espectros Raman derivados y PCA

Raman spectroscopic discrimination of pigments and tempera paint model samples by Principal Component Analysis on first-derivative spectra. (2010). N. Navas, **J. Romero-Pastor**, E. Manzano, C. Cardell. J. Raman Spectroscopy 41, 1486–1493.

Resumen

Continuando con el objetivo de poner a punto procedimientos y metodologías de análisis para el estudio de materiales pictóricos, este trabajo se centra en el estudio de réplicas pictóricas mediante el empleo de PCA de datos espectrales registrados mediante Microscopía Raman (RM). Dichas réplicas pictóricas se han elaborado a partir de pigmentos históricos blancos (blanco de plomo, calcita y yeso), azules (azurita, lapislázuli y esmalte) y rojos (cinabrio, minio y *Sienna*). Además, se han preparado réplicas puras de yema de huevo y sus correspondientes mezclas con cada pigmento, mediante recetas tradicionales de temples de huevo.

El estudio quimiométrico –PCA- de los datos espectrales se ha realizado de forma independiente para cada grupo de muestras (blancos, azules y rojos), incluyendo en cada caso los datos espectrales de las réplicas puras de yema de huevo. Previo al PCA, ha sido necesario llevar a cabo un estudio para seleccionar el pre-tratamiento matemático de los datos espectrales -diferente al usual centrado o autoescalado- más idóneo para una posterior aplicación del análisis multivariante. Concretamente, se ha evaluado la idoneidad de emplear el logaritmo o la primera derivada de los espectros Raman. A partir de los resultados obtenidos, se propone el empleo de la primera derivada, ya que tiene la ventaja de hacer más eficiente el reconocimiento de las muestras mediante PCA, pues permite poner de manifiesto pequeñas diferencias no reconocibles en los espectros Raman originales. No obstante, el PCA de los espectros Raman (sin derivar), aún no siendo totalmente eficaz en la discriminación de las muestras pictóricas en función de su composición, si ha mostrado capacidad para la detección de alteraciones de pigmentos, como el ocurrido con el minio por acción del láser durante la adquisición del correspondiente espectro Raman.

Research Article

Journal of RAMAN SPECTROSCOPY

Received: 14 September 2009 Accepted: 7 February 2010 Published online in Wiley Online Library: 26 March 2010

(wileyonlinelibrary.com) DOI 10.1002/jrs.2646

Raman spectroscopic discrimination of pigments and tempera paint model samples by principal component analysis on first-derivative spectra†

Natalia Navas,[a]* Julia Romero-Pastor,[b] Eloisa Manzano[a] and Carolina Cardell[b]

This work explores the application of principal component analysis (PCA) on first-derivative Raman spectra to investigate historical tempera paint model samples. Various paint model samples were prepared containing pure blue pigments (azurite, lapis lazuli and smalt), pure red pigments (cinnabar, minium and raw Sienna), pure white pigments (lead white, chalk and gypsum), pure egg yolk as binder and tempera model samples obtained by mixing each of the pigments with the binder, and further characterized by Raman spectroscopy. The corresponding Raman spectra were used to apply PCA in order to test whether spectral differences allowed discrimination of samples based on their composition. Multivariate analyses were performed separately on three data matrices, one for each color, namely, white, blue and red, corresponding to the model samples, and all containing the spectral data of the binder model sample. Different pretreatments, that is log and derivative spectra, were performed on the spectra since no pattern distributions were obtained when the original Raman spectra were analyzed. Nevertheless, the multivariate analysis of the original Raman spectra was able to track alterations of sensitive pigments due to laser interaction. Results showed the excellent ability of PCA, when applied to the derived Raman spectra, to discriminate model samples according to their differing compositions in the three groups of model samples tested. This is the first attempt to use this approach in the field of cultural heritage and demonstrates the potential benefits for identifying historical pigments and binders for purposes of conservation and restoration.

Keywords: historical painting; micro-Raman spectroscopy; principal component analysis; first-derivative spectra

Introduction

At present, Raman microscopy (RM) is considered a well-established analytical technique to characterize artworks and their degradation products, providing valuable data for diagnostic information, preservation and restoration of artistic objects.[1] In fact, RM has become one of the most widely used techniques to study painting materials both organic (varnishes, binders and dyes)[2–4] and inorganic (pigments and extenders).[5–8] This is due to the high spatial resolution and accuracy of RM, which in addition provides rapid, reliable and specific results regarding both inorganic and organic components in the same sample.[9,10]

Ancient paintings are complex, composite materials made up of heterogeneous mixtures of organic and inorganic components.[11–13] Thus, Raman spectral interpretation of these materials can be a challenging task. Most previous studies on characterization of model and historical paintings are based on separate and independent analyses of the different painting components, because of sample complexity.[5–8] In fact, problems arise when the identification of individual components (pigments or binders) in mixtures is attempted[14] since few studies have addressed both binders and pigments simultaneously.[9,10] To solve this problem, mathematical methods are applied to facilitate the study of the spectral contributions from different components of a mixture.[14–17]

The development of mathematical operations on spectra such as derivatives is a well-known procedure. In the case of Raman spectroscopy, the use of second derivatives to reduce the fluorescence in the spectra is frequent,[18,19] although this method has the limitation of reducing band sensitivity. First-derivative Raman spectra followed by principal component regression was also proposed for multivariate calibration of coating thickness in pharmaceutical tablets.[20] Micro-Raman spectroscopy, combined with several chemometric techniques, has also been applied to differentiate between synthetic and natural indigo samples.[21] In this last work, the best discrimination of the samples was obtained by principal component analysis (PCA) before applying linear discriminant analysis to the second-derivative Raman spectra. PCA on Raman spectra was also used for the study of ceramics and glasses, but cluster variation approaches appeared to be

* *Correspondence to: Natalia Navas, Department of Analytical Chemistry, University of Granada, Fuentenueva s/n, 18071 Granada, Spain. E-mail: natalia@ugr.es*

† *Paper published as part of the Art and Archaeology 2009 special issue.*

a *Department of Analytical Chemistry, University of Granada, 18071 Granada, Spain*

b *Department of Mineralogy and Petrology, University of Granada, 18071 Granada, Spain*

more efficient.[22] However, to the authors' knowledge the use of first-derivative Raman spectra with PCA has not been reported in the study of complex, ancient painting materials.

In recent years, chemometric techniques have been used increasingly in the field of cultural heritage since they can extract information from correlated data, such as spectroscopic sets.[23] Nowadays, chemometric evaluation of spectral data is well accepted as a powerful tool for different purposes, including sample identification and recognition.[24] Among the different chemometric tools, PCA is a powerful data-mining technique that reduces data dimensionality and provides a more interpretable representation of the system under investigation.[25,26] In addition, valuable information is also obtained about the most important variables involved in the process of interest. The benefits of applying combined diffuse reflectance infrared Fourier transform spectroscopy (DRIFTS) and PCA for identifying historical pigments and binders were highlighted recently.[16] A similar approach using Fourier transform infrared spectral data was applied to study the UV ageing process of proteinaceous paint binder.[17] The principles of quality control and multivariate statistical analysis of Raman spectral data were successfully applied to monitor the conservation state of pigmented and wooden works of arts.[27,28] PCA on the Raman spectra of proteinaceous materials used in paints proved to be a powerful tool to discriminate among protein media on the basis of their Raman spectra,[29] as well as among naturally and artificially aged protein-based paint media.[15] In brief, all of these works demonstrate the increasing importance of multivariate analytical methods in the field of cultural heritage and a new trend in confronting problems related with works of art.

This paper explores the innovation of applying PCA on first-derivative Raman spectra to investigate model tempera paint samples. Thanks to the study of various paint model samples that contain pure blue pigments (azurite, lapis lazuli and smalt), pure red pigments (cinnabar, minium and raw Sienna), pure white pigments (lead white, chalk and gypsum), pure egg yolk as binder and mixtures of each of the pigments with the binder (tempera samples), different aspects of the benefits of this novel analytical approach are highlighted. The PCA-on-derivative Raman spectra approach to discriminate model samples based on its composition is described throughout this work.

Experimental

Painting materials

For this work, three blue pigments (azurite, lapis lazuli and smalt), three red pigments (cinnabar, minium and raw Sienna), and three white pigments (lead white, chalk and gypsum) were selected for analysis. Pigments were chosen on the basis of their widespread use throughout history. The azurite and smalt pigments were purchased from Kremer Pigments GmbH & Co. KG (Madrid, Spain). The rest of the pigments were supplied by Caremi Pigmentos (Sevilla, Spain).

Azurite is the hydrated copper carbonate $Cu_3(CO_3)_2(OH)_2$, and was the most important pigment in European paintings until the later part of the 17th century.[30] Lapis lazuli is a pigment made by grinding the semiprecious rock lapis lazuli whose main constituent is lazurite (Na_8-$10Al_6Si_6O_{24}S_{2-4}$). A famous and expensive pigment used since the 6th century A.D. in Afghan temples, it was worth more than gold during the Renaissance.[31] Smalt is an artificial pigment made of coarsely ground potassium cobalt glass strongly colored with cobalt oxide, which became a substitute for azurite and lapis lazuli in the 17th century.[32]

Regarding the red pigments, cinnabar is mercuric sulfide (HgS) and widely used in antiquity (e.g. 2nd millennium B.C. in China and since Neolithic period in Europe[33]) and still in use, despite its toxicity.[30] Minium is red oxide of lead (Pb_3O_4), also highly poisonous and one of the earliest pigments artificially prepared and still in use today.[34] Sienna and natural red earths represent a large group of clay-rich materials having a complex composition (e.g. gypsum, anhydrite, quartz, calcite, dolomite, etc.). The main coloring agents are either some nonclay pigment, for example iron oxides (haematite, goethite, magnetite, manganese oxides, etc.) or a chromogenous element in the clay structure.[35] The original pigment was obtained from Siena in Italy, from which the term is adopted.[36]

Lead white or ceruse is the chemical compound $(PbCO_3)_2{\cdot}Pb(OH)_2$; one of the oldest manmade pigments, it dates back to the ancient Egyptians and Greeks. Lead white was the principal white of classical European oil paintings.[37] Chalk is a natural white pigment made of calcium carbonate ($CaCO_3$), mainly used for painting grounds and in *fresco* paintings.[30] Natural gypsum ($CaSO_4{\cdot}2H_2O$) has been used in all forms since the beginning of civilization for artistic purposes.[38] In paintings, it has been traditionally used in ground layers and as filler or extender similar to chalk.

The protein binder selected was natural egg yolk, which has been used since ancient times. It solidifies quickly and is favorably flexible, but remains soft for long time and resists mechanical abrasion.[39]

Model samples

Nineteen model paint samples were prepared according to 'Old Master recipes' to obtain egg yolk tempera painting standards similar to those used by medieval artists.[40] Tempera is a painting technique in which finely ground pigments are first mixed with water and later blended with a solidifying proteinaceous binding agent, such as egg, animal glue or casein.[41] The first 9 model samples were pure pigments and the 10th the pure egg yolk binder. The nine remaining model samples were paint binary mixture samples composed by each of the pure pigments mixed with the egg yolk binder.

To prepare the binder, the egg yolk was separated from the white by the usual method of pouring it back and forth in the half shells. It was then rolled onto a paper tissue to remove the layer of clinging egg white and most of the chalazae. The skin was punctured at the bottom by a pin and the liquid content poured into a jar.[39]

The preparation of the tempera model samples was as follows: approximately 0.5 g of each pigment powder was formed as a crater-shaped mass and several drops of beaten egg yolk (different amounts according to each pigment) were added to form a fluid paste. This procedure was adapted to emulate real paint layers with variable pigment concentrations as found in ancient paintings. Then, one layer of the obtained paste was spread with a paintbrush to a fine coat on a glass slide. To obtain the pure binder model sample, the beaten egg yolk was directly spread onto the glass slide. By contrast, the pure pigment samples did not require this preparation, so the Raman measurements were done directly on the pigment powder.

Raman technique

A Renishaw Invia Raman microscope system fitted with a Peltier-cooled CCD detector and a Leica DMLM microscope was

Table 1. Specific working conditions for each analyzed sample

Samples	Laser (%)	Objective	Exposure time (s)	Accumulation (number)	Wavenumber (cm^{-1})
Binder					
Egg yolk	100	20	13	3	300–3800
White pigments					
Lead white	100	20	15	10	250–1600
Chalk	100	20	15	10	250–1200
Gypsum	100	20	15	5	350–1250
Lead white–egg	100	20	15	5	300–3500
Chalk–egg	100	20	15	5	250–3400
Gypsum–egg	100	50	10	5	350–3400
Blue pigments					
Lapis lazuli	25	20	10	5	200–1200
Smalt	100	50	10	10	200–1200
Azurite	1	50	10	10	200–1650
Lapis–egg	50	50	10	10	300–3400
Smalt–egg	100	50	10	5	200–3400
Azurite–egg	100	50	20	7	200–3400
Red pigments					
Cinnabar	1	20	10	10	200–450
Minium	5	50	10	5	100–600
Raw sienna	20	50	10	10	200–500
Cinnabar–egg	15	20	10	7	200–3400
Minium–egg	25	50	20	1	200–3400
Raw sienna–egg	25	50	10	10	200–3400

used. Samples were excited with the 514.5-nm line of an Ar laser (Laser Physics, model 23S514), with an average spectral resolution of approximately 1 cm^{-1} over the wavenumber range of 3800–200 cm^{-1}. To improve signal/noise ratios, spectra from 20-s exposure were averaged (n = 10). The spectra were recorded by placing the samples on the microscope stage and observing them with t long-working-distance 20× and 50× objectives. The sampled areas were identified and focused using either a video camera or microscope binoculars. Precautions were taken not to cause any damage to the samples (i.e. laser-induced degradation of paint materials). This was done by reducing the laser intensity and visually confirming the absence of damage in the sampling area with the help of the camera. Thus, laser power was kept between 0.2 and 20 mW. Moreover to avoid sample alteration and to obtain the best sample spectrum, we varied the laser power (% of 20 mW maximum), the number of spectra accumulations and irradiation exposure times for the diverse samples, as shown in Table 1.

Every sample was characterized by ten spectra obtained from the same location on the model sample in order to avoid spatial variation. The egg yolk model samples were characterized by 20 Raman spectra. Raman signals were collected by the probe and transferred via fiber optics to the CCD detector (NIR-enhanced), controlled by the Wire 2.0 software running on a personal computer.

Principal component analysis

PCA was performed separately on Raman spectral data on the basis of the color of the model samples, that is white, blue or red model samples. Three data matrices were built, one for each color, which initially included the spectra of the tempera model samples (30 spectra), the pure pigment model samples (30 spectra) and the pure egg yolk binder model samples (20 spectra). In this way, each color matrix was initially formed by 90 spectra. The principal components (PCs) were obtained using both the covariance data matrices (scaling by mean-centered data) and the correlation data matrixes (scaling by unit variance). Similar to previous works,[16,17] results were better when PCA was performed on correlation data matrices, so the results shown and discussed here correspond to autoscaled data. A simple centering data procedure is often adopted for spectral data[42,43] because the commonly applied autoscaling procedure assigns the same relevance to each spectral region. Thus spectral regions with small variation – no relevant bands – can acquire the same importance as large bands related to important functional groups. This problem was avoided in this work because only regions containing relevant bands were selected to apply PCA. These spectral regions were selected on the basis of the presence of characteristic bands of the pigments contained in the pigment-laden samples. The best results were obtained for the spectral regions shown in Table 2. Pretreatment techniques – log and first-derivative Raman spectra – were performed on the original Raman spectra before extracting the PCs. Log spectra were calculated using Excel 2000 (Microsoft Corporation, USA). First-derivative spectra were obtained using Spectrum Viewer 2.1b freeware program. PCA was performed using the Statistical Product and Service Solutions program (SPSS, for Windows ver. 15, USA).

Results and Discussion

The chemometric method PCA was applied in order to differentiate model samples on the basis of their different compositions.

Table 2. PCA results

Data matrix	Raman spectral region (cm^{-1})	PC	Variance account (%)	Variance accumulated (%)
White model samples	1200–600	PC1	65.3	65.3
		PC2	12.2	77.6
		PC3	6.1	83.7
		PC4	2.7	86.4
Blue model samples	1100–600	PC1	42.0	42.0
		PC2	26.5	68.5
		PC3	21.1	89.6
		PC4	1.6	91.2
Red model samples	1700–200	PC1	52.2	52.2
		PC2	12.0	64.2
		PC3	5.8	70.0
		PC4	2.6	72.6

First, this analysis was performed directly on the recorded Raman spectra separately for each color, that is white model samples, blue model samples and red model samples. Different Raman spectral regions were tested, including those with information on the pigments and also those at shorter Raman shifts, since no signal from the pigments appears at longer Raman shifts. Results from these multivariate analyses were discarded since they were uninformative for the three kinds of color model samples studied and for the different spectral regions tested. No pattern distributions were detected when projecting the samples onto the space of the firsts PCs, and the score plots showed no relation between sample distribution and composition for all the three color samples studied. No meaningful distribution could be assigned to the graphs. This meant that PCA was not able to detect differences in the recorded Raman spectra on the basis of the different composition of the samples.

Thus, in order to discern variability in the original Raman spectra, two pretreatments were performed on the spectral data matrices before extracting the PCs. These pretreatments were the logarithm and derivative of the recorded Raman spectra. No improvements were observed when applying PCA to the log-Raman spectra, which again produced uninformative score plots for the model samples. By contrast, however, when first-derivative spectra were used, the results indicated successful discrimination of the samples based on their different compositions for the three kinds of color model samples (white, blue and red). Consequently, all of the results presented and discussed in the remainder of this paper correspond to first-derivative Raman spectra. The transformation of a single Raman spectral band into its maximum and minimum, by calculating the first derivative of the spectra, apparently modifies the structure of the data matrix in such a way that differences are evident when PCA is applied. Small spectral differences in the original Raman spectra are seen in the first-derivative spectra, making possible PCA discrimination among samples based on their different composition.

White model samples

PCA was performed on several spectral regions that contained characteristic spectral bands of the white pigments. The highest quality information was obtained using the spectral region in the Raman shift interval 1100–600 cm^{-1}. The main spectral bands of the three pigments are found in this interval, that is at 1057 cm^{-1} for lead white, at 1086 cm^{-1} for chalk and at 1007 cm^{-1} for gypsum. PCA in the interval 1100–600 cm^{-1} allowed separation of the model samples according to their composition. The score plot of the first two PCs shown in Fig. 1(a) reveals that the first-derivative Raman spectral characteristics of this region exhibited enough difference to cluster the samples on the basis of their different chemical compositions. The results of the corresponding PCA in terms of explained variance (%) and cumulative explained variance (%) are shown in Table 2. An in-depth examination of the score plot of these two first PCs, which accounted for 77.6% of the total variance, reveals that the lead white samples clearly differ from the rest of the samples, the first PC being sufficient to discriminate them from the rest of the samples. Similarly, the pure gypsum samples were discriminated via the second PC. The rest of the samples were discriminated using both PCs. The scores of the pure chalk samples were identical; thus they clustered in the space of the two first PCs, near the gypsum tempera samples. Although these two types of samples were placed into the same cluster, there were small derivative spectral differences between them that allowed their separation. Surprisingly, the score plot of PC2 and PC4, which accounted only for 15.0% of the total variance, improved the results, and samples were better discriminated despite the fact that PC4 accounted only for 2.7% of the total variance (Fig. 1(b)).

The loading values indicate the specific contribution of each Raman shift in the calculation of the total variance of the derivative spectral data. Therefore, the loading plot can identify those Raman shift intervals that are important in the PC. A closer examination of the loading plots combined with the score plots can also reveal the kind of contribution associated with the PC. Since the scores of PC1 and PC2 discriminated lead white samples and gypsum samples, respectively, it is clear that the derivative spectral data variances due to these samples are mainly described by these PCs. Nevertheless, the interpretation of the loading plots is difficult since they did not directly represent the Raman spectrum, but rather its derivative. For example, a zero loading value corresponds to either a maximum or a minimum (zero first derivative) in the Raman spectrum.

Taking this into account, the contribution of each of the three white pigments is observed in the PC1 loading plot. A maximum and a minimum centered at zero for the Raman shift, corresponding to the characteristic Raman band of each pigment, was detected as shown in Fig. 1(c). The PC2 loading plot clearly indicates the contribution of the gypsum-laden samples in this PC because of the presence of a maximum and a minimum corresponding to its characteristic Raman band, that is 1007 cm^{-1} (Fig. 1(d)). Finally, from the loading plot of PC4, the Raman shift around 1086 cm^{-1} (maximum of chalk), 811 and 717 cm^{-1} weighs more heavily on this PC (Fig. 1(e)). The score plot in the spaces of PC4 and PC2 allowed a complete discrimination of the samples based on their composition (Fig. 1(b)). The use of the PC3 to build the score plots did not improve the results, and so is not discussed.

Blue model samples

The best capability to discriminate among the model samples by PCA was found in the Raman spectral shift between 1100 and 600 cm^{-1}. The main band of the Raman spectrum of the azurite pigment (401 cm^{-1}) was not included in this spectral region, nor

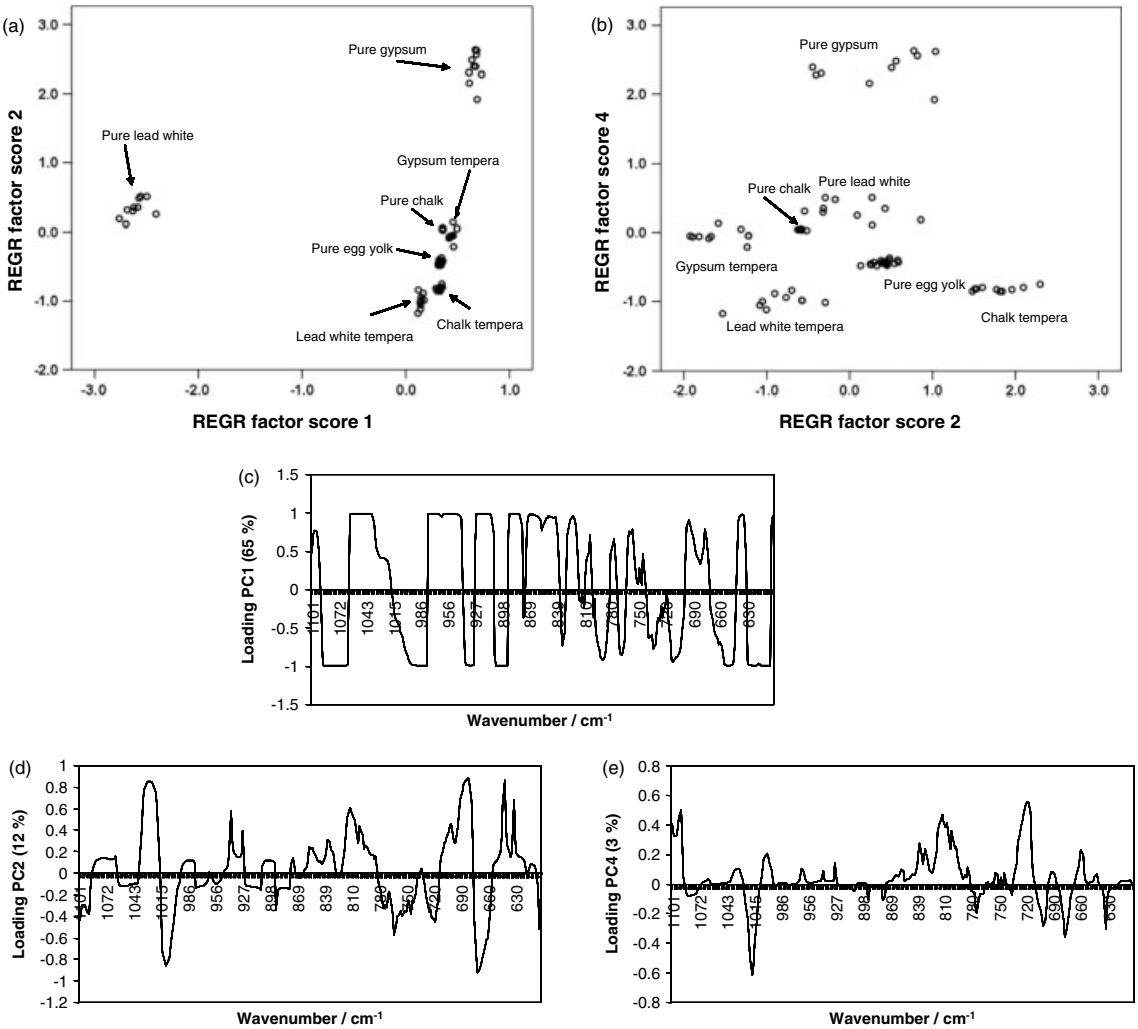

Figure 1. White model samples: (a) score plot of PC1 and PC2; (b) score plot of PC2 and PC4; (c) loading plot of PC1; (d) loading plot of PC2; (e) and loading plot of PC4.

was the main band of smalt (462 cm^{-1}). Bands at 761, 839, 933 and 1094 cm^{-1} were included; all these bands exhibited similar intensities. Also, for lapis lazuli its main spectral band was outside this spectral region (547 cm^{-1}). The spectral bands at 670, 802 and 1095 cm^{-1} were included, the latter having the highest intensity. The result of performing PCA on this spectral region is shown in Table 2. The first three PCs accounted for 89% of the total variance of the original Raman spectra studied (Table 2). The projection of the samples onto the spaces of the two first PCs, explaining 68% of the total variance, is shown in Fig. 2(a). This score plot shows the distribution of the samples in six groups based on the composition. Although the azurite model samples grouped near the smalt model samples in both Fig. 2(a) and (b), they did not cluster together in both score plots; rather, PC3 allowed slight separation of the azurite from the pure smalt (more negative scores).

Again, the interpretation of the information related to each PC was difficult since many spectral regions weighted the PCs as can be observed from the loading plots in Fig. 2(c)–(e). The analysis of the loadings of the first PC revealed that the spectral regions 1068–1009, 879–792 and 770–670 cm^{-1} had large positive values (Fig. 2(c)). Analysis of the derivative spectra of the model samples suggested that the first mentioned region could be related to the presence of egg yolk in the sample since its higher derivative band was located between 1045 and 929 cm^{-1}. The combination of the binder with the pigment could introduce small spectral changes in this region detected by the PCA, thus contributing to the discrimination of the samples. The most negative score value on PC1 was found for the azurite tempera model samples and the most positive value was for lapis lazuli tempera model samples, while the rest of the samples were characterized with score values near zero. The second and third regions could be related to the presence of the azurite pigment because its main derivative bands were located in this spectral region, that is between 863 and 718 cm^{-1}; nevertheless, the azurite tempera model samples had the most negative values. This result could be attributed to a significant change in the derivative spectra of the tempera with respect to those of the pure components (Fig. 2(c)). The second and third PCs also showed that the spectral region between 1092 and 1009 cm^{-1} gave large positive values (Fig. 2(d) and (c)). The score values of the tempera samples were positive on PC2, whereas those for pure pigment samples and egg yolk samples were negative. No improvement was found when using PC3 to project the samples (Fig. 2(b)).

Journal of RAMAN SPECTROSCOPY

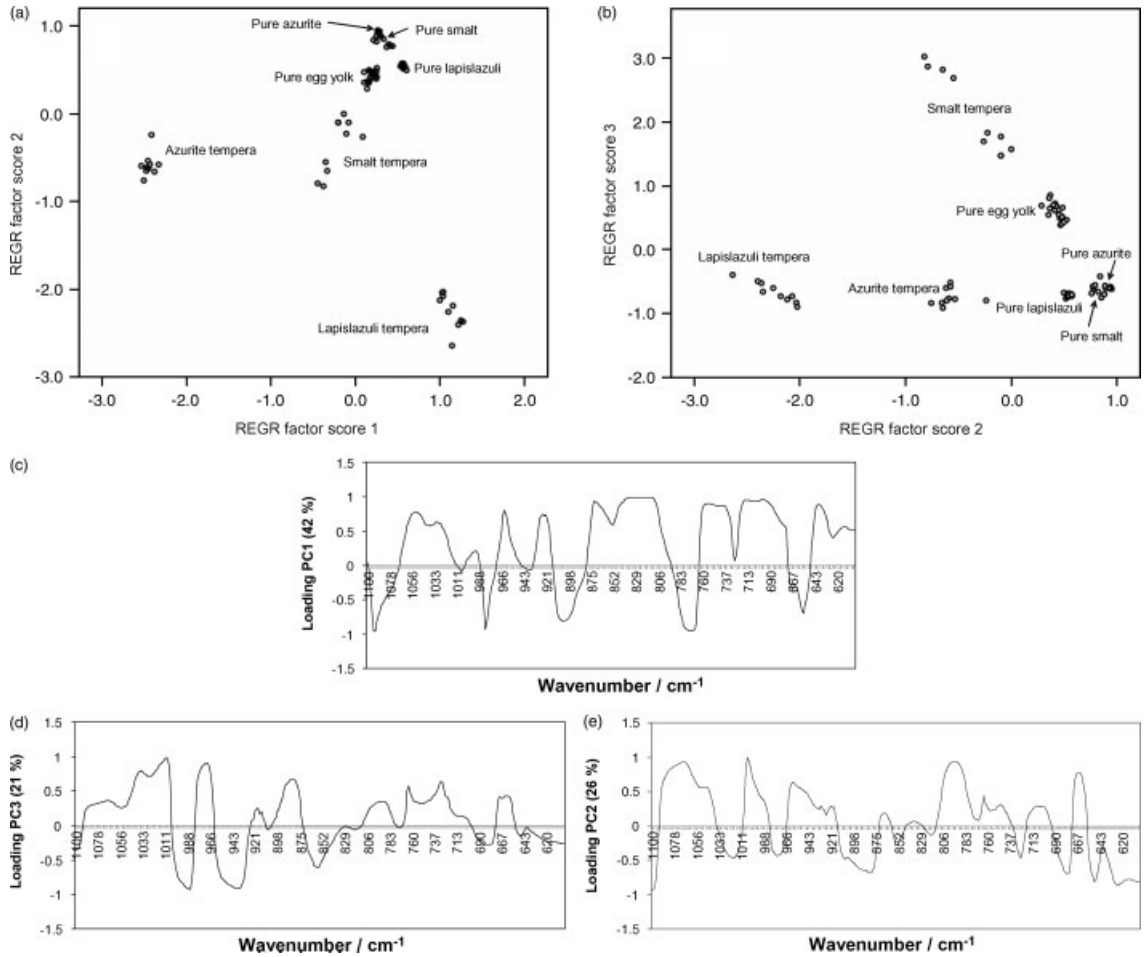

Figure 2. Blue model samples: (a) score plot of PC1 and PC2; (b) score plot of PC2 and PC3; (c) loading plot of PC1; (d) loading plot of PC3; (e) and loading plot of PC2.

Red model samples

Visual inspection of the minium Raman spectra and PCA (Fig. 3) revealed degradation of the minium samples by laser irradiation, in agreement with Burgio *et al.*[44] Consistent with the findings of these authors, minium degraded immediately when irradiated with the 514.5-nm excitation lines at any power, yielding a spectrum similar to that of massicot (orthorhombic PbO), with the main band at ~277 cm^{-1}. This degradation was detected only in the pure minium model samples, indicating protection of the pigment when mixed with the binder in its egg yolk tempera. The red model samples spectral differences were better discriminated when performing PCA on the Raman spectral data between 1700 and 200 cm^{-1} using centered data, where multiplicative effects were not eliminated. The score plot of the two PCs (Fig. 4(b)) accounting for 60.4% of the total variance, PC1 (41.7%) and PC2 (18.7%), shows a clear shift of the score distribution for the pure minium model sample, from the highest PC2 value for the first recorded Raman spectra to the much lower value for the last one. Thus, the degradation process of minium was mainly related to variance explained by PC2. PC1 mainly accounts for the discrimination of the egg yolk samples (positive values) from the rest of the samples containing pigments (negative values). From the score of the minium egg tempera grouped with the samples containing pigments, we infer that the egg yolk binder protected it from the degradation induced by the laser. Thus, this fact highlighted the capacity of PCA to track different degradation processes that may occur in pictorial samples by using Raman spectroscopic data.

In order to discriminate red samples on the basis of their composition, all the minium-laden samples were discarded from the original (recorded) and derivative spectral data matrixes. Thus, PCA was performed on data matrices with 60 spectra. As cited above, the best results were obtained when the derivative data matrix was used to apply PCA and the following results were obtained.

Again, different Raman shift intervals were tested for applying PCA. The highest quality information for discerning samples was obtained using the interval between and 1700 and 200 cm^{-1}. This includes the main Raman bands for the red pigments (at 251 and 343 cm^{-1} for cinnabar; at 214, 279 and 394 cm^{-1} for raw Sienna), and several characteristic Raman bands for the egg yolk (at 1156, 1440 and 1524 cm^{-1}). The results of the PCA are summarized in Table 2. Projection of the data samples from the original space into the plane of the two first PCs, explaining 64.2% of the total variance, is shown in Fig. 4(a). Three clear groups are distinguished. The first PC must be related to the presence of pigment in the model samples. The samples were divided in two groups in this PC, which score positive for the egg yolk model samples and negative for the rest of the model samples (each with a pigment in the composition), and gave negative score values.

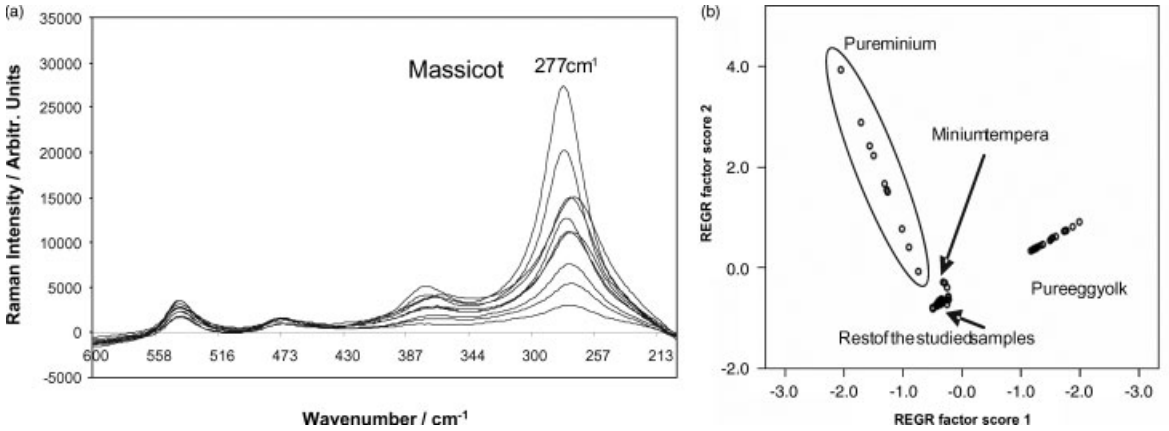

Figure 3. Minium degradation process: (a) spectra of massicot (277 cm^{-1}) obtained after irradiating minium with the Ar laser (514.5 nm); (b) score plot of the two principal components, PC1 and PC2. Raman spectra of all the red model samples were included in the PCA using centered data.

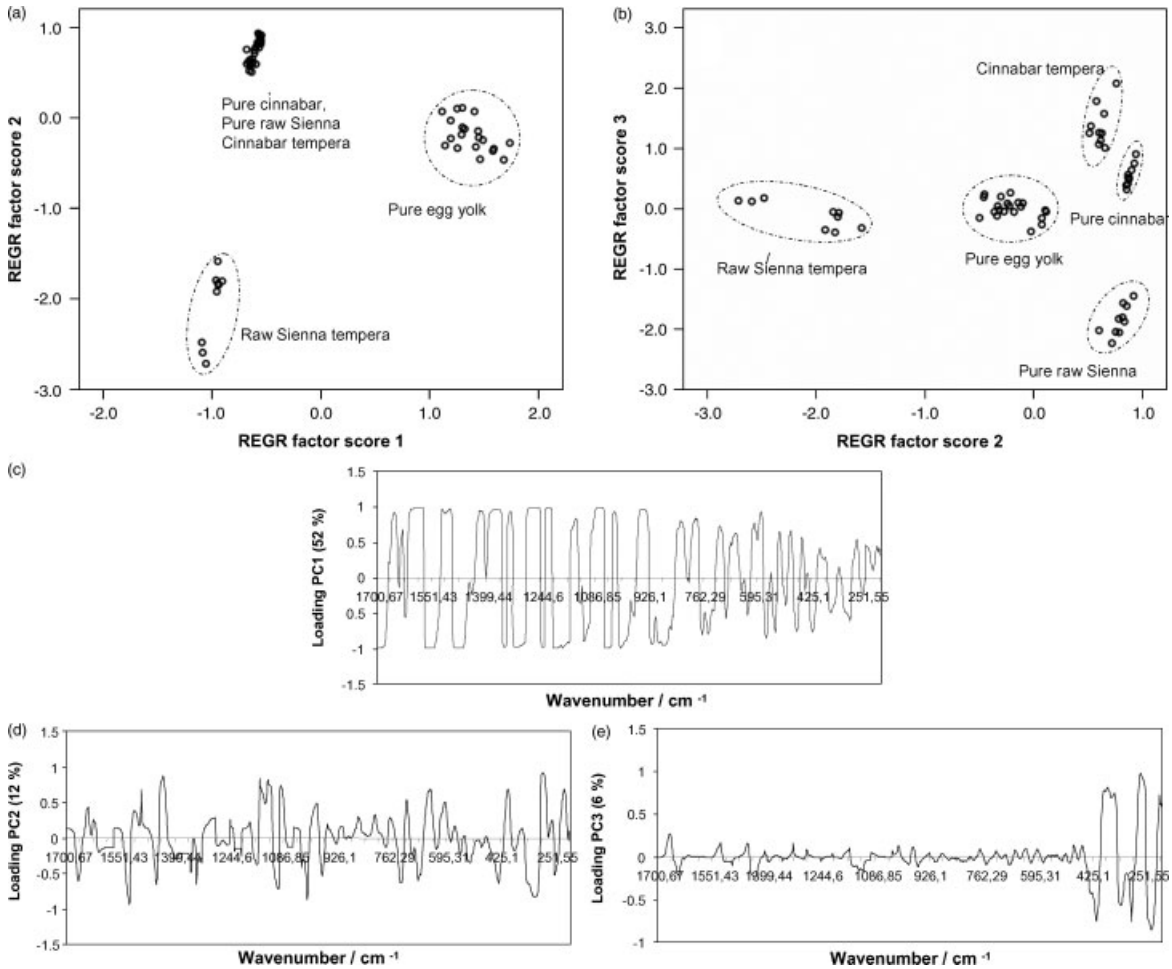

Figure 4. Red model samples: (a) score plot of PC1 and PC2; (b) score plot of PC2 and PC3; (c) loading plot of PC1; (d) loading plot of PC2; (e) and loading plot of PC3.

Loading plot for PC1 indicated that the whole spectral interval selected contributed to the score value, and thus the whole interval contributed to discriminate the presence of pigment in the model samples (Fig. 4(c)). In PC2, raw Sienna tempera model samples were separated from the rest of the studied samples by negative score values. Loading plot of this PC again indicated a contribution of the whole spectral interval in grouping the samples (Fig. 4(d)). Finally, the score plot of PC2 and PC3 grouped samples according to their composition as shown in Fig. 4(b). Five groups could be clearly discriminated, one for each type of model sample. From the loading plot of PC3, it is clear that this component is mainly related to the sample pigment composition (Fig. 4(e)). The spectral region weighting this derivative PC corresponds to the bands of the pigments (between 430 and 200 cm^{-1}).

Conclusions

In this study, PCA of first-derivative Raman spectra of pure and tempera model paint samples has demonstrated its capability to discriminate samples on the basis of their composition. This approach provides a novel and complementary method for discerning among egg yolk temperas used in ancient paintings. Model samples prepared following Old Master recipes were analyzed by RM, showing the usefulness of this technique to study artistic materials like pigments and egg yolk binder. In addition, laser degradation of the red pigment minium was detected by multivariate analysis. To validate the analytical approach, the PCA was performed separately on the derivative spectra of white, blue and red model samples. In all cases, the approach proved a powerful tool to discriminate tempera samples on the basis of their composition, including tempera and pigment. In future work, it would be very interesting to extend such study to different binders and attempt the study of real samples.

Acknowledgements

Financial support for this work was provided by Spanish Science Ministry Projects BHA2003-08671 and HUM-2006-09262/ARTE, the Andalusian Research Group RNM-179, and a research contract from the *Junta de Andalucía* awarded to C. Cardell. We thank A. Yebra-Rodríguez for helping with Raman microscopy using equipment from the University of Jaén, and A. Kowalski for English revision.

References

[1] P. Baraldi, A. Tinti, *J. Raman Spectrosc.* **2008**, *35*, 963.
[2] P. Vandenabeele, B. Wehling, L. Moens, H. Edwards, M. De Reu, G. Van Hooydonk, *Anal. Chim. Acta* **2000**, *407*, 261.
[3] P. Vandenabeele, S. Bodé, S. A. Alonso, L. Moensa, *Spectrochim. Acta; Part A* **2005**, *61*, 2349.
[4] G. Burrafato, M. Calíbrese, A. Cosentino, A. M. Gueli, S. O. Troja, A. Zuccarello, *J. Raman Spectrosc.* **2004**, *35*, 879.
[5] P. Vandenabeele, L. Moens, *Compr. Anal. Chem.* **2004**, *42*, 635.
[6] I. M. Bell, R. J. H. Clark, P. J. Gibbs, *Spectrochim. Acta, Part A* **1997**, *53*, 2159.
[7] L. Burgio, R. J. H. Clark, *Spectrochim. Acta; Part A.* **2001**, *57*, 1491.
[8] R. J. H. Clack, *J. Mol. Struct.* **2007**, *74*, 834.
[9] M. Pérez-Alonso, K. Castro, J. M. Madariaga, *Anal. Chim. Acta.* **2006**, *571*, 121.
[10] P. Vandenabeele, K. Castro, M. Hargreaves, L. Moensa, J. M. Madariaga, H. G. M. Edwards, *Anal. Chim. Acta.* **2007**, *588*, 108.
[11] A. M. Correia, M. J. V. Oliveira, R. J. H. Clark, M. I. Ribeiro, M. L. Duarte, *Anal. Chem.* **2008**, *80*, 1482.
[12] C. Cardell, L. Rodriguez-Simón, I. Guerra, A. Sánchez-Navas, *Archaeometry* **2009**, *51*, 637.
[13] A. Andreotti, I. Bonaduce, M. P. Colombini, G. Gautier, F. Modugno, E. Ribechini, *Anal. Chem.* **2006**, *78*, 4490.
[14] M. Breitman, S. Ruiz-Moreno, A. López-Gil, *Spectrochim. Acta; Part A* **2007**, *68*, 1114.
[15] A. Nevin, D. Anglos, A. Burnstock, S. Cather, M. Becucci, C. Fotakis, E. Castellucci, *J. Raman Spectr.* **2008**, *39*, 307.
[16] N. Navas, J. Romero-Pastor, E. Manzano, C. Cardell, *Anal. Chim. Acta* **2008**, *630*, 141.
[17] E. Manzano, N. Navas, R. Checa-Moreno, L. Rodríguez-Simón, L. F. Capitán-Vallvey, *Talanta* **2009**, *77*, 1724.
[18] A. O'Grady, A. C. Dennis, D. Denvir, J. J. McGarvey, S. E. J. Bell, *Anal. Chem.* **2001**, *73*, 2058.
[19] T. L. Weis, Y. Jiang, E. R. Grant, *J. Raman Spectrosc.* **2004**, *35*, 813.
[20] J. F. Kauffman, M. Dellibovi, C. R. Cunninghamb, *J. Pharm. Biomed. Anal.* **2007**, *43*, 39.
[21] P. Vandenabeele, L. Moens, *Analyst* **2003**, *128*, 187.
[22] P. Colomban, A. Tournier, *J. Cult. Herit.* **2007**, *8*, 242.
[23] M. F. Musumarra, *Chemometr. Intell. Lab. Syst.* **1998**, *44*, 363.
[24] P. Geladi, B. Sethson, J. Nystroem, T. Lillhonga, T. Lestander, J. Burger, *Spectrochim. Acta B* **2004**, *59*, 1347.
[25] S. Wold, K. Esbensen, P. Geladi, *Chemom. Intell. Lab. Syst.* **1987**, *2*, 37.
[26] J. E. Jackson, *A User's Guide to Principal Components*, John Wiley & Sons, Inc.: New York: **1991**.
[27] E. Marengo, E. Robotti, M. C. Liparota, M. C. Gennaro, *Anal. Chem.* **2003**, *75*, 5567.
[28] E. Marengo, E. Robotti, M. C. Liparota, M. C. Gennaro, *Talanta* **2004**, *63*, 987.
[29] A. Nevin, L. Osticioli, D. Anglos, A. Burnstock, S. Cather, E. Castelluci, *Anal. Chem.* **2009**, *79*, 6143.
[30] N. Eastaugh, V. Walsh, T. Chaplin, R. Siddall, *Pigment Compendium: A Dictionary of Historical Pigments*, Butterworth-Heinemann: Oxford, **2004**.
[31] D. Marano, I. M. Catalana, A. Monno, *Spectrochim. Acta A.* **2006**, *64*, 1147.
[32] I. Borgia, B. Brunettia, I. Mariania, A. Sgamellottia, F. Cariati, P. Fermob, M. Mellinic, C. Vitic, G. Padelettid, *Appl. Surf. Sci.* **2002**, *185*, 206.
[33] U. B. Mioc, P. Colomban, G. Sagon, M. Stojanovic, R. Rosic, *J. Raman Spectrosc.* **2004**, *35*, 843.
[34] M. Matteini, M. Arcanuelo, *La Química en la Restauración*, Editorial Nerea: Sevilla, **2001**.
[35] F. Froment, A. Tournie, P. Colomban, *J. Raman Spectrosc.* **2008**, *39*, 560.
[36] D. Hradil, T. Grygara, J. Hradilova, P. Bezdicka, *Appl. Clay Sci.* **2003**, *22*, 223.
[37] D. A. Scott, S. Warmlander, J. Mazurek, S. Quirke, *J. Archaeol. Sci.* **2009**, *36*, 923.
[38] A. Heywood, in *The Use of Huntite as a White Pigment in Ancient Egypt. Colour and Painting in Ancient Egypt*, British Museum Press: London, **2001**, pp 5.
[39] R. Mayer, in *The Artists Handbook of Materials and Techniques* (Ed.: S. Sheehan), The Viking Press: New York, **1991**.
[40] F. Pacheco, *El arte de la Pintura*, Cátedra: Madrid, **1990**.
[41] L. Masschelein-Kleiner, *Ancient Binding Media; Varnishes and Adhesives*, ICCROM: Rome, **1995**.
[42] E. Marengo, M. C. Liparota, E. Robotti, M. Bobba, M. C. Gennaro, *Anal. Bional. Chem.* **2005**, *381*, 884.
[43] D. L. Massart, B. G. M. Vanderginste, L. M. C. Buydens, S. De Jong, P. J. Lewi, J. Smeyers-Verbeke, *Handbook of Chemometrics and Qualimetrics. Part A*, Elsevier: Amsterdan, **1997**.
[44] L. Burgio, R. J. H. Clark, S. Firth, *Analyst* **2001**, *126*, 222.

Conclusiones

Los resultados obtenidos en este trabajo evidencian la capacidad del PCA para discriminar réplicas pictóricas en función de su composición específica, empleando para ello la primera derivada de los espectros Raman de los materiales pictóricos puros y sus temples de huevo. La validez de la metodología propuesta se ha corroborado empleando tres tipos de réplicas pictóricas en función del color, esto es, blanco, azul y rojo. En los tres casos, las muestras han podido ser discriminadas en función de su composición específica.

En el estudio de las réplicas blancas (blanco de plomo, calcita y yeso), la región del espectro Raman más informativa desde el punto de vista del análisis multivariante, es la comprendida entre 1100 y 600 cm^{-1}, intervalo en el que se encuentran localizadas las bandas características de los tres pigmentos estudiados. Tras el análisis, las réplicas que contienen los pigmentos puros blanco de plomo y yeso son claramente diferenciadas del resto de muestra, las cuales aunque son discriminadas, se localizan próximas entre si en los resultados, hecho posiblemente atribuible a la presencia del aglutinante en todas ellas, salvo en la réplica de calcita pura.

En cuanto a las réplicas azules (azurita, lapislázuli y esmalte), la discriminación realizada mediante el PCA parece estar nuevamente relacionada con la presencia de yema de huevo en las mismas, salvo que en estas réplicas y a diferencia con el estudio de las réplicas blancas, las que contienen aglutinante – temples – son las que mejor se discriminan, localizándose próximas entre si las que tienen pigmento puro. Las réplicas que contienen los pigmentos puros con azurita y esmalte no han podido ser discriminadas entre si, lo cual puede ser atribuido a que el intervalo del espectro Raman más informativo desde el punto de vista del análisis multivariante (1100 – 600 cm^{-1}) no incluye las bandas características de dichos pigmentos.

Son de resaltar los resultados obtenidos en el estudio mediante PCA de los datos espectrales de las réplicas rojas (cinabrio, minio y *Sienna*) que han puesto de manifiesto la degradación del minio debido a la acción del láser de 514 nm. Esta degradación es claramente observable a partir del PCA de los

espectros originales sin derivar. El estudio detallado de este proceso de alteración sugiere una modificación mineralógica del minio (Pb_3O_4) a *massicot* (masicotita; PbO), por lo que fue excluido para el estudio de discriminación de las réplicas mediante PCA de la primera derivada de los espectros Raman originales. No obstante, no se detecta degradación de este pigmento cuando se encuentra formando parte de su correspondiente temple. Este hecho sugiere que la cola debe de ejerce algún tipo de efecto protector sobre el mismo. Finamente, el análisis multivariante, realizado sin incluir las muestras de minio, permite una clara separación relacionada con la composición específica de cada réplica, en particular, los temples de *Sienna* se diferencian con claridad del resto de las réplicas estudiadas. El intervalo del espectro Raman que permite una mejor discriminación es el comprendido entre 1700 y 200 cm^{-1}, incluyéndose aquí las bandas características de los pigmentos estudiados.

En conclusión, esta metodología basada en el PCA de los espectros Raman plantea por primera vez el uso de la primera derivada para extraer de manera más efectiva información contenida en los espectros de réplicas pictóricas. Así pues, el PCA de los espectros derivados permite detectar ligeras diferencias espectrales asociadas a la composición de las muestras, es decir, las discrimina en función de su composición, lo cual no fue posible inicialmente empleando los espectros originales de las mismas.

6. Estudio de la interacción pigmento-aglutinante en temples de huevo en la región *CH stretching* mediante RM y PCA

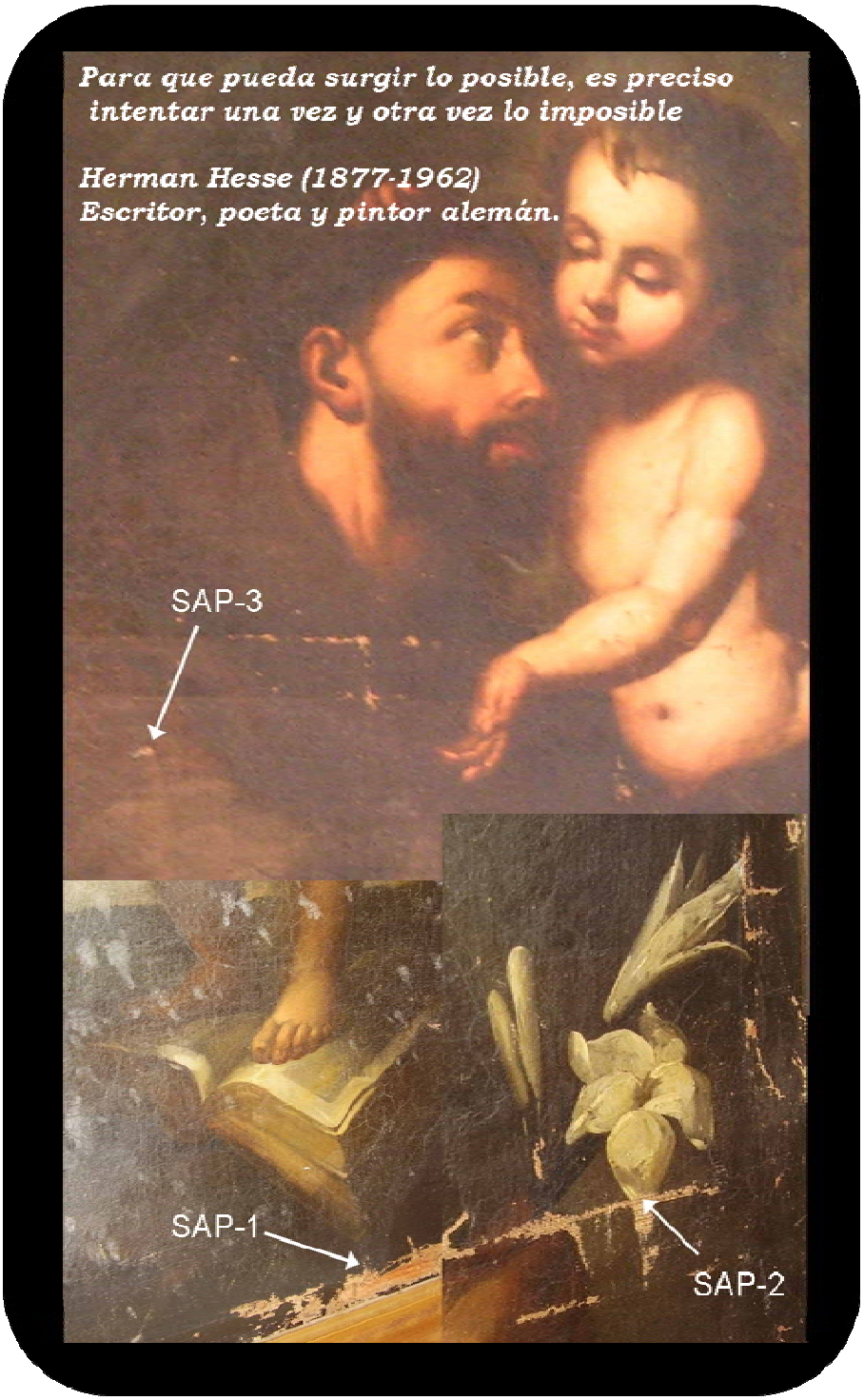

Assessment of Raman Microscopy coupled with Principal Component Analysis to examine egg yolk-pigment interaction based on the protein C-H stretching region (3100-2800 cm^{-1}). (2011). **J. Romero-Pastor,** C. Cardell, E. Manzano, Á. Yebra-Rodríguez, N. Navas. J. Raman Spectroscopy, (doi: 10.1002/jrs.2977).

Resumen

Una vez comprobada la capacidad del PCA de los datos espectrales obtenidos mediante Microscopía Raman en el estudio y caracterización de réplicas pictóricas (Capítulo 5), en el este trabajo se aborda el estudio de las interacciones físico-químicas entre los materiales pictóricos de las réplicas previamente caracterizadas en el capítulo anterior, es decir, de los temples de huevo de pigmentos históricos rojos, blancos y azules. El objetivo es investigar sobre la naturaleza específica de la posible interacción pigmento-aglutinante proteico. Para ello se propone estudiar bandas características del espectro Raman, concretamente el intervalo comprendido entre 3100 y 2800 cm^{-1}, en donde se localizan bandas de estiramiento del grupo funcional C-H tanto de la estructura proteica como de los ácidos grasos presentes en la yema de huevo. A destacar el hecho particular que en este intervalo del espectro Raman no se produce ningún tipo de absorción debida a los pigmentos investigados (cinabrio, *Sienna*, blanco de plomo, calcita, yeso, azurita, lapislázuli y esmalte), por lo que modificaciones en él pueden ser interpretadas como el resultado de cambios en la estructura de la yema de huevo por interacciones específicas con los pigmentos. Concretamente, se esperan *a priori* interacciones del material proteico con los cationes metálicos de los pigmentos, pero no se excluyen las interacciones también con los aniones.

Un examen visual de la zona del espectro Raman elegida (3100 y 2800 cm^{-1}) en las muestras de temple y de yema de huevo pura revela diferencias espectrales muy leves que dificultan la interpretación de los resultados, por lo que se propone abordar el estudio mediante análisis multivariante, PCA, con el objeto de identificar pautas de comportamiento en las muestras asociadas a las interacciones. En este trabajo se propone la existencia de una serie de interacciones pigmento-aglutinante en base a los resultados obtenidos de este análisis multivariante en la región antes citada del espectro Raman. Pare ello, la premisa es: las réplicas pictóricas de temples que se comporten de manera similar a las muestras de yema de huevo pura tras el PCA de la región espectral Raman característica del material proteico – muestras agrupadas en el PCA- no han experimentado cambios en dicha región, por lo que se puede asumir que no existe ningún tipo de interacción entre el correspondiente pigmento y el material proteico; por el contrario, si se produce una clara separación del temple con respecto a las muestras de yema de huevo puro,

puede ser interpretado como resultado de diferencias espectrales debidas a la presencia del pigmento, es decir, a modificaciones espectrales por la interacción pigmento-material proteico, dado que dicha interacción es la única que puede justificar tal modificación espectral.

Al igual que en el Capítulo 5, el estudio se ha abordado independientemente en cada grupo de muestras estudias: rojas, blancas y azules. No obstante, en este caso no fue necesario realizar pre-tratamientos matemáticos diferentes a centrados o autoescalado de los espectros Raman para obtener resultados fácilmente interpretables.

Research Article

Journal of RAMAN SPECTROSCOPY

Received: 27 January 2011 Accepted: 5 April 2011 Published online in Wiley Online Library:

(wileyonlinelibrary.com) DOI 10.1002/jrs.2977

Assessment of Raman microscopy coupled with principal component analysis to examine egg yolk–pigment interaction based on the protein C–H stretching region (3100–2800 cm^{-1})

Julia Romero-Pastor,[a] Carolina Cardell,[a] Eloisa Manzano,[b] África Yebra-Rodríguez[c] and Natalia Navas[b]*

This work seeks to identify the slight changes in the characteristic C–H stretching region (3100–2800 cm^{-1}) of a protein-based binder and fatty acid esters from egg yolk, which may occur in complex paint samples due to the presence of particular pigments. To date, this protein region – where historic pigments do not show characteristic Raman bands – has not been used to identify possible interactions between painting materials, in spite of its potential due to the mentioned feature. This study is based on the investigation of pure egg yolk model samples and tempera model samples prepared by mixing this binder with some historic pigments (cinnabar, raw Sienna, lead white, gypsum, calcite, azurite, lapis lazuli and smalt) as binary samples. All samples were analyzed in this region by Raman microscopy (RM) coupled with principal component analysis (PCA) for three color groups (red, white and blue) separately. The results show relevant spectral changes in the C–H stretching region of amino acids and polyunsaturated fatty acids esters of the egg yolk binder, particularly in the azurite, lead white and gypsum-based tempera samples. Lesser interactions were discerned in the tempera samples made with smalt, as well as shift in the region of polyunsaturated fatty acid esters of the egg yolk binder in the cinnabar and raw Sienna-based tempera paintings. No interactions were recognized between the egg yolk and the pigments calcite and lapis lazuli. The effectiveness of applying RM combined with PCA for identifying interaction processes between binders and pigments is demonstrated.

Keywords: proteinaceous binding media; historic pigments; C–H stretching region; Raman microscopy; PCA

Introduction

It is highly worthwhile to characterize artworks by nondestructive analytical techniques combined with statistical methods such as multivariate chemometric tools to extract the maximum information concerning composition, and to detect slight disparities in spectroscopic data.[1,2] One of the most applied chemometric analyses in the field of cultural heritage is principal component analysis (PCA). PCA has been used successfully for classification purposes on pottery and paintings,[3,4] identification of pigments and binders in historical and model paintings samples,[5] aging detection on painting materials,[6] dating purposes,[7,8] recognition of different sources of raw materials and characterization of alteration products.[9,10] Such analyses have been applied to data obtained by diverse analytical techniques such as inductively coupled plasma mass spectrometry, X-ray fluorescence, gas chromatography-mass spectrometry, Fourier transform infrared spectroscopy (FT-IR), diffuse reflectance infrared Fourier transform spectroscopy or Raman microscopy (RM). The main benefit of PCA is its capability to reduce data dimensionality to principal components (PCs), which contain more interpretable and representative information of the system under investigation.

At present, RM is one of the most commonly used analytical techniques to study painting materials both organic and inorganic simultaneously in the same sample, including binders, varnishes, pigments and dyes.[11] The identification of these compounds using RM is based on the detection of characteristic bands in the spectra, particularly in the fingerprint region.[12,13]

The study of protein-based binding media (e.g. animal glues, casein, egg, etc.) using Raman spectroscopy is centered on the main structure of amino acid compounds (with the general formula $H_2NCHRCOOH$, where R is an organic substitute). This formula varies according to the different amino acids present, and is based on an amine group (N–H bond), a carboxylic acid group (C═O bond) and its characteristic side chain.[14] According to the most

* *Correspondence to: Natalia Navas, Department of Analytical Chemistry, Science Faculty, University of Granada, Avda. Fuentenueva s/n, 18071 Granada, Spain. E-mail: natalia@ugr.es*

a *Department of Mineralogy and Petrology, Science Faculty, University of Granada, 18071 Granada, Spain*

b *Department of Analytical Chemistry, Science Faculty, University of Granada, 18071 Granada, Spain*

c *Department of Geology, Associated Unit IACT (CSIC-UGR), Faculty of Experimental Science, University of Jaén, 23071 Jaén, Spain*

recent studies, the main bands assigned to the presence of egg yolk are the amide bands I and III located at approximately 1670 and 1250 cm^{-1}, respectively.[15] In addition, egg yolk contains 40% fatty acid esters, with a characteristic Raman feature at 2940 cm^{-1}, and phenylalanine (Phe)and tyrosine (Try) (aromatic amino acids) both showing the C–H stretching modes at 3060 cm^{-1}. All these bands, found at high Raman wavenumbers, have been considered less for study since their spectral details are less than those in the fingerprint region.[15] However, this region has recently proved its importance in the identification of different kinds of proteins and in the discrimination of fresh *versus* aged protein model samples studied by RM.[15–17] Moreover, this region has also demonstrated its capability to discriminate complex painting model samples based on the aging state of the protein, using FT-IR spectroscopic data.[8,18] The importance of studying this characteristic region in complex painting samples with RM arises from the fact that historic pigments do not show characteristic bands here. Thus it provides an exceptional opportunity to track the interactions between the protein binder and diverse pigments.

It is well known that the characterization of proteinaceous binders (such as egg yolk) and their stability in complex paint samples can be conditioned by the presence of particular pigments and extenders.[18] Thus, the role of pigments in the study of proteinaceous binding media in paintings is an important task which must be investigated in depth. In this sense, the benefit of applying RM data coupled with PCA to detect pigments and protein binders in tempera model samples has been demonstrated.[19] Nevertheless, to the authors' knowledge, PCA has not been applied to RM data from paintings to detect changes and interferences in the C–H stretching region of proteinaceous binders.

This work demonstrates the application of PCA to this characteristic protein region (where the C–H stretching modes of amino acids and esters of fatty acids appear) in three different pigment colors (blue, red and white) by varied model painting samples.[20] The goal is to identify slight changes in these vibrational bands arising from the binder, i.e. natural egg yolk, as resulting from the interaction with some historic pigments, namely cinnabar and raw Sienna as red pigments; lead white, gypsum and calcite as white pigments; and azurite, lapis lazuli and smalt as blue pigments. In this way, it is expected to shed light on the interaction between this binder and the mentioned pigments in their temperas, as well as to probe the usefulness of using multivariate chemometric approaches on Raman spectroscopic data as a valuable tool for investigating and characterizing painting materials.

Materials and Methods

Painting materials

The azurite and smalt pigments were purchased from Kremer Pigments GmbH & Co. KG (Madrid, Spain), while the rest of the samples were supplied by Caremi Pigmentos (Sevilla, Spain). Cinnabar is mercuric sulfide (HgS) and raw Sienna is a natural iron-rich earth pigment, i.e. a clay-rich material having a complex composition (gypsum, anhydrite, quartz, calcite, dolomite, etc.). Regarding the white pigments, lead white or cerusite is the chemical compound ($PbCO_3$); calcite (or chalk) is a natural white pigment made of calcium carbonate ($CaCO_3$); and gypsum is calcium sulfate ($CaSO_4 \cdot 2H_2O$); the latter two having been used traditionally in ground layers and as fillers or extenders.[21–24] The blue pigments selected were the hydrated copper carbonate named azurite ($Cu_3(CO_3)_2(OH)_2$), lapis lazuli whose main constituent is lazurite ($Na_{8-10}Al_6Si_6O_{24}S_{2-4}$), and smalt which is a synthetic pigment made of coarsely ground potassium cobalt glass strongly colored with cobalt oxide.[23,25]

Painting model samples

Nine model paint samples were prepared according to 'Old Master recipes' to obtain egg yolk tempera painting standards similar to those used by medieval artists.[26] Tempera is a painting technique in which finely ground pigments are first mixed with water and later blended with a solidifying proteinaceous binding agent, such as egg, animal glue or casein.[27] The first model sample was the pure egg yolk binder. To prepare the binder, the egg yolk was separated from the white and spread out with a paintbrush in a fine coat on a glass slide.

The eight remaining model samples were paint binary mixture samples composed of pure pigments blended with the egg yolk binder; thus the tempera replicate samples were obtained. They were prepared by mixing the pigment with egg yolk. Approximately 0.5 g of each pigment powder was formed as a crater-shaped mass to which a few drops of egg yolk (different number according to each pigment) were added until a fluid paste was attained. Each mixture was applied to a glass slide to be studied directly by RM.

Raman technique

A Renishaw Invia Raman microscope system fitted with a Peltier-cooled CCD detector and a Leica DMLM microscope was used. Samples were analyzed with the 514.5-nm line of an Ar laser (Laser Physics, model 23S514), with an average spectral resolution of approximately 1 cm^{-1} over the wavenumber range of 3400–200 cm^{-1}. To improve signal-to-noise ratios, spectra from 20-s exposure were averaged ($n = 10$). Spectra were recorded by placing the samples on the microscope stage and observing them with 20× and 50× objectives. Sampled areas were identified and focused using either the microscope binoculars or a video camera. Precautions were taken not to damage the samples (i.e. laser-induced degradation of paint materials). This was done by reducing laser intensity and visually confirming the absence of damage in the sample area with the help of the camera viewfinder. Thus, laser power was kept at 8 mW. Moreover, to avoid sample alteration and obtain the best sample spectrum, the laser power, the number of spectra accumulations and the irradiation exposure times were varied for the diverse samples. The egg yolk model sample was characterized by 20 Raman spectra and the tempera paint samples were characterized by ten spectra. All spectra were obtained from the same location on the model sample to avoid spatial variation.

Principal component analysis

PCA was performed on the Raman spectral data from 3100 to 2800 cm^{-1} for each color group. Three data matrices were built that included the spectra of the pure egg yolk binder model samples and the spectra of the tempera model samples. In this way, the matrices were formed by 40 spectra for red tempera model samples and 50 spectra for white and blue tempera model samples. The PCs were obtained separately using both the covariance data matrices (scaling by mean-centered data) and the correlation data matrices (scaling by unit variance). The results were clearly better when PCA was performed on correlation data matrices (according to previous work),[2] since the autoscaled

Journal of RAMAN SPECTROSCOPY

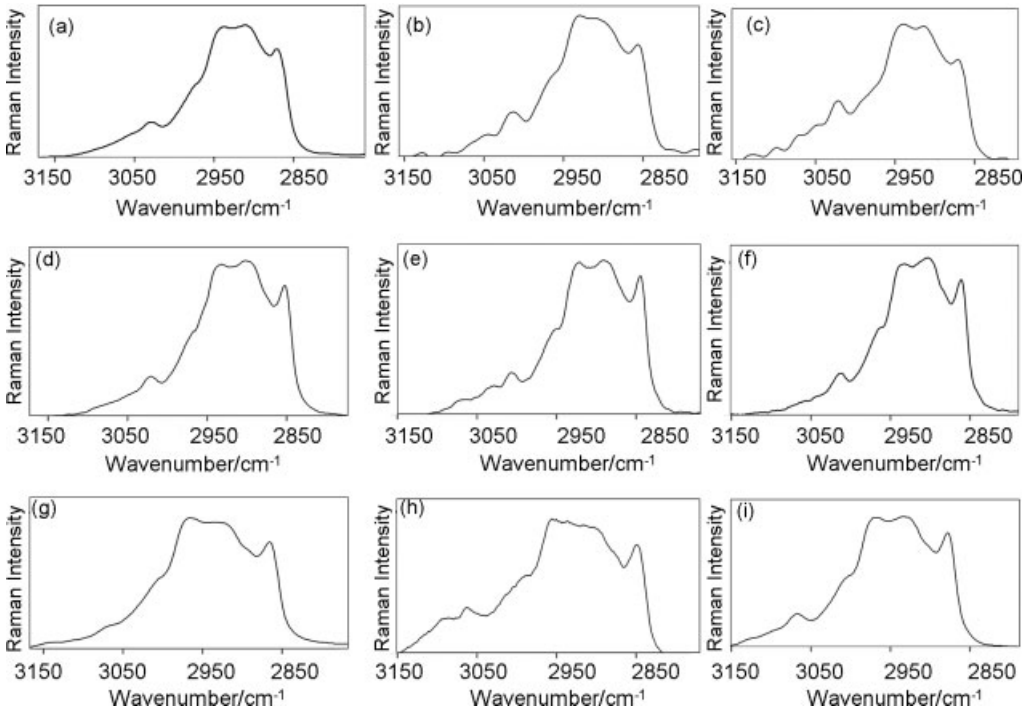

Figure 1. Raman spectra of the tempera model samples in the characteristic protein region of 3150–2800 cm^{-1} of: (a) pure egg yolk; (b) cinnabar; (c) raw Sienna; (d) lead white; (e) chalk; (f) gypsum; (g) azurite; (h) lapis lazuli and (i) smalt.

data normalize relative intensities among the samples. Indeed, this autoscaling procedure assigns the same relevance to each Raman spectral region, and, therefore, when applied to a small region – e.g. 3100–2800 cm^{-1} – it is very effective at extracting information.[19] Therefore, the results shown and discussed here correspond to these autoscaled data.

Results and Discussion

The tempera model and pure egg yolk samples were analyzed by RM in the wavenumber range 3400–200 cm^{-1}. However, considering the purpose of this work, the protein region between 3100 and 2800 cm^{-1} (C–H stretching modes region) was further studied to identify small changes that may occur due to the interaction with particular pigments, which otherwise show no absorption band in this spectral region.

With this aim, PCA was particularly performed in this protein Raman characteristic band and in the three color groups separately, where *a priori* the Raman spectra of all model samples showed an appearance similar to that seen in Fig. 1. Thus, visual inspection of the Raman C–H stretching region revealed no differences in the spectra of the samples. Nevertheless, the presence of a particular pigment could introduce slight changes in this Raman band as a result of the interaction between the protein and the specific pigment, if the pigment interacts with the amino acids involved in this specific Raman region. Bearing this in mind, the result of performing PCA to matrices containing the spectral data of the protein samples and the tempera samples should allow discrimination of the spectral variability associated with the presence of the particular pigment in the tempera due to its particular interaction with the protein.

From the PCA performed as described previously, the results obtained in terms of explained variance (%) and cumulative explained variance (%) for each group of studied color samples are shown in Table 1. Also, the specific Raman shift intervals analyzed in each case are pointed out.

Table 1. PCA results

Model sample	Raman spectral region (cm^{-1})	PC	Variance account (%)	Variance accumulated (%)
Red model samples	3120–2800	PC1	96.6	96.6
		PC2	1.9	98.6
White model samples	3050–2815	PC1	93.1	93.1
		PC2	5.1	98.3
Blue model samples	3070–2800	PC1	98.2	98.2
		PC2	1.3	99.6

From the results of Table 1, it is interesting to note that, in the three multivariate analyses performed, the first PC accounted for more that 90% of the variance present in the spectra (96.6% in the case of the red model samples, 93.1% in the case of the white model samples and 98.2% in the case of the blue model samples). This indicated mainly one source of variability in the spectra. Only in the case of the white model samples did the second PC account for 5.1% of the total variance. The remaining PCs explained <2% of the total variance contained in the corresponding spectral data. More detailed study of these results are discussed in the following sections.

Red tempera model samples

The PCA of the red tempera model samples allowed discrimination of the pure egg yolk samples from the red tempera samples. Figure 2(a) shows the score plot of the samples in the plane of

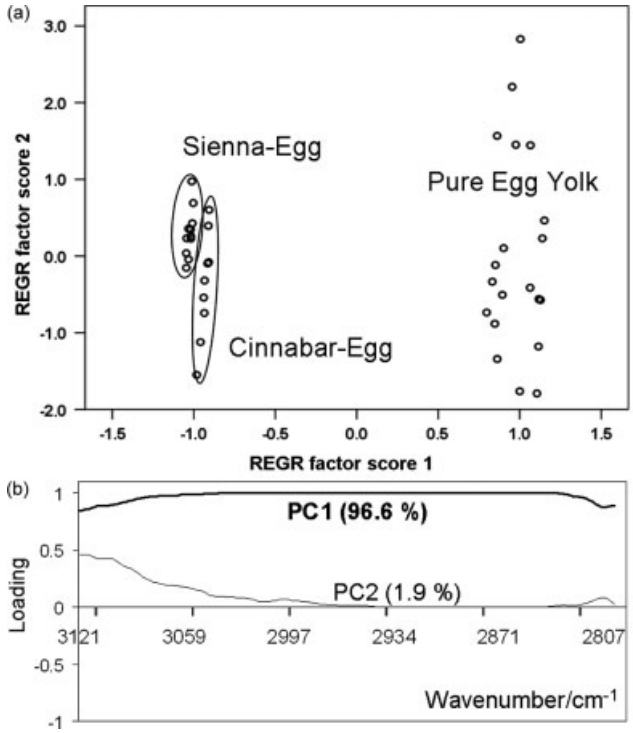

Figure 2. (a) Score plot of and (b) loading plot of PC1 and PC2 of red tempera model samples and pure egg yolk.

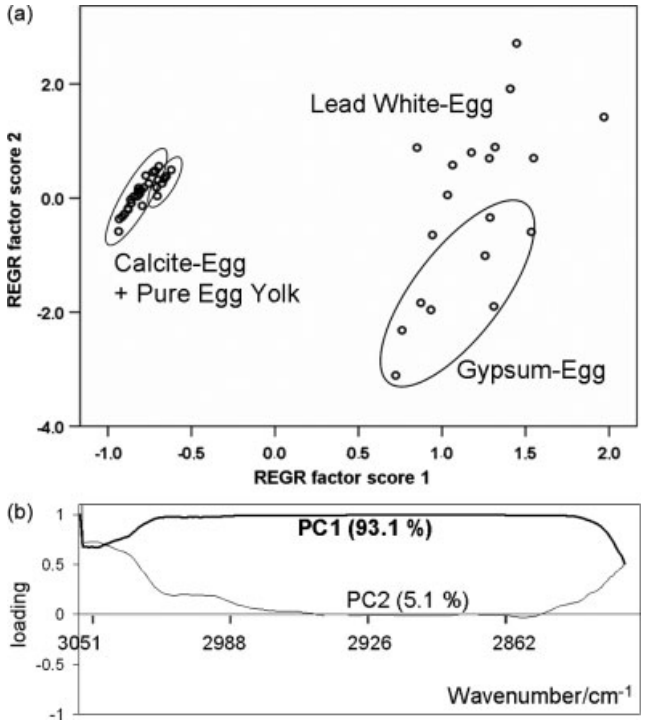

Figure 3. (a) Score plot and (b) loading plot of PC1 and PC2 of white tempera model samples and pure egg yolk.

PC1 and PC2. These two PCs accounted for 98.6% of the total spectral variance. As indicated above, the first PC accounted for 96.6% of the total variance; thus it can be inferred that there was a main source of variability in the original data, i.e. in the spectra. Only using this first PC the three kind of samples could be discriminated, i.e. pure egg yolk, raw Sienna tempera, and cinnabar tempera. Therefore, this variability could be associated with the different pigments present in the sample. Since the pigments show no Raman features in the spectral region here studied, it can be inferred that the pigments interact with the protein through the amino acids involved in this Raman spectral region.

The first PC separated the pure egg yolk (with positive scores) from both red tempera samples (raw Sienna-egg yolk sample showed slightly more negative scores) in the same cluster (Fig. 2(a)). The loading plot of PC1 showed a high weight in this whole band (3080 and 2830 cm^{-1}) in the component (Fig. 2(b)). As stated above, since the raw Sienna and the cinnabar tempera samples showed very different PC1 scores than those from the pure egg yolk samples, it could be concluded that these pigments interacted with the protein within this spectral region where the aliphatic and aromatic $C–H_x$ ($x = 1,2,3$) stretching modes of aromatic amino acids appear. In particular, Phe, tryptophan, histidine and Tyr show this band between 3060 and 3080 cm^{-1} in their spectra.[20,28] In addition, high loading at 2830 cm^{-1} could suggest the oxidation of double bonds in the fatty acid esters by the shifting from 2940 cm^{-1}.[15,16] Furthermore, the fact that the scores of each tempera samples were placed in the same cluster – although slightly separated from each other – (Fig. 2(a)) could indicate similar interactions between the pigments and the protein, i.e. both Hg- and Fe-based pigments interact through similar amino acids in the protein chain. The second PC, which accounted for a variance <2% only, expanded the scores through this PC and so was not associated with relevant information.

White tempera model samples

The goal in studying the white tempera model samples was similar to that of the red tempera samples, i.e. to obtain knowledge regarding interactions between the white pigments and the egg yolk-based protein using the C–H stretching Raman region where the white pigments do not present any bands in their Raman spectra. Thus, PCA was again performed on the spectral interval 3050–2815 cm^{-1} but using the white tempera model samples and the pure egg yolk samples. The result of the projection of the original spectral data into the plane of the two firsts PCs, carrying the 98.3% of the total variance, is shown in Fig. 3(a). Examination of the score values of the samples in the first PC, accounting for 93.1% of the total variance, evidenced that lead white tempera and gypsum tempera (with positive scores) clearly differ from the pure egg yolk and calcite tempera (with negative scores; Fig. 3(a)). Thus, this first PC must be related to the interaction of the white pigment and the protein. From the distribution of the scores in the PC, it can be inferred that the presence of calcite in the model sample did not affect the Raman spectra of the protein in the C–H stretching region, whereas the presence of lead white or gypsum affected this characteristic protein Raman interval.

Regarding the loading plot of this first PC (Fig. 3(b)), the highest spectral weight was located at 3050 cm^{-1}, where the amino acids Tyr, Phe and Trp show their C–H stretching mode. In addition, lower loading values were obtained between 2992 and 3010 cm^{-1} where the C–H stretching modes of threonine (2994 cm^{-1}), methionine (3002 cm^{-1}), alanine (3005 cm^{-1}), proline (3005 cm^{-1}) and cystine (2995 and 3008 cm^{-1}) are located.[20,28] All of this evidence suggests molecular changes in this particular spectral region when lead white and gypsum (i.e. Pb- and Ca-based pigments) were mixed with the binder (egg yolk) in the tempera samples.

The second PC was not useful despite accounting for 5.1% of the total variance. Nevertheless, a closer observation of the cluster

Journal of RAMAN SPECTROSCOPY

of pure egg yolk and calcite tempera samples shows a slight separation between the two kinds of samples when using the two first PCs, which are not randomly mixed in the cluster. Thus, it was possible to discriminate all types of samples when using this second PC along with the first PC (Fig. 3(a)).

Blue tempera model samples

Application of PCA on the blue tempera model samples also used the pure egg yolk samples to obtain the spectral data matrix. The two first PCs were used to project all samples in the new variable space in order to evaluate whether differences could be identified as a result of the presence of the different blue pigments (Fig. 4(a)). The percentage of total variance explained by these two PCs was 99.6%, with 98.2% explained by the first PC. Once again, it can be inferred that the interaction of blue pigment and protein was related to the first PC. The score of the samples on this first PC showed three clusters representing pure egg yolk samples joined to lapis lazuli tempera samples (placed at highest negative score values), smalt tempera samples (placed around zero value) and azurite tempera samples (placed at highest positive score values). The loading plot of the first PC is shown in Fig. 4(b). The high loading values in this whole specific Raman region (3100–2800 cm^{-1}) could be associated with the large effect on this region caused by the occurrence of the azurite pigment, since tempera samples prepared with azurite were characterized by the highest positive score values on this component. Also, it suggests that the C–H stretching modes of the amino acids and polyunsaturated fatty acids esters contained in the egg yolk were affected by the contribution of the azurite, i.e. they changed as a result of the interaction with the azurite pigment. The smalt pigment also interacts with the binder, though not in a similar way as azurite does (they are clearly separated, Fig. 4(a)). On the contrary, the presence of the pigment lapis lazuli did not affect the Raman C–H stretching mode of the protein (both samples are in the same cluster); thus it can be concluded that lapis lazuli does not interact with the protein in the same way as azurite (Cu-based pigment) and smalt (Co-based pigment) do.

Although PC2 explained only 1.3% of the total spectral variance, its contribution is useful for a clear observation of the three clusters cited above. The projection of the samples into the plane of PC1 and PC2 allowed a satisfactory discrimination among those three clusters. Also, pure egg yolk samples and lapis lazuli tempera samples could be discriminated in the cluster where they were placed.

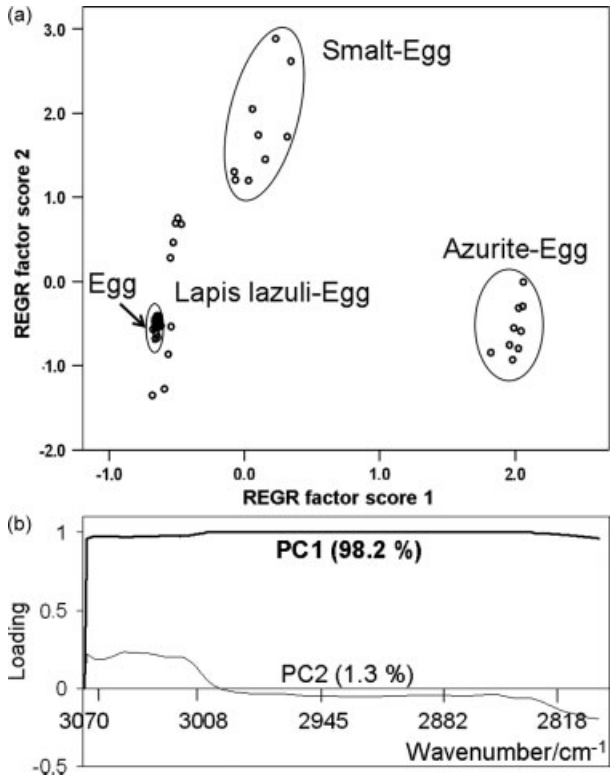

Figure 4. (a) Score plot of and (b) loading plot of PC1 and PC2 of blue tempera model samples and pure egg yolk.

Conclusions

In this study, an original method to gain insight into interactions between historical pigments and a proteinaceous binder (egg yolk) was successfully demonstrated. The combination of Raman spectroscopic data and a multivariate analysis of those data demonstrated the potential of the approach to discriminate samples on the basis of the interaction between the pigments and the egg yolk-based binder. The novelty of the approach lies in the performance of PCA of a particular Raman characteristic protein region where the pigments do not exhibit any Raman feature. Differences in the Raman C–H stretching region of the protein due to the presence of a specific historical pigment were highlighted by the PCA. In particular, it was possible to infer interactions on the C–H stretching modes of aromatic amino acids and fatty acids esters of egg yolk in the case of cinnabar, raw Sienna, lead white, gypsum, azurite and smalt (Hg-, Fe-, Pb-, Ca-, Cu- and Co-based pigments). By contrast, calcite and lapis lazuli did not interact with the protein through this characteristic Raman spectral region, since no spectral variations with respect to the pure protein were discriminated by the PCA. Therefore these results suggest that the pigments containing (transition or alkali-earth) metals interact with the proteinaceous binder depending on the stability of the complex formed between the metal and the binder's amino acids. If the complex is more stable than its initial form in the pigment, protein–pigment interaction will occur. This could explain the fact that azurite (Cu) and gypsum (Ca) interact differently to lapis lazuli (Ca, Na) or calcite (Ca). It could be proposed that Cu – a transition metal – interacts in the case of azurite (carbonate-based pigment) because it forms a stable complex with the proteinaceous binder, while this is not the case for lapis lazuli since this silicate is chemically more stable. Similar arguments can be used in the case of the alkali-earth metal Ca: the Ca–protein complex is more stable than $CaSO_4 \cdot 2H_2O$, but less stable than $CaCO_3$.

This approach will be further applied to investigate the interactions taking place after exposing similar model samples to sunlight and air pollutants, in order to gain knowledge about the behavior of historical paintings damaged by environmental exposure. Also, it would be interesting to extend the study to different pigments in order to better understand the roles of metals and anions in the interaction between a pigment and a proteinaceous binder.

Acknowledgements

This study was supported by Research Groups RNM325, FQM118 and RNM179 (CICE, JA, Spain). The authors acknowledge financial

support from the *Ministerio de Educación y Cultura, Dirección General de Enseñanza Superior* (Spain), Project HUM2006-09262. They also thank 'Servicios Técnicos de Investigación' of the University of Jaén, Spain) for Raman spectroscopy experiments and A. Kowalski for the English revision. Finally, the insightful comments and suggestions of one anonymous referee are acknowledged.

References

[1] T. L. Weis, Y. Jiang, E. R. Grant, *J. Raman Spectrosc.* **2004**, *35*, 813.
[2] N. Navas, J. Romero-Pastor, E. Manzano, C. Cardell, *Anal. Chim. Acta.* **2008**, *630*, 141.
[3] E. Marengo, M. Aceto, E.Robotti, M. C. Liparota, M. Bobba, G. Pantò, *Anal. Chim. Acta.* **2005**, *537*, 359.
[4] K. Castro, A. Sarmiento, M. Maguregui, I. Martínez-Arkarazo, N. Etxebarria, M. Angulo, M. U. Barrutia, J. M. González-Cembellín, J. M. Madariaga, *Anal. Bioanal. Chem.* **2008**, *392*, 755.
[5] E. Marengo, E. Robotti, M. C. Liparota, M. C. Gennaro, *Talanta* **2004**, *63*, 987.
[6] E. Robotti, M. Bobba, A. Panepinto, E. Marengo, *Anal. Bioanal. Chem.* **2007**, *388*, 1249.
[7] T. Trafela, M. Strlic, J. Kolar, D. A. Lichtblau, M. Anders, D. P. Mencigar, B. Pihlar, *Anal. Chem.* **2007**, *79*, 6319.
[8] E. Manzano, J. Romero-Pastor, N. Navas, L. Rodríguez-Simon, C. Cardell, *Vib. Spectrosc.* **2010**, *53*, 260.
[9] Q. Ma, A. Yan, Z. Hu, Z. Li, B. Fan, *Anal. Chim. Acta.* **2000**, *406*, 247.
[10] M. Bacci, M. Fabbri, M. Picollo, S. Porcinai, *Anal. Chim. Acta.* **2001**, *446*, 15.
[11] G. Burrafato, M. Calabrese, A. Cosentino, A. M. Gueli, S. O. Troja, A. Zuccarello, *J. Raman Spectrosc.* **2004**, *35*, 879.
[12] P. Vandenabeele, B. Wehling, L. Moens, H. Edwards, M. De Reu, G. Van Hooydonk, *Anal. Chim. Acta.* **2000**, *407*, 261.
[13] L. Burgio, R. J. H. Clark, *Spectrochim. Acta A* **2001**, *57*, 1491.
[14] V. N. Uversky, E. A. Permyakov, *Analysis Vibrational, Methods in Protein Structure and Stability*, Biomedical: New York, **2007**.
[15] A. Nevin, I. Osticioli, D. Anglos, A. Bursnstock, S. Cather, E. Castellucci, *J. Raman Spectrosc.* **2008**, *39*, 993.
[16] O. F. Van den Brink, J. J. Boon, P. B. O'Connor, M. C. Duursma, R. M. A. Heeren, *J. Mass Spectrom.* **2001**, *36*, 479.
[17] A. Nevin, I. Osticioli, D. Anglos, A. Bursnstock, S. Cather, E. Castellucci, *Anal. Chem.* **2007**, *79*, 6143.
[18] E. Manzano, N. Navas, R. Checa-Moreno, L. Rodriguez-Simón, L. F. Capitán-Vallvey, *Talanta* **2009**, *77*, 1724.
[19] N. Navas, J. Romero-Pastor, E. Manzano, C.Cardell, *J. Raman Spectrosc.* **2010**, *41*, 1196.
[20] N. K. Howell, G. Arteaga, S. Nakai, E. C. Y. Li-Chan, *J. Agric. Food Chem.* **1999**, *47*, 924.
[21] A. Heywood, *Colour and Painting in Ancient Egypt*, British Museum Press: London, **2001**.
[22] D. Hradil, T. Grygara, J. Hradilova, P. Bezdicka, *Appl. Clay Sci.* **2003**, *22*, 223.
[23] N. Eastaugh, V. Walsh, T. Chaplin, R. Siddall, *Pigment Compendium. A Dictionary of Historical Pigments*, Butterworth-Heineman: Oxford, **2004**.
[24] D. A. Scott, S. Warmlander, J. Mazurek, S. Quirke, *J. Archaeol. Sci.* **2009**, *36*, 923.
[25] J. R. Barnett, S. Miller, E. Pearce, *Opt. Laser Technol. 38*, **2006**, 445.
[26] F. Pacheco, *El arte de la pintura*, Cátedra: Madrid, **1990**.
[27] D. V. Thompsons Jr, *The Practice of Tempera Painting, Materials and Methods*, Dover: New York, **1962**.
[28] P. Lunven, C. Le Clement de St Marcq, E. Carnovale, A. Futon, *J. Nutr.* **1973**, *30*, 189.

Conclusiones

A partir de los resultados obtenidos en este estudio se propone la existencia de interacciones concretas entre determinados pigmentos históricos y los componentes de la yema de huevo en temples pictóricos. Esta interacción ha sido evidenciada debido a las leves diferencias espectrales en la región del espectro Raman correspondiente al estiramiento del grupo C-H del material orgánico –mayoritariamente proteico- de la yema de huevo tras el análisis de los espectros mediante PCA. Concretamente, los resultados han revelado cambios espectrales notables en la región de la banda de estiramiento de C-H de los aminoácidos y ácidos grasos de la yema de huevo en presencia de azurita, blanco de plomo, yeso, esmalte, cinabrio y *Sienna*. Por el contrario, la presencia de calcita y lapislázuli no da lugar a modificaciones en dicha región espectral, por lo que se asume que no se produce interacción entre estos pigmentos y la estructura del material orgánico antes citado.

La hipótesis propuesta en base a estos resultados es que los pigmentos que contienen metales alcalinotérreos o metales de transición, (concretamente Hg, Fe, Pb, Ca, Cu y Co en los pigmentos estudiados), interaccionarán o no con la yema de huevo –fundamentalmente con el material proteico- dependiendo de la estabilidad del complejo metal/proteína a qué den lugar, es decir, se producirá interacción si el complejo metal/proteína es de mayor estabilidad que el enlace inicial del metal en el correspondiente pigmento. Esta hipótesis podría explicar el hecho de que unos pigmentos interaccionen y otros no. Así pues, en el caso de la azurita, el cobre –elemento metálico de transición presente en él – interacciona para formar un complejo estable con el material proteico de la yema de huevo, mientras que en el caso del lapislázuli, que es un aluminosilicato que contiene cationes de sodio y calcio muy estable, no da lugar a interacción. Argumento similar puede ser empleado para explicar el diferente comportamiento de los pigmentos con calcio, como el yeso y la calcita. En el caso del yeso, la interacción apreciada podría deberse a la formación de un complejo Ca-aglutinante más estable que el compuesto de Ca en el pigmento original. Por contra, en el caso de temples de calcita, la ausencia de interacción pigmento/proteína puede asumirse como consecuencia de una menor estabilidad del complejo pigmento/proteína con respecto al pigmento de partida, esto es, la propia calcita.

Además del estudio particular de las interacciones estudiadas, este trabajo propone y demuestra la gran utilidad de un novedoso enfoque en el uso del PCA para poder abordar interacciones pigmento-aglutinante.

7. Estudio mediante T-FTIR y PCA de la interacción entre azurita y cola de conejo por efecto de la radiación UV

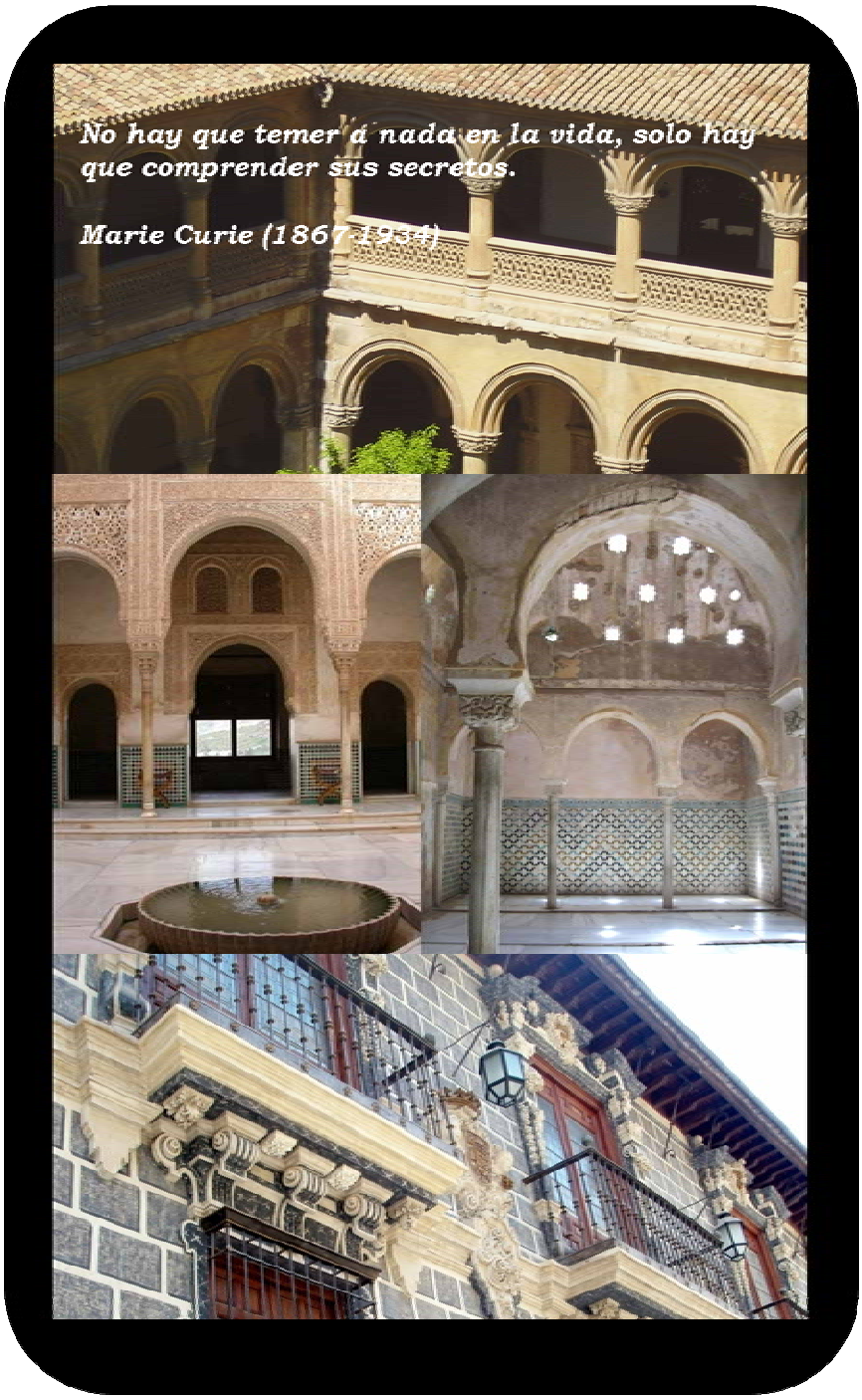

A study of the interaction between rabbit glue binder and blue copper pigment under UV radiation: A spectroscopic and PCA approach. (2010). E. Manzano, **J. Romero-Pastor**, N. Navas, L.R. Rodríguez-Simón, C. Cardell. Vibrational Spectroscopy 53, 260–268.

Resumen

En los Capítulos 4, 5 y 6 se han puesto a punto procedimientos y metodologías para el estudio de materiales pictóricos mediante el uso de FTIR, DRIFT y RM mediante PCA. Además, se ha abordado de manera particular el estudio de interacciones las físico-químicas entre el pigmento y el aglutinante sin intervención de agentes de alteración externos (Capítulo 6). Para continuar con la consecución de los objetivos marcados en esta Tesis Doctoral (Capítulo 2), este Capítulo 7 aborda el estudio del proceso de envejecimiento por la acción de la radiación UV de temples pictóricos. Para ello, se han elaborado réplicas pictóricas empleando materiales ampliamente utilizados a lo largo de la historia: azurita y cola de conejo, según recetas medievales. Además, con objeto de evaluar el papel de la concentración en el envejecimiento de los materiales pictóricos, se han preparado temples azurita-cola de conejo en diferentes proporciones (concentración de aglutinante baja, media y alta). Por tanto, son cinco réplicas pictóricas las estudias: azurita y cola de conejo puros así como sus mezclas a tres proporciones de aglutinante distintas.

En este trabajo se han evaluado los cambios físico-químicos y cromáticos inducidos por el efecto de la radiación UV en las réplicas antes descritas. Para ello, una vez preparadas, se han analizado periódicamente por SEM-EDS, XRD, Espectrofotometría y T-FTIR para el control topográfico-elemental, mineralógico, colorimétrico y estructural, respectivamente. Una vez finalizado el proceso de envejecimiento (3000 horas de exposición), los datos espectrales obtenidos por T-FTIR han sido analizados mediante PCA. El estudio multivariante se llevó a cabo de forma independiente en los seis grupos de réplicas con objeto de comparar los resultados y determinar si la diferente composición de las réplicas ejerce algún tipo de influencia en el envejecimiento por exposición a la radiación UV. Los resultados han mostrado la degradación de la cola pura debido a la radiación UV y la estabilidad de la azurita tanto pura como en los temples a esa misma radiación. Además, con este estudio es posible proponer una primera evidencia sobre el poder fotoestabilizador de la azurita ante el proceso de envejecimiento de la cola de conejo, aspecto que se volverá a abordar en esta Tesis Doctoral en el Capitulo 9, proporcionando nuevas evidencias sobre este efecto.

Vibrational Spectroscopy 53 (2010) 260–268

Contents lists available at ScienceDirect

Vibrational Spectroscopy

journal homepage: www.elsevier.com/locate/vibspec

A study of the interaction between rabbit glue binder and blue copper pigment under UV radiation: A spectroscopic and PCA approach

E. Manzano[a,*], J. Romero-Pastor[b], N. Navas[a], L.R. Rodríguez-Simón[c], C. Cardell[b]

[a] Dept. of Analytical Chemistry, University of Granada, Fuentenueva s/n, 18071 Granada, Spain
[b] Dept. of Mineralogy and Petrology, University of Granada, Fuentenueva s/n, 18071 Granada, Spain
[c] Dept. of Paint and Restoration, University of Granada, Av. Andalucía s/n, 18071 Granada, Spain

ARTICLE INFO

Article history:
Received 6 November 2009
Received in revised form 15 April 2010
Accepted 15 April 2010
Available online 22 April 2010

Keywords:
FT-IR spectroscopy
Spectrocolorimetry
Principal component analysis
Azurite pigment
Glue binder
Historical paintings

ABSTRACT

The effects of a UV-accelerated ageing test on model samples of azurite glue tempera, pure azurite and pure rabbit glue, all elaborated according to medieval recipes, were studied. The color changes and modifications in composition and texture for both pure and mixed samples are shown and discussed. Special attention is given to the physico-chemical interactions occurring when azurite and glue are combined. Ageing effects on the model samples after up to 3000 h of UV irradiation were periodically analyzed by scanning electron microscopy (SEM) with X-ray energy dispersive spectrometer (EDS) microanalysis, X-ray diffraction (XRD), reflectance spectrophotometry and Fourier-transform infrared spectroscopy (FT-IR). Once the ageing process ended, a chemometric study using principal component analysis (PCA) of the FT-IR data was carried out independently for every model sample and for all the azurite-laden samples. Loadings from the significant principal components were analyzed to identify the FT-IR frequency (cm^{-1}) involved in the degradation process. PCA proved capable of identifying significant changes in pure glue samples. Also this work showed the lack of photochemical effects of UV irradiation on both pure azurite samples and those mixed with glue, in agreement with the SEM-EDS, XRD and colorimetrics results. Nevertheless PCA revealed that the azurite FT-IR spectral variability decreased in the presence of glue, being more affected by exposure to the IR region between 2100 cm^{-1} and 3600 cm^{-1}, where the azurite band is located. In addition, PCA managed to separate the azurite/glue mixture samples from pure azurite samples.

1. Introduction

In heritage science considerable attention is given to model studies on the effects of environmental factors on artists' materials [1–4]. In the particular case of paint artworks, the main goal is to characterize painting components and interacting processes under diverse conditions to promote painting conservation. Ancient paintings are complex microlayered composite materials made by heterogeneous mixtures of organic and inorganic components [5–7]. Throughout a paint stratigraphy (from inside to out: ground layer, priming layer and coloring layers), micrometer-scale pigments are mixed with binders. Over time, historical paintings transform due to exposure to diverse environmental conditions which promote reactions between painting components [1–5]. Particularly important in affecting color of paintings are ultraviolet (UV) and visible (vis) irradiation [1,3–4,8–9]. Effects induced by radiation on paints include chemical changes and color modifications that cause aesthetic damage. This makes characterization of ancient paintings a challenging task.

Especially sensitive to alteration are organic components used as binders, such as linseed oil, egg, casein, animal glue or dammar resin. The stability of protein binders exposed to various atmospheric conditions is said to be exceptional as compared with the yellowing and brittleness of aged oils and resins. The high susceptibility of oils and resins to light-induced damage has promoted numerous studies concerning their ageing processes, whereas fewer studies have analyzed ageing of protein binders in paintings or just mixed with pigments [8,10–12].

Concerning stability of pigments, diverse authors have investigated the light-induced damage to a variety of pigments [13], including copper pigments [3]. Azurite is a basic copper carbonate of formula $Cu_3(CO_3)_2(OH)_2$ used for centuries as blue pigment, particularly during the Middle Ages and Renaissance. Azurite on its own is remarkably stable under ordinary conditions [14], but the stability of azurite combined with different binders is different under natural conditions. Thus it turns into green tones when mixed with oil and egg yolk [15], while proteinaceous binders seem to protect azurite from color degradation, as found in the Van Eyck

* Corresponding author. Tel.: +34 958243388; fax: +34 958 243328.
E-mail address: emanzano@ugr.es (E. Manzano).

0924-2031/$ – see front matter © 2010 Elsevier B.V. All rights reserved.
doi:10.1016/j.vibspec.2010.04.003

brothers' painting [16]. Thermal (DSC and TGA) and spectroscopic (XPS) studies have revealed that azurite egg tempera is altered by thermal ageing and pollutants, while less changes occurred under exposure to light irradiation [17]. In fact, the latest direct laser irradiation tests at IR, vis and UV wavelengths on azurite-laden paint samples corroborate that azurite is more stable than the majority of ancient pigments, both alone and when mixed with binders. Among others techniques, colorimetry, vibrational spectroscopies, SEM-EDS and XRD have been used to discern ageing processes [18].

Fourier-transform infrared spectroscopy (FT-IR) is commonly used to characterize organic and inorganic paintings materials present in art works [19]. A main advantage of this technique is that it provides complex data sets represented by samples' spectra suitable for being treated with multivariate analysis techniques. In fact, in recent years chemometric techniques have been increasingly used in the field of Cultural Heritage since they can extract information from correlated data sets, such as spectroscopic sets [8,20–22].

Assessments of physico-chemical changes induced in painted models by UV–vis irradiation using SEM-EDS, XDR and colorimetrics techniques are routine but essential tools, principally in the field of laser interaction with polychromy. In fact variation in colorimetric characteristics is the major type of side-effect in light ageing processes of paintings, triggered mainly by chemical modifications but also through modification of pigment morphology and textural relations of pigment-binder systems [9,23].

Despite the above, numerous areas remain open for research, including colorimetric behavior and chemical and texture interactions when azurite is blended with glue binders, as well as the application of chemometric tools to the obtained data to detect minor ageing variations. The present work investigates modifications in terms of changes in color, composition, texture and chemical interactions occurring on model samples of azurite rabbit glue tempera, pure azurite and pure rabbit glue under accelerated UV irradiation. The aim is to assess the stability of both painting components when standing alone and also when combined to further clarify the interaction process between them. Analysis of samples was periodically performed by measuring colorimetrical changes and recording their FT-IR spectra before and throughout increased UV radiation doses. In addition composition and texture characteristics were examined by SEM-EDS and DRX. PCA was applied to FT-IR spectra to reduce its multidimensional space in order to extract information about the azurite and glue ageing process by studying similarities in the samples.

2. Materials and methods

2.1. Reagents

The azurite pigment was purchased from Kremer Pigments GmbH & Co. KG. Pigment reference is 10,200 natural azurite (CI: PB 30.77420) with particle size 0–120 μm. The standard protein binder used was rabbit skin glue (collagen) purchased from Sigma (Barcelona, Spain). This binder has been used since ancient times, mostly in traditional woodworking, gilding and paintings due to its high strength, viscosity and elasticity.

2.2. Model samples

Five painting model samples were prepared according to Old Master recipes to obtain standards similar to those used by medieval artists [24]. The first model comprises the pure azurite pigment and the second model the pure rabbit glue binder. The third, fourth and fifth model samples include azurite/rabbit glue mixtures in various ratios (w/v).

Preparation of the pure azurite model sample was as follows: 5 g of powder azurite was formed as a crater-shaped mass and six drops of pure water (total volume of 30 μl) were added to form a dense paste. Then, four layers of this azurite paste were sequentially spread in fine coats onto a glass slide with a paintbrush. Each layer dried thoroughly before the next was applied. This is the traditional way to obtain an opaque paint layer guaranteeing full luminosity of the color. The pure glue binder model sample was prepared as follows: 10 g of rabbit glue was diluted to 10% by w/v in deionized water (MilliQ-System Millipore, Bedford, MA) by gently adding the glue to the water during 24 h, and stirring periodically. Next the obtained blend was gradually heated in a bain-marie water bath below 50 °C to obtain a homogeneous mixture. Then the glue was carefully spread on a glass slide with a paintbrush in six successive fine coats, each applied after the previous layer had dried to a constant weight using a gel air dryer system.

Azurite/rabbit glue mixture model samples were prepared by blending the azurite with the glue both components previously prepared as described above in various ratios (w/v): 5.2/1; 5.2/0.4 and 5.2/3. Next, these mixtures were spread on glass slides in three fine coats. This procedure was adapted to emulate real paint layers with variable pigment concentrations as found in ancient paintings. In addition, this enables discrimination among contributions from each pure painting material, i.e. azurite and rabbit glue, in terms of the physico-chemical changes occurring between them when interacting under UV exposure. The different ratios examined were: (i) 5.2/1 (w/v) for the so-called "ideal" combination, following the old recipes; (ii) 5.2/0.4 (w/v) to obtain a mixture with less glue (1/3 less in volume) for a sample overly rich in azurite; and (iii) 5.2/3 (w/v) to obtain a mixture with extra glue (1/3 more in volume).

2.3. UV-accelerated ageing test

The painting model samples on the glass slides were aged in a UV-accelerated test chamber. To avoid azurite transformation into malachite the temperature was maintained at 30 ± 5 °C and the relative humidity at 15 ± 5%. Before UV irradiation exposure (time = 0) fresh samples of each type were removed and stored in glass vials in the dark to be further analyzed. These are the blank samples to be compared with the aged samples. All the azurite-laden samples were UV irradiated during 3000 h, when the test was judged to have finalized and no color changes had been observed. At the start of the test at 200 h, 500 h, 800 h, 1500 h, 2500 h and at 3000 h spectrocolorimetry analyses were performed. Throughout the test at the above mentioned times, aged micro-samples were removed from the slides in order to analyze their composition and morphology (DRX and SEM-EDS) and to measure their IR spectra. Regarding the pure glue binder model samples, due to the higher susceptibility of the binder to UV damage (compared to the azurite-laden samples) color changes were checked at earlier UV exposure times, i.e. 24 h, 48 h, 72 h, 96 h, 120 h, 144 h, 200 h and at 500 h. Colorimetric analysis at 500 h was not possible due to the need for an even surface to obtain suitable data, whereas 500 h of UV irradiation left the glue surface cracked, blistered and flaked. Micro-sampling and analyses similar to those performed for the azurite-laden samples were applied for the pure glue sample at analogous times, i.e. from the start of the test and at 200 h, 500 h, 800 h, 1500 h and 3000 h.

2.4. Instrumentation and software

A high-speed exposure unit SUNTEST CPS, Heraeus (Hanau, Germany), equipped with a Xenon lamp was used for the ageing test. A special UV glass filter was employed for limiting the radiation at wavelengths greater than 295 nm, corresponding to outdoor solar exposure. Irradiance was set at 765 W m^{-2}, and range of temperature on the samples was kept at 30 ± 5 °C and 15 ± 5% relative

humidity measured by the thermohygrometer Station OREGON, mod. EMR812HGN (Portland, Oregon, USA).

The diffuse spectral reflectance of each model sample was measured with a Hunterlab Ultrascan spectrophotometer. Spectra were acquired in the visible range of 375–750 nm at 5 nm intervals, with diffuse illumination and 8° from specimen-normal viewing, 25 mm circular area. Once the spectral reflectance curves were drawn, the CIE-1931 chromaticity coordinates were calculated under illuminant D65. The CMC (2:1) version of the color difference formula [25] was used to colorimetrically compare the samples. In general terms, these differences will be visually perceptible when the values change by more than three units.

The FT-IR spectra were collected using a NICOLET spectrometer 20SXB, working in transmission mode. The instrument was connected to a Pentium 200 and the instrument software was OMNIC v 4.1, running under Windows 2000 Professional (Microsoft Corporation, USA). The FT-IR spectra were registered from 400 cm^{-1} to 4000 cm^{-1} with a resolution of 2 cm^{-1} and 200 scan. Each model sample on the glass slide was characterized by five FT-IR spectra at the start of the test (fresh samples) and at each of the selected times above mentioned (aged samples). These spectra were obtained from five KBr pellets that were prepared by homogeneously mixing ~50 μg of sample powder removed from five randomly places from the glass slide. In this way, FT-IR spectra were independent from the position where the powder was taken in the glass slide.

Powder XRD was used to determine the mineral composition of all azurite-laden samples at each check time. A Philips PW-1710 diffractometer was used with the Bragg-Brentano focusing geometry, a graphite secondary monochromator, Cu Kα radiation (λ = 1.5405) and automatic divergence 1° slit. Diffraction patterns were obtained using continuous scan mode exploring an area over 3–64° 2θ, with 0.01° 2θ s^{-1} goniometer speed. The voltage was 40 kV and the tube current 40 mA. Samples were slightly milled in agate mortar to <40 μm particle size and then analyzed. Automatic acquisition, evaluation and identification of minerals were carried out with the Xpowder software [26].

An SEM-EDS technique was used to study the chemical composition and morphology of the models. An Inca 350 version 17 Oxford Instrument was used. Analyses were done in secondary electron mode (SE) and backscattered electron mode (BSE). Both operating modes are complementary, though SE-mode provides information on texture and structure and BSE-mode on elementary composition, based on the different grey range of regions, a consequence of the atomic numbers of the elements constituting the materials. The SEM-EDS working conditions were 1.3 nA beam current measured in Faraday cage, 20 ev/ch resolution and acquisition time of 50 s. Samples requiring no preparation were mounted on a tee and coated with carbon for microanalysis purposes (azurite-laden samples), and with gold to visualize morphology in the pure glue samples.

A system of Gel Air Dryer, BIO-RAD Laboratories S.A. (Madrid, Spain) was used for drying the painting layers. Analytical balance METTLER-TOLEDO model AE163, with range of weighed 0–30 and 0–160 g, and precision 0.01 and 0.1 mg, respectively was used for weighting the painting compounds.

Chemometric data treatments were performed using Statistical Product and Service Solutions program (SPSS, for Windows ver. 15, USA).

3. Results and discussion

3.1. Spectrocolorimetry analysis

For all azurite-laden model samples a slight difference in the reflectance values is seen throughout the UV exposure times, particularly in the range of c.a. 450–500 nm and mainly in the pure azurite model samples. For the pure rabbit glue model samples a darkening seems to occur in the first 24 h of UV irradiation, principally beneath 550 nm. However, these changes in reflectance require a specific reworking of the data on the basis of the color coordinates (CIE-1976) to obtain via color difference formulae CMC (2:1): the color differences ΔE_{cmc} (total color), ΔL^* (brightness), ΔC^* (chroma) and ΔH^* (hue). These values shown in Tables 1 and 2 indicate whether the apparent chromatic differences observed in diffuse reflectance spectra are due to perceptible visual changes, achieved only when ΔE_{cmc} exceeds three units [27].

Table 1
Colorimetric values calculated for UV-aged pure azurite samples (Az) and azurite/rabbit glue mixture samples (see text for explanation). IMixt = ideal azurite/glue mixture; Mixt-g = mixture with less glue; Mixt-G = mixture with extra glue.

	Color	Check	Time			
Samples	400	850	1400	2100	2600	3000
Az						
ΔE_{cmc}	**0.84**	1.29	1.52	1.75	2.33	**2.10**
ΔL^*	−0.23	−0.04	−1.12	−1.22	−1.30	−1.39
ΔC^*	−0.54	−0.81	−0.94	−1.00	−1.50	−1.33
ΔH^*	−0.60	−1.01	−0.41	−0.76	−1.22	−0.84
IMixt						
ΔE_{cmc}	**2.17**	1.92	1.67	1.71	1.53	**1.43**
ΔL^*	−0.84	−0.71	−0.53	−1.00	−1.12	−0.90
ΔC^*	1.16	0.93	0.70	0.75	0.58	0.70
ΔH^*	1.63	1.53	1.42	1.17	0.87	0.87
Mixt-g						
ΔE_{cmc}	**1.00**	2.10	0.52	0.82	1.15	**0.66**
ΔL^*	0.96	1.09	0.48	0.26	0.91	0.58
ΔC^*	0.28	1.28	−0.17	0.45	0.61	−0.10
ΔH^*	−0.07	1.26	−0.11	0.64	0.35	−0.30
Mixt-G						
ΔE_{cmc}	**1.63**	2.21	1.01	1.09	1.06	**1.22**
ΔL^*	−1.15	−0.65	−0.03	−0.03	0.63	1.10
ΔC^*	−0.09	0.43	−0.31	−0.05	−0.02	−0.38
ΔH^*	−1.15	2.07	0.96	1.09	0.85	0.36

Table 1 shows the results of ΔE_{cmc}, ΔL^*, ΔC^* and ΔH^* in azurite-laden samples. The scattered data across the color-check times reveals the important role of the spreading of painting materials on the glass slides, where obtaining a homogeneous surface is key for spectrophotometric evaluation. Further differences can arise due to the spreading of painting materials on the glass slides, where obtaining a homogeneous surface is key for spectrophotometric evaluation to positioning errors. In fact, the difficulty in systematically recording the same area in a studied sample is well known. Nonetheless taking into account these results, some indications can be made regarding the chromatic behavior of these samples.

The UV radiation effect on all azurite-laden model samples is a variation in total color, however imperceptible in terms of visual perception due to the fact that ΔE_{cmc} is less than three units, i.e. ΔE_{cmc} equals 2.10 at t = 3000 h (Table 1). In the pure azurite model sample the decrease of ΔL^* and ΔC^* accounted for the ΔE_{cmc} increases during the 3000 h of UV irradiation because changes of ΔH^* are too small to be significant. This result is in agreement with the findings of Price [16] who indicated that chroma is critical in

Table 2
Colorimetric values calculated for UV-aged pure rabbit glue samples.

Check time	ΔE_{cmc}	ΔL^*	ΔC^*	ΔH^*
24	1.72	0.36	−1.67	−0.16
48	2.11	0.53	−2.04	−0.07
72	2.37	0.62	−2.29	−0.16
96	2.53	0.67	−2.43	−0.16
120	2.67	0.69	−2.58	−0.12
144	2.79	0.64	−2.71	−0.14
200	3.15	0.70	−2.74	−0.17

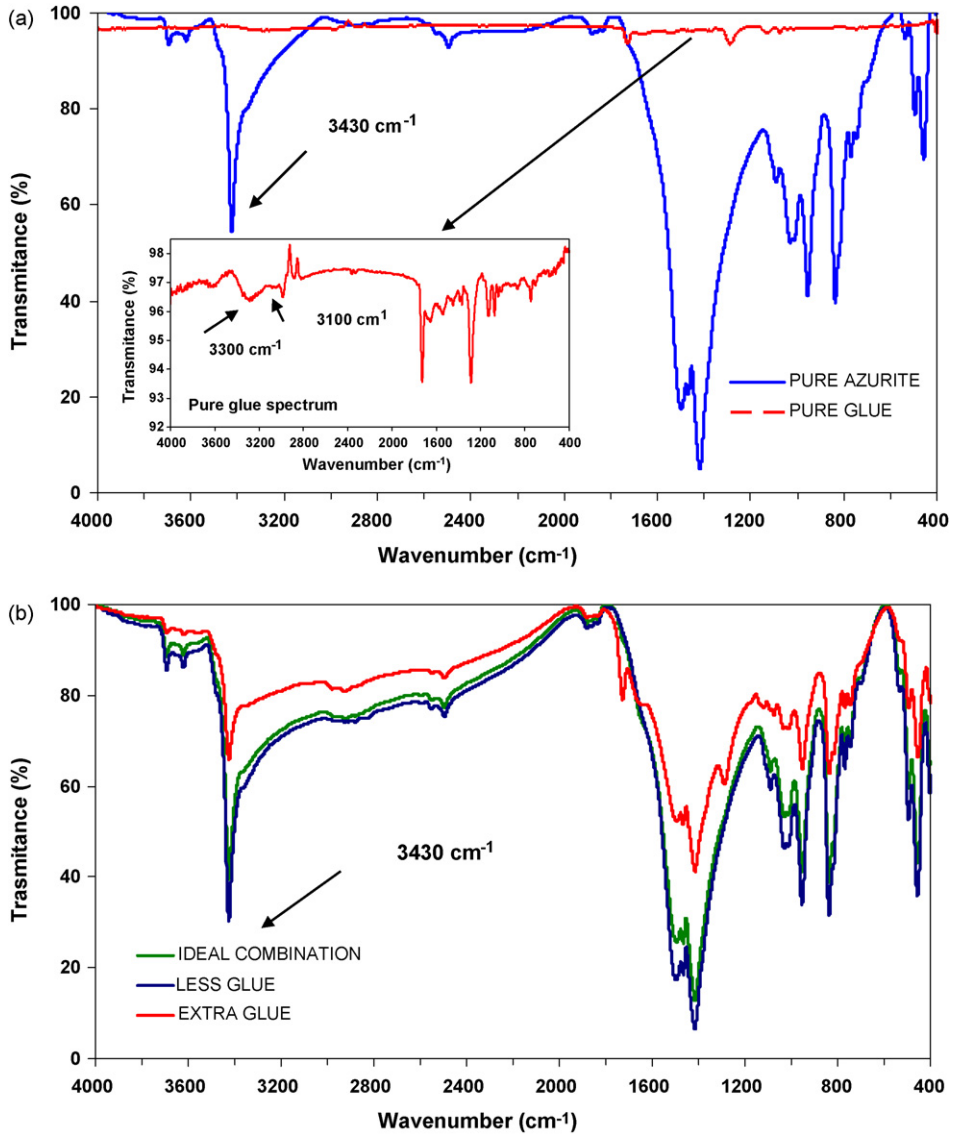

Fig. 1. FT-IR spectra of fresh samples: (a) pure glue sample and pure azurite sample; (b) azurite/glue mixtures in the different ratios studied.

Table 3
PCA results.

Data matrix	FT-R region (cm^{-1})	PC	Variance account (%)	Variance accumulated (%)
Glue	2900–3600	PC1	93.9	93.9
		PC2	4.9	98.9
Azurite	2100–3600	PC1	43.4	43.4
		PC2	29.1	72.5
		PC3	11.4	83.9
		PC4	7.2	91.1
		PC5	4.4	95.6
Azurite/Glue (less glue)	2100–3600	PC1	97.7	97.7
		PC2	1.4	99.1
Azurite/Glue (ideal mixture)	2100–3600	PC1	95.0	95.0
		PC2	3.5	98.6
		PC3	1.1	99.7
Azurite/Glue (extra glue)	2100–3600	PC1	93.9	93.9
		PC2	4.5	98.4
		PC3	0.9	99.3
All azurite samples (pure and mixed with glue)	2100–3600	PC1	93.5	93.5
		PC2	3.8	97.3
		PC3	1.6	98.9

azurite color changes. In the azurite/glue mixture samples the differences in ΔE_{cmc} are even smaller than in the pure azurite sample after 3000 h of UV irradiation (Table 1).

Table 2 shows the results of ΔE_{cmc}, ΔL^*, ΔC^* and ΔH^* in the pure rabbit glue model samples. An increase in ΔE_{cmc} and a decrease in ΔC^* values are seen, as in the pure azurite model sample, although by contrast a slight increase in ΔL^* is detected. Our results indicate that azurite is photostable after 3000 h of UV irradiation (no color changes detectable by human eye occurred). Nonetheless the results for the pure glue sample indicate that beyond 200 h of UV irradiation exposure a color change takes place. However when glue is mixed with azurite this tendency to darken is not observed, which suggests that the presence of azurite promotes photostabilization of the glue and thus permanency in the overall paint system. This result agrees with the preliminary findings of Price regarding the stability of azurite mixed with diverse protein binders under ordinary conditions [16].

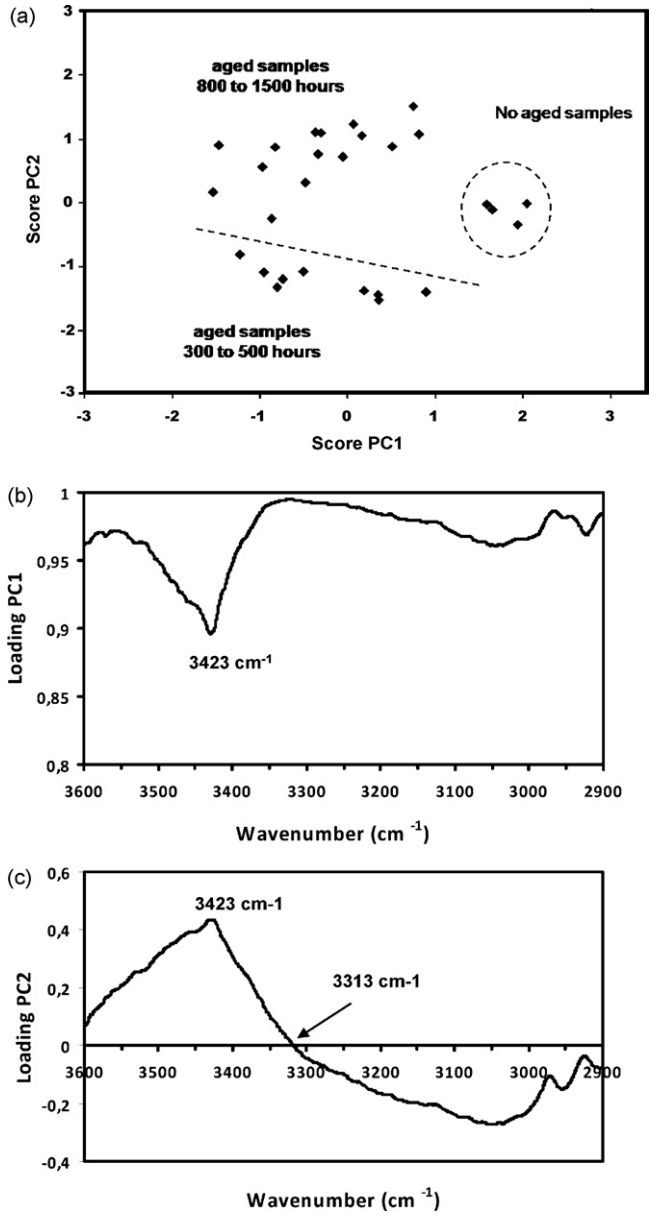

Fig. 2. PCA performed on the IR region between 2900 cm^{-1} and 3600 cm^{-1} of the pure glue sample: (a) score plot of PC1 and PC2; (b) loading plot of PC1; (c) loading plot of PC2.

3.2. PCA analysis on FT-IR data. SEM-EDS and XRD results

The FT-IR spectra were registered from 400 cm^{-1} to 4000 cm^{-1} and they were formed by 3734 data points. At each check time studied, the five model samples were characterized by five FT-IR spectra. Fig. 1 shows the FT-IR spectra of pure glue sample (Fig. 1a), pure azurite sample (Fig. 1a), and the different azurite/glue mixture samples (Fig. 1b).

Several IR regions were selected to perform the PCA analysis in accordance with the sample composition. Fingerprint was selected in all samples by its unique absorption pattern (600–1450 cm^{-1}). The IR region between 1500 cm^{-1} and 1750 cm^{-1}, representative of adsorption bands due to carbonyl stretching, and the IR region between 2900 cm^{-1} and 3600 cm^{-1}, that includes the amide bands A (around 3300 cm^{-1}) and B (around 3100 cm^{-1}) were tested in the PCA of the pure glue samples. The IR regions (600–1450 cm^{-1}, 1455–1600 cm^{-1} and 2100–3600 cm^{-1}) used to perform PCA in azurite-laden samples were selected from the visual analysis of the azurite FT-IR spectra. These regions include, in addition to the fingerprint, FT-IR regions between 1455 cm^{-1} and 1600 cm^{-1} (small absorption band) and between 2100 cm^{-1} and 3600 cm^{-1} (characteristic azurite absorption band).

The PCAs were performed on the data matrices of every model sample. These data matrices were constructed using the IR spectra of the model samples at the different UV irradiation check times and also including fresh samples. In this way, as samples were checked seven times and every check was characterized by five IR spectra, 35 IR spectra were represented in every data matrix (five data matrices, one for each studied model sample). The PCs were obtained using both the covariance data matrices (scaling

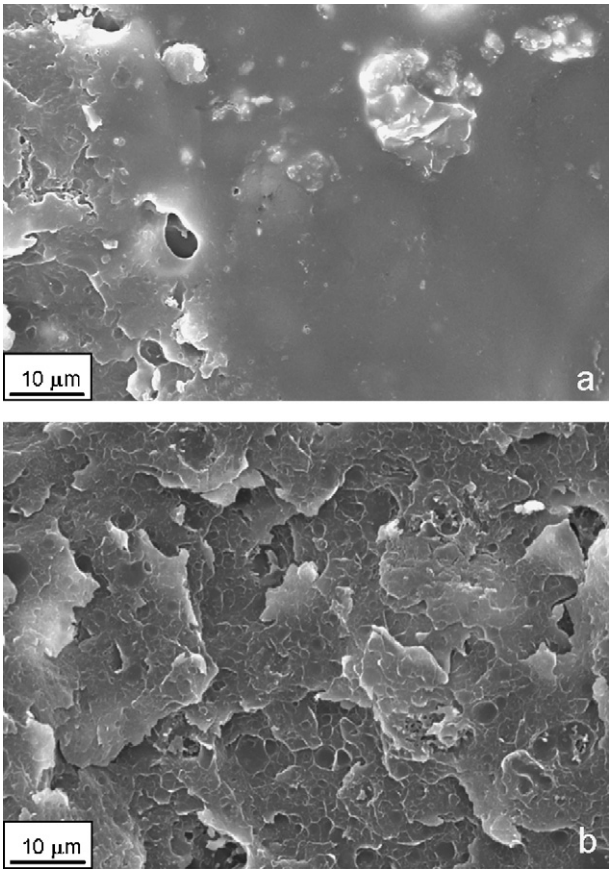

Fig. 3. SEM photographs of pure glue samples showing: (a) the smooth surface of the fresh glue sample; (b) the polygonal cracking developed on the surface of the glue sample aged by 1500 h of UV irradiation.

by mean-centered data) and the correlation data matrices (scaling by unit variance). The results were clearly better when PCA were performed on the correlation data matrices, so the results shown and discussed here correspond to autoscaled data. A simple data-centering procedure is often adopted for spectral data [28,29], because the applied autoscaling procedure assigns the same relevance to each IR spectral region. Thus spectral regions with small variation – no relevant IR bands – can acquire the same importance as large IR bands related to important functional groups. Therefore in this work, only IR bands containing the greatest variability were selected to apply PCA (not the whole IR spectrum). This may explain why results were more interpretable when data were autoscaled since no relevant bands were included in the PCA. The results of the PCA in terms of explained variance (%) and cumulative explained variance (%) for each model sample are shown in Table 3.

In accordance with previous work [8], PCA successfully detected changes associated with ageing processes in the glue model sample. In the score plots of PC1 and PC2 (Fig. 2a), accounting for 98.89% of the total spectral variance, there is a clear separation between aged and fresh samples. PC1 alone separated fresh samples from aged ones, so this PC accounts mainly for the separation of aged and fresh glue samples with a 93.94% of the total spectral variance. Fresh samples gave the highest scores on this PC. From the corresponding loading plots (Fig. 2b), it could be assumed that the IR region between 2900 cm^{-1} and approximately 3333 cm^{-1} suffered a general IR transmittance decreased when glue samples were aged because this IR region had the highest weight on the scores. The band at 3423 cm^{-1} on the loading plot was no discriminant on this PC1 since its weight was the smallest. Nevertheless, the information related with this band was explained on PC2, where this band showed larger weights (highest loading values). Scores for PC2 separated samples aged up to 500 h from samples aged more than 500 h; fresh samples gave zero scores or lightly negative score. From the analysis of the corresponding loading plots, it is clear that samples with negative scores had high IR transmittances in the band between 2900 cm^{-1} and 3313 cm^{-1}, and samples with positive scores had high IR transmittances in the 3423.99 cm^{-1} band. In fresh samples, the transmittance values of these two IR bands compensated each other. Nevertheless a combination of both components, PC1 and PC2, was needed to separate samples aged at different times. Again in agreement with previous work [8], these results show that the UV irradiation on glue samples causes changes mainly in the IR region between 2900 cm^{-1} and 3600 cm^{-1}, where the amide bands A and B are included.

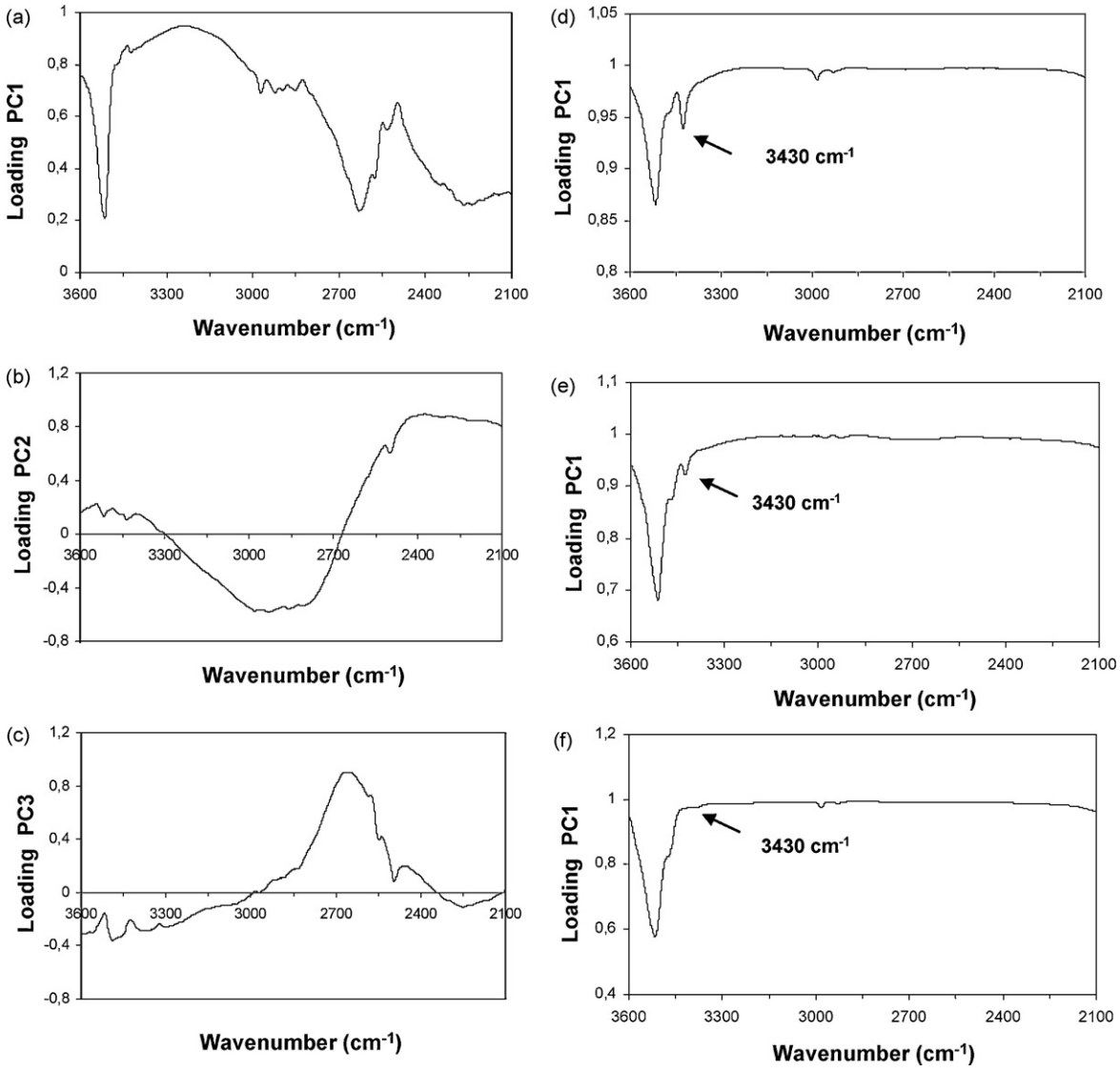

Fig. 4. Loading plots of azurite-laden samples for the IR region between 2100 cm^{-1} and 3600 cm^{-1}: (a), (b) and (c) correspond to the PC1, PC2 and PC3 of the pure azurite sample respectively; and (e), (f) and (g) correspond to the PC1 of the less-, ideal- and extra-glue contents in the azurite-laden samples respectively.

The SEM study in SE-mode of the pure glue samples' microstructure at different UV exposure times revealed that damage processes occurred prior to 200 h of UV irradiation (first inspection time). Damage intensified with increased UV irradiation doses, leading to a polygonal crack pattern in the surface of the glue (Fig. 3).

PCA of the different azurite-laden sets gave no information related to the UV-ageing test in the IR regions studied. The distribution of the scores plots related to ageing was indistinct. For example, Fig. 4 shows the scores plot of azurite/glue ideal mixture when PCA was performed on the IR region between 2100 cm^{-1} and 3600 cm^{-1}. Although glue was present in the three model of mixture samples, PCA could not detect changes associated with the UV test – contrary to what was obtained for pure glue samples. The lack of an interpretable pattern in azurite-laden model samples (both pure and mixture samples) suggests that the UV-ageing process did not introduce systematic chemical changes that could be detected by multivariate analysis of the IR spectrum. Therefore it seems that the pigment is UV-photostable either when alone or mixed with glue as already reported in the literature [16]. Moreover this finding suggests that azurite could prevent the glue UV-photodegradation when both components are blended, irrespective of their concentrations in the mixture, since the pure glue model samples degrade under UV irradiation, as mentioned above.

In fact, XRD revealed that azurite (ICDD card 11-682) was the main crystalline phase in all fresh samples, with quartz, SiO_2 (ICDD card 46-1045) being present only in minor amounts (c.a. 2%). Throughout the UV-ageing test no changes in mineral composition took place in any of the azurite-laden samples, neither in the pure samples nor in the azurite/glue mixture samples. The SEM-EDS study in BSE-mode provided elementary composition information. Results from fresh pure samples revealed the occurrence of grains made of Cu, O and Si (Fig. 5a) that were attributed to azurite and quartz respectively, in agreement with the XRD results. In addition grains containing Fe, Mg, Al, and Si apart from Cu and O were detected with this technique and ascribed to clay minerals, Fe–Mg-rich aluminosilicates (Fig. 5b). SEM analyses performed at different UV irradiation times in both pure and mixed samples did not yield interpretable results in terms of mineral changes, since the same elements were analyzed.

Nevertheless differences in the PCA results were found in all azurite-laden samples mainly in the IR region 2100–3600 cm^{-1}, where the characteristic band of azurite is located, together with the amide bands A and B of the glue. Table 3 shows that the first five PCs accounted for 95% of the total spectral variance when the PCA was performed on the azurite pure data matrix, whereas the PC1 s accounted for more than 90% of the spectral variance when the PCA was performed on the different kind of azurite/glue mixed data matrices. No interpretable results were found when analyzing the score plots and the loading plots of the corresponding PCA. Fig. 6 shows how the loadings of the PCs of the pure azurite model sample were characterized by great variability in their weights (Fig 6a–c). Instead the PC1s for azurite/glue mixtures were a weighted average of the intensities from 2100 cm^{-1} to approximately 3300 cm^{-1} (Fig. 6d–f), contributing all this variable (wavenumber) to the scores with similar weight. The PC2 in the three azurite/glue mixtures accounted for the information related to the band at 3518 cm^{-1}. This band corresponds to the characteristic band of azurite, and could be related to the different azurite contents in the KBr pellet. From these results it can be inferred that the presence of glue in azurite samples removed different sources of spectral variability.

As revealed by SEM analyses in ES-mode, which provide information on particle morphology (size and shape) and on overall sample micro-texture characteristics, when both fresh azurite and glue are mixed, glue wraps azurite particles but these remain independent of each other (Fig. 5a). With increasing UV-irradiation

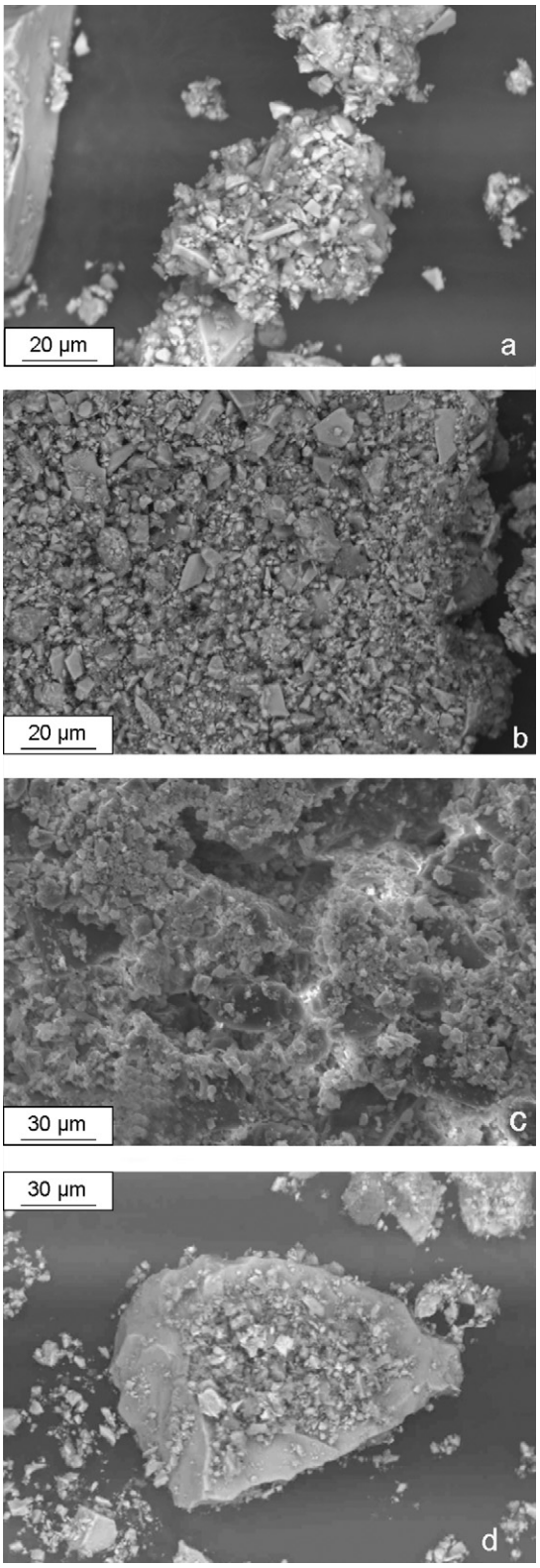

Fig. 5. SEM photographs of azurite-laden samples: (a) glue wrapping azurite crystals leading to the formation of isolated azurite-glue clusters; (b) continuous and homogeneous azurite-glue paste; (c) glue film adsorbing azurite particles onto its surface; (d) irregular azurite particles covered with "dust" made of smaller azurite crystals and impurities.

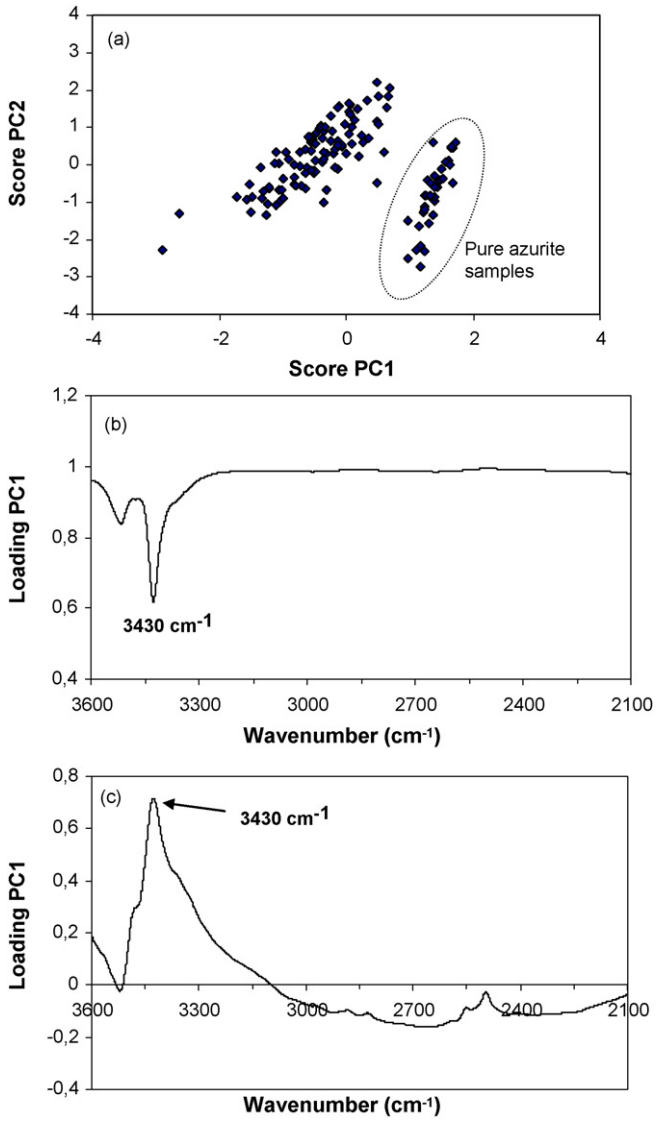

Fig. 6. PCA performed on the IR region between 2900 cm^{-1} to 3600 cm^{-1} of all azurite-laden samples (pure and mixed): (a) score plot of PC1 and PC2; (b) loading plot of PC1; (c) loading plot of PC2.

doses, particles start to form clusters enlarging in size, until a homogeneous azurite/glue paste is formed at 1500 h of UV irradiation (Fig. 5b). Thus, higher UV-irradiation doses cause glue to behave as an adhesive tending to adsorb loose azurite particles onto its surface (Fig. 5c, to be compared with Fig. 3b). Similar trends were observed in the mixtures with less glue and with extra glue. This encasement of azurite particles in the layer of glue could justify why variations in the IR spectral data were not detected. Additionally it could be the cause of the increased stability of the glue when combined with azurite.

Instead, when azurite stands alone – pure azurite samples – SEM images show loose and irregular particles of uneven size ranging from <1 μm to around 120 μm. Additionally, particles are covered with "dust" (Fig. 5d) that according to Price [16] corresponds to impurities of smaller crystals normally associated with this natural pigment. In our case impurities of quartz and clays were confirmed by SEM-EDS. Both this "dust" and the variation in azurite particle size could be responsible for the different sources of variability in the IR spectral data, since both can vary the amount of light reflected, refracted and transmitted in the azurite single particles.

Finally, PCA was performed on a data matrix constructed using all the FT-IR spectra of all azurite-laden samples, both pure and mixture samples samples at (w/v) different ratios. The FT-IR regions (600–1450 cm^{-1}, 1455–1600 cm^{-1} and 2100–3600 cm^{-1}) were used to perform PCA on mean-centered data and autoscaled data.

The most informative FT-IR region was again that between 2100 cm^{-1} and 3600 cm^{-1}, but using mean-centered data. The results of this PCA are shown in Table 3 and the projection of the original data onto the plane of the first two PCs, explaining 97.3% of the total variance, is shown in Fig. 6a. Two clear groups can be distinguished, one containing all azurite/glue mixture samples and the other containing pure azurite samples, with both PCs necessary to separate the samples. Loading plots of PC1 (Fig. 6b) indicate that the IR region between 2100 cm^{-1} and approximately 3250 cm^{-1} dominates the distinction between azurite samples with or without glue. The presence of glue in the samples decreased the IR transmittances in this IR region, since samples without glue showed the highest score on PC1. No pattern distribution was identified into the groups. PC2 accounts for the information related to the azurite band at around 3430 cm^{-1} (Fig. 6c). Although the FT-IR spectra were quite similar for all samples containing pigment, PCA was capable of distinguishing whether glue was present or not in the samples.

4. Conclusions

This work represents a study of artificial UV-ageing processes of a blue copper pigment-glue tempera painting technique, particularly on azurite and rabbit skin glue, focused mainly on component interactions, thus emulating real situations that can be found in historical paintings. The study shows the successful application of several analytical techniques to this aim. Spectrocolorimetry together with PCA on FT-IR data supplied valuable information in this regard; in addition to detecting physico-chemical changes occurring in painting model samples, these techniques were capable of providing insights into age-induced alterations. SEM-EDS and XRD analyses were essential to corroborate the obtained results.

Moreover, the results show that the glue binder alone suffers strong degradation after UV irradiation. By contrast, the presence of azurite seems to improve the photostabilisation of the glue against UV damage, thus promoting the permanency of the overall paint system, whatever the glue concentration used in the analyzed model samples. This finding suggests that azurite protects the glue binder against UV degradation.

Acknowledgements

Financial support for this work was provided by Spanish Science Ministry Projects BHA2003-08671 and HUM-2006-09262/ARTE, the Andalusian Research Group RNM-179, and a research contract from the Junta de Andalucia awarded to C. Cardell. We wish to thank A. García-Beltrán for assistance and A. Kowalski for English revision.

References

[1] J. Aze, J.M. Vallet, M. Pomey, A. Baronnet, O. Grauby, Eur. J. Miner. 19 (2007) 883.
[2] V. Brezová, J. Pigosová, B. Havlínová, D. Dvoranová, M. Durovi, Dyes and Pigments 6 (2) (2004) 177.
[3] P. Ballirano, A. Maras, Eur. J. Miner. 18 (2006) 589.
[4] S. Gaspard, M. Oujja, P. Moreno, C. Mendez, A. García, C. Domingo, M. Castillejo, Appl. Surf. Sci. 255 (2008) 2675.
[5] A. Andreotti, I. Bonaduce, M.P. Colombini, G. Gautier, F. Modugno, E. Ribechini, Anal. Chem. 78 (2006) 4490.
[6] R. Checa-Moreno, E. Manzano, G. Mirón, L.F. Capitán-Vallvey, J. Sep. Sci. 31 (2008) 3817.
[7] C. Cardell, L. Rodríguez-Simón, I. Guerra, A. Sánchez-Navas, Archaeometry 51 (4) (2009) 637.

[8] E. Manzano, N. Navas, R. Checa-Moreno, L. Rodriguez-Simón, L.F. Capitán-Vallvey, Talanta 77 (2009) 1724.
[9] E. Marengo, M.C. Liparota, E. Robotti, M. Bobba, Vib. Spectrosc. 40 (2006) 225.
[10] M.P. Colombini, F. Modugno, J. Sep. Sci. 27 (3) (2004) 147.
[11] M.P. Colombini, F. Modugno, R. Fuoco, A. Tognacci, Microchem. J. 73 (2002) 175.
[12] A. Karpowicz, Stud. Conserv. 26 (1981) 153.
[13] M. Bacci, C. Cucci, E. Del Federico, A. Ienco, A. Jerschow, J.M. Newman, M. Picollo, Vib. Spectrosc. 49 (2009) 80.
[14] J.L. Pérez-Rodríguez, C. Maqueda, C. Jiménez de Haro, P. Rodríguez-Rubio, Atmos. Environ. 32 (1998) 993.
[15] F. Capitelli, J. Anal. Appl. Pyrol. 71 (2004) 405.
[16] M. Price, Leonardo 33 (2000) 281.
[17] M. Odlyha, N.S. Cohen, G.M. Foster, R. West, Thermochim. Acta 365 (2000) 53.
[18] J. Striova, M. Camaiti, M. Matteini, A. Sansonetti, A. De Cruz, R. Palmer, E.M. Castellucci, A. Anderotti, M.P. Colombini, Lasers in the Conservation of Artworks (LACONA VII), PA-20, S-118, 2007.
[19] S. Bruni, F. Cariati, F. Casadio, L. Toniolo, Vib. Spectrosc. 20 (1999) 15.
[20] N. Navas, J. Romero-Pastor, E. Manzano, C. Cardell, Anal. Chim. Acta 630 (2008) 141.
[21] E. Marengo, E. Robotti, M.C. Liparota, M.C. Gennaro, Anal. Chem. 75 (20) (2003) 5567.
[22] R. Checa-Moreno, E. Manzano, G. Mirón, L.F. Capitán-Vallvey, Talanta 75 (2008) 697.
[23] M. Chappé, J. Hildenhagen, K. Dickmann, M. Bredo, J. Cult. Herit. 4 (2003) 264.
[24] F. Pacheco, El arte de la pintura (Ed.), Cátedra, Madrid, Spain, 1990.
[25] CMC: Calculation of small colour differences for acceptability, in: ATCC Technical Manual. AATCC Test Method, American Association of Textile Chemists and Colorists, vol. 173, 1989.
[26] J.D. Martín-Ramos, Using XPowder: A Software Package for Powder X-Ray Diffraction Analysis. (GR 1001/04. ISBN 84-609-1497-6), 2004.
[27] J. Rodríguez-Gordillo, M.P. Saéz-Pérez, J. Durán-Suárez, A. García-Beltrán, Color Res. Appl. 32 (2007) 65.
[28] E. Robotti, M. Bobba, A. Panepinto, E. Marengo, Anal. Bioanal. Chem. 388 (2007) 1249.
[29] D.L. Massart, B.G.M. Vanderginste, Handbook of Chemometrics and Qualimetrics, Elsevier, Amsterdam, 1997.

Conclusiones

Con este trabajo queda demostrada la potencialidad del empleo conjunto de una serie de técnicas espectroscópicas junto con análisis multivariante –PCA- para obtener información sobre los procesos de envejecimiento de muestras pictóricas, particularizado en el estudio del fotoenvejecimiento de temples de azurita. El PCA de los espectros de T-FTIR ha permitido extraer información sobre el comportamiento de dichos materiales frente a la radiación UV. Además, los análisis por colorimetría, SEM-EDS y XRD han sido esenciales para corroborar los resultados obtenidos por PCA.

En particular, el estudio de las réplicas de cola pura ha revelado un deterioro apreciable tras 200 horas de exposición. Estos resultados se han deducido a partir de la información del PCA en la región del infrarrojo comprendida entre 2100 y 3600 cm^{-1}, donde se encuentran localizadas las bandas amida A y B características de la cola, junto con el estudio de las imágenes de electrones secundarios de la cola pura obtenidas por SEM. Además, a partir de estos resultados se infiere que la degradación producida debe de estar relacionada con alteraciones de los grupos amida. Sin embargo, cuando se aplica la metodología propuesta al estudio de las muestras de temples de azurita, tanto en réplicas puras como en los distintos temples de cola, los resultados obtenidos por PCA de los espectros de T-FTIR, además de la información derivada de los análisis por SEM-EDX, DRX y colorimetría, revelan la estabilidad de la azurita frente a la acción dañina de la radiación UV.

A destacar también como conclusión, que el proceso de envejecimiento por radiación UV es independiente de la concentración de aglutinante en las réplicas estudiadas, siendo el factor determinante la presencia o no del pigmento azurita. Por otra parte, y viniendo a corroborar trabajos anteriores no incluidos en esta Tesis Doctoral, la zona del aglutinante más afectada por el envejecimiento, y por tanto, aquella más informativa desde el punto de vista del análisis mediante PCA, es la región infrarroja comprendida entre 2100 y 3600 cm^{-1}.

8. Uso de patrón mineral de control y PCA para validación de los datos espectrométricos de muestras compuestas alteradas térmicamente

Mejor no mirar atrás con rabia, o adelante con miedo, sino alrededor de ti con conciencia.

James Grover Thurber (1894-1961)
Escritor estadounidense

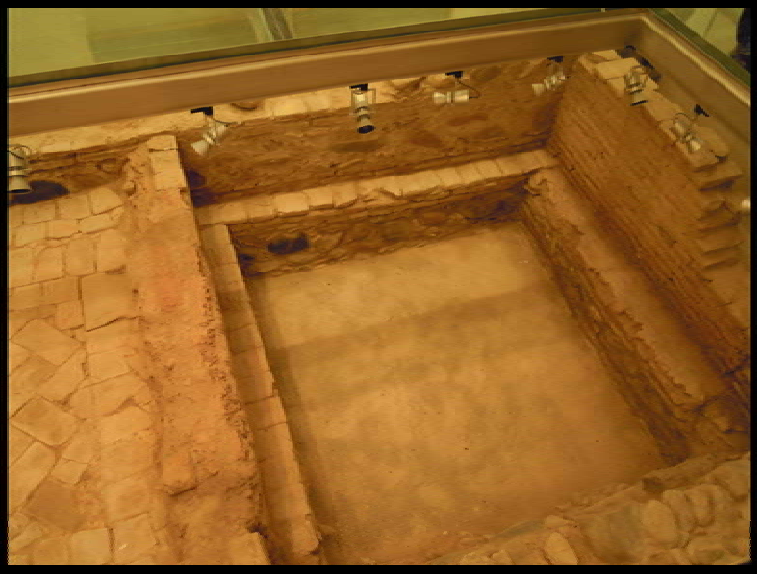

Internal mineral standard and PCA as tools to validate the quality of spectroscopy data of thermally aged composite materials (2011). **J. Romero-Pastor**, C. Cardell, A. Yebra-Rodríguez, A. B. Rodríguez- Navarro. J. European Mineralogy. (submitted paper, April 2011).

Resumen

Este trabajo aborda la capacidad del PCA para validar la calidad de los datos espectrales obtenidos mediante RM y ATR-FTIR de réplicas pictóricas envejecidas a baja temperatura (<250ºC). Para este estudio se analizaron con RM mezclas de cuarzo-albúmina (proteína presente en el huevo) en diferente proporción y mediante ATR-FTIR muestras de hueso natural de gallina (compuesto por hidroxiapatito y materia orgánica) sometidas a diferentes temperaturas. Para validar la calidad de los datos espectrales obtenidos se analizaron mediante PCA los intervalos espectrales que contienen tanto las bandas características del cuarzo y del hidroxiapatito, como las bandas de absorción características del material orgánico presente en las muestras. El cuarzo y el hidroxiapatito son estables al tratamiento térmico aplicado y, por tanto, sus bandas espectrales deben permanecer constantes a lo largo del ensayo de alteración. En consecuencia, estas fases minerales pueden ser utilizadas como patrones de control de proceso de degradación del material orgánico con los que se encuentran mezclados.

Los resultados de este estudio permiten determinar que en el caso de las réplicas de cuarzo-albúmina, la proporción más adecuada para el uso de cuarzo como patrón de control es del 70% (en peso). Por otra parte, en las muestras de hueso sometidas a envejecimiento térmico se usó la señal del hidroxiapatito (principal componente del hueso) como control interno. Los resultados obtenidos mediante RM demuestran la capacidad del PCA para detectar cambios en los componentes orgánicos presentes en el hueso (que son susceptibles a la degradación térmica), mientras que la señal del hidroxiapatito permanece estable a lo largo del proceso de alteración térmica. Además, este método ha puesto de manifiesto que el PCA es independiente respecto de factores instrumentales, preparación de la muestra, o técnicas de análisis utilizadas durante el proceso de medida.

Internal mineral standard and PCA as tools to validate the quality of spectroscopy data of thermally aged composite materials

Julia ROMERO-PASTOR[1], Carolina CARDELL[1], Africa YEBRA-RODRÍGUEZ[2], Alejandro B. RODRÍGUEZ-NAVARRO[1]*

[1]Dept. Mineralogy and Petrology. Faculty of Science, University de Granada. Campus Fuentenueva s/n, 18071 Granada, Spain.

[2]Dept. Geology–Associated Unit IACT (CSIC-UGR), Faculty of Experimental Science, University of Jaén, Campus Las Lagunillas s/n, 23071 Jaén, Spain

*anava@ugr,es

Abstract. This work shows the capability of Principal Component Analysis (PCA) to detect molecular, chemical and mineralogical changes in composite materials subjected to a thermal ageing test (<250ºC). To this end transformation processes in two sets of samples containing two mineral phases (quartz and hydroxyapatite) and two organic compounds (albumin and collagen) were investigated. Quartz/albumin-laden samples were studied using Attenuated Total Reflectance–Fourier Transform Infrared (ATR-FTIR) spectroscopy, and Raman microscopy (RM) was applied to characterise hydroxyapatite/collagen samples. The chosen minerals behaved as internal standards during the experiments since they are chemically inert at the tested temperatures. The set of samples made of four different quartz/albumin mixtures having quartz contents of 30%, 50%, 70% and 90% (w/w) were designed to identify the ideal proportion of internal standard to be validated by ATR-FTIR and PCA, determined to be 70%. The other set of tested samples was chicken bone composed of the mineral hydroxyapatite (70%) and organic compounds, mainly collagen (30%). Results demonstrated the capability of PCA to detect changes in the molecular structures of the organic

components while the mineral used as an internal standard remained stable. Moreover, the results of PCA analyses were independent of instrumental and technical factors, as well as sample collecting and handling.

Key-words: PCA, thermal ageing test, internal standard, mineral phase, proteinaceous binders, ATR-FTIR and RM.

1. Introduction

The study of alteration processes of painting artworks is challenging due to the complexity of the composition of these materials and the variety of alteration mechanisms to which they might be subjected, as well as interferences among them. Paintings contain pigments, mainly mineral phases (i.e., azurite, cinnabar, minium), and a specific binding media such as calcium carbonate, protein binders or drying oils (Mayer, 1988; Vandenabeele *et al.*, 2000; Hradil *et al.*, 2002, 2003, 2004; Cardell & Navarrete-Aguilera, 2006, Cardell *et al.*, 2009a). Painting materials are very sensitive to the influence of atmospheric pollution and varying environmental conditions associated with climate change (Ballirano and Maras, 2006; Aze *et al.*, 2007; Marengo *et al.*, 2004, 2005, 2006; Mazzeo & Joseph, 2007, Manzano *et al.*, 2010). Recent studies show how pigments and organic binders are subjected to mineralogical changes and chemical modifications when exposed to different environmental factors (i.e., sunlight, humidity) (Aze *et al.*, 2006, 2007; Cotte *et al.*, 2006; Van Der Snickt *et al.*, 2009; Manzano *et al.*, 2010). For instance, Aze and co-workers (2006) revealed that red lead pigment (Pb_3O_4) transformed into cerussite ($PbCO_3$) and anglesite ($PbSO_4$) during the natural ageing of *frescos*. Other studies describe how organic components are even more easily degraded

than pigments due to oxidation or denaturalisation processes produced by varying environmental conditions such as temperature, humidity or UV radiation (Marengo *et al.*, 2004, 2005, 2006).

The identification of painting materials and their alteration products is used to define the painting techniques and preservation state of the artwork, and to determine which alteration mechanisms are at play. Moreover, knowing the stability and/or chemical modification of painting materials is critical to designing the right strategy for the conservation or restoration of painting artworks (Aze *et al.*, 2006; Cotte *et al.*, 2006; Cardell *et al.*, 2006, 2009a; Monico *et al.*, 2011). In any case, a combination of advanced analytical techniques is necessary to fully characterise all the organic and mineral constituents in a painting (Ballirano & Maras, 2006; Monico *et al.*, 2011).

Regarding advanced analytical techniques, Infrared and Raman spectroscopies provide a wealth of information regarding chemical composition and structural characteristics of inorganic and biomolecular compounds (Fuchs *et al.*, 2001; Thongnopkun & Ekgasit, 2006; Mazzeo & Joseph, 2007; Doménech-Carbó, 2008; Cardell *et al.*, 2009b). These analytical techniques are increasingly applied to characterise complex materials (i.e., plastics, nanocomposites, ceramics, artefacts) and to study their chemical behaviour during formation or transformation processes (Franco *et al.*, 2006; Furlan *et al.*, 2007, Mazzeo and Joseph., 2007; Muik *et al.*, 2007; Benavente *et al.*, 2008). However, the complexity of analytical data from painting materials makes necessary the use of sophisticated statistical and mathematical methods for data analysis. In this regard, there has been increasing interest in the application of chemometric tools to spectral data, to assist in the characterisation of Cultural Heritage materials with complex composition (Trafela *et al.*, 2007; Navas *et al.*, 2008; Gambaro *et al.*, 2009; Colao *et al.*, 2010; Rosi *et al.*, 2010). Thus, methods of multivariate data analysis that allow data reduction are

especially useful to extract the most relevant information from the spectral data; Principal Component Analysis (PCA) is one of the most commonly used of these methods. In fact, PCA greatly facilitates analytical data interpretation and helps to classify or group samples according to their similarities, for instance, in composition and/or molecular conformation (Wilcken & Schulten, 1996; Dyrby *et al.*, 2005; Furlan *et al.*, 2007). In the case of paintings, simulations of natural ageing processes such as oxidation, UV-radiation or thermal degradation to which these painting materials are subjected are especially relevant. In fact, the application of PCA to spectral data from these objects helps to identify significant changes in painting components, and thus to recognise the most sensitive materials which may require special protection (Marengo *et al.*, 2004, 2005, 2006; Verbi-Pereira & Silveira-Bueno, 2009; Manzano *et al.*, 2010). In particular PCA has been used to study in detail chemical changes ocurring in organic components subjected to a thermal test (Le Blond *et al.*, 2009).

Nevertheless, spectral data are highly dependent on multiple factors such as instrument settings, sample preparation and handling or acquisition time. Additionally, instrumental miscalibration or measurement errors can substantially modify spectral data including changes in peak intensities or positions, or even the apparence of spurious peaks. In any case, these changes in spectral data can induce the misclassification of samples with similar characteristics in different groups when using PCA methods. This in turn may induce erroneous conclusions about alteration processes or mechanisms to which they have been subjected. Also, sensitive components can be altered during analysis, for example by laser exposition during Raman analysis. In this regard, Navas and co-workers (2010) noticed that a minium pigment readily degraded when irradiated with the 514.5 nm excitation line at any power, yielding a spectrum similar to that of massicot (orthorhombic PbO), with the main band at 277 cm^{-1}.

In order to detect and correct these systematic and other instrumental errors it is necessary to evaluate data quality by measuring substances with well-known and accurate spectral data (Ramos & Ruisánchez, 2005). The spectra generated by these standard substances can be compared with the tabulated spectral data to check for any changes arising from differences in sample handling, instrument miscalibration, or other problems which may arise during sample measurement. The standard substances can be a natural component of the studied sample or can be intentionally added. Ideally, standards must be chemically stable in the face of the treatment to which the samples are subjected, and should not react with any sample components, so that their contribution to the spectra is constant throughout the test and measurement period.

This work describes a methodology based on the use of internal standards to validate the results of PCA. To this end, we have studied the molecular and mineralogical changes, during an accelerated thermal aging test, on two sets of samples, i.e. quartz (SiO_2)/albumin and chicken bone (composed mainly of hydroxyapatite, Hap, $Ca_{10}(PO_4)_6(OH)_2$ and collagen). To characterise these samples, respectively, Attenuated Total Reflectance Fourier Transform Infrared (ATR-FTIR) spectroscopy and Raman Microscopy (RM) were used. Subsequently, the spectral data were analysed by PCA. In both cases, quartz and hydroxyapatite were selected as internal standard minerals since they are stable through the thermal tests (< 250ºC), and their spectral bands do not overlap the bands of albumin and collagen. To validate the PCA results, spectral signals associated with the internal standards must remain constant.

2. Experimental Section

Reagents and samples. Pure quartz (SiO_2) was mixed with albumin (Kremer Pigments GmbH & Co.KG; CI:PB 63250) to prepare four different quartz/albumin mixtures with quartz contents of 30%, 50%, 70% and 90% (w/w). The use of quartz as an extender is very frequent in historical paintings (Mayer, 1988; Cardell *et al.*, 2006, 2009a). For the other set of experiments, fresh chicken bone (femur) composed of hydroxyapatite (70%) and organic material (30%, mainly collagen, a protein-based material) were selected and ground using a cryomill (CertiPrep 6750, Freezer/Mill,SPEX). Powdered burned bones have been traditionally used as white or black pigments (Mayer, 1988; Eastaugh *et al.*, 2004; Van Loon and Boon, 2004; Correia *et al.*, 2007, Cardell *et al.*, 2009b). In addition, the use of albumin and collagen as organic binders is common in historical paintings. For instance, albumin is present in egg which is a traditional media used in the *tempera grassa* painting technique (Cennini, 1988; Mayer, 1988). On the other hand, collagen extracted from animal skins, bones or fishes has been used as a binder since Ancient Egypt (Chiavari *et al.*, 1995). Non-aged (untreated) samples were used as blanks and analysed.

Thermal-aging processes. The quartz/albumin mixtures were divided into four fractions. One fraction was used as a blank sample (control sample) and the other three were heated to different temperatures, i.e. 150ºC, 200ºC and 250ºC using a muffle Thermo Scientific Thermolyne, mod. F4791026 (USA) during 15 minutes. Subsequently, the resultant samples were analysed by ATR-FTIR. Similarly, the powdered bone sample was divided into four fractions. One fraction was used as control sample and the other three were heated in the same oven to 100ºC, 150ºC and 250ºC. Afterwards, such samples were analysed by RM.

Attenuated Total Reflectance Fourier Transform Infrared (ATR-FTIR) Spectroscopy. A JASCOFTIR6200 spectrometer (JASCO, Tokyo, Japan) equipped

with an ATR diamond crystal plate (MIRacle^{TM} ATR accessory, PIKE Technology) was used to analyse the quartz/albumin mixtures samples treated at different temperatures. For each measurement, 200 scans were co-added with a resolution of 2 cm^{-1} in the region of 650 cm^{-1} to 4000 cm^{-1}. Smoothing and baseline fitting were performed using the JASCO software Spectra Manager v.2. Each sample was consecutively measured 10 times for subsequent statistical analyses.

Raman Microscopy (RM). A Renishaw Invia Raman microscope system fitted with a Peltier-cooled CCD detector and a Leica DMLM microscope was used to analyse the inorganic and organic compounds present in the bone samples. Samples were excited with a 785 nm diode laser over the range of 400 – 3200 cm^{-1} with an average spectral resolution of approximately 1 cm^{-1}. To improve signal-to-noise ratios, 10 spectra collected consecutively during 15s each were averaged. Spectra were taken by placing the samples on the microscope stage and focusing on them with a 50x objective. The video camera attached to the microscope enabled selection of the sample area to be analysed and laser focus. To avoid any damage to the samples, 50% laser power (150 mW) was employed. Each sample treated at different temperatures was consecutively analysed 10 times for statistical analyses.

Statistical analyses. The spectra acquired from the studied samples subjected to different thermal treatments were combined on an Excel spreadsheet and the resulting data matrices were used as input data for the PCA analyses. PCA analyses were performed using the Statistical Product and Service Solutions program (SPSS, for Windows v.15, USA). Specifically, in the case of the quartz/albumin mixtures, four different data matrices were prepared containing spectra data from each mixture prepared at different ratios, which included 10 spectra of the quartz/albumin samples at

each temperature studied (fresh and aged samples). In this way, each matrix was initially formed by 40 spectra. The principal components (PCs) were obtained using both the covariance data matrices (scaling by mean-centered data) and the correlation data matrices (scaling by unit variance). PCA results from correlation data matrices were better, as showed in previous works (Navas *et al.*, 2008, 2010). Thus, the results shown and discussed here correspond to autoscaled data. In this work only regions containing relevant bands were selected to apply PCA. Similarly, for the bone samples a correlation data matrix was prepared containing the information from 40 spectra.

3. Results and Discussion

In the case of the quartz/albumin mixtures (quartz contents of 30%, 50%, 70% and 90%), the spectral region from 600 to 1770 cm^{-1} containing the characteristic bands of quartz (779, 796, 1060 and 1089 cm^{-1}) and the albumin (1156, 1440, 1524 and 1660 cm^{-1}) were analysed by PCA (Bosch-Reig *et al.*, 2002; Furlan *et al.*, 2007). In this work, the optimum amount of quartz contained in the composite samples has to be established to determine the quartz signal strong enough to be detected without interfering with the albumin bands. Four PCA analyses were carried out, one for each quartz/albumin mixture. Table 1 summarises the explained variance for the PCA analyses on each group of samples. The best results were clearly obtained when the proportion of quartz in the quartz/albumin mixture samples was 70% (Fig.1).

Table 1. PCA results in the quartz/albumin mixture samples.

	ATR-FTIR region (cm^{-1})	PC	Variance explained (%)	Accumulated variance explained (%)
30% quartz/albumin	760-1700	PC1	73.6	73.6
		PC2	23.3	96.9
50% quartz/albumin	950-1730	PC1	77.4	77.4
		PC2	21.7	99.1
70% quartz/albumin	650-1730	PC1	95.1	95.1
		PC2	3.7	98.8

Figure 1

The PCA results for samples containing 30% and 50% of quartz showed a greater variability in their weights (Fig.2-3). In these multivariate analyses, the first calculated PC accounted for more than 70% of the variance present in the spectra. In particular as Table 1 shows it is 73.3% in the case of the 30% quartz/albumin samples, 77.4% in the case of the 50% quartz/albumin samples, and 95.1% in the case of the 70% quartz/albumin samples. This indicates mainly one source of variability in the spectra being observed mainly in 70% albumin/quartz.

In particular, scores plots for 30% quartz/albumin samples showed separation of samples in groups according to the temperature of treatment, i.e. four groups were clearly discriminated when the first two PCs were plotted against each other (Figure 2a). These two first PCs account for 96.9% of the total variance (see Table 1). The loading plot of the PC1 showed a high weight for the whole band between 1200 and 1700 cm^{-1} where some characteristic Raman bands of albumin appear. Additionally, the corresponding plots of PC2 loadings showed the highest weight at 1690 cm^{-1} revealing a shift in the position of the amide I band from 1636 to 1690 cm^{-1} (Fig. 2b). This result indicates an alteration of three dimensional structure of albumin associated with its thermal degradation, in agreement with Furlan and co-workers (2007).

Figure 2

On the contrary, only three clusters were identified for 50% quartz/albumin mixture samples when plotting the PC1 against the PC2 (these two PC accounted for 99.1% of the total variance). Specifically, the untreated (fresh) samples had negative scores for PC1; while the samples treated at 150ºC and 200ºC were grouped in one cluster around zero scores for both PCs (Fig. 3a). Another group with positive score for PC1 was identified, which included data from samples treated at 250ºC. In these samples, the corresponding loading plot was less informative than for the 30% mixture samples. A broad region of high weight resulted and no relevant information was obtained (Fig. 3b).

Figure 3

In the case of the quartz/albumin mixtures containing 70% of quartz, the score plot of PC1 (95.1%) versus PC2 (3.7%) accounted for 98.8% of the total variance, and the samples treated at the same temperature were grouped in the same cluster with clusters of samples treated at different temperatures well separated, i.e. four groups were identified in the first two component projection (Fig.4a). The information contained in the loading plot of this PC when plotted versus the wavenumber values analysed showed that the values with the lowest weight were those at 779 cm^{-1}, 1060 cm^{-1} and 1089 cm^{-1}, which correspond to the characteristic bands of quartz (Fig. 4b). This is due to the fact that quartz is stable in the temperature range of the test and thus its spectral bands are unaffected by the thermal treatments, as expected. On the contrary, PC2 did not add relevant information to the first PC, accounting for less than 5% of the variance. On the other hand, in the case of the 90% quartz/albumin mixture sample, the PCA results were not interpretable since the quartz bands masked the characteristic spectral bands of albumin (not shown). Thus, in this later case, the excessive amount of quartz in

the mixture prevented the gathering of high quality data for the albumin, and it was not possible to distinguish in which way albumin was altered by the thermal test.

Figure 4

Figure 5 shows the Raman spectra of the bone samples treated at different temperatures in the region between 400 and 3200 cm^{-1} where thermal degradation is evident. The PCA analysis of the spectral data was focused on the region from 650 to 1730 cm^{-1} which included the main characteristic Raman bands of the principal chemical component of bones, i.e. the phosphate band of the Hap mineral and the amide or C-H groups of proteins and lipids (Le Blonde *et al.*, 2009). The two first principal components explained 99.97% of the total variance of the data (Fig. 5). Scores for PC1 and PC2 showed that data from bone samples treated at the same temperature were grouped in the same cluster, and the clusters of samples treated at different temperatures separated well. In particular, PC1 (accounting for 94.6% of total variance) distinguishes fresh untreated bone samples with positive scores from aged bone samples heated at 100ºC, 150ºC and 250 ºC, which showed negative scores (Fig. 6a). On the other hand, the information contained in PC2 (accounting for 5.1% of total variance) was associated with the thermal degradation of samples up to 250ºC (with negative scores), separating aged samples from the rest of the bone samples studied, which showed positive scores (Fig.6a).

In addition, the analysis of the corresponding values of loadings plots of PC1 and PC2 revealed strongly negative values for the wavenumbers associated with the main phosphate band of Hap (around 958 cm^{-1}; Fig.6b). This result indicates that the spectral bands of the Hap mineral remain unchanged during the heating test. This result was expected since Hap is stable over the temperature range selected in this work, and more importantly, it confirms the quality of the results of the PCA analyses and that the data

aquired are correct. On the contrary, bands associated with proteins and lipids showed positive weight of the loadings plots of PC2 (Fig. 6b), indicating that these components are strongly affected by the thermal test. In particular, the PC2 loading plot clearly showed that these bands have an important contribution and are more strongly affected in samples heated at 250ºC. In this case, the most notable changes –to the amide I band at about 1640 – 1670 cm^{-1}, i.e. ט C=O (α helix) and for ט (CCtrans) at 1125 cm^{-1} of phospholipids and proteins– could be indicative of a conformational change of protein secondary structure (Furlan et al., 2007; Fig. 5). The bands at 1295 cm^{-1} and 1438 cm^{-1} associated with lipids were also notably affected by the temperatures of the test in agreement with results from other authors (Furlan *et al.*, 2007; Le Blond *et al.*, 2009).

Figure 5

Figrure 6

4. Conclusions

This work has demonstrated the capability of PCA to distinguish changes in the molecular structures of organic components present in complex samples containing both mineral phases and organic compounds, due to an accelerated thermal aging test. The quality of the data and the validity of the PCA results were assessed by the use of quartz or hydroxyapatite as internal standards added to different samples containing either albumin or collagen. The refered minerals remained unaltered in the studied samples during the thermal tests, contributing constantly to the spectra. In addition, this validation method made possible identification of the suitable proportion of internal standard to be added to a sample, in such a way that it can be used to validate results of PCA analyses. Basically, the amount of the mineral used for internal standard has to be

enough to produce a relatively high intensity peak so that it can contribute significantly to the spectra. For instance, in this study the concentration of the mineral used as internal standard should be around 70% (by weight) in the mixture (inorganic-organic) sample to obtain a good spectral signal from both type of compounds.

Regarding the spectrometric techniques used to characterise the composite samples, both ATR-FTIR and RM showed similar capability to validate the quality of the PCA results. However, RM provided higher spectral resolution and thus a better discrimination of samples by PCA analyses.

Based on the results of this study, we propose the following recommendations in order to validate results of spectra data analysed by PCA obtained from complex samples. The substance used as an internal standard should be stable and chemical inert for the test conditions, i.e. stable against temperature or other parameters or agents such as acids or UV radiation. Regarding thermal aging processes, we propose the use of mineral phases such as quartz, apatite or hydroxyapatite which are stable within a large temperature range. The material of choice to be used as a standard also should ideally have a simple spectrum, with a single or few characteristic spectral bands, which in addition should not mask the key bands of the organic or inorganic compounds present in the analysed sample.

The validation methodology of PCA described here, based on the use of a stable mineral standard, might be also valid for many mineralogical studies, such as archeological investigations involving transformation or reaction processes of minerals. For instance, it can be applied to better understand the alteration of mineral pigments (clay minerals, realgar, minium, etc.) commonly found in buried archaeological artefacts (metals or potteries) . Additionally, it can be useful to determine the compatibility or reaction of materials introduced during restoration interventions, with the original ones.

5. Acknowledgements. This research was supported by Projects P08-RNM-04169 and Research Groups RNM-179 and RNM-325 (CICE, JA, Spain). The authors thank "Centro de Instrumentación Científico Técnica" of the University of Jaén, Spain. We wish to thank Dr. A. Kowalski for English revision.

6. References

Aze, S., Vallet, M., Baronnet, A., Grauby, O. (2006): The fading of red lead pigment in wall paintings: tracking the physico-chemical transformations by means of complementary micro-analysis techniques. *Eur. J. Mineral.,* **18,** 835-843.

Aze, S., Vallet, M., Pomey, M., Baronnet, A., Grauby, O. (2007): Red lead darkening in wall paintings: natural ageing of experimental wall paintings versus artificial ageing tests. *Eur. J. Mineral.,* **19**, 883–890.

Ballirano, P. & Maras, A. (2006): In-situ X-ray transmission powder diffraction studi of the light-induced alteration of realgar (α-As_4S_4). *Eur. J. Mineral.*, **18**, 589–599.

Benavente, D., Cultrone G., Gómez-Heras, M. (2008): The combined influence of mineralogical, hygric and thermal properties on the durability of porous building stones. *Eur. J. Mineral.*, **20**, 673–685.

Bosch-Reig, F., Gimeno-Adelantado, J.V., Moya-Moreno, M.C.M. (2002): FTIR quantitative analysis of calcium carbonate (calcite) and silica (quartz) mixtures using the constant ratio method. Application to geological samples. *Talanta,* **58,** 811–821.

Cardell-Fernández, C., Navarrete-Aguilera, C. (2006): Pigment and plasterwork analyses of nasrid polychromed lacework stucco in the Alhambra (Granada, Spain). *Stud. in Conserv.,* **51**, 161–176.

Cardell, C., Rodríguez-Simón, l., Guerra, I., Sánchez-Navas A. (2009a): Analysis of Nasrid Polychrome Carpentry at the Hall of the Mexuar Palace, Alhambra Complex (Granada, Spain), combining microscopic, chromatographic and spectroscopic methods. *Archaeometry* **51**, 637–657.

Cardell, C., Guerra, I., Romero-Pastor, J., Cultrone, G., Rodríguez-Navarro, A. (2009b): Innovative Analytical Methodology Combining Micro-X-Ray Diffraction, Scanning Electron Microscopy-Based Mineral Maps, and Diffuse Reflectance Infrared Fourier Transform Spectroscopy to Characterize Archeological Artifacts. *Anal. Chem.* **81**, 604–611

Cennini, C., (1988): El Libro del Arte, Ed. Akal. Madrid.

Chiavari, G., Fabbri, D., Galletti, G. C., Mazzeo, R. (1995): Use of analytical pyrolysis to characterize Egyptian painting layers. *Chromatographia,* **40**, 594–600.

Colao, F., Fantoni, R., Ortiz, P., Vázquez, M.A., Martín J.M., Ortiz R., Idris N. (2010): Quarry identification of historical building materials by means of laser induced breakdown spectroscopy, X-ray fluorescence and chemometric analysis. *Spectrochim. Acta B,* **65**, 688–694.

Correia, A. M., Clark, R. J. H., Ribeiro, M. I. M., Duarte, M. L. T. S. (2007): Pigment study by Raman microscopy of 23 paintings by the Portuguese artist Henrique Pousao (1859–1884). *J. Raman Spectrosc.* **38**, 1390–1405.

Cotte, M., Susini, J., Metrich, N., Moscato, A., Gratziu, C., Bertagnini, A., Pagano, M. (2006): Blackening of Pompeian cinnabar paintings: X-ray microspectroscopy analysis. *Anal. Chem.* **78**, 7484–7492.

Doménech-Carbó M.T., Kuckova S., de la Cruz-Cañizares J., Osete-Cortina L. (2006). Study of the influencing effect of pigments on the photoageing of terpenoid resins used as pictorial media. *J. Chromatogr. A* **1121**, 248–258.

Doménech-Carbó M.T. (2008): Novel analytical methods for characterising binding media and protective coatings in artworks. *Anal. Chim. Acta*, **621**, 109–139.

Dyrby, M., Baunsgaard, D., Bro R., Engelsen, S. B. (2005): Multiway chemometric analysis of the metabolic response to toxins monitored by NMR. *Chemometr. Intel.l Lab.,* **76**, 79– 89.

Eastaugh, N., Walsh, V., Chaplin, T., Siddall, R. (2004): Pigment Compendium. A Dictionary of Historical Pigments. Elsevier Butterworth-Heinemann: Oxford.

Franco, F., Pérez-Maqueda, L. A., Ramirez-Valle, V., Pérez-Rodriguez, J. L. (2006): Spectroscopic study of the dehydroxylation process of a sonicated antigorite. *Eur. J. Mineral.*, **18**, 257–264.

Fuchs, Y., Mellini, M., Memmi, I. (2001): Crystal-chemistry of magnesiocarpholite: controversial X-ray diffraction, Mössbauer, FTIR and Raman results. *Eur. J. Mineral.*, **13**, 533–543.

Furlan, P.Y., Scott, S.A., Peaslee, M.H. (2007): FTIR-ATR study of pH effects on egg albumin secondary structure. *Spectrosc. Lett.* **40**, 475-482.

Gambaro, A., Ganzerla, R., Fantin, M., Cappelletto, E., Piazza, R., Cairns, W. (2009): Chemical and statistical characterization of selected documents from the archives of the Palazzo Ducale (Venice, Italy). *Anal. Chim. Acta*, **651**, 139–148.

Hradil, D., Hradilová, J., Hrebícková, B. (2002): Clay minerals in pigments of mediaeval and baroque paintings. *Geol. Carpath.,* **53**, 123–126.

Hradil, D., Grygar, T., Hradilová, J., Bezdička, P. (2003): Clay and iron oxide pigments in the history of painting. *Appl. Clay Sci.,* **22**, 223–236.

Hradil, D., Grygar, T., Hrusková, M., Bezdicka, P., Lang, K., Schneeweiss, O., Chvátal, M. (2004): Green earth pigment from the Kadan region, Czech Republic: Use of rare Fe-rich smectite. *Clay Clay Miner.,* **52**, 767–778.

Le Blond, S., Guilminot, E., Lemoine, G., Huet, N., Mevellec, J.Y. (2009): FT-Raman spectroscopy: A positive means of evaluating the impact of whale bone preservation treatment. *Vib. Spectrosc,* **51**, 156–161.

Manzano, E., Romero-Pastor, J., Navas, N., Rodríguez-Simón, L.R., Cardell, C. (2010): A study of the interaction between rabbit glue binder and blue copper pigment under UV radiation: A spectroscopic and PCA approach. *Vib. Spectrosc,* **53**, 260–268.

Marengo, E., Robotti, E., Liparota, M. C., Gennaro, M. C. (2004): Monitoring of pigmented and wooden surfaces in accelerated ageing processes by FT-Raman spectroscopy and multivariate control charts. *Talanta,* **63**, 987–1002.

Marengo, E., Liparota, M. C., Robotti, E., Bobba, M., Gennaro, M. C. (2005): The state of conservation of painted surfaces in the presence of accelerated ageing processes monitored by use of FT-Raman spectroscopy and multivariate control charts. *Anal. Bioanal. Chem.* **381**, 884–895.

Marengo, E., Liparota, M. C., Robotti, E., Bobba, M. (2006): Monitoring of paintings under exposure to UV light by ATR-FT-IR spectroscopy and multivariate control charts. *Vib Spectrosc,* **40**, 225–234.

Mayer, R. (1988): Materiales y Técnicas del Arte. Ed. Hermann Blume. Madrid.

Mazzeo, R. & Joseph, E. (2007): Attenuated total reflectance microspectroscopy mapping for the characterisation of bronze corrosion products, *Eur. J. Mineral.*, **19**, 363–371.

Monico, L., Van der Snickt, G., Janssens, K., de Nolf, W., Miliani, C., Dik, J., Radepont, M., Hendriks, E., Geldof, M., Cotte, M. (2011): Degradation Process of Lead Chromate in Paintings by Vincent van Gogh Studied by Means of Synchrotron X-ray Spectromicroscopy and Related Methods. 2. Original Paint Layer Samples. *Anal. Chem.,* **83**, 1224–1231.

Muik, B., Lendl, B., Molina-Diaz, A., Valcarcel, M., Ayora-Canada, M. J. (2007): Two-dimensional correlation spectroscopy and multivariate curve resolution for the study of lipid oxidation in edible oils monitored by FTIR and FT-Raman spectroscopy. *Anal. Chim. Acta*, **593**, 54–67.

Navas, N., Romero-Pastor, J., Manzano, E., Cardell, C. (2008): Benefits of applying combined diffuse reflectance FTIR spectroscopy and principal component analysis for the study of blue tempera historical painting. *Anal. Chim. Acta*, **630**, 141–149.

Navas, N., Romero-Pastor, J., Manzano, E., Cardell, C. (2010): Raman spectroscopic discrimination of pigments and tempera paintmodel samples by principal component analysis on first-derivative spectra. *J. Raman Spectros.,* **41**,1196–1203.

Ramos, P.M. & Ruisánchez, I. (2005). Noise and background removal in Raman spectra of ancient pigments using wavelet transform. *J. Raman Spectrosc.*, **36**, 848–856.

Rosi, F., Miliani, C., Clementi, C., Kahrim, K., Presciutti, F., Vagnini, M., Manuali, V., Daveri, A., Cartechini, L., Brunetti, B. G., Sgamellotti, A. (2010): An integrated spectroscopic approach for the non-invasive study of modern art materials and techniques. *Appl. Phys A.,* **100**, 613–624.

Thongnopkun, P. & Ekgasit, S. (2006): Attenuated total reflection Fourier transform infrared spectra of faceted diamonds. *Anal. Chim. Acta*, **576**, 130–135.

Trafela, T., Strlič, M., Kolar, J., Lichtblau, D.A., Anders, M., Mencigar, D.P., Pihlar, B. (2007): Nondestructive analysis and dating of historical paper based on IR spectroscopy and chemometric data evaluation. *Anal. Chem.*, **79**, 6319–6323.

Vandenabeele, P., Wehling, B., Moens, L., Edwards, H., De Reu, M., Van Hooydonk, G. (2000): Analysis with micro-Raman spectroscopy of natural organic binding media and varnishes used in art. *Anal. Chim. Acta.* **407**, 261–274.

Van Der Snickt, G., Dik, J., Cotte, M., Janssens, K., Jaroszewicz, J., De Nolf, W., Groenewegen, J., Van Der Loeff, L. (2009): Characterization of a degraded cadmium yellow (CdS) pigment in an oil painting by means of synchrotron radiation based X-ray techniques. *Anal. Chem.* **81**, 2600–2610.

Van Loon, A. & Boon, J. J. (2004): Characterization of the deterioration of bone black in the 17th century Oranjezaal paintings using electron-microscopic and micro-spectroscopic imaging techniques. *Spectrochim. Acta B* **59**, 1601–1609.

Verbi-Pereira, F. M. & Silveira-Bueno, M. I. M. (2009): Evaluation of varnish and paint films using digital image processing, energy dispersive X-ray fluorescence spectrometry and chemometric tools. *J. Coat. Technol. Res.*, **6**, 445–455.

Wilcken, H. & Schulten, H.R. (1996): Quality control of paints: Pyrolysis-mass spectrosmetry and chemometric. *Anal. Chim. Acta*, **336**, 201–208.

Figure Captions

Fig.1. ATR-FTIR spectra of 70% quartz/albumin sample from 650 to 4000 cm^{-1} fresh and treated at 150ºC, 200ºC and 250ºC.

Fig.2. PCA of the thermal ageing of the 30% quartz/albumin sample in the ATR-FTIR region between 760 and 1700 cm-1 a) Scores plots and b) loading plots for PC1 and PC2. Figure includes ageing at different temperature (Fresh; 150ºC; 200ºC and 250ºC).

Fig.3. PCA of the thermal ageing of the 50% quartz/albumin sample in the ATR-FTIR region between 950 and 1730 cm^{-1}. a) Scores plots and b) loading plots for PC1 and PC2. Figure includes ageing at different temperature (Fresh; 150ºC; 200ºC and 250ºC).

Fig.4. PCA of the thermal ageing of the 70% quartz/albumin samples in the ATR-FTIR region between 650 and 1730 cm^{-1} a) Scores plots and b) loading plots for PC1 and PC2. Figure includes ageing at different temperature (Fresh; 150; 200 and 250ºC).

Fig.5. Thermal ageing of bone samples. RM spectra of fresh and aged bone samples at 100ºC, 150ºC and 250ºC from 400 to 3200 cm^{-1}.

Fig.6. PCA in the RM region between 650 and 1730 cm^{-1}; a) Scores plots and b) loading plots for PC1 and PC2.

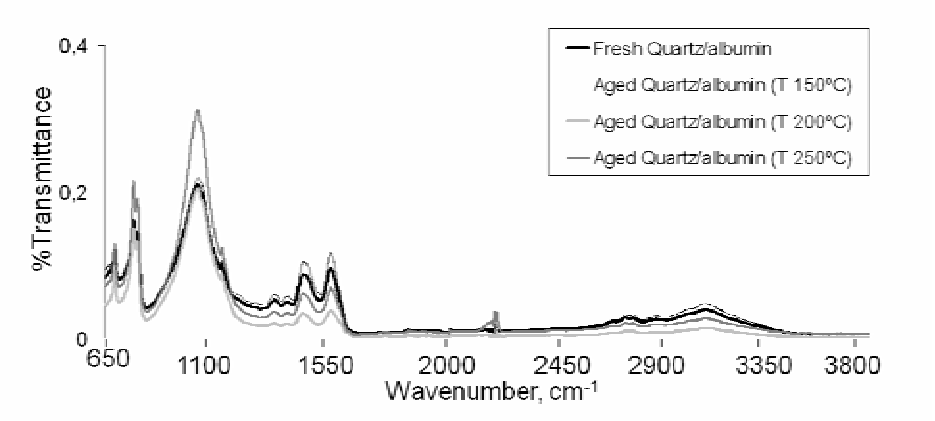
Fresh Quartz/albumin
Aged Quartz/albumin (T 150ºC)
Aged Quartz/albumin (T 200ºC)
Aged Quartz/albumin (T 250ºC)
%Transmittance
0,4
0,2
0
650
1100
1550
2000
2450
2900
3350
3800
Wavenumber, cm-1

Fig.1.

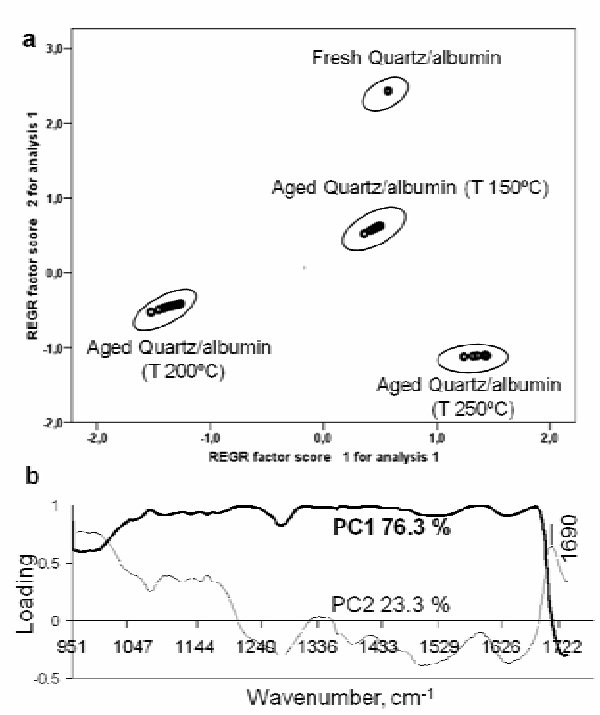
a
Fresh Quartz/albumin
Aged Quartz/albumin (T 150ºC)
Aged Quartz/albumin
(T 200ºC)
Aged Quartz/albumin
(T 250ºC)
REGR factor score 2 for analysis 1
REGR factor score 1 for analysis 1
b
PC1 76.3 %
PC2 23.3 %
1690
Loading
951
1047
1144
1240
1336
1433
1529
1626
1722
Wavenumber, cm-1

Fig.2.

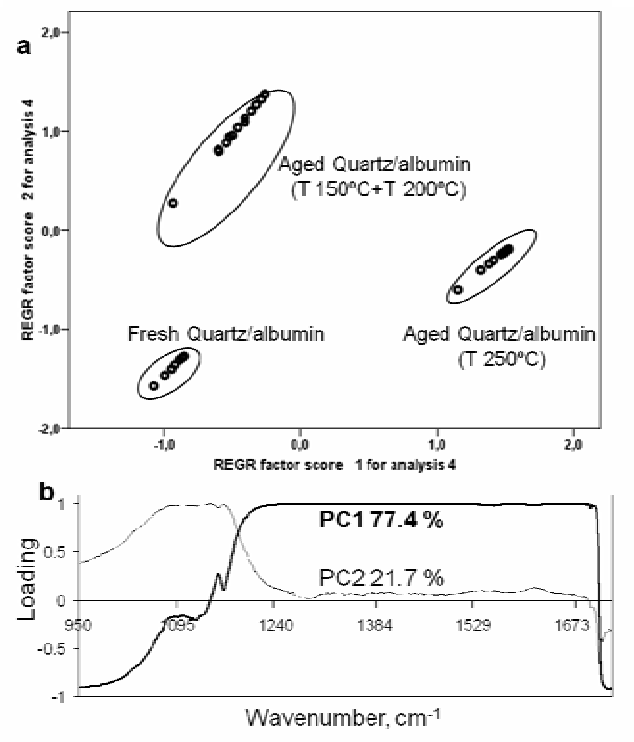
a
Aged Quartz/albumin
(T 150°C+T 200°C)
Fresh Quartz/albumin
Aged Quartz/albumin
(T 250°C)
REGR factor score 2 for analysis 4
REGR factor score 1 for analysis 4
b
PC1 77.4 %
PC2 21.7 %
Loading
Wavenumber, cm-1

Fig.3.

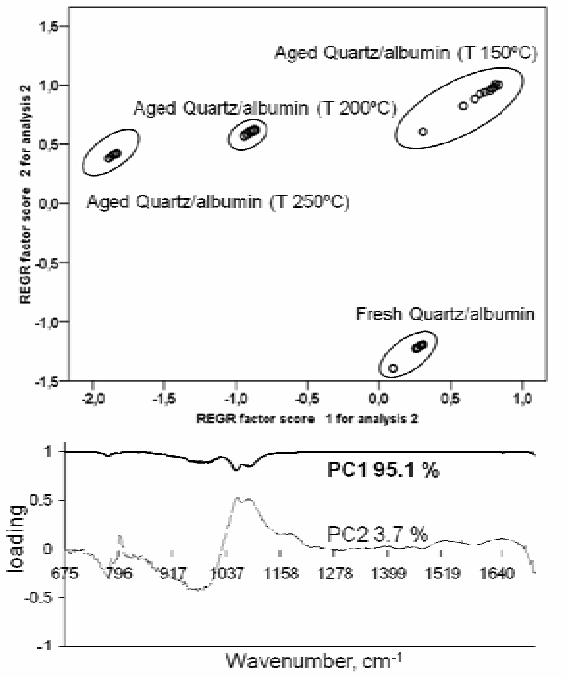
Aged Quartz/albumin (T 150°C)
Aged Quartz/albumin (T 200°C)
Aged Quartz/albumin (T 250°C)
Fresh Quartz/albumin
REGR factor score 2 for analysis 2
REGR factor score 1 for analysis 2
PC1 95.1 %
PC2 3.7 %
loading
Wavenumber, cm-1

Fig.4.

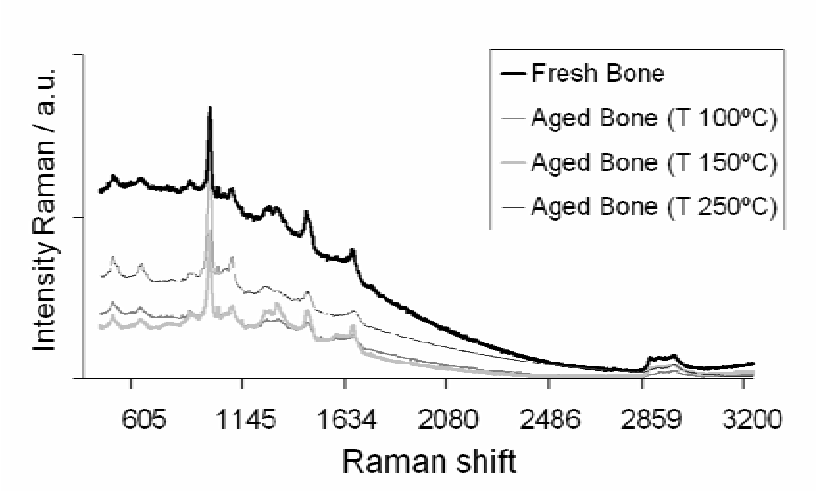
Fresh Bone
Aged Bone (T 100ºC)
Aged Bone (T 150ºC)
Aged Bone (T 250ºC)
Intensity Raman / a.u.
605
1145
1634
2080
2486
2859
3200
Raman shift

Fig.5.

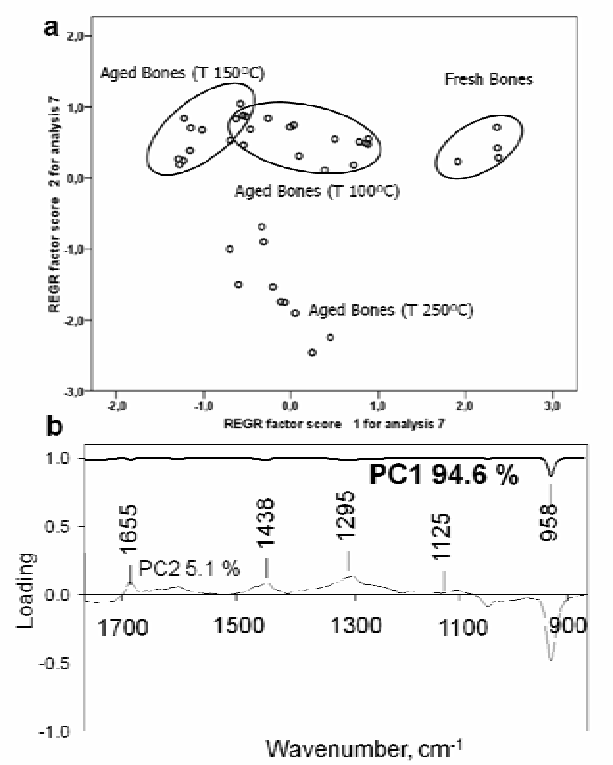
a
Aged Bones (T 150ºC)
Fresh Bones
Aged Bones (T 100ºC)
Aged Bones (T 250ºC)
REGR factor score 2 for analysis 7
REGR factor score 1 for analysis 7
b
PC1 94.6 %
PC2 5.1 %
1655
1438
1295
1125
958
Loading
1700
1500
1300
1100
900
Wavenumber, cm-1

Fig.6.

Conclusiones

Este trabajo demuestra la utilidad de usar de manera conjunta un estándar mineral interno y el PCA para evaluar la calidad de los datos espectrales obtenidos por RM y ATR-FTIR en muestras complejas como son las muestras pictóricas. En particular, esta metodología se ha aplicado al estudio de muestras binarias (mineral y materia orgánica) envejecidas a baja temperatura (< 250ºC). El análisis multivariante – PCA – de los datos espectrales confirma la estabilidad de la fase mineral al envejecimiento térmico, mientras que permite evaluar la alteración del material orgánico. Este comportamiento se pone de manifiesto cuando la proporción de la fase mineral genera una señal espectral lo suficientemente intensa para contribuir significativamente al espectro; en concreto, cuando la proporción de éste es del 70% (en peso). Asimismo, el estudio de los datos espectrales ha permitido identificar los cambios químicos y estructurales de los componentes orgánicos debido a la alteración térmica.

Con respecto a las técnicas espectrométricas utilizadas, tanto RM como ATR-FTIR muestran similar resultado para la aplicación de dicha metodología. Sin embargo, RM proporciona una mayor definición en las bandas espectrales y, por lo tanto, una mejor capacidad al aplicar PCA para separar las muestras en función de la temperatura de envejecimiento. Asimismo, este trabajo demuestra el beneficio del uso de fases minerales como cuarzo e hidroxiapatito como patrón de control dada a su estabilidad mineralógica a baja temperatura y por generar bandas de absorción simples, las cuales no enmascaran las bandas de material orgánico o inorgánico presente.

9. Estudio de la interacción pigmento-aglutinante en temples envejecidos por radiación UV mediante MALDI-TOF MS, PCA y T-FTIR

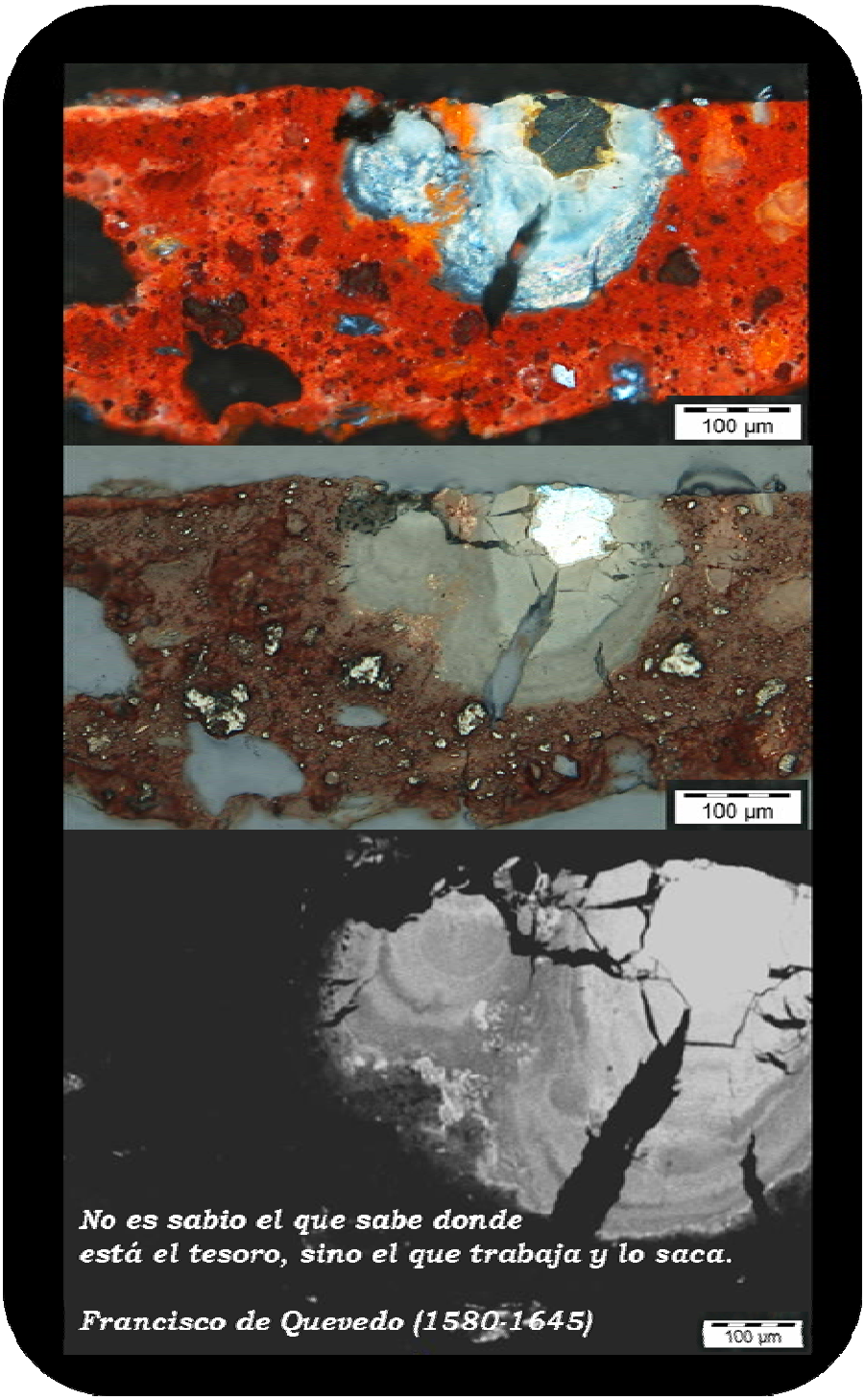

Pigment-proteinaceous binder interaction study under UV ageing conditions by MALDI-TOF-MS and Principal Component Analysis (2011). **J. Romero-Pastor**, N. Navas, S. Kuckova, A. Rodríguez-Navarro, E. Manzano, C. Cardell. Journal of Mass Spectroscopy. (Submitted paper, July 2011).

Resumen

El Capítulo 9 continúa la investigación iniciada en el Capítulo 7 sobre el estudio de los procesos de alteración de temples históricos por exposición controlada a radiación UV. Este trabajo tiene entre sus objetivos dar respuesta a las evidencias obtenidas en el Capítulo 7 sobre el diferente proceso de envejecimiento de la cola de conejo cuando se encuentra pura o cuando forma parte de temples. En este trabajo, se presenta además una nueva metodología para el estudio de réplicas pictóricas basada en un enfoque proteómico junto con en el análisis multivariante – PCA - de los mapas peptídicos obtenidos por MALDI-TOF MS, y todo ello complementado con el estudio de la estructura secundaria de la proteína mediante T-FTIR.

Concretamente, en este Capítulo se aborda el estudio de la interacción pigmento-aglutinante en temples de azurita y temples de cinabrio elaborados con recetas tradicionales, evaluando el papel del pigmento mineral en el proceso de alteración de la cola de conejo por acción de la radiación UV. Además, se lleva a cabo el estudio del envejecimiento de la cola bajo las mismas condiciones de radiación UV para poder comparar los resultados de dicho proceso en presencia y ausencia de pigmento. Paralelamente, se evalúa también la idoneidad de la metodología propuesta en el estudio de materiales pictóricos.

Concretamente, el proceso de envejecimiento se evalúa tras la exposición de las réplicas, tanto del aglutinante puro como de los temples de azurita y cinabrio, a radiación UV durante 200, 500, 800, 1500, 2500 y 3000 horas. Para ello, se analiza una pequeña cantidad de muestra de las réplicas sometiéndola a digestión con tripsina, con el objeto de obtener los correspondientes mapas peptídicos mediante MALDI-TOF MS. El análisis quimiométrico –PCA– de estos mapas peptídicos se lleva a cabo para cada tipo de réplica pictórica por separado, esto es, cola pura, temples de azurita y temples de cinabrio, incluyendo además en los análisis los datos – mapas peptídicos - de las muestras sin envejecer. De forma complementaria, se aborda el estudio de la conformación del colágeno mediante T-FTIR a partir del desplazamiento de la banda amida I (próxima a 1660 cm^{-1}) para cada tiempo de exposición a la radiación UV.

Los resultados obtenidos de todos estos estudios corroboran el diferente comportamiento frente al envejecimiento por exposición a radiación UV de la cola de conejo pura y sus mezclas con pigmentos, así como la idoneidad de la metodología propuesta para llevar a cabo el estudio propuesto. Esto es, la información obtenida gracias a las técnicas empleadas permite proponer mecanismos específicos de interacción entre el aglutinante y los pigmentos estudiados, así como posibles degradaciones debidas al envejecimiento de la cola de conejo en las réplicas pictóricas evaluadas.

Journal of Mass Spectrometry

Pigment-proteinaceous binder interaction study under UV ageing conditions by MALDI-TOF-MS and Principal Component Analysis

Journal:	*Journal of Mass Spectrometry*
Manuscript ID:	Draft
Wiley - Manuscript type:	Research Article
Date Submitted by the Author:	n/a
Complete List of Authors:	Romero Pastor, Julia; University of Granada, Department of Mineralogy and Petrology Navas, Natalia; University of Granada, Analytical Chemistry Kuckova, Stepanka; Charles University, Chemistry and Chemical Education Manzano, Eloisa; University of Granada, Analytical Chemistry Rodriguez-Navarro, Alejandro; Unversity of Granada, Department of Mineralogy and Petrology Cardell, Carolina; Unversity of Granada, Department of Mineralogy and Petrology
Keywords:	MALDI-TOF MS, Principal Component Analysis, Pigment-Proteinaceous Binder Interaction, FT-IR Protein Conformational tudy, Collagen

Pigment-proteinaceous binder interaction study under UV ageing conditions by MALDI-TOF-MS and Principal Component Analysis

Julia Romero-Pastor[a]. Department of Mineralogy and Petrology, University of Granada, Campus Fuentenueva s/n, 18071 Granada, Spain.

Natalia. Navas[b*]. Department of Analytical Chemistry, University of Granada, Campus Fuentenueva s/n, 18071 Granada, Spain.

Stephanca Kuckova[c]. Charles University, Department of Chemistry and Chemical Education, M.D. Rettigové 4, 116 39 Prague 1, Czech Republic. Institute of Chemical Technology, Department of Biochemistry and Biotechnology, Technická 5 166 28 Praha 6, Czech Republic.

Eloisa Manzano[b]. Department of Analytical Chemistry, University of Granada, Campus Fuentenueva s/n, 18071 Granada, Spain.

Alejandro Rodríguez-Navarro[a]. Department of Mineralogy and Petrology, University of Granada, Campus Fuentenueva s/n, 18071 Granada, Spain.

Carolina Cardell[a]. Department of Mineralogy and Petrology, University of Granada, Campus Fuentenueva s/n, 18071 Granada, Spain.

Corresponding author: Natalia Navas, e-mail: natalia@ugr.es; Fax: ++ 34 958 243328

ABSTRACT

This study focuses on acquiring information on the degradation process of proteinaceous binders due to UV radiation and the possible interaction owing to the presence of two historical mineral pigments. To reach this purpose, this paper proposes a novel methodology combining Principal Component Analysis of mass spectra registered by Matrix-Assisted Laser Desorption/Ionization-Time of Flight Mass Spectrometry (MALDI-TOF MS) and the conformational study by Fourier Transform Infrared (FTIR) Spectroscopy of the secondary structure of the aged collagen. The PCA has not been applied yet to MALDI-TOF MS data from art paintings with the aim of investigating compositional changes of proteinaceous binders in the ageing process, or the evidence provided by interactions between proteinaceous binder and inorganic pigments in tempera samples. The modifications in the rabbit glue binder (collagen) were periodically checked on tempera paintings of cinnabar and azurite elaborated according to medieval recipes, evaluating pure rabbit glue samples to compare the results. The approach succeeded discriminating among replica model samples based on their aged state and conformational changes due to the different role for every pigment.

Introduction

The application of organic materials in artworks is well-known, for instance, substances like oils, gums, proteins or waxes are used as traditional binders in diverse painting techniques. [1,2] In particular, proteinaceous binders have been used as binders since ancient times, e.g. egg, skin animal glue or milk, to elaborate the named tempera painting. [3,4] In the past, some researches have focused on the identification of the different types of proteins or in alteration processes. [5-11] Despite these works, the ageing processes of proteinaceous paint binders are little studied due to their complex composition and structure. Amino acids are arranged in linear chains linked by peptide bonds between the carboxyl and amino groups of adjacent amino acid residues. These chains fold into unique 3-dimensional structures which might be modified (protein denaturation) regarding to the type of alteration induced by natural or artificial processes. [12-14] Moreover, few works have centered their investigation on the role of inorganic pigments in the ageing processes of proteinaceous binders. [11,15]

The study of proteinaceous material has been performed by High Performance Liquid Chromatography (HPLC), Gas-Chromatography (CG), Fluorescence Spectroscopy (FS), Raman Microscopy (RM) or Fourier Transform Infrared Spectroscopy (FTIR). [2,5,8,9,11,16] In addition, FTIR has been used to gain molecular and conformational information via the observed shift of amide I maximum. Hydrogen bonds linking the peptide bond NH of a glycine residue with a peptide carbonyl (C═O) group in an adjacent polypeptide help hold the triple-helical structure of collagen. [17] These bands, particularly amide I band, are conformationally sensible, and are often used to determine protein secondary structure caused by intramolecular and intermolecular hydrogen bonding of amide groups. [14,18-20] In particular, amide I band (carbonyl stretching vibrations) gives information of α-helix (1647-1660 cm^{-1}), β-sheet (1615-

1640 cm^{-1}), β-turn (1660-1680 cm^{-1}), β-antiparallel sheet contents (1681-1692 cm^{-1}) or unordered structures as random coil (1646-1641 cm^{-1}). [14,19,20] Moreover, the conformational changes observed could suggest the formation of non-covalent interactions and ionic bonds. [13]

In the field of artistic materials, Matrix-Assisted Laser Desorption/Ionization Time of Flight Mass Spectroscopy (MALDI-TOF-MS) has been proposed to study fresh and photo-aged di- and triterpenoid varnish resins. [21] Also, MALDI Fourier Transform Mass Spectrometry (MALDI-FTMS) has demonstrated to be useful when investigated egg tempera. [22, 23] Recently, mass spectrometric proteomic approaches have been used in the field of Heritage Science. In particular, Matrix-Assisted Laser Desorption/Ionization Time of Flight Mass Spectroscopy (MALDI-TOF MS) is one of the most sensible MS techniques and routinely used for biomolecular analysis. [24] In fact, MALDI-TOF MS has been applied in the study and authentication of artworks during the last decade mainly due to its microdestructive character, the minimum sampling and its high identification ability. These studies have focused on the analysis of proteins from painting samples by peptide mass mapping or identification of amino acids sequence. [15,25-28]

Currently, the application of multivariate techniques such as Principal Component Analysis (PCA) is gaining relevance in the study of materials used in the Fine Arts field, and particularly, from artistic painting samples. Techniques such as T-FTIR, DRIFTS (Diffuse Reflectance FTIR Spectroscopy), GC–MS and HPLC [2,11,30-33] provide vast number and systematic data to be investigated by multivariate analysis.

In this paper, an accelerated UV test was carried out on painting model samples of pure rabbit glue (collagen) and on two mixtures with historical inorganic pigments (cinnabar and azurite). A novel combined methodology based on multivariate analysis,

i.e. PCA of MALDI-TOF mass data, and the FTIR spectra evaluation is proposed to study the UV ageing of glue-based painting samples. The multivariate analysis facilitated the interpretation of the alteration process and the estimation of the role played by the mineral pigment in the tempera samples. In addition, the visual inspection of the FTIR spectra of the samples helped detect complementary conformational changes in the secondary structure of collagen during the photoageing of these samples.

Experimental

Materials

The standard protein binder was rabbit glue (hydrolyzed collagen) purchased from *Productos de Conservación* (Madrid, Spain). Animal glue has been used as binder since ancient Egypt to elaborate historical tempera paintings. [3] Cinnabar (HgS) was acquired from *Caremi Pigmentos*, reference PR106 (Seville, Spain) with particle size <30 μm. Cinnabar was well known as pigment to the Romans and its use was related to the Almaden mines (Spain) which were the most important source of mercury in the world. [34] The azurite pigment ($Cu_3(CO_3)_2(OH)_2$) was purchased from Kremer Pigments GmbH & Co. KG (Barcelona, Spain). Pigment reference is 10200, natural azurite (CI: PB 30.77420) with particle size 80-120 μm. Azurite was used especially throughout the Middle Ages and the Renaissance. [34]

All reagents were of analytical reagent grade unless stated otherwise. Reverse-osmosis type quality water (purified with a Milli-RO plus Milli-Q station from Millipore) and HPLC quality were used throughout. Trypsin was supplied by Promega Corporation (UK). Acetonitrile, ammonium hydrogen carbonate, trifluoroacetic acid and 2,5-dihydroxybenzoic acid (DHB) were supplied by Sigma (Prague, Czech Republic).

Model samples

The painting model samples (i.e. paint reconstruction samples) were prepared according to Old Master recipes to obtain standards similar to tempera used by medieval artists. [3,11] The first painting model sample comprises the pure rabbit glue (PG) prepared as describe elsewhere. [11] The second and third tempera model samples include cinnabar-rabbit glue (Cin-G) and azurite-rabbit glue (Azu-G) mixtures (i.e. corresponding to tempera model samples) in 5.2/1 (w/v) for the called "ideal" combination (according to Old Recipes, Manzano et al., 2010). Next, the painting model samples were spread on three glass slides in five fine coats.

UV accelerated ageing test

The painting model samples were aged in a UV accelerated test chamber for 3000 h. A high-speed exposure unit SUNTEST CPS, Heraeus (Hanau, Germany), equipped with a Xenon lamp was used for the ageing test. A special UV glass filter was employed to limit the radiation at wavelengths greater than 295 nm, corresponding to outdoor solar exposure. Irradiance was set at 765 $W \cdot m^{-2}$ (XenoCal sensors to measure and calibrate irradiance). The possible chemical changes of the protein fraction in the painting model samples (PG, Cin-G and Azu-G) were checked periodically at 200, 500, 800, 1500, 2500 and 3000 h by taking the corresponding MALDI-TOF mass and IR spectra. Prior to the UV irradiation exposure (time = 0) fresh micro-samples from each painting model sample were removed and stored in glass vials in darkness to be further analyzed. These samples were considered as reference samples to be compared with the aged samples throughout the mass and IR spectral data registered. The environmental conditions during the UV ageing test were set at 30±5 ºC and the relative humidity at 15±5 % to

avoid mineralogical transformation of azurite into malachite. The measurement was registered by a thermohygrometer (OREGON Scientific, mod. EMR812HGN; Portland, Oregon, USA).

Trypsin digestion method and MALDI-TOF MS analysis

The analysis by MALDI-TOF MS requires the previous digestion and purification of the painting model samples to fragment the glue in its characteristic peptides and to eliminate the inorganic pigments and the possible impurities respectively. The digestion and purification processes involve the treatment of the sample by the trypsin digestion method cited by Kuckova et al., 2007. [27] After that, 10 drops (1.5µl) of the digested sample solution were taken and placed in spots of the stainless steel MALDI target and dried at room temperature. A mass spectrum was taken for each drop between 0 to 5000 m/z using a Bruker-Daltonics Biflex IV MALDI-TOF mass spectrometer equipped with standard nitrogen laser (337 nm) in reflector mode and employing the XMASS software (Bruker). At least 200 laser shots were collected for each mass spectrum. The recalibration of the mass spectrometer with a commercial standard of peptide mixture (Pepmix, Bruker) was performed every twenty mass spectra recorded.

MS data pre-treatment and PCA

In order to apply the multivariate analysis, mass data were pre-treated using the M-mass 2.3.0 and Delphi 6.0 softwares for conversion of the mass data into ASCII file format. [35] PCA analyses were performed using the Statistical Product and Service Solutions program (SPSS, for Windows ver. 15, USA). This chemometric tool has been applied for different purposes, including the interpretation of ageing process of painting model samples due to its capability to identify changes of painting materials produced

by different agents. [11] In particular, PCA is a powerful data-mining technique that reduces data dimensionality obtaining more interpretable representation of the system under investigation. [36] PCA was performed independently on three matrixes on the peptide mass fingerprint interval (from 1000 to 2500 m/z). Each matrix contains information about fresh and aged painting model samples (UV-exposition times 0, 200, 500, 800, 1500, 2500 and 3000 h). In the case of the pure glue data matrix, mass spectra at 800 h of ageing were discarded due to experimental errors; therefore they were not included in the multivariate analysis. Hence, PG, Cin-G and Azu-G data matrixes were constructed with sixty, seventy and seventy mass spectra (10 spectra per check time) respectively. The Principal Components (PCs) were obtained using the correlation data matrices (scaling by unit variance).

Fourier Transform Infrared Spectroscopy (FTIR)

The FTIR spectra were collected using a NICOLET spectrometer 20SXB working in transmission mode. The instrument was connected to a Pentium 200 and the instrument software was OMNIC v 4.1, running under Windows 2000 Professional (Microsoft Corporation, USA). The FTIR spectra were registered from 4000 cm^{-1} to 400 cm^{-1} with a resolution of 2 cm^{-1} and 200 scan. The IR spectra were obtained from five KBr pellets that were prepared by homogeneously mixing 50μg of sample powder removed from five randomly places from the glass slide. The FTIR analysis was carried out on fresh and aged PG, Cin-G and Azu-G model samples at 200, 500, 800, 1500, 2500 and 3000 h.

Results and Discussion

MALDI-TOF mass spectral features

In order to characterize the pure collagen, i.e. type I or II, a mass spectrum was obtained after sample digestion with trypsin using the method developed in Kuckova et al., 2007 (Figure 1). [27] The visual exam of this fresh pure collagen mass spectrum evidenced a collagen type II thanks to the presence of peptides with molecular weights higher than 4000 m/z. [37] This type II represents the major collagen in cartilage.

An evaluation of the paint samples by means of the mass spectra feature was also carried out. The mass spectra of fresh and aged painting model samples at 3000 h were visual compared for pure glue and for the two tempera model samples. Figure 2 shows the mass spectra of fresh pure glue and the tempera with cinnabar and azurite, and also the mass spectra of the pure aged glue and their aged temperas. Comparing the fresh painting model samples (Figure 2 a,c,e), it can be note that the fragmentation patterns in the mass spectra of the digested glue (collagen) significantly differs when pure or mixed with cinnabar or azurite pigments. In fact, the number of m/z peak signals was higher in the case of the tempera samples than in pure glue samples. This fact evidenced changes in the glue structure before trypsin digestion that could be attributed to the interaction with the particular pigment. Comparing the fresh and aged painting model samples (Figure 2) from a same kind of samples, the m/z patterns were also different, indicating changes in the protein structure due to the UV ageing process. Moreover, the mass patterns of the aged samples differs depending on their composition, i.e. pure glue or temperas (see Figure 2 b,d,f).

Complementary procedures such as PCA on the mass spectra and FTIR analysis were also applied to provide further evidences of the interaction of the particular pigment with the collagen, and the effect on the ageing process of the proteinaceous binder. Particularly, PCA was used to confirm pattern of samples discrimination based on the

mass spectra since *a priori* mass spectral differences could be attributed, for instance, to different ionization process in the MALDI interfase.

Insert Figure 1

Insert Figure 2

PCA on MALDI-TOF MS data

PCA was performed on the m/z data matrices of every model samples which included the m/z data at the different UV irradiation check times and also the m/z data from the fresh samples. The m/z intervals selected to perform the PCA were those exhibiting the highest number of fragment ions, corresponding with the more representative of the peptides of the glue. [28,38] In particular, for the PG samples, the m/z interval was from 1400 to 2500 m/z (900 data). However, the great number of m/z data for the case of the tempera samples required to split the data into two intervals to perform the PCA by SPSS software, i.e. between 1000-1760 m/z (760 data) and 1760-2500 m/z (740 data) for the Cin-G samples; and between 1090-1900 m/z (810 data) and between 1900-2500 m/z (600 data) for Azu-G samples (Table 1). The PCs were obtained using both the covariance data matrices (scaling by mean-centered data) and the correlation data matrixes (scaling by unit variance). The results were better when PCA was performed on correlation data matrixes, so the results shown and discussed here correspond to autoscaled data.

The results of the multivariate analyses in terms of explained variance (%) and cumulative explained variance (%) for each model sample are shown in Table 1. From the results of Table 1, it is interesting to note that in the three multivariate analyses performed, the first PC accounted for more than 74 % of the total variance present in the mass spectra (91.7 % in the case of the PG samples, 80.4 and 74.8 % in the case of the

Cin-G samples, and 86.5 and 87.5 % in the case of the Azu-G samples). This indicated mainly one source of variability in the spectra.

Insert Table 1

Pure glue model samples

PCA discriminated PG samples up to 1500 h of ageing. The results of the projection of the samples into the plane of the two PCs are shown in Figure 3a. PC1 (accounting for 91.7 % of the total variance) discriminated samples up to 500 h of ageing (negative scores) from the rest of the aged samples (placed at positive scores). Despite explaining only 2.3 % of the total variance, PC2 allowed discrimination of the initial ageing stage, i.e. fresh PG and aged PG samples at 200 h (both with positive scores) from more aged samples (with negative scores) (Figure 3a). These PCA results suggested chemical modifications of the pure glue due to the ageing process by means of UV radiation after 200 h of exposure as was previously demonstrated. [11] The combination of both components, PC1 and PC2 was necessary to distinguish among check times up to 1500 h of ageing. Therefore, this result evidence protein changes due to the ageing process that was detected by PCA up to 1500 h of UV irradiation. After that time of exposure, no changes were discriminated by the multivariate analysis performed. It could be inferred that not relevant protein change occurred.

The loading values indicated the specific contribution of each m/z signal in the calculation of the total variance of the mass spectral data. Therefore, the loading plot helped identify those peptide ions that were important in the PCs. A closer examination of the loading plots combined with the score plots also revealed the kind of contribution associated with the PC. Since the scores of PC1 and PC2 discriminated samples aged up to 1500 h, the m/z spectral data variances due to these samples were mainly described

by these PCs. The unknown peptide ions at 1872, 1888, 2055, 2081, 2097, 2113, 2128 and 2130 m/z exhibited the higher negative loading values in the PC1 and the higher positive loading values in the PC2. Thus, they could be related with the aged PG samples discriminated up to 200 h.

Insert Figure 3

Cinnabar tempera model sample

As mentioned above, PCA was performed separately in two different intervals from the mass spectrum. On the 1000-1760 m/z interval, the two first PCs accounted for 87 % of the total variance in the Cin-G samples. Nevertheless the projection of the samples into the plane of these two components was not informative since they were randomly distributed and no changes associated with the UV test were discriminated. Hence, this interval was discarded to evaluate the alteration process of collagen. However, the PCA on the mass spectrum between 1760 and 2500 m/z allowed discrimination between different ageing check times by projecting the samples into the three-dimensional space defined by the three first PCs as shown in Figure 4a. The first PC (accounting for 89.2 % of total variance) separated fresh Cin-G samples, with positive scores, from the rest of the samples, with negative scores, being the aged Cin-G samples at 3000 h located at the more negative score (Figure 4a). The aged Cin-G samples at 500 h could be discriminated (with positive score values) from the rest of the ageing check times in the PC2, which accounted for 10.5 % of the total variance. Finally, scores for PC3, which only accounted for 3.90% of the total variance, clearly discriminated samples aged at 3000 h (positive scores) from the rest of the samples. The loading plot of PC1 and PC2 showed high variability in the values (Figure 4b) that made difficult their interpretation. Nevertheless, compared to the pure glue discussed above, different fragment ions were

implicated when discriminating Cin-G samples. Therefore this suggests that different collagen ageing processes depends on the presence of the pigment cinnabar.

Insert Figure 4

Azurite tempera model samples

The best ability for discriminating among aged Azu-G samples was found in the m/z interval between 1760 and 2500 m/z (containing 600 data points). The m/z interval between 1090 and 1900 m/z (810 data) required the combination of the PC1 and PC2 (89.6 % of total variance) to discriminate aged Azu-G samples up to 500 h (with positive scores in both PCs) from the rest of the samples; nevertheless the groups were not clearly separated and the results were not further investigated.

The projection of the scores onto the plane of the first two PCs performed on the m/z data from 1900 to 2500 m/z showed the distribution of the Azu-G samples in three groups based on the ageing occurred. In particular, fresh samples, aged samples at 200 h and samples aged more than 500 h were discriminated. Regarding the PC1 that accounting for 87.52% of total variance, the fresh and aged Azu-G samples at 200 h (positive scores) were discriminated from the rest of the samples (negative score). Despite the fact that PC2 accounted for 3.84% of the total variance (Figure5a), it allowed discrimination between fresh and aged Azu-G at any time of UV exposure. Again, the results demonstrated that the UV ageing process introduced changes in this tempera model samples that could be detected by PCA. Also, it suggested no changes in the tempera after 500 h of UV ageing that could be detected by PCA; thus it could be inferred that these changes were minimal. Then, the ageing process of this particular tempera containing azurite as pigment is carried out at the first stages of the UV exposure (up to 200 h). After that, the tempera remains stable. Indeed, these results upon collagen stability in presence of azurite confirmed similar conclusions obtained

elsewhere. [11,39]

Insert Figure 5

In order to interpret these multivariate results for Azu-G samples, the formation of a metal complex or coordination compound could be the key to explain the evident photostability of collagen in presence of azurite. In fact, the literature extensively describes the formation of chemical species of protein-copper complex even at lower pH values. [40] This chemical reaction is widely employed as method for protein detection and quantification. In particular, the Biuret Test is based on the formation of a violet-colored complex between the Biuret reactive (containing Cu^{2+} ions in alkaline solution) and the amino groups from the peptide bonds (–HN-CO_2-N–) of the proteins (Figure 6). According to the color intensity of the complex measured by colorimetric analysis, the protein concentration is calculated. [41]

Insert Figure 6

On the other hand, the study of loading plots of Azu-G samples showed different peptide ions involved in the discrimination of the fresh and aged samples compared to those found for PG and Cin-G samples (see the loading plot in Figure 3, 4 and 5). It can be concluded, that the ageing process of glue when mixed with azurite pigment was different to those detected for pure glue (collagen) or when mixed with cinnabar pigment.

Conformational analysis by FTIR

The conformational structure of the proteinaceous binder (collagen) was studied from the analysis of the FTIR spectrum of the PG, Azu-G and Cin-G samples, fresh and aged at the checked times. Also, the FTIR spectra were used to track changes in the collagen due to the UV ageing test and the influence of a particular pigment in the process.

Figure 7 shows the most informative FTIR spectra for each kind of samples. In the case of PG samples these spectra were those from fresh and aged samples at 200 h, 500 h and 3000 h (Figure 7a); for Cin-G samples (Figure 7b) the spectra were from fresh sample and aged samples at 500 h and 3000 h; and for the Azu-G samples, were those from fresh and aged samples at 200 h, 500 h and 3000 h (Figure 7c). The IR amide bands I (carbonyl stretching vibrations) and II (NH bending vibrations) can be observed at around 1660 cm^{-1} and 1550 cm^{-1} respectively for fresh and aged samples as expected. The conformational study was mainly based on the analysis of these two proteinaceous characteristics bands. Nevertheless, it was corroborated in all the FTIR spectra that the position of the amide band II was not affected by the ageing process since it was always placed at 1550 cm^{-1}. Thus, the discussion about conformational changes were based on amide I band features.

Since the aged samples at 200 h (for PG and Azu-G samples) or 500 h (for Cin-G samples) were well discriminated in the PCA performed previously on the mass data, it was inferred that the ageing process at these checked times could introduce important initial changes. Therefore, a comparative study between these fresh and aged samples was carried out tracking the modification. In the case of PG samples, the IR band at 1663 cm^{-1} attributed to β-turn structure was detected in fresh samples; [20] nevertheless the β-turn structure decreased during irradiation and the amide band I shifted to α-helix structure at 1655 cm^{-1} for samples aged at 200 h. [14,19] Moreover, this fact was also evidenced for the rest of the aged samples, as can be noted in Figure 7a for samples aged at 500h and 3000 h. Thus, this suggested that the PG samples underwent conformational changes in their secondary structure of pure glue due to slight shift in the amide I band. The β-turn structure is based on two or more polypeptide chains running alongside each other which are linked in a regular manner by hydrogen bonds

between the main chain C=O and N-H groups. [17] The FTIR results suggested that the UV irradiation could break these bonds and the chains of collagen became independent turning to α-helix structure as the basic structural unit.

In a similar way, conformational changes were also evaluated for Cin-G samples. Before the ageing process, for fresh samples, the amide band I was located at 1648 cm^{-1}, which is assigned to random coil according to the consulted bibliography (Figure 7b). [14,20] Thus, this result revealed an absence of secondary structure in presence of cinnabar even before the UV exposure. [18-20] In fact it is well known that the denaturation process disrupts the normal α-helix and β-sheets in a protein and uncoils it into a random shape. Therefore, in this particular case, it suggested the denaturation effect of cinnabar on the collagen occurred previously to the ageing test. The harmful properties of mercury are well established, producing the protein degradation of tissues. [42,43] For the next state of ageing tested, i.e. at 500 h of UV exposition, a shift of the amide band I to 1627 cm^{-1} was observed, which is labelled as β-sheet structure. This was surprising, and this shift could be related to denaturation and aggregation processes [14,20] more than reorganization in a β-sheet structure. Finally, the conformational study at 3000 h (maximum time of ageing) showed a shift to 1688 cm^{-1}. When the amide band I is located between 1670 and 1690 cm^{-1} is indicative of random coil. [20] Thus, the study of the collagen conformational properties throughout the ageing test revealed the denaturation of the collagen by different disordered structures, such as aggregates at 500 h and random coil for the aged final state.

The ageing process of AZ-G samples is showed in Figure 7c. For fresh samples, the position of amide band I was at 1663 cm^{-1}, which was attributed to β-turn structure. When aged, this amide band I remained stable at 1663 cm^{-1} for all checked times studied, i.e. 200, 500 h or 3000 h. Therefore, the β-turn structure of the glue when

mixed with the pigment azurite remained stable despite the exposure to UV irradiation. This suggests that no changes in the second conformational structure of collagen occurred when mixed with the pigment azurite. On the other hand, it is well known that cupper ions (Cu^{2+}) bonds to amide groups to form a particular complex protein-Cu^{2+}. This complex is formed by four N–H groups from two collagen chains and two groups from each chain stabilizing the β-turn structure of collagen (Figure 6). Thus it could be inferred that the formation of this complex prevented conformational changes in the secondary structure of the binder collagen.

Insert Figure 7

Conclusions

This work is part of an ongoing investigation on interactions between historical pigments and proteinaceous binders. The present study suggests some possible answers about the interaction and the role of two mineral pigments, i.e. cinnabar and azurite, in the UV ageing process of collagen when present in tempera paintings. The combined use of analytical techniques (MALDI-TOF MS and FTIR) and the novel application of PCA on mass data allowed discrimination of significant differences in mass fragmentation patterns of glue, and conformational changes in its structure due to the UV irradiation. Results also show that these chemical or structural changes occurred in different forms when these pigments are present, indicating diverse ways of interaction between pigment-collagen.

This new approach facilitates the analysis and interpretation of ageing process versus traditional methods due to more sensible mass data registered, whole structural information and the small sample size needed for this specific analysis. In addition, this work proposes that the formation of a protein-copper complex could justified the additional photostabilization of the tempera when azurite is present, as suggested by

Price (2000) and Manzano et al. (2010). [11,39] Moreover, this paper suggests that the alteration mechanism of collagen detected by PCA is likely due to secondary dimensional structure alteration.

In addition, this approach based on MALDI-TOF MS, PCA and FTIR can be employed to further study protein binders affected by other degradation agents. For instance, environmental factors as such gaseous pollutants including SO_2 and NO_2 from industrial and urban pollution could be studied in depth. Also chemical modifications due to the presence of inorganic salts could be evaluated, and possible interactions with other organic compounds (e.g. varnishes, oils, organic pigments, etc.) which are commonly present in paintings.

Acknowledgment

Financial support was provided by Research Groups RNM-179 and FQM-118 (CICE, Junta de Andalucía) and Project P08-RNM-04169. We would like to thank Dr. L. Rodríguez-Simón for collaborating with sampling preparation.

References

[1] P. Vandenabeele, B. Wehling, L. Moens, H. Edwards, M. De Reu, G. Van Hooydonk. Analysis with micro-Raman spectroscopy of natural organic binding media and varnishes used in art. *Anal. Chim. Acta.* **2000**, *407*, 261.

[2] A. Nevin, D. Comelli, G. Valentini, R. Cubeddu. Total synchronous fluorescence spectroscopy combined with multivariate analysis: Method for the classification of selected resins, oils, and protein-based media used in paintings. *Anal. Chem.* **2009**, *81*, 1784.

[3] F. Pacheco. *El arte de la pintura*, 1st ed., Cátedra, Madrid, **1990**.

[4] G. Leo, I. Bonaduce, A. Andreotti, G. Marino, P. Pucci, M. P. Colombini, L. Birolo. Deamidation at asparagine and glutamine As a major modification upon deterioration/aging of proteinaceous binders in mural paintings. *Anal. Chem.* **2011**, *83*, 2056.

[5] M.P. Colombini, F. Modugno, E. Menicagli, R. Fuoco, A. Giacomelli. GC-MS characterization of proteinaceous and lipid binders in UV aged polychrome artefacts. *Microchem. J.* **2000**, *67*, 291.

[6] J.V. Gimeno-Adelantado, R. Mateo-Castro, M.T. Domenech-Carbó, F. Bosch-Reig, A. Domenech-Carbó, M.J. Casas-Catalan, L. Osete-Cortina. Identification of lipid binders in paintings by gas chromatography: Influence of the pigments. *J. Chromatogr. A.* **2001**, *922*, 385.

[7] M.T. Doménech-Carbó, S. Kuckova, J. de la Cruz-Cañizares, L. Osete-Cortina. Study of the influencing effect of pigments on the photoageing of terpenoid resins used as pictorial media. *J. Chromatogr. A* **2006**, *1121*, 248.

[8] A. Nevin, L. Osticioli, D. Anglos, A. Burnstock, S. Cather, E. Castellucci. Raman spectra of proteinaceous materials used in paintings: A multivariate analytical approach for classification and identification. *Anal. Chem.* **2007**, *79*, 6143.

[9] A. Nevin, I. Osticioli, D. Anglos, A. Bursnstock, S. Cather, E. Castellucci. The analysis of naturally and artificially aged protein-based paint media using Raman spectroscopy combined with Principal Component Analysis. *J. Raman Spectrosc.* **2008**, *39*, 993.

[10] E. Manzano, N. Navas, R. Checa-Moreno, L. Rodríguez-Simón, L.F. Capitán-Vallvey. Preliminary study of UV ageing process of proteinaceous paint binder by FT-IR and principal component analysis. *Talanta* **2009**, *77*, 1724.

[11] E. Manzano, J. Romero-Pastor, N. Navas, L. Rodríguez-Simón, C. Cardell. A study of the interaction between rabbit glue binder and blue copper pigment under UV radiation: A spectroscopic and PCA approach. *Vib. Spectrosc.* **2010**, *53*, 260.

[12] M. Jackson, L.P. Choo, E.H. Watson, W.C. Halliday, H.H. Mantsch. Beware of connective tissue proteins: Assignment and implications of collagen absorptions in infrared spectra of human tissues. *Biochim. Biophys. Acta.* **1995**, *1270*, 1.

[13] K. Dif, C. Pepe, J. Peduzzi, B. Lavedrine, C. Chahine. An approach of a study of the interaction between collagen and sulphur dioxide by using ESI and MALDI-TOFMS. *J. Cult. Herit.* **2002**, *3*, 317.

[14] P.R. Palaniappan, V. Vijayasundaram. Fourier transform infrared study of protein secondary structural changes in the muscle of Labeo rohita due to arsenic intoxication. *Food Chem. Toxicol.* **2008**, *46*, 3534.

[15] O.F. Van den Brink, J. J. Boon, P. B. O'Connor, M.C. Duursma, R.M.A. Heeren. Matrix-assisted laser desorption/ionization Fourier transform mass spectrometric analysis of oxygenated triglycerides and phosphatidylcholines in egg

tempera paint dosimeters used for environmental monitoring of museum display conditions. *J. Mass Spectrom.* **2001**, *36*, 479.

[16] I. Osticioli, N.F.C. Mendes, S. Porcinai, A. Cagnini, E. Castellucci. Analysis of natural and artificial ultramarine blue pigments using laser induced breakdown and pulsed Raman spectroscopy, statistical analysis and light microscopy. *Anal. Bioanal. Chem.* **2009**, *394*, 1033.

[17] H. Lodish, A. Berk, S.L. Zipursky, P. Matsudaira, D. Baltimore, J.E. Darnell. *Molecular Cell Biology*, 4th ed., New York, Freeman W.H., **2000**.

[18] M. Jackson, H.H. Mantsch. The use and misuse of FTIR Spectroscopy in the determination of protein structure. *Crc Cr Rev Bioch Mol.* **1995**, *20*, 95.

[19] J. Kneipp, L.M. Miller, M. Joncic, M. Kittel, P. Lasch, M. Beekes, D. Naumann. In situ identification of protein structural changes in prion-infected tissue. *Acta Bioch Bioph Sin.* **2003**, *1639*, 152.

[20] J. Kong, S. Yu. Fourier Transform Infrared Spectroscopic analysis of protein secondary structures. *Acta Bioch Bioph Sin.* **2007**, *39*, 549.

[21] D. Scalarone, M. C. Duursma, J. J. Boon, O. Chiantore. MALDI-TOF mass spectrometry on cellulosic surfaces of fresh and photo-aged di- and triterpenoid varnish resins *J. Mass Spectrom.* **2005**, *40*, 1527.

[22] M. Castillejo, M. Martín, M. Muijja, D. Silva, R. Torres, A. Manousaki, V. Zafiropulos, O.F. Van der Brink, R.M.A. Heeren, R. Teule, A. Silva, H. Gouveia. Analytical Study of the Chemical and Physical Changes Induced by KrF Laser Cleaning of Tempera Paints *Anal. Chem.* **2002**, *74*, 4662.

[23] O. F. van den Brink, J. J. Boon, P. B. O'Connor, M. C. Duursma and R. M. A. Heeren. Matrix-assisted laser desorption/ionization Fourier transform mass spectrometric analysis of oxygenated triglycerides and phosphatidylcholines in egg

tempera paint dosimeters used for environmental monitoring of museum display conditions *J. Mass Spectrom.* **2001**, *36*, 479.

[24] M. D'Imperio, A. Della Corte, A. Facchiano, M. Di Michele, G. Ferrandina, M. B. Donati, D. J. Rotilio. Standardized sample preparation phases for a quantitative measurement of plasma peptidome profiling by MALDI-TOF. *Proteomics* **2010**, *73*, 1355.

[25] C. Tokarski, E. Martin, C. Rolando, C. Cren-Olivé. Identification of proteins in Renaissance paintings by proteomics. *Anal. Chem.* **2006**, *78*, 1494.

[26] S. Kuckova, I. Nemec, R. Hynek, J. Hradilova, T. Grygar. Analysis of organic colouring and binding components in colour layer of art works. *Anal. Bioanal. Chem.* **2005**, *382*, 275.

[27] S. Kuckova, R. Hynek, M. Kodicek. Identification of proteinaceous binders used in artworks by MALDI-TOF mass spectrometry. *Anal. Bioanal. Chem.* **2007**, *388*, 201.

[28] S. Kuckova, M. Crhova, L. Vankova, A. Hnizda, R. Hynek, M. Kodicek. Towards proteomic analysis of milk proteins in historical building materials. *Int. J. Mass Spectrom.* **2009**, *284*, 42.

[29] G. Musumarra, M. F*ichera.* Chemometrics and cultural heritage. *Chemom. Intell. Lab. Syst.* **1998**, *44*, 363.

[30] R. Aruga, P. Mirti, A. Casolli, G. Palla. Classification of ancient proteinaceous painting media by the joint use of pattern recognition and factor analysis on GC/MS data. *Anal. Chem.* **1999**, *36*, 559.

[31] G. Gautier, M.P. Colombini. GC–MS identification of proteins in wall painting samples: A fast clean-up procedure to remove copper-based pigment interferences. *Talanta* **2007**, *73*, 95.

[32] N. Navas, J. Romero-Pastor, E. Manzano, C. Cardell. Benefits of applying combined diffuse reflectance FTIR spectroscopy and principal component analysis for the study of blue tempera historical painting. *Anal. Chim. Acta.* **2008**, *630*, 141.

[33] W. Fremout, M. Dhaenens, S. Saverwyns, J. Sanyova, P. Vandenabeeled, D. Deforce, L.Moensb. Tryptic peptide analysis of protein binders in works of art by liquid chromatography–tandem mass spectrometry. *Anal. Chim. Acta.* **2010**, *658*, 156.

[34] N. Eastaugh, V. Walsh, T. Chaplin, R. Siddall. *Pigment Compendium: A Dictionary of Historical Pigments, 1st ed., Butterworth-Heinemann*, Oxford, **2004**.

[35] C.D. Calvano, A. Aresta, M. Iacovone, G.E. De Benedetto, C.G. Zambonin, M. Battaglia, P. Ditonno, M. Rutigliano, C. Bettocchi. Optimization of analytical and pre-analytical conditions for MALDI-TOF-MS human urine protein profiles. *J. Pharm. Biomed. Anal.* **2010**, *51*, 907.

[36] J. E. Jackson. *A User's Guide to Principal Components,* John Wiley & Sons, Inc., New York, **1991**.

[37] G. Zhang, A. Sun, W. Li, T. Liu, Z. Su. Mass spectrometric analysis of enzymatic digestion of denatured collagen for identification of collagen type. *J. Chromatogr A.* **2006**, *1114*, 274.

[38] Y.V. Sungurov, N.L. Eremeev, A.T. Lebedev, O.A. Maloshitskaya, G.N. Rudenskaya, S.A. Semenova. A mass-spectrometric approach to primary screening of collagenolytic enzymes. *Russ. J. Biorgan. Chem.* **2008**, *34*, 353.

[39] M. Price. A Renaissance of color: particle separation and preparation of azurite for use in oil painting. *Leonardo.* **2000**, *33*, 281.

[40] G. Drochioiu, N.E. Damoc, M. Przybylski. Novel UV assay for protein determination and the characterization of copper–protein complexes by mass spectrometry. *Talanta.* **2006**, *69*, 556.

[41] P.K. Smith, R.I. Krohn, G.T. Hermanson, A.K. Mallia, F.H. Gartner, M.D. Frovenzano, E.K. Fujimoto, N.M. Goeke, B.J. Olson, D.C. Klenk. Measurement of protein using bicinchoninic acid. *Anal. Biochem.* **1985**, *19*, 76.

[42] G. Sener, O. Sehirli, A. Tozan, A. Velioglu-Ovunc, N. Gedik, G.Z. Omurtag. Ginkgo biloba extract protects against mercury (II)-induced oxidative tissue damage in rats. *Food Chem. Toxicol.* **2007**, *45*, 543.

[43] M. Wang, Y. Wang, J. Wang, L. Lin, H. Hong, D. Proteome profiles in medaka (Oryzias melastigma) liver and brain experimentally exposed to acute inorganic mercury. *Wang, Aquat. Toxicol.* **2011**, *103*, 129.

Table 1. PCA results.

Data matrix	m/z Interval	Data number	PC	Variance account (%)	Variance accumulated (%)
Pure Glue (PG)	1400-2500	900	PC1 PC2 PC3	91.7 2.2 1.6	91.7 93.9 95.6
Cinnabar-Glue (Cin-G)	1000-1760	760	PC1 PC2 PC3	80.4 7.3 2.5	80.4 87.7 90.2
	1760-2500	740	PC1 PC2 PC3	74.8 10.5 3.9	74.8 85.3 89.2
Azurite-Glue (Azu-G)	1090-1900	810	PC1 PC2 PC3	86.5 3.1 2.3	86.5 89.6 92.0
	1900-2500	600	PC1 PC2 PC3	87.5 3.8 2.1	87.5 91.3 93.5

Figure Captions

Figure 1. Mass spectra obtained by MALDI-TOF MS of digested collagen (type II).

Figure 2. Mass spectra obtained by MALDI-TOF MS of fresh and aged collagen at 3000 h of UV irradiation for: a, b) Pure Glue; c) d) Cin-G and e) f) Azu-G samples, respectively.

Figure 3. Scores plots (a) and loading plots (b) for PC1 and PC2 of the UV ageing of the pure rabbit glue (Pure Glue) in the mass interval between 1400 and 2500 Da. Figure shows the ageing at different times (Fresh, 200, 500, 1500, 2500 and 3000 h).

Figure 4. Score plots (a) and loading plots (b) of the Cin-G samples into the tridimensional space of the PC1, PC2 and PC3. PCA performed on m/z between 1760 and 2500 m/z. Figures show the ageing at different times (Fresh, 200, 500, 800, 1500, 2500 and 3000 h).

Figure 5. Scores plots (a) and loading plots (b) for PC1 and PC2 of the UV ageing of the azurite tempera model samples (Azu-G) in the mass interval between 1760 and 2500 m/z. Figures show the ageing at different times (Fresh, 200, 500, 800, 1500, 2500 and 3000 h).

Figure 6. Copper complex obtained by Biuret reaction.

Figure 7. Infrared spectra of fresh and aged collagen in: a) pure glue (aged PG at 200 h); b) Cinnabar tempera (aged Cin-G at 200 h) and c) Azurite tempera model samples (aged Azu-G at 200 h).

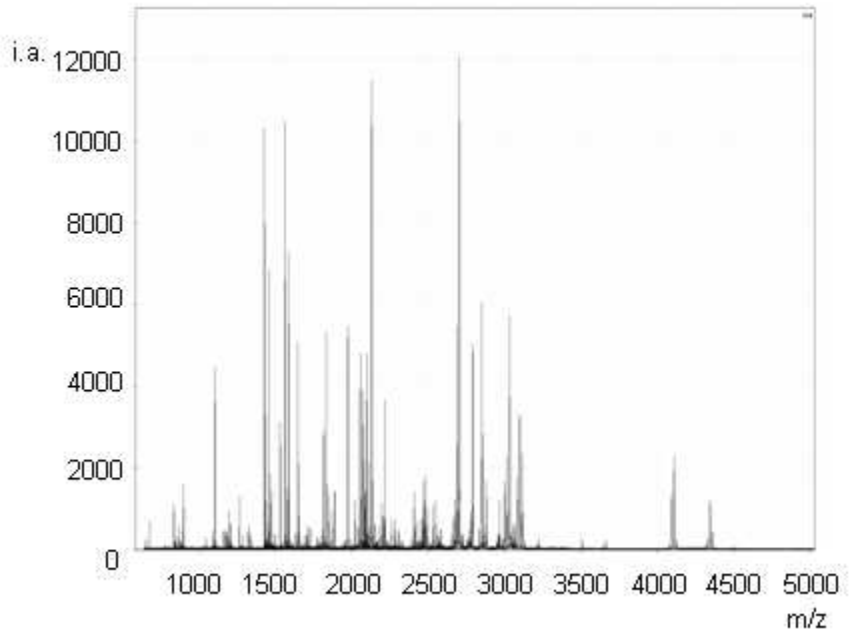

Figure 1. Mass spectra obtained by MALDI-TOF MS of digested collagen ,type II
77x60mm (150 x 150 DPI)

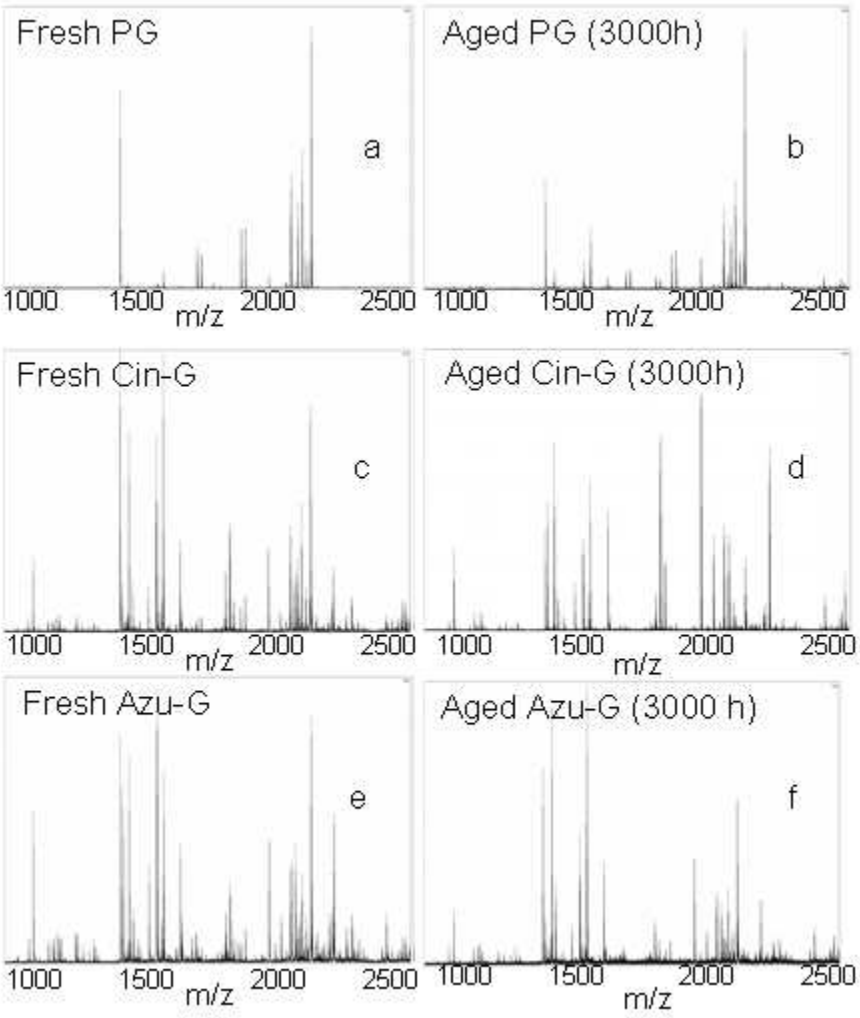

Figure 2. Mass spectra obtained by MALDI-TOF MS of fresh and aged collagen at 3000 h of UV irradiation for: a, b) Pure Glue; c) d) Cin-G and e) f) Azu-G samples, respectively.
75x88mm (150 x 150 DPI)

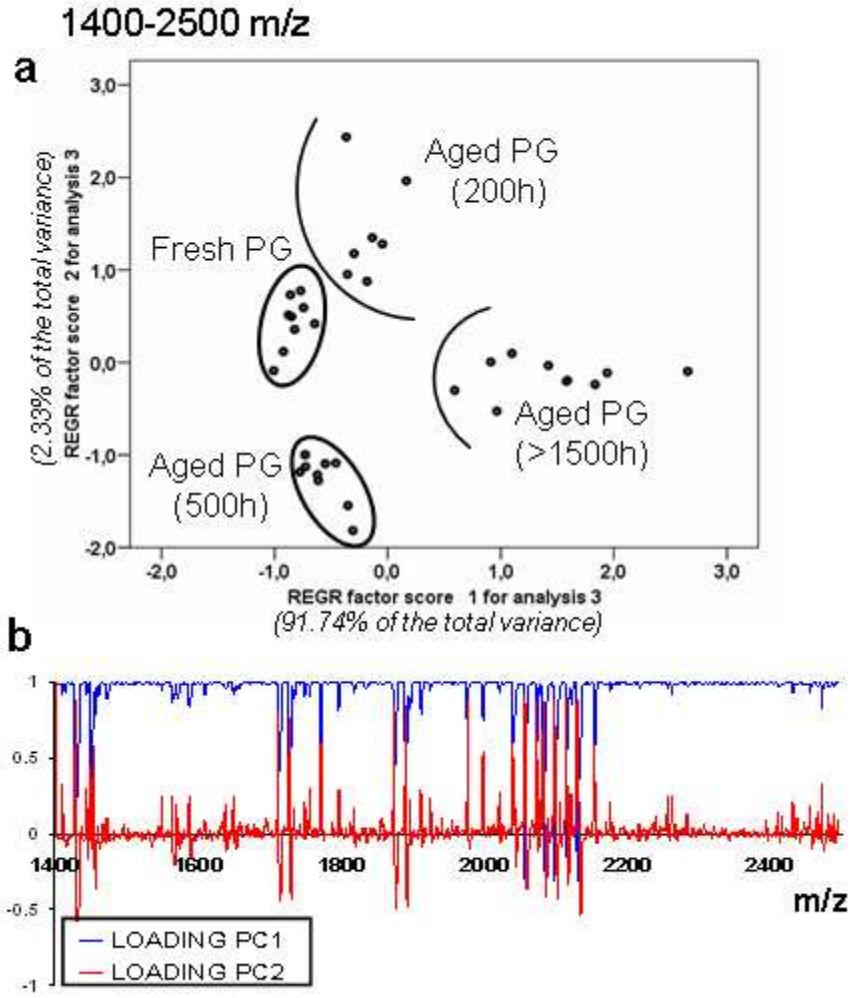

Figure 3. Scores plots (a) and loading plots (b) for PC1 and PC2 of the UV ageing of the pure rabbit glue (Pure Glue) in the mass interval between 1400 and 2500 Da. Figure shows the ageing at different times (Fresh, 200, 500, 1500, 2500 and 3000 h).
75x88mm (150 x 150 DPI)

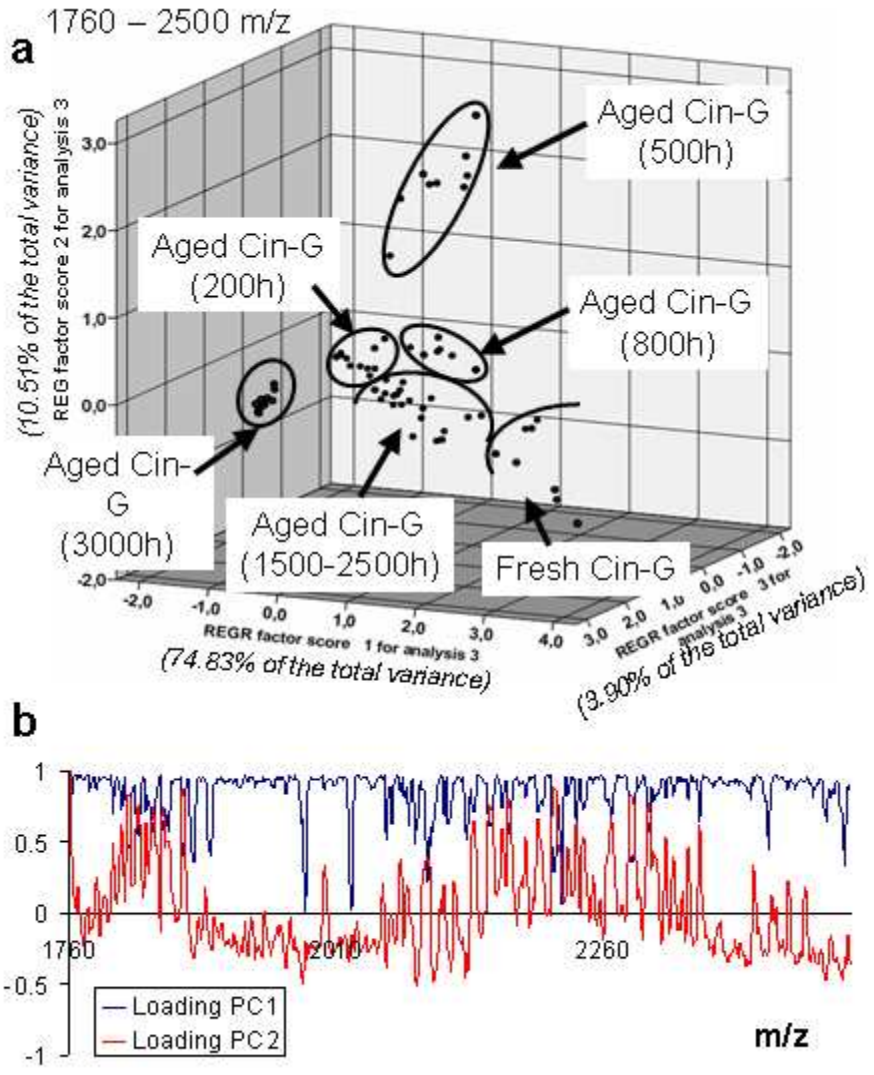

Figure 4. Score plots (a) and loading plots (b) of the Cin-G samples into the tridimensional space of the PC1, PC2 and PC3. PCA performed on m/z between 1760 and 2500 m/z. Figures show the ageing at different times (Fresh, 200, 500, 800, 1500, 2500 and 3000 h).
77x96mm (150 x 150 DPI)

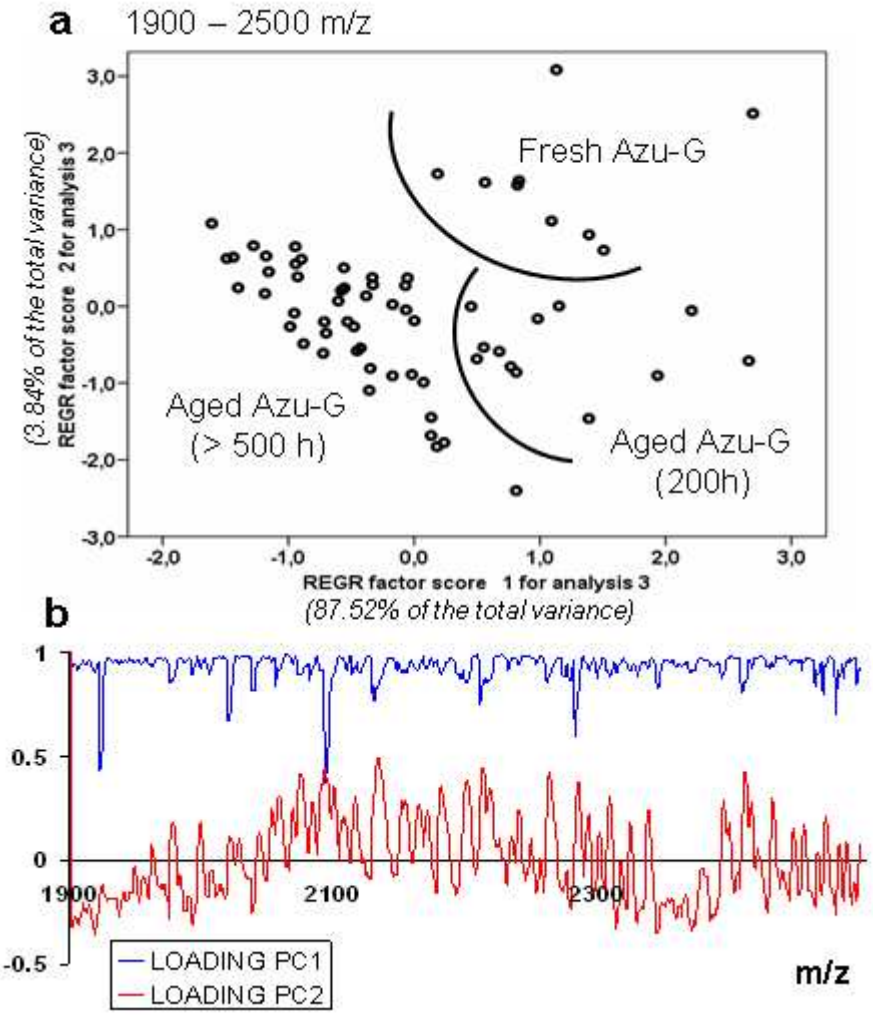

Figure 5. Scores plots (a) and loading plots (b) for PC1 and PC2 of the UV ageing of the azurite tempera model samples (Azu-G) in the mass interval between 1760 and 2500 m/z. Figures show the ageing at different times (Fresh, 200, 500, 800, 1500, 2500 and 3000 h).
75x88mm (150 x 150 DPI)

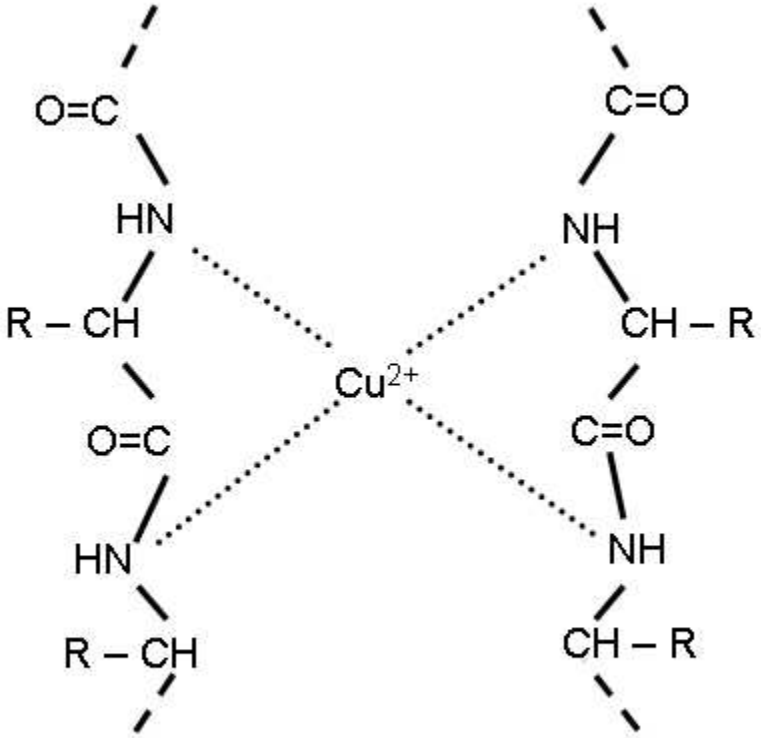

Figure 6. Copper complex obtained by Biuret reaction.
75x75mm (150 x 150 DPI)

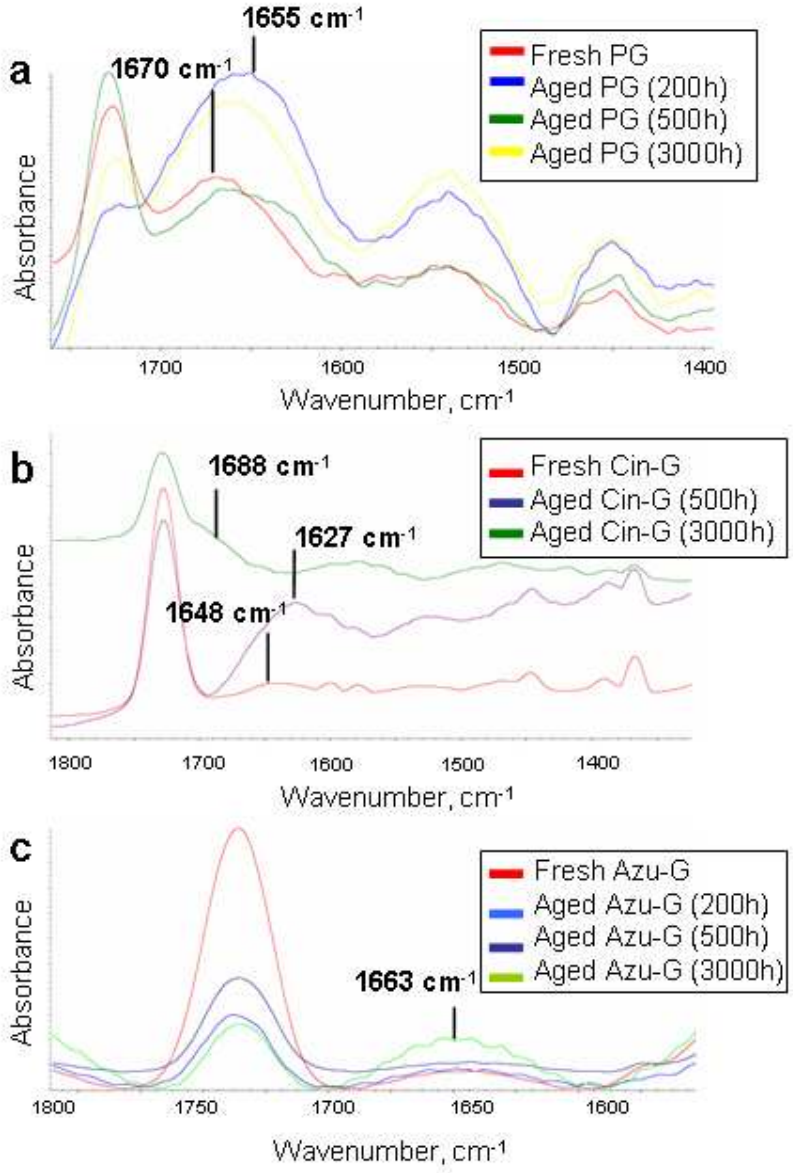

Figure 7. Infrared spectra of fresh and aged collagen in: a) pure glue (aged PG at 200 h); b) Cinnabar tempera (aged Cin-G at 200 h) and c) Azurite tempera model samples (aged Azu-G at 200 h).
75x108mm (150 x 150 DPI)

Conclusiones

Esta nueva metodología basada en el uso combinado de MALDI-TOF MS y T-FTIR y la aplicación de PCA a los mapas peptídicos obtenidos mediante MALDI-TOF MS, permite detectar diferencias significativas en el proceso de alteración de la cola de conejo e identificar cambios en la estructura secundaria del colágeno debido a la radiación UV, tanto en las réplicas puras como en las mezclas con azurita y cinabrio. De acuerdo con los resultados del PCA realizado con los datos de masas de los tres grupos de réplicas pictóricas (i.e. cola pura, temples de azurita y temples de cinabrio), puede concluirse que la cola de conejo se comporta de manera diferente en cada tipo de réplica con respecto al envejecimiento producido por la radiación UV. Este hecho se manifiesta a partir de los diferentes patrones de fragmentación obtenidos en los correspondientes mapas peptídicos. Este análisis sugiere, por tanto, el establecimiento de interacciones específicas pigmento-aglutinante según el tipo de pigmento, y que van a influir en el estado de alteración de la cola de conejo a lo largo del ensayo. En consecuencia, el empleo de la espectrometría de masas facilita la detección e incluso la interpretación del estudio de los procesos de envejecimiento gracias a la información estructural que proporciona, y presenta además el valor añadido en el estudio de muestras pictóricas, de la pequeña cantidad de muestra necesaria para realizar el análisis.

En particular, el PCA para la cola pura en el intervalo del espectro de masas entre 1400 y 2500 m/z discrimina las réplicas pictóricas en función del envejecimiento hasta 1500 horas, desde este tiempo de exposición las réplicas envejecidas se muestran agrupadas, sugiriendo que no existen modificaciones relevantes de la cola de conejo frente a la radiación UV por encima de 1500 horas. En cambio, la separación de los temples de cinabrio envejecidos es posible a todos los tiempos de exposición a la radiación UV estudiados. Este resultado del PCA indica que los temples de cinabrio sufren modificaciones detectables a todos los tiempos de exposición y, por tanto, se puede decir que el efecto dañino de la radiación UV es activo sobre ellos hasta el final de la exposición (i.e. 3000 horas). Sin embargo, el PCA de los temples de azurita discrimina claramente las muestras frescas de las envejecidas, las cuales se agrupan juntas a partir de 200 horas de exposición en adelante. Este

resultado sugiere que el efecto de la alteración de la radiación UV en presencia de azurita tiene lugar principalmente antes de las 200 horas, tiempo tras el cual el temple de azurita se mantiene estable frente a la irradiación UV. Por tanto, esto es una evidencia de como la presencia de azurita puede inferir en el mecanismo de alteración de la cola de conejo, confiriéndole mayor estabilidad frente a la radiación UV, como ya se puso también de manifiesto en el Capítulo 7 de esta Tesis Doctoral. También en el Capítulo 6 se indicó la existencia de una interacción específica cobre-aglutinante, justificada por una mayor estabilidad de la interacción con respecto al compuesto de partida (i.e. azurita).

Este diferente comportamiento de la cola de conejo detectado en las diferentes réplicas pictóricas frente a la radiación UV, justifica la propuesta de diversas hipótesis para interpretar las evidencias extraídas de los anteriores resultados del PCA. En concreto, se propone la posible formación de complejos cobre-proteína para explicar la fotoestabilidad de la cola de conejo en presencia de azurita. Además, los estudios de la conformación del colágeno realizados para los temples envejecidos azurita-cola de conejo mediante los espectros T-FTIR corroboran la estabilidad de la estructura secundaria del colágeno. Se propone por tanto, la formación de un complejo entre el Cu^{2+}– presente en el pigmento azurita y dos cadenas de colágeno, lo cual mantendría estable la estructura *β-turn* a lo largo de la exposición a la radiación UV. Es un hecho bien conocido la formación de complejo entre el Cu^{2+} y los enlaces peptídicos de las proteínas, empleándose esta reacción en la detección de proteínas en diversos medios (por ejemplo, la reacción del Biuret).

En cuanto a los temples de cinabrio, el estudio de su conformación mediante T-FTIR parece indicar una desnaturalización de la proteína desde las primeras fases del ensayo (temples frescos de cinabrio), lo cual no es sorprendente, pues son conocidos los efectos nocivos que ejerce el mercurio sobre tejidos orgánicos, que bien podrían estar relacionados con modificaciones o interacciones en las estructuras proteicas. En particular, el estudio detallado de los correspondientes espectros de T-FTIR sugiere que la radiación UV modifica la estructura secundaria del colágeno a diferentes estructuras desordenadas a lo largo de la exposición UV debido a procesos de agregación y desnaturalización de la proteína. Esto podría explicar las diferencias

observadas en los patrones de fragmentación de la cola de conejo detectadas por PCA para los diferentes tiempos de exposición estudiados cuando el cinabrio está presente.

A la luz de todas las conclusiones que pueden ser extraídas de los resultados de la aplicación de la metodología propuesta en este capitulo, puede concluirse que es una herramienta con una gran potencialidad a la hora de analizar, caracterizar e interpretar resultados en muestras pictóricas.

10. Caracterización cuantitativa de la composición y de la microtextura de pinturas históricas mediante μ-XRD y RM

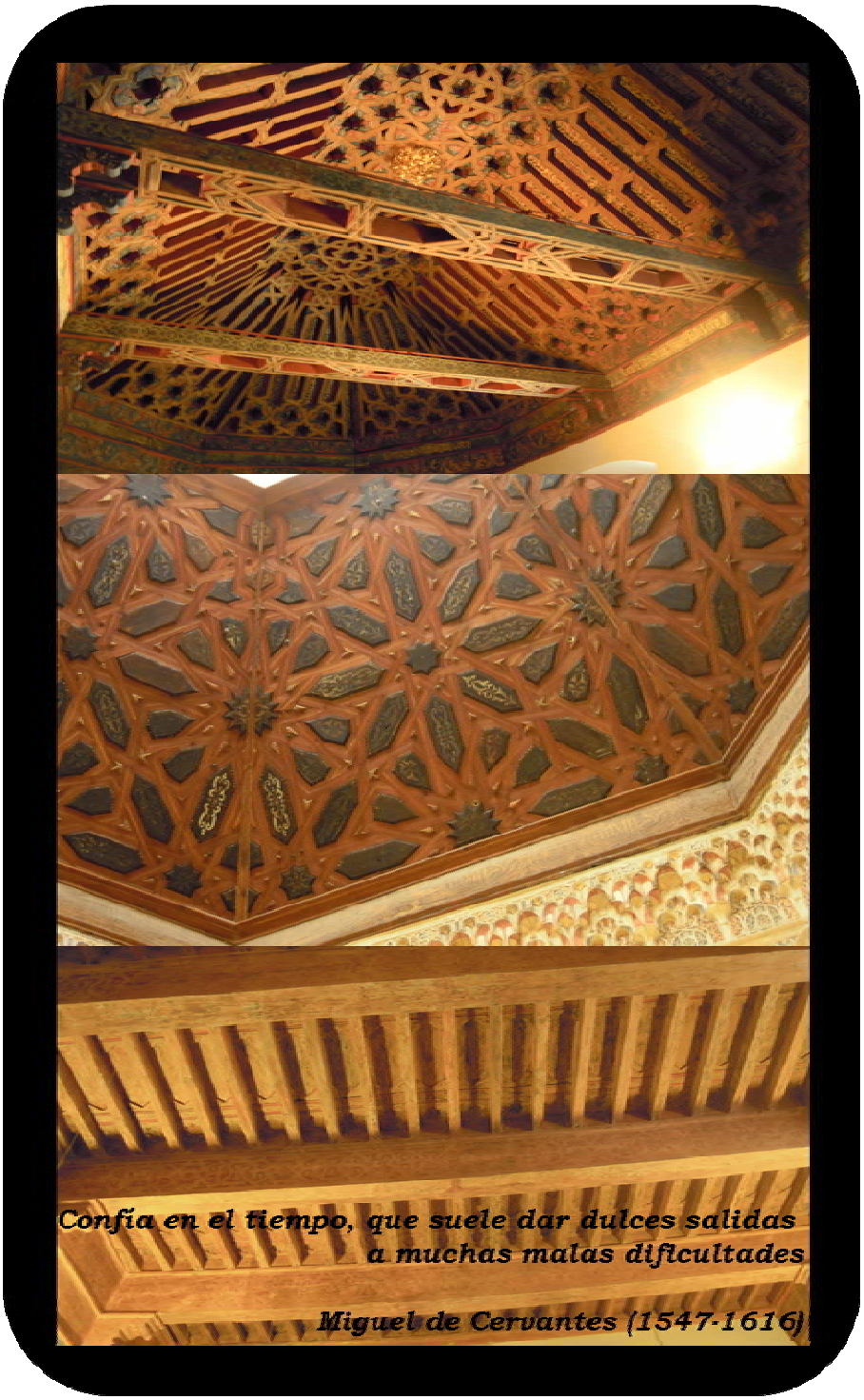

Compositional and quantitative microtextural characterization of Historic Paintings by means of Micro-X-Ray Diffraction and Raman Microscopy (2011). **J. Romero-Pastor**, A. Durán, A. B. Rodríguez- Navarro, R. Van Grieken, C. Cardell. Analytical Chemistry. (Accepted paper, June 2011).

Resumen

Este Capítulo 10 aborda el último de los objetivos marcados en esta Tesis Doctoral, es decir, proponer metodologías de análisis *ad hoc* para el estudio de muestras pictóricas reales a partir de diversas técnicas de análisis. Aquí se exponen los beneficios de la caracterización de pinturas históricas mediante μ-XRD y RM. La novedad de este trabajo reside en el uso de μ-XRD no sólo para la identificación en detalle de todas las fases cristalinas presentes en las estratigrafías pictóricas, sino también para la cuantificación de las características texturales de fases cristalinas a partir de patrones de difracción en dos dimensiones (anillos de Debye-Scherrer). Este método de caracterización de la microtextura ofrece una alterativa al tratamiento de imágenes por microscopía, la cual resulta más tediosa y no proporciona de manera tan eficiente, rápida y fácil la cuantificación del tamaño y cantidad de granos cristalinos presentes en las muestras pictóricas. Además, el estudio microtextural mediante μ-XRD puede realizarse a todas las fases cristalinas presentes en una capa pictórica a partir del mismo análisis de μ-XRD, lo cual facilita en gran medida su estudio.

En este Capítulo 10, el uso de las características microtexturales, tales como el número de granos minerales (TNP) y el tamaño de grano (API), estimados a partir de la intensidad y continuidad de los anillos de Debye-Scherrer, ha permitido por primera vez dar información acerca de la manufactura de pigmentos y de procesos de alteración, e.g. procesos de recristalización mineral y pérdida de capas pictóricas. Además, la información textural de una determinada fase cristalina ha podido correlacionarse con las características texturales de una fase cristalina similar en diferentes muestras pictóricas. Esta comparación de texturas ha permitido en el Palacio de la Madraza de Granada: i) identificar capas pictóricas procedentes de intervención históricas, ii) poner de manifiesto diferente molienda de un pigmento según la función de la capa pictórica en la estratigrafía pictórica y iii) relacionar la cantidad y el tamaño del pigmento con tonalidades cromáticas en diferentes capas pictóricas.

El uso combinado de μ-XRD, RM, SEM-EDS y CG-MS ha permitido la caracterización completa de las decoraciones pictóricas del Palacio de la Madraza, así como reconocer intervenciones históricas. En este edificio histórico se han caracterizado las policromías sobre diferentes sustratos en tres dependencias. En el Oratorio, la única habitación conservada de época Nazarí (siglo XIV), se han estudiado las yeserías policromadas, habiéndose confirmado la existencia de restos pictóricos originales más una intervención cristiana. En la Sala de Entrada y en el Salón de Caballeros, ambas construidas en el siglo XVI, las referencias bibliográficas mencionan numerosas intervenciones acometidas desde el siglo XVIII hasta la actualidad. Nuestros resultados obtenidos en maderas policromadas de los techos y en pinturas murales confirman la existencia de diversas intervenciones gracias a la identificación de determinados pigmentos minerales y la variedad de aglutinantes orgánicos.

Compositional and Quantitative Microtextural Characterization of Historic Paintings by means of micro-X-ray diffraction and Raman microscopy

Journal:	*Analytical Chemistry*
Manuscript ID:	Draft
Manuscript Type:	Article
Date Submitted by the Author:	n/a

Complete List of Authors:	Romero-Pastor, Julia; University of Granada, Mineralogy and Petrology Duran, Adrian; Materials Science Institute of Seville (CSIC-UNSE) Rodríguez Navarro, Alejandro; University of Granada, Mineralogy and Petrology Vangrieken, Rene; University of Antwerp, Department of Chemistry Cardell, Carolina; University of Granada, Mineralogy and Petrology

Compositional and Quantitative Microtextural Characterization of Historic Paintings by means of micro-X-ray diffraction and Raman microscopy

Julia Romero-Pastor[†], *Adrian Duran*[‡], *Alejandro Basilio Rodríguez-Navarro*[†], *René Van Grieken*[§] *and Carolina Cardell*[†*]

[†]Department of Mineralogy and Petrology, University of Granada, Av/Fuentenueva s/n, 18071 Granada, Spain

[‡]Centre de Recherche et de Restauration des Musées de France (CNRS-C2RMF), 14 quai François Mitterrand, Palais du Louvre, 75001 Paris, France – Materials Science Institute of Seville (CSIC-UNSE), Americo Vespucio 49, 41092 Seville, Spain

[§]Micro and Trace Analysis Centre, Department of Chemistry, University of Antwerp, Universiteitsplein 1, 2610 Antwerp, Belgium

Corresponding author: * Tel: + 34 958 242725. Fax: + 34 958 243368. E-mail: cardell@ugr.es

ABSTRACT: This work shows the benefits of characterizing historic paintings via compositional and microtextural data from micro-X-ray diffraction (μ-XRD) combined with molecular information acquired with Raman microscopy (RM) along depth profiles in paint stratigraphies. The novel approach was applied to identify inorganic and organic components from paintings placed at the 14th century Islamic University –*Madrasah Yusufiyya*– in Granada (Spain), the only Islamic University still standing

from the time of *Al-Andalus* (Islamic Spain). The use of μ-XRD to obtain quantitative microtextural information of crystalline phases provided by two dimensional diffraction patterns to recognize pigments nature and manufacture, and decay processes in complex paint cross sections, has not been reported yet. A simple *Nasrid* (14th century) palette made of gypsum, vermilion and azurite using the *tempera* painting technique was identified in polychromed stuccos. Here also a Christian intervention was found via the use of smalt, barite, hematite, Brunswick green and gold; oil was the painting technique employed. On mural paintings and wood ceilings more complex palettes dated to the 19th century were found, made of gypsum, anhydrite, barite, dolomite, calcite, cerussite, hydrocerussite, hematite, minium, ultramarine, and black carbon. The painting techniques identified were *tempera*, *tempera grassa* and oil technique.

INTRODUCTION

Many analytical techniques have been used to study historic paints with the goals of determining palette´s manufacture and to enable conservation/restoration interventions. Characterizing historic pigments and binders is a challenging task due to the complex composition of the artworks and their artistic and historic value, demanding the use of micro- or non- destructive analytical techniques. [1-3] Moreover, the use of a lone technique is generally insufficient to provide evidence of dating, pigment manufacture, execution technique, retouches and/or alteration phenomena. Instead, coupling complementary techniques allows us to overcome limitations of each individual technique and increase confidence in the results. Some techniques disclose molecular information as Fourier Transform Infrared Spectroscopy (FTIR) and Raman Microscopy (RM), while others identify chemical elements present in inorganic pigments and extenders (X-Ray Fluorescence, XRF), or detect crystalline phases in samples (X-ray diffraction, XRD). [1,3,5-11] In particular, the use of RM and μ-XRD allows unambiguous identification of organic and inorganic paintings materials present in the same sample.[10-12] Thus, while RM identifies amorphous, poorly ordered and crystalline compounds of small grains thanks to its high

spatial resolution (~1μm), μ-XRD clearly identifies most crystalline phases present in paintings according to their abundance and crystallinity degree.

This paper presents a novel methodology combining μ-XRD and RM to characterize real painting samples at molecular, mineralogical and microtextural levels to unravel their composition, pigments manufacture, execution technique and chronology. Other complementary analytical techniques used were Gas Chromatography-Mass Spectroscopy (GC-MS), Scanning Electron Microscopy-Energy Dispersion X-ray Spectrometry (SEM-EDX) and Optical Microscopy (OM). The novelty of this work is the determination of the crystallinity and microtextural characteristics of the crystalline phases composing the samples. These physical properties were determined by analyzing Debye-Scherrer rings recorded on two dimensional (2D) diffraction patterns collected with in-house μ-XRD equipment. [12-15] The intensity profile along Debye-Scherrer rings was used to estimate sizes and number of grains of the main crystalline phases present in the samples.

In this regard, small crystal sizes may suggests a meticulous pigment manufacture or imply alteration processes. For instance, Cu-based pigments such as malachite ($CuCO_3.Cu(OH)_2$) when altered into Cu-chlorides show smaller crystal sizes.[4] By contrast, gypsum recrystallization in wall ground layers yields an increase in their crystal sizes.[16] Moreover, grain morphology (size and shape) can provide information regarding pigments origin. Thus homogeneous HgS crystal sizes suggest a synthetic pigment (vermilion), as opposed to the natural pigment cinnabar, which commonly shows heterogeneous HgS crystals. Similar arguments can be used to distinguish between lapis lazuli and blue ultramar.[4,17]

The combined use of μ-XRD and RM to obtain detailed molecular, mineralogical and microtextural information of crystalline phases provided by 2D diffraction patterns, has not been reported in previous studies. Thus, this is the first attempt to use this approach to fully characterize real paint samples, recognize the nature and manufacture of pigments and decay processes, and track historic interventions. The ultimate goal is to draw historic and archaeological conclusions to help clarify the confusing chronology of the paintings at the *Madrasah* palace of Granada.[18]

EXPERIMENTAL SECTION

Sampling site

The *Madrasah* palace of Granada was built by *Yusuf I* (of the *Nasrid* dynasty, 1238-1492 AD) in 1349 AD in the religious and trading centre of the ancient *Madinat Garnata* (Granada, Southern Spain). The original *Madrasah Yusufiyya* was the first Islamic University of Granada and the only extant Islamic University dating back to the time of *Al-Andalus*. Soon after the Christian conquest in 1492 AD, the *Madrasah* became the city council. Since then the building has undergone numerous reforms including incorporation of new rooms such as "the Hall room" and "the Knight room", and restoration interventions such as that currently undertaken by the University of Granada. At present, the only original *Nasrid* room in the *Madrasah* is "the Oratory room"; however, it has undergone several interventions since the 18th century particularly in 1893.[18] In the 16th century "the Hall room" and "the Knight room" were constructed and decorated, later undergoing further interventions starting in the 18th century.[20] Nevertheless, the full chronology remains unclear.

Painting samples

Nineteen samples were taken from the *Madrasah* palace (Table 1). The sampling procedure was guided by i) location in the building, ii) color observed on different substrates (stucco, wood, mural) and iii) possible historic interventions. Colors studied were white, red, blue, green, black and gold. Results are organized according to room to facilitate identification of similarities or differences of painting materials and thus enable tracking historic interventions chronologically.[3,4]

Locate Table 1

Analytical Techniques

Paint stratigraphies were prepared as polished thin sections for microscopic analyses. They were first examined using a polarized light microscope in transmitted and reflected light (Olympus BX60) to obtain an overview of the paint layers disposition, morphology and color. The system was equipped with a digital camera for microphotography (Olympus DP10). Then a detailed chemical and morphological

analysis was performed with a scanning electron microscope SEM Leo 1430VP coupled with an EDX microanalysis (SEM-EDX) INCA 350 version 17 Oxford Instrument. Single point elemental analyses were registered in every layer of sample stratigraphies. SEM-EDX working conditions were 500 pA filament current, 20 keV beam energy and 10 eV/ch resolution.

Micro-X-Ray Diffraction (μ-XRD) analyses were used to identify crystalline components and for microtextural study. Analyses were performed on paint stratigraphies prepared as double-polished thin-sections as described elsewhere.[3] A μ-XRD system developed at the Centre de Recherche et de Restauration des Musées de France at the Louvre Museum was used. The μ-XRD system was equipped with a Cu high-flux, micro-focus X-ray tube (Rigaku MSC MicroMax equiped with a Kirkpatrick-Baez mirror). Imaging plates were used as 2D detectors which allow reasonably fast data collection (10 min per sample spot) with good angular resolution.[5,12,19] μ-XRD analyses were done in reflection mode with an incidence angle around 10 degrees using a 200 µm collimator for microanalysis. For each sample, a set of analyses was performed across a 1 mm line every 10 to 50 µm in each paint stratigraphy starting from the outermost external layer toward the interior. Due to the small thickness of some layers (down to 10 µm as identified by the microscopic techniques), the different measurements do not always correspond exactly to individual paint layers. Nevertheless, as demonstrated by Duran and co-workers,[12] useful information of composition evolution along sample depth profiles can be obtained. The FIT2D software was used to transform 2D images into standard one-dimensional (1D) XRD diagrams (2Theta scan).[5,12,19] The EVA and/or XPower software programs were employed to identify crystalline phases using the PDF-2 database (JCPD) from calculated XRD diagrams and to perform quantitative analysis.[20]

Microtextural features of crystalline phases was done by analyzing the concentric Debye-Scherrer rings (2D diffraction patterns) with the software XRD2Dscan.[13,15] Each ring correspond to a specific set of {hkl} crystallographic planes of a particular mineral phase, and is formed by reflection spots of all mineral grains illuminated by the X-ray beam that are oriented with a set of {hkl} planes to fulfill the Bragg diffraction condition. According to sample characteristics, the rings display particular variations

in intensity and continuity. Thus, for a fix beam size, depending on grain size, the number of grains illuminated is very large for nano- or microcrystalline materials, or very small for coarse grained materials. Also continuous rings are formed by superposition of many reflections in the case of fine-grained minerals, and broad rings will be obtained when nano- or microcrystalline phases are present. Instead spotty rings form by isolated reflection spots produced by a reduced number of coarse mineral grains. Additionally, the total number of peaks (TNP) of one ring is a gauge of the number of grains illuminated and of their sizes. Another textural characteristic obtained is the average intensity of peaks (API) along a Debye-Scherrer ring, which is related to the crystal sizes of mineral grains. Indeed, the intensity of these peaks is directly proportional to grain sizes, allowing size quantification.[13,14] Moreover, this technique enables quantification of grain sizes of different mineral phases (independently) that might be present by analyzing rings associated with each mineral.

Raman microscopy analyses were performed with a Renishaw Invia Raman microscope system fitted with a Peltier-cooled CCD detector and a Leica DMLM microscope to identify inorganic and organic compounds present in the paint samples. Samples were excited with a 785 nm diode laser. Spectra were collected with an average resolution of 1 cm^{-1} within the wavenumber range of 200-3000 cm^{-1}. To improve signal/noise ratios, a series of recorded spectra (n = 10) with exposure time = 20 s were collected in each sample spot and averaged. Spectra were taken by placing the samples on the microscope stage and observing them using 20X and 50X objectives. A video camera was employed to identify particular locations in the painting stratigraphies. Precautions were taken to not cause any damage to samples (i.e. laser-induced degradation of paintings). Thus laser power was kept between 0.2 and 20 mW to avoid paint component alteration and obtain the best spectra.[21] In this work, key Raman bands and main diffraction peaks are given only the first time that a specific paint compound is mentioned in the text. *Gas Chromatography/Mass Spectroscopy* (GC-MS) analyses were done on chips samples to determine the organic binders as described elsewhere.[3]

RESULTS AND DISCUSSION

Oratory room

Seven samples were studied showing different surface colors, i.e. red, blue, green and gold (applied on stucco) and white (used for wood ceiling, Table 1). According to μ-XRD, the red sample OR-R-NE was composed of HgS (main diffraction peaks at 26.5º and 31.2º 2θ; JCPD: 06-0256). Its presence was confirmed by RM analysis thanks to Raman spectra showing key bands at 251 cm^{-1} and 343 cm^{-1} (the distinction between cinnabar and vermilion based on μ-XRD textural analysis is explained below). The red color was applied over a ground layer of gypsum ($CaSO_4.2H_2O$, key diffraction peaks at 29.2º and 31.2º 2θ; JCPD: 33-0311 and main Raman bands at 418, 497, 628, 1005 and 1140 cm^{-1}). SEM-EDX analyses identified Hg, S and Ca, confirming these results (Table 1). No X-ray diffraction peaks were detected from the blue sample OR-BL-E; instead a broad band indicated its amorphous nature. RM analysis identified blue smalt via the Raman band at 470 cm^{-1}. Blue smalt is an artificial pigment made of fine to coarsely ground potassium cobalt glass. In Europe it was used as early as the 15th century up to recent times;[22] thus this is not an original *Nasrid* paint layer. This finding was supported by the scarce literature available in this regard claiming that lapis lazuli and azurite were the only blue pigments used in *Nasrid* polychromes.[3,4,23] In this superficial blue layer also barite ($BaSO_4$) was identified by both techniques; indeed, Raman spectrum exhibited its key band at 989 cm^{-1} and the barite XRD pattern showed typical peaks at 28.8º and 42.6º 2θ (JCPD: 24-1035). The barite identified as an extender in this blue layer points to an intervention dated no earlier than the 19th century, since barite pigment was introduced in the market in that century.[24] In addition, an irregular layer of HgS was detected under the blue smalt. This feature, together with the fact that the HgS layer was applied over a similar ground layer made of gypsum, suggests that the red layer is originally *Nasrid*. SEM-EDX analyses identified Ba, Hg, S, Ca, confirming these results, in addition to K, Na, Si, and Al attesting for clay mineral dust particles (Table 1).

The green samples (Table 1) were made of Brunswick green a pigment composed of Prussian blue, chrome yellow and barite commercialized in the 19th century.[24] RM analyses identified the main Raman bands of barite, chrome yellow (359, 377, 401 and 840 cm^{-1}) and Prussian blue (275, 530, 2075, 2150

and 2153 cm^{-1}); however μ-XRD only detected barite. SEM-EDX analyses confirmed these pigments by detecting Ba, Cr, Pb, S and Fe (Table 1). In both samples the green layers were applied over a white ground layer made of gypsum and calcite ($CaCO_3$, key diffraction peaks at 29.4º and 47.6º 2θ; JCPD: 05-0586 and key Raman band at 1086 cm^{-1}).

The characterization of the golden sheet (Figure 1a) exemplifies the benefits of the applied methodology. Figure 1b shows the OM image of the paint stratigraphy. A golden sheet was applied over a thick white layer and both lie on top of an irregular blue layer. μ-XRD analyses identified gold (Au) at the surface (key diffraction peaks at 38.3º and 44.5º 2θ; JCPD: 04-0784), gypsum and calcite in the white layer, and azurite grains ($Cu_3(CO_3)\cdot 2(OH)_2$) in the inner-most layer (main diffraction peaks at 25.23º 2θ; JCPD: 11-0682) (Figure 1c,d). SEM-EDX analyses identified Au, Ca, S and Cu confirming the above results.

The detection of gypsum, calcite and azurite were corroborated by RM analyses via the recognition of their key Raman bands: gypsum and calcite (cited) and azurite at 401 cm^{-1}. In this sample, azurite was believed to be an original *Nasrid* pigment considering its identification in other early *Nasrid* polychromes characterized in Granada[3,4,23], and the fact that other layers (gypsum and gold) were applied on top. Thus, the above gilding should be attributed to a later intervention. Although there are not enough data to ascribe this intervention to a particular period, we suggest that it may belong to the 19th century, since results in others samples from this room (e.g. OR-BL-E) so suggest.

RM analyses could not detect the presence of gold. Though the high spatial resolution of RM (~1 μm) allows the analysis of individual grains, which is ideal for the identification of small crystals such as those comprising a gold sheet (<10μm in diameter), in this study the slight gold key Raman bands were masked by the strong intensity bands of gypsum and calcite from the underneath layer. Moreover, it should be noted that in this sample gold could be detected by μ-XRD due to its abundance (the gold layer is homogeneous and continuous). As mentioned in the experimental section, though μ-XRD explores a large sample area (in this work a 200 μm collimator was used), to detect a crystalline phase there must be enough grains of this phase properly oriented to satisfy the Bragg diffraction condition.

Thus, the higher the number of crystal phases, the bigger the probability of satisfying the diffraction condition; so it is difficult to detect scarce and isolated coarse grains with μ-XRD.[15]

The μ-XRD microtextural study of the OR-G-NE sample indicated the presence of microcrystalline gold, as revealed by the broad and continuous rings produced by this phase in the 2D diffraction pattern (Figure 1c), and corroborated by 1D XRD diagram (Figure 1d). Additionally, the green line in Figure 1e shows a low and constant intensity profile along the diffraction rings associated with gold, different from the spotty rings for other mineral phases present in this sample. In particular, the rings attributed to gypsum (Figure 1e) have very strong reflection spots due to the large size of gypsum grains in the ground layer and/or also due to recrystallization events due to alteration processes.[16] The crystal size of these neoformed grains was estimated to be ~ 40 μm *vs*. the 15 μm size of the unaltered gypsum crystals present in the same layer, as shown by the pink line in Figure 1e (note the sharp gypsum peaks). The rings associated with calcite (Figure 1c and 1e-yellow line) showed strong isolated reflection spots, indicating that calcite grains were relatively large (few tens of microns). Microtextural analysis was not done on the azurite pigment since, as explained before, only scarce grains were present (which would justify the mentioned historic gilding intervention), and so an estimation of grain size based on μ-XRD could not be achieved.

Insert Figure 1

The OM study of sample OR-R-S revealed two red layers of different hues applied over a coarse white ground layer. The outermost red layer was identified as hematite (Fe_2O_3, key Raman bands at 293, 410 and 616 cm^{-1}) applied over the remains of another red layer identified as HgS. HgS was clearly detected by μ-XRD unlike hematite which showed very weak peaks. The characterization of iron oxide-hydroxides using μ-XRD was difficult due to the small amount of these pigments and their low reflecting power compared to the main crystalline phases present in the sample. Another difficulty in identifying hematite is the strong X-ray fluorescence of Fe-bearing minerals when analyzed using Cu radiation.[25] The white ground layer was made of gypsum and calcite according to μ-XRD and RM analyses. SEM-EDX analyses identified Fe, Hg, Ca and S, confirming the above results (Table 1). The

white sample OR-W-S taken from the wood ceiling was composed mostly of zincite (ZnO, with key Raman band at 434 cm^{-1} and diffraction peaks at 31.8º and 36.3º 2θ, JPCD: 05-0664), corresponding to the zinc white pigment. Other minerals identified were gypsum and calcite. The occurrence of zinc white indicates a 19th century intervention, since this pigment was industrially commercialized around 1845.[24] This datum is chronologically compatible with the identification of blue smalt in the polychromed stucco of "the Oratory room".

To further demonstrate the benefits of our methodology, we assessed the microtextural properties of diverse samples from "the Oratory room" which correspond to different periods (according to our results). Thus, grain sizes of HgS and gypsum layers were studied analyzing their corresponding 2D diffraction patterns. Results revealed that HgS was very similar in grain size (tens of microns) in samples OR-R-NE and OR-BL-E, as seen in Figure 2a. On the contrary, grain size of HgS in sample OR-R-S was notably smaller (a few microns). In fact, the API data of sample OR-R-S showed lower values (385) than the other two samples (621 and 702), implying smaller crystal size. Moreover, the corresponding averaged TNP data revealed lower number of HgS grains (10) in OR-R-S sample compared to the other two samples (27 and 25).

Insert Figure 2

Diverse studies conducted in *Nasrid* palaces in Granada have identified HgS either as cinnabar or vermilion in their polychromed decoration.[3,4,23] Cinnabar and vermilion are names assigned to HgS of different origin: cinnabar is a natural compound used as pigment since ancient times (China), and vermilion (wet/dry-process type) is a synthetic pigment known since the 8th century.[26] No differences in their composition or crystal structure can be recognized, though slight morphological disparities between them may help in its determination, as well as the existence of impurities in natural cinnabar.

Considering our microtextural results, the presence of wet-process vermilion can be excluded in our samples on the basis of the absence of very fine crystals (<1 μm) and even particle size distribution typical of this pigment.[17] Moreover the wet method is thought to have been known since the late 17th century.[26] On the other hand, cinnabar must be excluded since no impurities were detected with

SEM–EDX in any of the studied red layers. Thus it seems that dry-process type vermilion (introduced to the West by the Arabs in the 9th century) was the pigment used in the three studied samples. Nevertheless, our microtextural study revealed different vermilion grain sizes that may suggest different periods of painting execution. However, microscopic evidence from paint layers in sample OR-R-S suggests that the vermilion layer in this sample is of *Nasrid* origin similar to the other two samples. Indeed, the hematite layer above the vermilion layer in sample OR-R-S supports this idea, suggesting that the hematite layer was applied in a later intervention due to the deterioration of the vermilion layer, where only few grains remain as revealed by OM. We hypothesize that the deterioration of the vermilion layer in this sample may have loosened the biggest crystals.

In "the Oratory room" also gypsum crystal sizes appearing in different layers were studied (see layers in Table 1). Microtextural analyses showed that gypsum grain sizes were notably different depending on the position of the studied layer in the paint stratigraphies (Figure 2b). According to API data grain sizes were smaller (~ 10 μm) at the outer most layers (surface layer) in OR-W-S than in interior layers (ground layers) of the rest of samples (~ 50 μm). In addition, TNP data revealed that gypsum crystals were more abundant in ground layers than in surface layers. Here differences in crystal sizes cannot be ascribed to diverse paint execution periods, but rather to the role of the paint layer in the painting structure. Normally coarse grains are present in ground layers to assist adherence between the substrate and the overlying paint layers. On the contrary finer grained pigments are used in surface paint layers to improve paint finish.[24]

Regarding binders of "the Oratory room" samples, RM analyses identified glue binders (proteinaceous binder) in all layers of sample OR-R-NE, the vermilion layer of sample OR-R-S, and all ground layers of the stucco samples (Table 1) via the detection of: a sharp aromatic ring breathing band at 1002 cm^{-1}, the amide III band at 1245 cm^{-1}, and the N–H and C–C (stretching modes) bands of Phenylalanine and Tyrosine at 1578 cm^{-1} and 1607 cm^{-1} respectively.[8] Though Raman spectra of protein binders are rather similar they can be distinguished by differences in band position and relative intensity, particularly of bands near 1000 and 1450 cm^{-1}. [10,27] However, in this work fluorescence problems did not allow us to

discern the type of protein present. Instead an oleinaceous binder was identified in all layers (blue smalt, hematite, green and white) attributed to a Christian intervention (19th century). Oil binders were recognized by RM through the C-H deformation bands of olefinic molecules shown at 1310 cm^{-1} (in-phase methylene twist) and at 1445 cm^{-1} (scissoring mode of methylene $\delta(C_{H2})$, the cis double bond stretching ν(C=C) band shown at 1660 cm^{-1} and the band at 1747 cm^{-1} (ester stretching ν(C=O)). [28-30] Oil discrimination was not possible due to high fluorescence which masked other characteristic Raman features. GC-MS further confirmed the presence of oils via the recognition of azelaic acid (A, $C_9H_{16}O_4$, characteristic component of aged oils), palmitic acid (P, $C_{16}H_{32}O_2$) and stearic acid (S, $C_{18}H_{36}O_2$).[31] Quantitative determination of percentage contents of fatty (P and S) acids and dicarboxylic (azelaic and suberic) acids allows discrimination between different types of drying oil (e.g. linseed, walnut and poppy seed) on the basis of characteristic acid ratios A/P and P/S.[32] Here however, the non-distinct percentages prevented oil discrimination.

Hall Room

Six samples taken from the wall and the wood ceiling were studied (Table 1). The polychromy of this room is based on white and red (different hues) applied over a white ground layer. The identified red pigments (see Table 1) were hematite (key Raman bands at 293, 410 and 616 cm^{-1}) and minium (PbO, key Raman bands at 237, 316, 394 and 550 cm^{-1} and diffraction peaks at 34.1º and 47.6º 2θ; JCPD: 41-1493). All ground layers were made of gypsum and/or anhydrite and/or barite as identified by μ-XRD and RM (Table 1). Both techniques allowed clear discrimination between the two types of calcium sulfates, i.e. gypsum ($CaSO_4 \cdot 2H_2O$) and anhydrite ($CaSO_4$). Anhydrite was identified via Raman bands at 422, 503, 615, 681, 1010 and 1128 cm^{-1} and diffraction peaks at 38.8º and 40.8º 2θ (JCPD: 37-1496). Also in ground layers traces of red pigments were identified, namely minium in sample W-R3-N and hematite in samples W-R2-N and AL-W. Hematite was not detected by *μ*-XRD for the reason explained above. Also blue ultramarine (a pigment synthesized in 1828) was identified in AL-W sample via the detection of the key Raman band at 549 cm^{-1}.[26] Instead ultramarine was not detected by *μ*-XRD due to the scarce pigment crystals.

For this room we present the results of evolution in composition along the depth profile of the white sample AL-W. Figure 3a is an OM view of the sample which consists of five layers. Figure 3b shows the RM analyses of each layer. In layer 1 (Figure 3a) dolomite ($CaMg(CO_3)_2$), key Raman bands at 1099 cm^{-1}), anhydrite and gypsum were identified, while in layer 2 and 3 gypsum and anhydrite were found. Barite, anhydrite and ultramarine were detected in layer 4, and hematite in layer 5. Figure 4c shows the μ-XRD results. Calcite and dolomite were identified in the surface layer, barite was found in the underlying layers and gypsum and anhydrite appeared in all layers. In the most internal layer hematite was not detected with μ-XRD probably due to its low concentration and/or strong X-ray fluorescence as discussed before. The elements detected with SEM-EDX in all layers confirmed the presence of the above mentioned minerals (Table 1).

Insert Figure 3

In "the Hall room" the microtextural study was restricted to gypsum and anhydrite crystals present at surface and the ground layers from all samples. The API data suggested that gypsum had smaller grain sizes than anhydrite in both the surface and ground layers (927 and 532 *vs* 1582 and 714 respectively). However, when analyzing in detail the intensity profile of the two minerals it was deduced that both had similar grain sizes (estimated size c.a. 10-20 μm) with the exception of few larger anhydrite grains (c.a. 50 μm in size) which produced some high intensity peaks. Moreover, the averaged TNP data showed a higher number of gypsum grains than anhydrite grains in all layers (42 and 33 *vs* 26 and 17 respectively). This result suggests that gypsum is the main mineral phase in these layers as confirmed by XRD quantitative analysis (67% gypsum).

The variable composition of binders in this room is shown in Table 1. Proteinaceous binders were detected with RM in almost all layers in all samples. In particular, egg yolk was identified through key protein bands at 1360, 1586 and 1603 cm^{-1} (from Tryptophan, Tyrosine and Phenilalanine aromatic amino acids)[8] and the characteristic carbonyl vibration at 1740 cm^{-1}. [31] Also RM detected oil in samples W-R2-N and AL-R via the key Raman bands at 1307, 1445 and 1660 cm^{-1}. These results were confirmed by GC-MS. In particular, egg yolk was recognized thanks to a high proportion of palmitic

acid, and linseed oil binder was identified via the P/S value around 1.18.[32] The inconsistent binder composition together with the variable ground layer composition suggests that diverse historic interventions took place in this room.

Knight Room

Six samples from the wood ceiling showing white, ochre, red and black color at the surface were studied (Table 1). Results obtained along depth profiles with RM and μ-XRD revealed that the white surface samples were made mainly of hydrocerussite ($Pb_3(CO_3)_2(OH)_2$) and cerussite ($PbCO_3$) with minor amounts of calcite (C-W1) or gypsum (C-W2). Key Raman bands for hydrocerussite were found at 970 and 1051 cm^{-1} and for cerussite at 680, 1051, 1214, 1330 cm^{-1}. The surface of the ochre C-OC sample was made of hydrocerussite, cerussite, calcite and hematite. μ-XRD analyses confirmed the presence of the mentioned minerals; thus hydrocerussite was identified via characteristic peaks at 34.2º and 40.4º 2θ (JCPD: 13-0131) and cerussite via peaks at 24.8º and 45.1º 2θ (JCPD: 05-0417). According to RM and μ-XRD data, minium was detected at the surface in red samples and scarce calcite grains in C-R2 (Table 1). Carbon black (vegetal carbon) was identified by RM at the surface in sample C-BK via a wide band at 1590 cm^{-1}. All layers described were applied over ground layers with diverse composition made mostly of gypsum, hydrocerussite and cerussite and/or lower amounts of anhydrite, minium (C-W1), calcite and quartz (see Table 1, results were confirmed by SEM-EDX). Quartz was identified with RM via the key band at 467 cm^{-1} and by μ-XRD through the main peaks at 26.7º 2θ (JCPD: 33-1161).

Regarding organic binders, RM analysis identified oil in all layers of all samples (Table 1) by way of key Raman bands at 1310, 1445, 1660 and 1747 cm^{-1}.[29-31] Once again the type of oils could not be identified with RM due to fluorescence problems. However GC-MS analyses identified suberic, azelaic, palmitic and stearic acids. The calculated P/S ratio = 1 confirmed the presence of linseed oil. [32]

In this room the application of our methodology was particularly valuable to study the white C-W2 sample. As Figure 4 shows strong Raman fluorescence in the 750 - 1250 cm^{-1} region hindered the recognition of bands corresponding to gypsum, anhydrite, hydrocerussite and cerussite. On the contrary

their identification by μ-XRD was easier as seen in the depth profile of Figure 4c. In fact minium was detected together with hydrocerussite, cerussite and small amounts of gypsum at the surface layer. In the intermediate layer minium was not found, and in the ground layer gypsum, anhydrite and quartz were identified by μ-XRD.

Insert Figure 4

Here the microtextural μ-XRD study was restricted to minium crystals from the surface layers in CR1 and CR2 (red layers) and CW2 (white layer) samples. According to API and TNP values, minium crystal sizes and the number of grains were slightly different for red and white layers. The averaged API values suggested that minium was manufactured similarly in CR1 and CR2 red samples (1590 and 1987, respectively) to obtain crystal sizes around tens of microns, versus the minium used in the white C-W2 sample where the API value (1007) indicated smaller crystal sizes. Averaged TNP data showed a vaguely lower number of minium grains in the red samples (26 and 28) than in the white sample (32). These results suggest that different procedures in paint execution of the red and white samples were employed, most probably due to the color sought rather than different execution periods. In addition, though API and TNP data of minium are similar for both "the Knight room" and "the Hall room" (averaged TNP=26 and API=1212 for this latter room), a coincident intervention has to be excluded based on the different nature of the binders (egg in "the Hall room" and oil in "the Knight room").

CONCLUSIONS

This study is a part of an ongoing investigation of Hispano-Muslim archaeological artifacts[15] and polychromes[3,4] on diverse substrates (plasterwork, marble, wood) in Granada (Spain), to clarify historic and artistic issues and to track the technical evolution of *Nasrid* art. The ultimate goal is to fill gaps in the history of pigments where Islamic pigments and painting techniques have systematically been omitted. In this paper our novel methodology based on microtextural μ-XRD information combined with RM analyses allowed identification of inorganic and organic paintings components from the 14th century Islamic University –*Madrasah Yusufiyya*.

The *Madrasah Yusufiyya* was built in 1349 by the *Nasrid* ruler *Yusuf I*, who also built the Comares Palace at the Alhambra[4]. In the only original *Nasrid* room (Oratory room) still standing in the *Madrasah* we found a simple *Nasrid* palette made of vermilion and azurite to polychrome stucco (named *yesería* by *Nasrids*). Azurite was also identified in other monuments of Granada from the first period of *Nasrid* art (1237–1314), for instance the Partal Palace in the Alhambra[4] and the *Qubba Dar al-Manjara l-kubra*[23], in contrast to lapis lazuli used during the later *Nasrid* period in the Alhambra (e.g. in the Lions Palace built by *Muhammad V*, 1362–1391).

In the *Madrasah* palace, Christian interventions were also recognized in the *Nasrid* Oratory room and in other two Christian rooms. Traditionally historic interventions, forgeries, dating and chronological uncertainties in paintings have been tackled using pigments as benchmarks.[3,10] However, as demonstrated in this study, information provided by microtextural characteristics of pigments and organic binders was crucial to identify historic interventions. In "the Oratory room" *Nasrid* ground (gypsum) and paint layers (vermilion and azurite) were blended with glue binder (tempera technique) whereas Christian paint layers (smalt, hematite, chrome green, zinc white and gilding) were mixed with oil binder (oil technique). Here the identified pigments attest to a 19th century intervention.

Regarding the Christian rooms, in "the Hall room" the variable composition of ground layers and binders suggest that diverse historic interventions took place. Here most ground layers were typically prepared using either gypsum or anhydrite, or both, together with barite and egg yolk as binder (*tempera grassa* technique). To be consistent with our reasoning, we propose that those ground layers containing barite were applied during a 19th century intervention. Other ground layers were prepared either with glue (*tempera* technique) or linseed oil (oil technique). In "the Knight room" all ground layers were mostly made of cerussite, hydrocerussite and gypsum mixed with linseed oil (oil technique). Here it is difficult to date the polychromy since the pigments used are not indicative of a particular epoch. However it can be argued that this painting was executed contemporarily with the oil technique painting of "the Hall room", since linseed oil was identified in both.

Microtextural data such as grain size and amount of crystalline phases present in a dense assemblage, as that usually found in complex paint layers, are not easy to determine with conventional microscopic techniques like OM or SEM. Usually identification and quantification of a sufficient number of mineral grains require tedious sample preparation and time-consuming image analysis procedures. As shown in this work, our μ-XRD procedure has provided quantitative grain size data and crystal amount of all crystalline phases present in a paint layer in a more efficient, faster and easier way than using microscopic techniques. In particular results have shed light on the nature, manufacture and weathering of pigments. Thus it seems that dry-process type vermilion was the red pigment used by *Nasrids*. Though different vermilion grain sizes and quantities were found in the three studied samples which may suggest different paint execution times, complementary microscopic studies revealed that paint layer deterioration was behind that observation. This fact attests the need to characterize painting samples coupling complementary analytical techniques.

Additionally μ-XRD results disclosed different grain sizes of similar pigments according to the role of the different coats in the paint stratigraphy; for instance, smaller gypsum crystals at the surface than in ground layers. Also recrystallized gypsum could be identified in ground layers. As well our method was able to quantify in the same layer the proportion of pigments present and their size. Thus in gypsum and anhydrite-rich surface and ground layers, gypsum was found to be the main pigment although anhydrite had larger crystal size. Moreover this method was able to discern different crystal sizes and the amount of minium pigment used by artists to achieve different tonalities at the surface. Our future perspectives in relation with the microtextural information obtained with μ-XRD in real painting samples is to explore its capability as a tool to date historic paintings.

ACKNOWLEDGMENT Financial support was provided by Research Group RNM-179 (CICE, (Junta de Andalucía), Project P08-RNM-04169 and contracts MEC FULLBRIGHT 2008-2010, JAEDoc088 and MAT2010-20660 (Spanish Government). The authors gratefully acknowledge AGLAE and C2RMF staffs (especially Dr Jacques Castaing). We thank E. Sebastián and P. Salmerón for authorizing this

research and J. Ramos from "Restauración del Patrimonio S.L." for collaborating with sampling campaign. We wish to thank A. Kowalski for English revision.

REFERENCES

(1) Castro, K.; Pessanha S.; Proietti, N.; Princi, E.; Capitani, D.; Carvalho, M. L.; Madariaga, J. M. *Anal. Bioanal. Chem*. **2008**, 391, 433–441.

(2) Švarcová, S.; Hradil, D.; Hradilová, J.; Kočí, E.; Bezdička, P. *Anal. Bioanal. Chem.* **2009**, 395, 2037–2050.

(3) Cardell, C.; Rodríguez-Simón, L.; Guerra, I.; Sánchez-Navas, A. *Archaeometry*. **2009**, 51, 637–657.

(4) Cardell-Fernández, C.; Navarrete-Aguilera, C. *Stud. Conserv.* **2006**, 51, 161–176.

(5) Duran, A.; Pérez-Rodríguez, J. L.; Jiménez de Haro, M. C. *Anal. Bioanal. Chem.* **2009**, 394, 1671–1677.

(6) Schmidt, C. M.; Walton, M. S.; Trentelman, K. *Anal. Chem.* **2009**, 81, 8513–8518.

(7) Appolonia, L.; Vaudan, D.; Chatel, V.; Aceto, M.; Mirti, P. *Anal. Bioanal. Chem.* **2009**, 395, 2005–2013.

(8) Nevin, A.; Anglos, D.; Burnstock, A.; Cather, S.; Becucci, M.; Fotakis, C.; Castellucci, E. *J. Raman Spectrosc.* **2008**, 39, 307–313.

(9) Franquelo, M. L.; Durán, A.; Herrera, L. K.; Jiménez de Haro, M. C.; Pérez-Rodríguez; J.L.J. *Mol. Struct.* **2009**, 924/926, 404–412.

(10) Correia, A. M.; Oliveira, M. J. V.; Clark, R. J. H.; Ribeiro, M. I.; Duarte, M. L. *Anal. Chem.* **2008**, 80, 1482–1492.

(11) Brostoff, L. B.; Centeno, S. A.; Ropret, P.; Bythrow, P.; Pottier, F. *Anal. Chem.* **2009**, 81, 6096–6106.

(12) Durán, A.; Sigüenza, M.B.; Franquelo, M.L.; Jiménez de Haro, M.C.; Justo, A.; Perez-Rodriguez, J.L., *Anal. Chim. Acta* **2010**, 671, 1–8.

(13) Rodríguez-Navarro, A. B. *J. Appl. Cryst.* **2006**, 39, 905–909.

(14) Rodríguez-Navarro, A. B.; Álvarez-Lloret, P.; Ortega-Huertas, M.; Rodríguez-Gallego, M. J. *Am. Ceram. Soc.* **2006**, 89, 2232–2238.

(15) Cardell, C.; Guerra, I.; Romero-Pastor, J.; Cultrone, G.; Rodríguez-Navarro, A. *Anal. Chem.* **2009**, 81, 604–611.

(16) Cardell, C.; Rodríguez-Gordillo, J. *Bol. Soc. Esp. Mineral.* **2003**, 26, 113–121

(17) Mactaggart, P.; Mactaggart A. PigmentID. CD issue version 2.4-d. **2004**.

(18) Gómez-Moreno, M. Guía de Granada, 1892. Ed.; Facsímil. Universidad de Granada-Fundación Gómez-Moreno: Granada, **1982**; 2; pp 195.

(19) Duran, A.; Castaing, J.; Walter, P. *Appl. Phys. A.* **2010**, 99, 333–340.

(20) Martín-Ramos, J. D. Using XPowder, A software package for Powder X-Ray diffraction analysis. (ISBN 84–609–1497–6), Spain, **2004**.

(21) Navas, N.; Romero-Pastor, J.; Manzano, E.; Cardell, C. *J. Raman Spectrosc.* **2010**, 41, 1196–1203.

(22) Mühlethaler. B.; Thissen J. *Stud. Conserv.* **1969**, 14, 47–61

(23) García-Bueno, A.; Medina-Flores, V. J. *Cult. Heritage.* **2004**, 5, 75–89.

(24) Mayer, R. Materiales y Técnicas Pictóricas. Ed. Hermann Blume **1988**.

(25) Herrera, L. K.; Montalbani, S.; Chiavari, G.; Cotte, M.; Solé, V. A.; Bueno, J.; Durán, A.; Justo, A.; Pérez-Rodríguez, J. L. *Talanta* **2009**, 80, 71–83.

(26) Eastaugh, N.; Walsh, V.; Chaplin, T.; Siddall, R. Dictionary of Historic Pigments; Pigment Compendium. A. Butterworth-Heineman: Oxford, **2004**.

(27) Vandenabeele, P.; Wehling, B.; Moens, L.; Edwards, H.; De Reu, M.; Van Hooydonk, G. *Anal. Chim. Acta* **2000**, 407, 261–274.

(28) Baeten, V.; Hourant, P.; Morales, M. T.; Aparicio, R. *J. Agr. Food Chem.* **1998**, 46, 2638–2646.

(29) Burgio, L.; Clark, R. J. H. *Spectrochim. Acta A*. **2001**, 57, 1491–1521.

(30) Muik, B.; Lendl, B.; Molina-Díaz, A.; Ayora-Cañada, M. *J. Chem. Phys. Lipids,* **2005**, 134, 173–182.

(31) Blaskov, J.; Kubinec, R.; Husoba, B.; Prikryl, P.; Pacakova, V.; Stulik, C.; Hradilova, J. *J. Sep. Sci.* **2008**, 31, 1067–1073.

(32) Mills, J. S.; White, R. The organic chemistry of the museum objects, 2nd ed.; Butterworth Heinemann Ltd: Oxford, **1994**.

Table 1. Samples analyzed in the 14th century Islamic University –*Madrasah Yusufiyya*– of Granada (Southern Spain).

Location	Sampling	Samples	Surface color	Pigments in surface	Pigments in underlying layers	Elements in all layers	Binders in all layers
Oratory room (Nasrid period 14th century)	Polychromed stucco (14th century)	OR-R-NE	red	V, Gy	Gy	Hg, S, Ca	glue: AL
		OR-BL-E	blue$^{\phi}$	Sm, B, Gy	V, Gy	Ba, Hg, S, Ca, K, Na, Si, Al	glue: GL oil: Sm
		OR-GR-E	green$^{\phi}$	B, BG, Gy, C	Gy, C	Ba, Cr, Pb, S, Fe, Ca	glue: GL oil: CG
		OR-GR-NE	green$^{\phi}$	B, BG, Gy, C	Gy, C	Ba, Cr, Pb, S, Fe, Ca	glue: GL oil: GC
		OR-G-NE	gold$^{\phi}$	G	Gy, C, Az	Au, Ca, S, Cu	glue: white layer
		OR-R-S	red$^{\phi}$	H	V, Gy, C	Fe, Hg, Ca, S	glue: GL and V oil: He
	Wood ceiling (19th century)	OR-W-S	white	ZW, Gy, C	No present	Zn, Ca, S	oil: white
Hall room (16th century)	Wall (mural painting, 19th century)	W-R1-N	red	Mi, Anh	Anh, B	Pb, S, Ca, Ba, Fe, Si, K, Al	egg: AL
		W-R2-N	red	Mi, Anh	Gy, Anh, H, B	Ba, Ca, Fe, S, Pb	oil: He egg: GL and M
		W-R3-N	red	H, Mi, Anh, Gy	Gy, Anh, B, Mi	S, Ca, Fe, Pb	egg: AL
		W-R4-N	red	H, Gy, Anh, C	Gy	Fe, Ca, S	glue: AL
	Wood ceiling (19th century)	AL-R	red	H, Mi	Anh	Fe, Pb, Ca, Si, S	oil: AL
		AL-W	white	Dol, C, Anh, Gy	H, Ult, Gy, Anh, B	Mg, Ca, S, Ba	egg: AL
Knights room (16th century)	Wood ceiling (? century)	C-W1	white	Hy, Cer, C	Hy, Cer, C, Mi	Pb, Ca	oil: AL
		C-W2	white	Hy, Cer, Gy, Mi	Gy, Anh, C, Q	Ca, S, Pb	oil: AL
		C-OC	ochre	Hy, Cer, C, H	Hy, Cer	Pb, Fe, Ca	oil: AL
		C-R1	red	Mi	Gy, Hy, Cer, Anh, C	Pb, Ca, S	oil: AL
		C-R2	red	Mi, C	Gy, C	Pb, Ca, S	oil: AL
		C-BK	black	BC	Cer, Hy, Gy, C	Pb, Ca, S	oil: AL

($^{\phi}$) = Christian intervention; Pigments identified by μ-XRD and RM; elements identified by SEM-EDX; binders identified by RM and GC-MS. Acronyms for pigments: V=vermilion; Gy=gypsum; C=calcite; B=barite; Sm=smalt; BG= Brunswick green; G=gold; H=hematite; ZW=zinc white; Mi=minium; Anh=anhydrite; Dol=dolomite; Hy=hydrocerussite; Cer=cerussite; BC=black carbon; Az=azurite; Ult=ultramarine; Q=quartz; AL=all layers; GL=ground layer

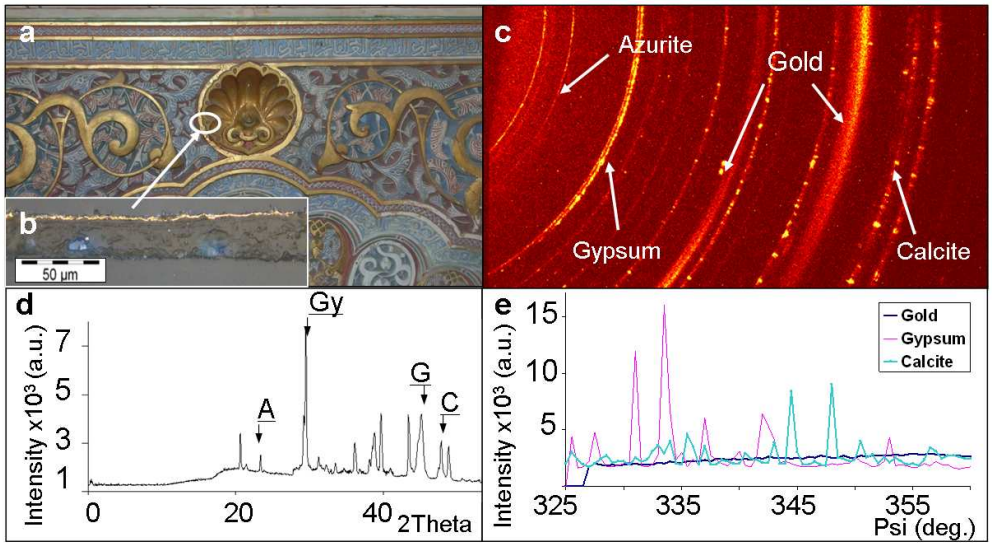

Gold sample (OR-G-NE) from "the Oratory room": a) Detail of the analyzed area; b) paint stratigraphy seen by OM (reflected light, crossed Nicols); c) 2D diffraction pattern of crystalline phases. d) 2Theta scan calculated from the 2D pattern: azurite (A), gypsum (Gy), gold (G) and calcite (C). e) Intensity profiles along the main diffraction rings associated with each mineral.
206x114mm (150 x 150 DPI)

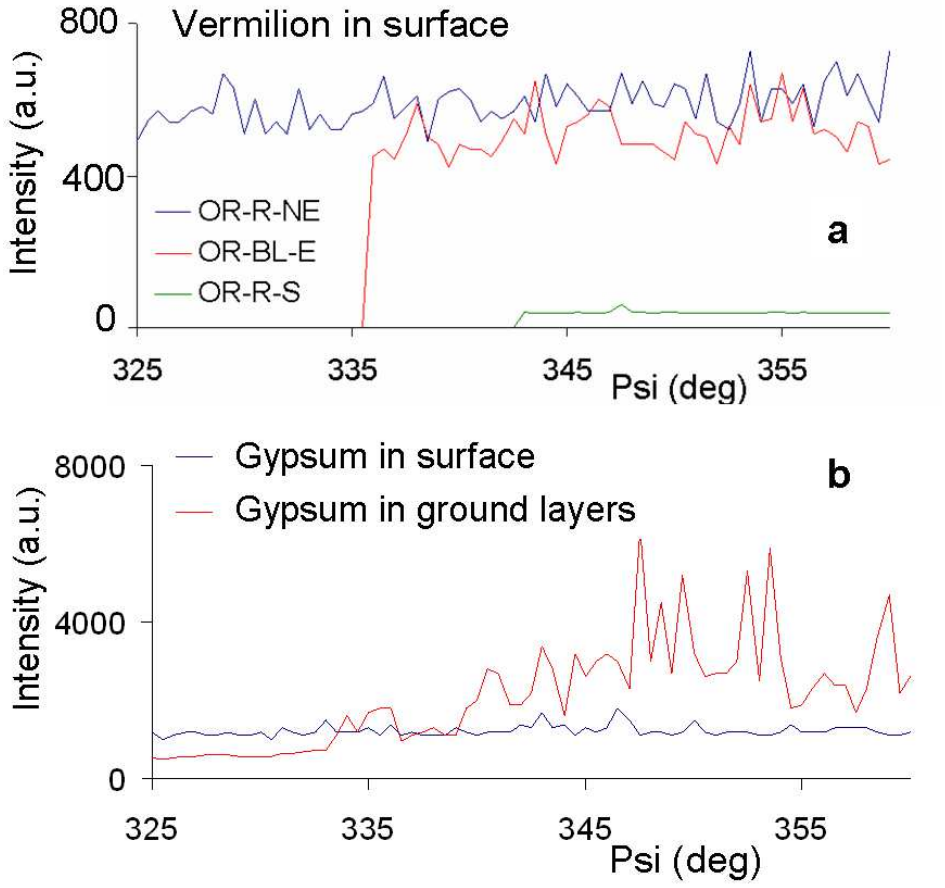

Graphics showing the intensity profile along the strongest diffraction rings of a) vermilion at 26.5º 2θ corresponding to three surface layers from "the Oratory room" samples, and b) gypsum at 31.2º 2θ at the surface and at underlying layers (ground layers) in all "the Oratory room" samples.
155x155mm (150 x 150 DPI)

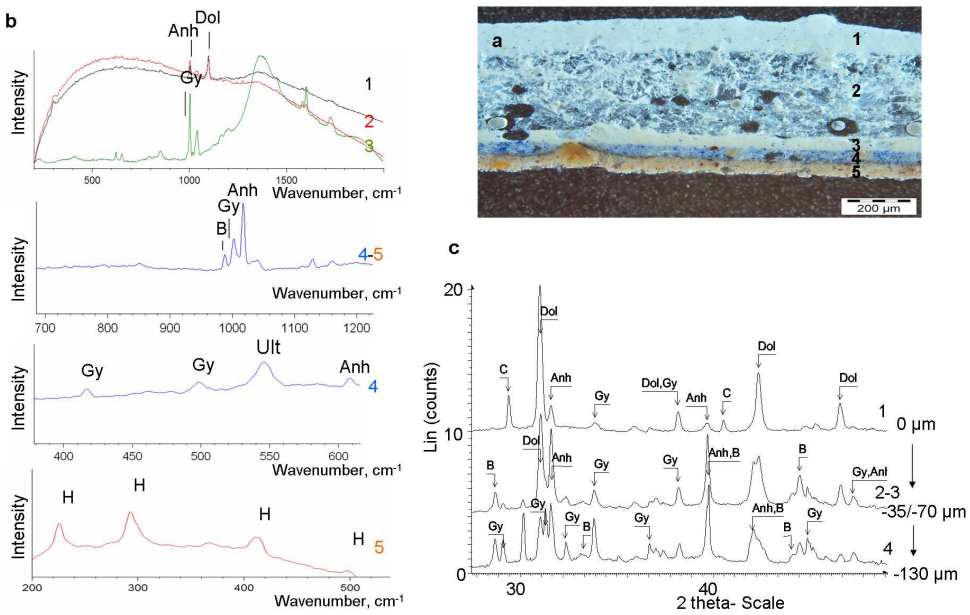

AL-W sample from "the Hall room": a) Paint stratigraphy as seen by OM (reflected light, crossed Nicols); b) Raman spectra of each layer and magnifications of spectrum 4 and 5; c) Diffractogram at 0 (1), 35 and 70 (2-3) and 130 µm (4) from the surface. H=Hematite, Anh=Anhydrite, Gy=Gypsum, Dol=Dolomite, B=Barite, Ult= ultramarine and C=Calcite.
320x205mm (150 x 150 DPI)

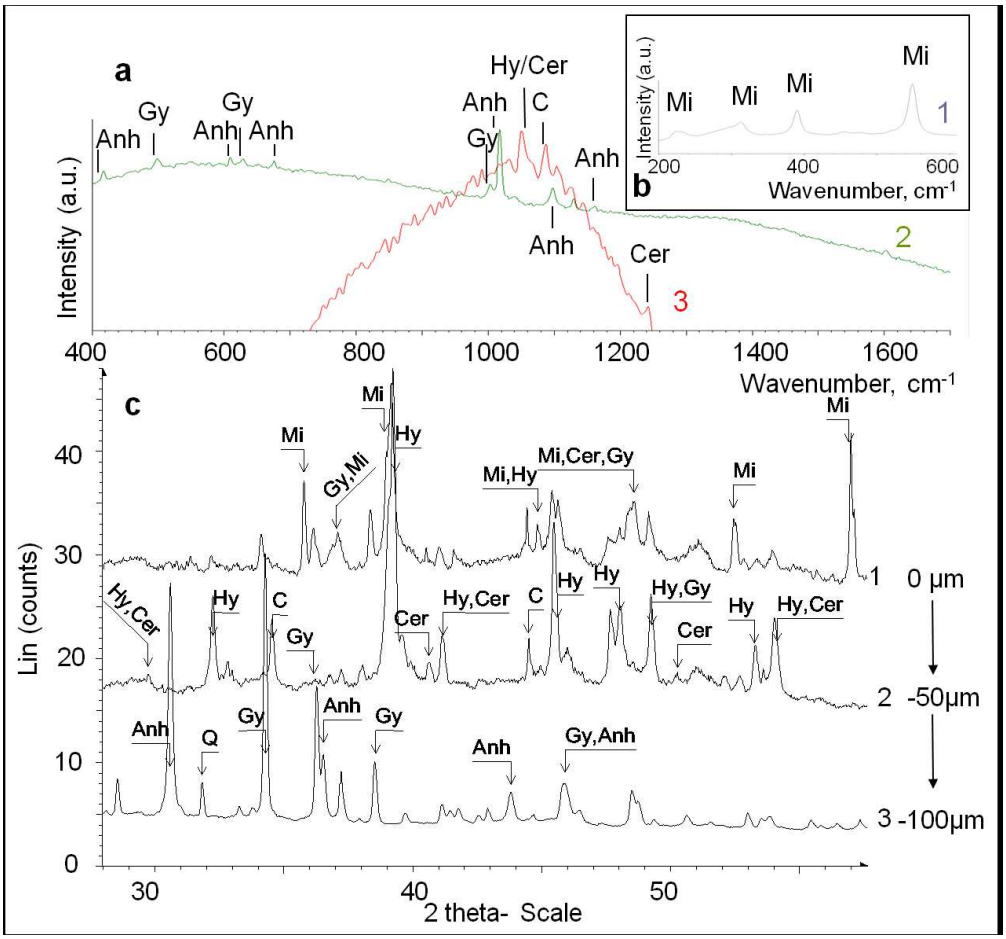

C-W2 sample from "the Knight room": a) Raman spectra of the white surface in the 400 to 1700 cm-1 range; b) Raman spectra of the surface in the 200 and 600 cm-1 range; c) XRD diffractograms along the depth profile from the surface inward (measurements every 50 µm). See acronyms above.
215x200mm (150 x 150 DPI)

Conclusiones

Este estudio pone de manifiesto la capacidad de la metodología basada en la combinación de RM, µ-XRD y técnicas complementarias como SEM-EDX y GC-MS para analizar muestras pictóricas reales a nivel molecular, mineralógico y microtextural, con objeto de identificar su composición, manufactura de pigmentos, técnicas de ejecución y cronología.

En particular, en la Sala del Oratorio los resultados han permitido confirmar el uso de bermellón como pigmento rojo de origen Nazarí usado en la decoración de las yeserías. Se sugiere que el bermellón fue elaborado según el método seco, puesto que los datos microtexturales de µ-XRD desechan la posibilidad de que hay sido elaborado según el método húmedo (i.e. ausencia de cristales homogéneos < 1 µm), y los resultados de SEM-EDX confirman la ausencia de impurezas típica del cinabrio o pigmento natural. En esta sala, además de bermellón, únicamente se ha encontrado azurita como pigmento original Nazarí; ambos fueron aglutinados con cola y aplicados sobre una preparación de yeso. En esta sala las características microtexturales del yeso revelan procesos de deterioro por recristalización mineral, gracias a la presencia de granos neoformados de mayor tamaño. Además se ha puesto de manifiesto que los cristales de yeso de las capas de preparación son más abundantes y tienen mayor tamaño que el yeso de las capas superficiales. La identificación en las yeserías de azul de esmalte, barita, hematites, verde de Brunswick y dorado (oro nanocristalino según datos microtexturales de µ-XRD) mezclados con un aglutinante oleoso, indica la existencia de una intervención Cristiana datada a partir del siglo XIX, tal y como sugieren los pigmentos presentes.

En la Sala de Entrada los pigmentos hallados en los muros fueron hematites y minio sobre capas de preparación a base de yeso y/o anhidrita, identificándose una gran variedad de aglutinantes, a saber, huevo, cola y aceite. En la policromía sobre madera se detectó blanco de yeso y anhidrita sobre escasos restos de azul ultramar sintético y barita mezclado con huevo, y rojo de minio y hematites aglutinado con aceite de linaza. Los datos microtexturales del yeso y anhidrita en las capas superficiales y las de preparación indican que sus tamaños de grano son similares, con la excepción de unos pocos cristales de anhidrita de mayor dimensión. Por otro lado, el yeso es más abundante (67%) que la anhidrita en todas las capas.

El techo policromado de la Sala de Caballeros presenta en superficie capas en rojo (minio), blanco (blanco de plomo, yeso y anhidrita) y negro (de carbón) aplicadas sobre preparaciones de composición diversa (yeso, anhidrita, blanco de plomo, calcita, cuarzo). En todas las capas el aglutinante identificado fue aceite de linaza. Los datos de μ-XRD han revelado que el tamaño de grano del pigmento minio es diferente en las capas rojas en comparación con el presente en las capas blancas, así como su cantidad, menor en las capas rojas. En esta sala es arriesgado realizar una datación de la policromía ya que los pigmentos identificados no lo permiten. No obstante, puede proponerse que estas policromías se ejecutaron contemporáneamente a las policromías del techo de la Sala de Entrada, al identificarse en ambas el mismo aglutinante a base de aceite de linaza.

11. Conclusiones. Conclusions

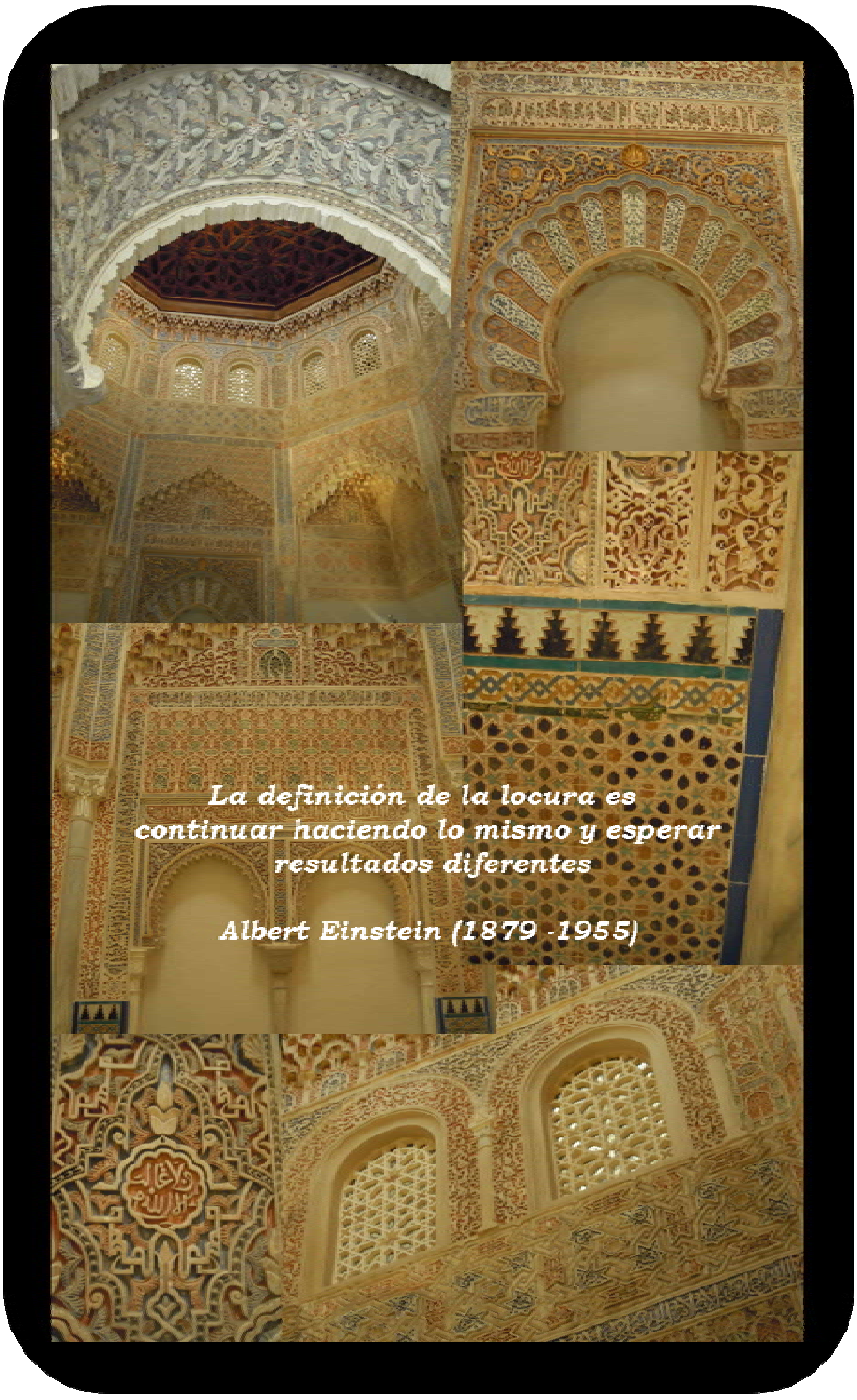

Este Capítulo 11 muestra las conclusiones generales extraídas de esta Tesis Doctoral.

This Chapter 11 shows the main conclusions of this Doctoral Thesis.

11. Conclusiones

Las principales conclusiones de esta Tesis Doctoral están relacionadas con el beneficio generado por la aplicación del análisis quimiométrico, concretamente, el análisis de componentes principales –PCA-, a diferentes datos espectrales adquiridos a partir de materiales pictóricos. En particular, los resultados obtenidos de la aplicación de diversas técnicas analíticas (esto es, T-FTIR, DRIFT, RM, MALDI-TOF MS y ATR-FTIR) y el empleo de PCA, han permitido caracterizar en detalle los materiales pictóricos estudiados, así como sus interacciones físico-químicas. Además, se han estudiado los efectos de procesos de envejecimiento en dichos materiales. Los resultados de estos todos estudios han llevado a proponer nueva metodología analítica para abordar la caracterización y el estudio del comportamiento de materiales pictóricos. Asimismo, en este capítulo 11 de Conclusiones Generales se describen las ventajas de usar técnicas de análisis combinadas en el estudio de muestras pictóricas reales.

Beneficios del empleo del PCA en el estudio de réplicas pictóricas

- El análisis de los espectros FTIR obtenidos en modo Reflectancia Difusa (DRIFT) proporciona una mejor información sobre la composición de pigmentos inorgánicos (i.e. azurita, lapislázuli y esmalte) que la proporcionada por los espectros registrados en modo Transmitancia (T-FTIR). Este hecho se debe a la presencia de bandas vibracionales más intensas de los pigmentos en los espectros DRIFT. Sin embargo, el modo Transmitancia, T-FTIR, es más adecuado para obtener información sobre el aglutinante proteico, dado que su espectro de infrarrojo presenta bandas de absorción muy características. Sin embargo, el estudio mediante PCA, pone de manifiesto la mayor utilidad de los datos DRIFT, ya que permite una mejor discriminación de las muestras según su composición específica.

- El análisis de la primera derivada de espectros Raman mediante PCA permite la diferenciación de réplicas pictóricas puras (i.e. pigmentos puros y aglutinante puro) y sus temples de huevo en función de su composición específica. Se demuestra que el análisis quimiométrico requiere el cálculo previo de la primera derivada del espectro Raman, ya que así es posible detectar cambios espectrales muy sutiles, que de otra forma pasarían desapercibidos. Esta metodología permite eficientemente discriminar la presencia o no del aglutinante -yema de huevo- en réplicas pictóricas. Por otra parte, la degradación de pigmentos por acción del láser, puede ser fácilmente detectada mediante PCA de espectros Raman originales.

- El PCA de espectros Raman originales –sin necesidad de calcular la primera derivada- presenta una gran potencialidad en el estudio de temples proteicos. Esto es debido a que se puede detectar leves diferencias espectrales en la región del estiramiento del grupo C-H característico exclusivamente del aglutinante (yema de huevo en el caso particular). Estas diferencias se asocian a las interacciones entre determinados pigmentos inorgánicos y el aglutinante. Así pues, con esta metodología propuesta se permite sugerir interacciones concretas pigmento-aglutinante. Concretamente, se propone la existencia de interacción cuando están presentes los siguientes pigmentos: cinabrio, *Sienna* natural, blanco de plomo, yeso, azurita y esmalte. La interacción con estos pigmentos modifica la estructura de las proteínas y los ácidos grasos contenidos en la yema de huevo de tal manera que da lugar a pequeños cambios espectrales discriminados mediante PCA. Estas interacciones puede deberse a la formación de complejos metal-proteína entre determinados componentes de la yema de huevo (principalmente, el componente de naturaleza proteica) y los pigmentos. Por el contrario, en presencia de calcita y lapislázuli no se observan estos cambios en dicha región espectral del aglutinante, indicación que la proteína permanece inalterada.

- El empleo conjunto de una serie de técnicas espectroscópicas junto con análisis multivariante –PCA- presenta una gran potencialidad en la obtención de información sobre procesos de envejecimiento de muestras pictóricas. Concretamente, el PCA de los espectros de T-FTIR ha permitido extraer información sobre el comportamiento de temperas de azurita-cola de conejo frente a la radiación UV. Además, los análisis por colorimetría, SEM-EDS y XRD han sido esenciales para corroborar los resultados obtenidos por PCA. En particular, en las réplicas que contienen sólo cola de conejo se pone de manifiesto una significativa degradación de este componente debida a la radiación UV, que también se corrobora por análisis de SEM. En cambio, la azurita no sufre alteración debida a la radiación UV en las réplicas pictóricas tanto puras como mezcladas con el aglutinante; este hecho es corroborado por SEM-EDX, DRX y colorimetría. Por tanto, estos resultados sugieren un efecto protector de la azurita en la fotoestabilidad de la cola frente a la radiación UV, con independencia de la concentración de la mezcla azurita-cola en la muestra pictórica.

- El uso combinado de MALDI-TOF MS y T-FTIR y la aplicación de PCA a los mapas peptídicos obtenidos mediante MALDI-TOF MS, permite detectar diferencias significativas en el proceso de alteración de aglutinante proteico, - cola de conejo - e identificar cambios en la estructura secundaria del colágeno debido a la radiación UV, tanto en las réplicas puras como en temples -mezclas con azurita y cinabrio-. Se revela, por tanto, ésta como una metodología muy adecuada para el estudio de procesos de alteración de materiales pictóricos en general. De forma particular, el estudio de las réplicas azurita-cola de conejo aplicando esta nueva metodología corrobora que la presencia de azurita mejora la fotoestabilidad de la cola frente a la radiación UV, favoreciéndose así la estabilidad del temple. Estos resultados se encuentran en línea con resultados previamente obtenidos. Se sugiere además la formación de un complejo cobre-proteína para los temples de azurita-cola. En el caso concreto de los temples de cinabrio, se evidencia

modificaciones del mismo a todos los niveles de envejecimiento estudiados.

- El estudio de la estructura secundaria del colágeno de la cola de conejo analizada mediante Espectrometría FTIR en los temples de cinabrio revela que se produce una desnaturalización de la cola debido a la acción degradante del cinabrio, atribuible en principio a la presencia de mercurio. Además, el efecto de la radiación UV sobre dichos temples origina sucesivos cambios conformacionales del colágeno a diferentes estructuras desordenadas.

- El estudio de la alteración térmica de réplicas pictóricas y hueso natural mediante ATR-FTIR y RM, respectivamente, y el análisis de estos datos espectrales mediante PCA demuestra la estabilidad de la fase mineral (i.e. cuarzo y hidroxiapatito) en las muestras, y la alteración de los componentes orgánicos involucrados. Además, se ha establecido la cantidad y fase mineral más adecuada que permite una valoración de la calidad de los resultados espectrales obtenidos por RM y ATR-FTIR. Ambas técnicas permiten separar las muestras de acuerdo con el tratamiento térmico recibido. Sin embargo, RM discrimina mejor las muestras, atribuible a su mayor resolución espectral.

Beneficios de aplicar metodologías analíticas ad hoc en el estudio de muestras pictóricas reales: Palacio de la Madraza (Granada, España).

- Se demuestra la capacidad e idoneidad de la metodología basada en la combinación de técnicas analíticas tales como RM, μ-XRD junto con otras técnicas complementarias (i.e. SEM-EDS, CG-MS) para la caracterización de materiales pictóricos inorgánicos y orgánicos. Esta metodología se aplicó a muestras pictóricas reales procedentes del *Palacio de la Madraza, en Granada*.

- En particular, se demuestra que el uso de µ-XRD no sólo permite identificar las fases minerales presentes en las muestras pictóricas, sino que proporciona información microtextural de éstas (i.e. tamaño y número de granos de cada fase cristalina). Esta información se obtiene a partir del análisis de patrones de difracción bidimensiones de las muestras. Esta es la primera vez que se utiliza información microtextural para reconocer el tipo de manufactura y naturaleza de algunos pigmentos minerales, así como para identificar procesos de deterioro en las pinturas estudiadas, tales como recristalización de yeso en las capas de preparación o pérdida de capas pictóricas.

- Esta novedosa metodología analítica ha permitido identificar policromías Nazaríes en el Oratorio de la Madraza (siglo XIV) así como intervenciones Cristianas posteriores en ésta y otras dependencias del monumento. Esta estimación cronológica se ha realizado gracias a la identificación de pigmentos característicos de determinadas épocas históricas, y el uso particular de aglutinantes en las distintas estancias estudiadas.

Conclusions

The main conclusions of this PhD Thesis are based on the benefits of the combined use of chemometric analysis on spectral data from painting materials. In particular, the results of different analytical techniques (i.e. T-FTIR, DRIFT, RM, MALDI-TOF MS o ATR-FTIR) and the application of PCA allow the characterization in depth of the painting materials studied and physico-chemical interactions between them. In addition, the alteration processes have been studied due to alteration agents. Also, new analytical methodology has been proposed focused to characterise and to study the behaviour of the painting materials. On the other hand, the benefits of the

combined use of analytical techniques have been focused on the study of real paintings.

Benefits of the application of PCA to the study of painting model samples

- PCA performed on DRIFT spectral data of blue pigments (i.e. azurite, lapis lazuli and smalt) and their tempera model samples has marked advantages when compared to the results obtained with the same approach but using T-FTIR spectral data. Multivariate analysis of DRIFT data demonstrated better ability to discriminate replica samples according to known composition. Moreover, it was possible to group in different clusters samples that differed only in terms of the presence of glue. The spectral data registered by DRIFT achieve high intensity bands of inorganic pigments. However, T-FTIR spectral data give more number of IR bands of rabbit glue.
- The application of PCA on first-derivative Raman spectra to investigate inorganic pigments and tempera paint model samples. The Raman spectra were used to apply PCA in order to test whether spectral differences allowed discrimination of samples based on their composition. This goal was achieved only when the first derivative Raman spectra where used. This could be attributed to the fact that the use of first derivative allows detection of small chemical changes on the RM spectra which could not be noted when using original Raman. Nevertheless, the original Raman spectra were useful to detect damage in the particular pigment minium by laser irradiation.
- The PCA performed on original RM spectra allows the identification of slight changes in the characteristic C–H stretching region (3100–2800 cm^{-1}) of a protein-based binder and fatty acids from egg yolk, which may occur in complex paint samples due to the presence of particular pigments. These interactions were evident in cinnabar, natural Sienna, white lead, gypsum, azurite and smalt. Therefore these results suggest that the pigments containing metals interact with the proteinaceous

binder depending on the stability of the complex formed between the metal and the binder's amino acids.

- The study of artificial UV-ageing processes of a blue copper pigment-glue tempera painting technique, particularly on azurite and rabbit skin glue allow discrimination among painting model samples based on their againg state due to UV irradiation. In particular, the pure glue undergoes strong degradation after UV irradiation, which is corroborated by SEM. However, the azurite shows photostability against the UV exposure, both when pure and mixture in model samples, as also was revealed by SEM-EDS, reflectance spectrophotometry and XRD analyses. This finding suggests that azurite protects the glue binder against UV degradation.
- The PCA performed on MALDI-TOF MS data from paintings model samples (i.e. pure glue and tempera model samples) discriminates samples based on the different ageing state after different UV time exposure. The results of azurite tempera model samples reveal the photostabilization of the glue against UV irradiation, i.e. high photostability of the tempera when azurite is present. In addition, conformational study of tempera shows the structural stability of collagen in the ageing process when is mixed with azurite. This approach based on MALDI TOF MS, PCA and FTIR proposes that the formation of the complex protein-copper could justify the additional photostabilization of the tempera when azurite is present.
- The conformational study of cinnabar tempera model samples by FTIR shows the denaturation of collagen due to the harmful properties of mercury. In addition, the study of the UV ageing process of glue when cinnabar is present in tempera reveals conformational changes by different disordered structure due to UV exposure.
- The study of thermal degradation of painting model samples and natural bones (made of hydroxyapatite mixed with collagen) by ATR-FTIR and RM spectra, respectively, and the PCA to both spectral data allow the identification of the mineral stability of two internal

standards (i.e. quartz and hydroxyapatite) and the alteration process of organic compounds. In addition, the adequate amount and type of mineral phases is proposed to evaluate the quality of spectral data. Both analytical techniques allow discrimination in samples based on the thermal stages. However, RM achieves better discriminations among samples due to its higher spectral resolution.

Benefits of the application of analytical methodology for the study of real painting samples: Madrasah Palace (Granada, Spain).

- The novel methodology based on microtextural µ-XRD information combined with RM analyses allowed identification of inorganic and organic paintings components from the 14th century Islamic University –*Madrasah Yusufiyya*.

- The µ-XRD procedure has provided microtextural data such as quantitative grain size data and crystal amount of all crystalline phases present in a paint layer in a more efficient, faster and easier way than using microscopic techniques. In particular results have shed light on the nature, manufacture and weathering of pigments. Additionally µ-XRD results disclosed different grain sizes of similar pigments according to the role of the different coats in the paint stratigraphy, also recrystallized gypsum could be identified in ground layers. Moreover this method was able to discern different crystal sizes and the amount of minium pigment used by artists to achieve different surface tonalities.
- In the *Madrasah* Palace, Christian interventions were recognized in the Oratory room on Nasrid paintings. The methodology based on RM, µ-XRD, SEM-EDS and CG-MS allows discriminating historic interventions using pigments and binders. Moreover, information provided by the painting techniques was crucial in clarifying the confusing chronology of the paintings at the *Madrasah*.

12. Perspectivas futuras

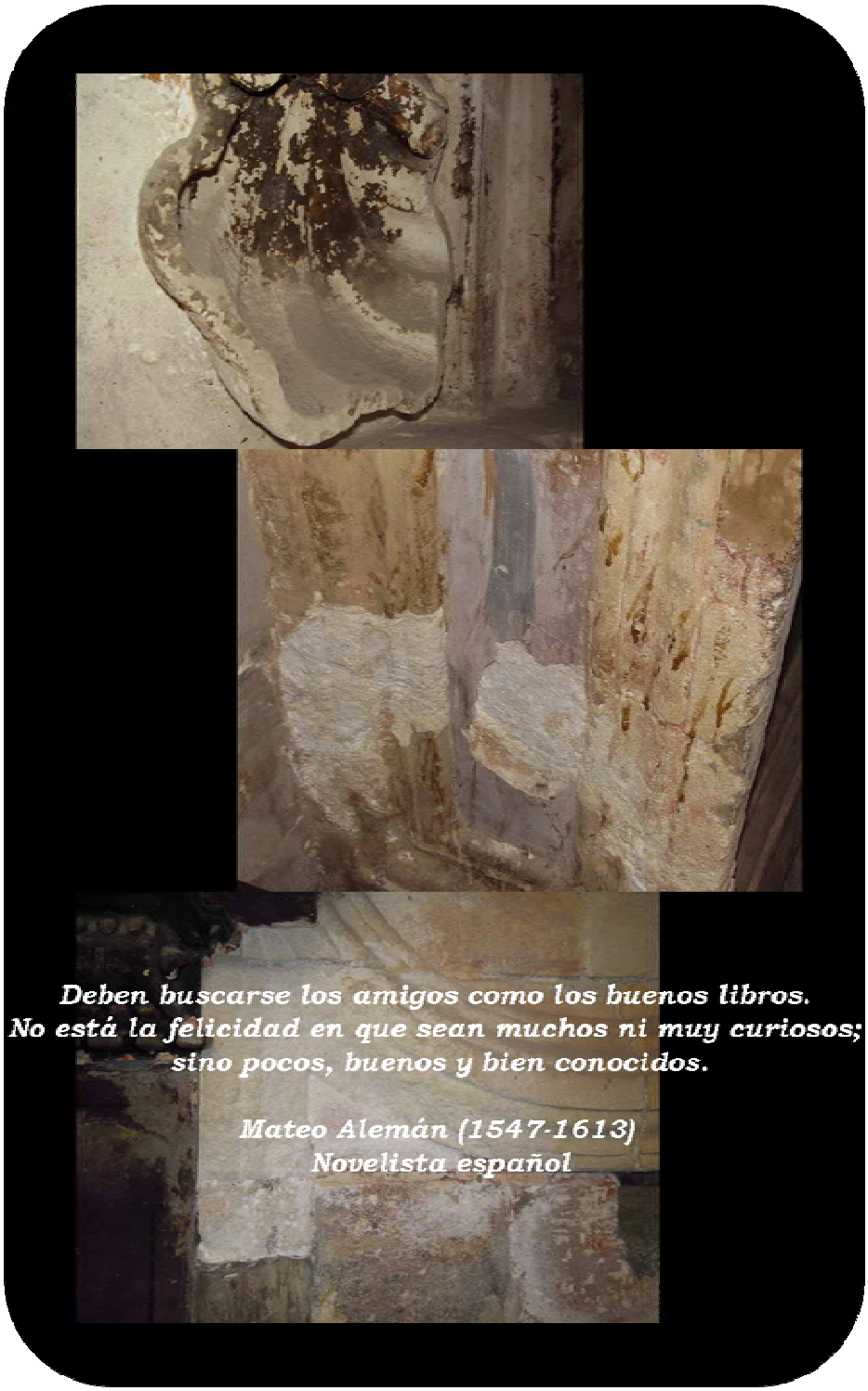

Deben buscarse los amigos como los buenos libros.
No está la felicidad en que sean muchos ni muy curiosos;
sino pocos, buenos y bien conocidos.

Mateo Alemán (1547-1613)
Novelista español

En el Capítulo 12 “Perspectivas futuras” se exponen las líneas de trabajo abiertas tras el desarrollo de esta Tesis Doctoral.

This Chapter 12 “Future perspectives” shows some future work perspectives based on the research of this Doctoral Thesis.

12. Perspectivas futuras

La investigación realizada en esta Tesis Doctoral ha supuesto profundizar en una línea previamente iniciada y dirigida al estudio y caracterización mediante técnicas quimiométricas de materiales pictóricos, particularmente centrada en aquellos materiales en los que el aglutinante es de naturaleza proteica. Concretamente, la presente Tesis doctoral se ha centrado en la evaluación del uso combinado de técnicas analíticas, novedosas en el campo del Patrimonio Pictórico, y el PCA para el estudio y caracterización de materiales pictóricos, sus interacciones físico-químicas y sus procesos de alteración bajo determinadas condiciones ambientales. Este uso combinado de diferentes técnicas de análisis es altamente recomendable para la identificación de materiales y técnicas pictóricas, el reconocimiento de intervenciones históricas, así como de procesos de alteración sufridos por una obra pictórica a lo largo de su historia. Esta información es imprescindible para un conocimiento profundo de tal obra, así como para su catalogación y/o intervención. Para poder abordar estas cuestiones en el futuro se pretenden realizar los siguientes estudios:

i) Análisis de procesos de envejecimiento acelerado de muestras pictóricas expuestas a aerosoles marinos (NaCl) y gases contaminantes (NO_x y O_3). Este tipo de agentes de alteración ambientales son especialmente dañinos para el Patrimonio Histórico (ya identificados en monumentos de la Ciudad de Granada, tales como el Monasterio de San Jerónimo y la Alhambra) y su estudio es de gran interés para el desarrollo de procesos adecuados de restauración-conservación. De ahí la necesidad de evaluar su impacto perjudicial sobre réplicas pictóricos, con el objetivo de correlacionar posteriormente las conclusiones obtenidas al estudio de obras pictóricas reales.

ii) Desarrollar metodologías de análisis *ad hoc* para el estudio de pigmentos negros en temples de caseína (i.e. temples de leche). Estos materiales pictóricos se han aplicado de manera extendida a lo largo de la Historia en obras pictóricas. Sin embargo, hay pocos estudios que analicen este tipo de pigmentos en obras pictóricas reales y su interacción con el aglutinante en temples de caseína. Para ello, será necesaria la aplicación de técnicas analíticas, como la Microdifracción y Microfluorescencia de Rayos X, la Espectrometría de Absorción de Rayos X y la aplicación de la Microscopía Electrónica de Barrido acoplada a Espectrometría Raman (Sistema SCA). Este tipo de análisis se realizará en un futuro en el Sincrotrón Alba (Barcelona, España), en el Sincrotrón ESRF (Grenoble, Francia) o el Centro Instrumentación Científica (Granada, España).

iii) Además, se están desarrollando metodologías analíticas novedosas para la caracterización detallada de obras pictóricas reales del Patrimonio Histórico de la ciudad de Granada, basadas en el uso conjunto de μ-XRD, RM, MALDI-TOF MS y CG-MS. Como ya ha quedado demostrado en esta Tesis Doctoral, estas técnicas de análisis son muy valiosas por la información que proporcionan y por su carácter no destructivo o microdestructivo. El objetivo es el estudio de policromías sobre estuco y mármol procedentes de los Palacios Nazaríes de la Alhambra, así como policromías y pinturas murales de la Iglesia del Monasterio de San Jerónimo (Granada, España).

iv) Se prevé también incorporar muestras pictóricas reales que serán estudiadas mediante metodologías analíticas basadas en PCA, así como el empleo de las diversas herramientas quimiométricas ya usada durante el desarrollo de esta Tesis Doctoral. El objetivo es abordar estudios de clasificación e identificación de dichas muestras reales mediante metodologías de análisis no invasivas y que maximicen la información obtenida de ellas.

PhD Thesis
Department of Mineralogy and Petrology
University of Granada

This PhD Thesis represents an advance in the field of Cultural Heritage and particularly in studying historical tempera paints. It deals with the characterization of historical painting materials (pigments and proteinaceous binders), the study of their interaction and the deterioration caused by accelerated ageing processes triggered by their exposure under diverse environmental conditions. This Thesis shows for the first time the benefits of applying a multivariate analysis tool, in particular, Principal Component Analysis (PCA) to data from routine and novel spectrometric techniques in the field of Cultural Heritage (e.g. Diffuse Reflectance Infrared Fourier Transform Spectroscopy, Raman Microscopy and Matrix-Assisted Laser Desorption/Ionization, Time of Flight Mass Spectrometry) to study model painting samples. The diverse analytical routines presented in this PhD Thesis allow discrimination of painting model samples according to their differing composition, states of ageing, or the interactions among their different components. The final goal is to discern compatibility of pigments and proteinaceous binders in real painting samples. In this regard, an ad hoc novel analytical approach based on Micro X-Ray Diffraction μ-XRD and Raman Microscopy was applied to identify inorganic and organic components from polychromes from the 14th century Islamic University –*Madrasah Yusufiyya*– in Granada (Spain). In particular, results have shed light on the nature, manufacture and weathering of pigments. Moreover, information provided by the painting techniques was crucial in clarifying the confusing chronology of the paintings at the *Madrasah*.